International Journal of Polymer Science

Natural Fibers, Bio- and Nanocomposites

Guest Editors: Susheel Kalia, Luc Avérous, James Njuguna, Alain Dufresne, and Bibin Mathew Cherian

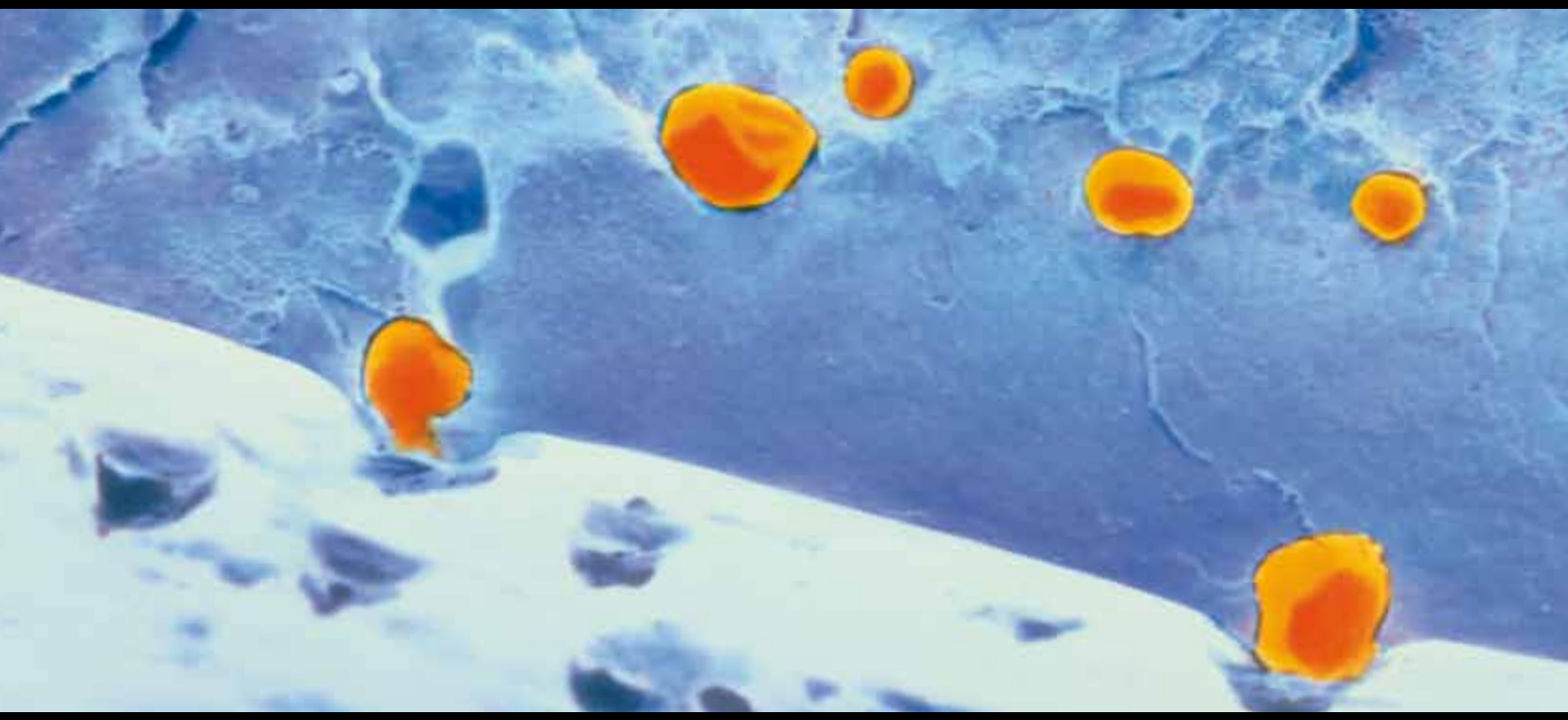

Natural Fibers, Bio- and Nanocomposites

International Journal of Polymer Science

Natural Fibers, Bio- and Nanocomposites

Guest Editors: Susheel Kalia, Luc Avérous, James Njuguna, Alain Dufresne, and Bibin Mathew Cherian

Editorial Board

Contents

Hindawi Publishing Corporation
International Journal of Polymer Science
Volume 2011, Article ID 735932, 2 pages
doi:10.1155/2011/735932

Editorial
Natural Fibers, Bio- and Nanocomposites

Susheel Kalia,[1] Luc Avérous,[2] James Njuguna,[3] Alain Dufresne,[4] and Bibin Mathew Cherian[5]

[1] *Department of Chemistry, Shoolini University of Biotechnology and Management Sciences, District Solan (Himachal Pradesh), Bajhol-173 229, India*
[2] *LIPHT-ECPM, EAC (CNRS) 4375, University of Strasbourg, 25 rue Becquerel, 67087 Strasbourg Cedex 2, France*
[3] *School of Applied Sciences, Cranfield University, Bedfordshire MK43 0AL, UK*
[4] *Grenoble Institute of Technology, The International School of Paper, Print Media and Biomaterials (Pagora), BP 65, 38402 Saint Martin d'Hères Cedex, France*
[5] *Department of Natural Resources, Sao Paulo State University (UNESP), Botucatu 18610-307, SP, Brazil*

Correspondence should be addressed to Susheel Kalia, susheel_kalia@yahoo.com

Received 12 October 2011; Accepted 12 October 2011

Natural fibers have received great interest as reinforcing material for polymer-based matrices because of the environmental issues in combination with their lowcost and some intrinsic interesting properties (density, shape ratio, mechanical behavior). From natural fibers, we can obtain cellulose whiskers in a multistep process. Cellulose nanofibers reinforced polymer composites is a fast-growing area of research because of their enhanced mechanical, thermal, and biodegradation properties. Nanocomposites based on cellulose nanofibers are increasingly regarded as an alternative to conventional composites. The properties of nanocomposites depend not only on the properties of their individual constituents but also on their morphology and interfacial (matrix/nanofiller) characteristics. This rapidly expanding field is generating many exciting new materials with novel properties. This special issue will be interesting for researchers working in the field of natural fibers, isolation of cellulose nanofibers, pretreatments of natural fibers and their application as reinforcement in bio- and nanopolymer composites.

The first paper of this special issue "Cellulose-based bio- and nanocomposites: A review," is an overview, which reviewed the surface modification of cellulose fibers by various methods. Applications of cellulose nanofibers for the development of composites are discussed in this review. Processing methods, properties, and various applications of nanocellulose and cellulosic composites are also discussed.

The second paper of this special issue "Kenaf bast Fibers—Part I: Hermetical alkali digestion" developed a hermetical alkali digestion process to obtain single cellulosic fibers from kenaf bast. Hermetical alkali digestion process effectively removed the lignin and hemicelluloses from kenaf bast fibers at 160°C. The α-cellulose content of the fibers was 92%. The increase of cellulose content of the digested fibers resulted in an improved fiber surface hardness and elastic modulus. The digestion temperature had a significant effect on tensile modulus and tensile strength properties of the kenaf fiber.

The third paper "Isolation of cellulose nanofibers: Effect of biotreatment on hydrogen bonding network in wood fibers" briefly describes a novel enzymatic fiber pretreatment developed to facilitate the isolation of cellulose microfibrils and explores the effectiveness of biotreatment on the intermolecular and intramolecular hydrogen bonding in the fiber. Hydrogen bond-specific enzyme and its application in the isolation of new generation cellulose nanofibers can be a huge leap forward in the field of nanobiocomposites.

Paper four of this issue "Effect of sisal fiber surface treatment on properties of sisal fiber reinforced polylactide composites" dealt with the modification of sisal fiber using two different macromolecular coupling agents. Sisal fiber-reinforced polylactide composites that were prepared by injection molding. It has been shown that surface-treatment of sisal fiber increased the mechanical properties for composites systems.

In paper five "Time effects on morphology and bonding ability in mercerized natural fibers for composite reinforcement," kenaf fibers were alkali treated, and the surface and morphology were analyzed to determine how treatment time affected the bonding sites in natural fibers. Tensile testing of fibers reported a 61% increase in strength and a 25% increase in modulus for fibers treated for 16 hours. The increase in tensile properties was assumed to result from increased intermolecular interaction and increased crystallinity in cellulose.

Paper six of this issue "Role of polysaccharides on mechanical and adhesion properties of flax fibres in flax/PLA biocomposite" dealt with the effect of alkali and enzymatic treatments on morphology, mechanical, and adhesion properties of flax fiber. This paper highlights the important role of amorphous polymers, hemicelluloses, and pectin in the optimization of the adhesion and mechanical properties of flax fibers in biocomposites systems.

In paper seven "Mechanical and Thermal Behaviour of Ecofriendly Composites Reinforced by *Kenaf* and *Caroà* Fibers," two kinds of environmental friendly composites were prepared reinforced by *Caroà* and *Kenaf* fibers. The obtained composites were compared in terms of moisture tolerance, thermal and mechanical properties, and thermoregulation ability.

In paper eight of this special issue "Effect of different parameters on mechanical and erosion wear behavior of bamboo fiber-reinforced epoxy composites," an attempt has been made to study the utilization potential of bamboo fiber in polymer composites and the effect of various parameters on mechanical and erosion wear performance of bamboo fiber-reinforced epoxy composites.

The ninth paper of this special issue "Manufacturing and structural feasibility of natural fiber-reinforced polymeric structural insulated panels for panelized construction" mainly focuses on the manufacturing feasibility and structural characterization of natural fiber-reinforced structural insulated panels (NSIPs) using natural fiber reinforced polymeric (NFRP) laminates as skin. The natural fibers were bleached before their use as reinforcement.

The tenth paper "Natural fibre-reinforced biofoams" dealt with natural fiber reinforced biofoams using starch and polylactic acid. This paper investigates the improvement of their morphology and properties through processing and materials parameters. The influence of a fiber surface treatment was investigated for both foams.

The eleventh paper "Kenaf bast fibers-Part II: Inorganic nanoparticle impregnation for polymer composites" used an inorganic nanoparticle impregnation (INI) technique to improve the compatibility between kenaf bast fibers and polyolefin matrices. The final paper of this special issue "A study of nanoclay reinforcement of biocomposites made by liquid composite molding" reports on a study of biobased composites reinforced with nanoclay particles. A soy-based unsaturated polyester resin was used as synthetic matrix, and glass and flax fiber fabrics were used as reinforcement. The last paper "A study of nanoclay reinforcement of biocomposites made by liquid composite molding" aims to improve mechanical and flammability properties of reinforced composites by introducing nanoclay particles in the unsaturated polyester resin.

Susheel Kalia
Luc Avérous
James Njuguna
Alain Dufresne
Bibin Mathew Cherian

Hindawi Publishing Corporation
International Journal of Polymer Science
Volume 2011, Article ID 837875, 35 pages
doi:10.1155/2011/837875

Review Article

Cellulose-Based Bio- and Nanocomposites: A Review

Susheel Kalia,[1] Alain Dufresne,[2] Bibin Mathew Cherian,[3] B. S. Kaith,[4] Luc Avérous,[5] James Njuguna,[6] and Elias Nassiopoulos[6]

[1] *Department of Chemistry, Shoolini University of Biotechnology and Management Sciences, Bajhol-173 229, District Solan (Himachal Pradesh), India*
[2] *Grenoble Institute of Technology, The International School of Paper, Print Media and Biomaterials (Pagora), Grenoble Institute of Technology, BP 65-38402 Saint Martin d'Hères, Grenolde, France*
[3] *Department of Natural Resources, Sao Paulo State University (UNESP), Botucatu 18610-307, SP, Brazil*
[4] *Department of Chemistry, Dr. B.R. Ambedkar National Institute of Technology, Punjab, Jalandhar 144011, India*
[5] *LIPHT-ECPM, EAC (CNRS) 4375, University of Strasbourg, 25 rue Becquerel, 67087 Strasbourg Cedex 2, France*
[6] *School of Applied Sciences, Cranfield University, Bedfordshire MK43 0AL, UK*

Correspondence should be addressed to Susheel Kalia, susheel_kalia@yahoo.com

Received 16 June 2011; Accepted 1 August 2011

Academic Editor: Jose Ramon Leiza

Cellulose macro- and nanofibers have gained increasing attention due to the high strength and stiffness, biodegradability and renewability, and their production and application in development of composites. Application of cellulose nanofibers for the development of composites is a relatively new research area. Cellulose macro- and nanofibers can be used as reinforcement in composite materials because of enhanced mechanical, thermal, and biodegradation properties of composites. Cellulose fibers are hydrophilic in nature, so it becomes necessary to increase their surface roughness for the development of composites with enhanced properties. In the present paper, we have reviewed the surface modification of cellulose fibers by various methods. Processing methods, properties, and various applications of nanocellulose and cellulosic composites are also discussed in this paper.

1. Introduction

Cellulose-fiber-reinforced polymer composites have received much attention because of their low density, nonabrasive, combustible, nontoxic, low cost, and biodegradable properties. A lot of research works have been performed all over the world on the use of cellulose fibers as a reinforcing material for the preparation of various types of composites. However, lack of good interfacial adhesion, low melting point, and water sensitivity make the use of cellulose-fiber-reinforced composites less attractive. Pretreatments of the cellulose fibers can modify the fiber surface, such as chemical functionalization stop the moisture absorption process and increase the surface roughness [1].

The production of nanoscale cellulose fibers and their application in composite materials have gained increasing attention due to their high strength and stiffness combined with low weight, biodegradability, and renewability. Application of cellulose nanofibers in polymer reinforcement is a relatively new research field [2]. The main reason to utilize cellulose nanofibers in composite materials is because one can potentially exploit the high stiffness of the cellulose crystal for reinforcement. This can be done by breaking down the hierarchical structure of the plant into individualized nanofibers of high crystallinity, with a reduction of amorphous parts [3].

In this paper we describe various approaches to the synthesis of nanofibers from plant resources. Potential use of macro- and nanofibers as reinforcing material for the development of polymers composites with enhanced properties and application of these composites in various fields are also discussed.

2. Cellulose Fibers

Cellulose fibers are being used as potential reinforcing materials because of so many advantages such as abundantly available, low weight, biodegradable, cheaper, renewable, low abrasive nature, interesting specific properties, since these are waste biomass, and exhibit good mechanical properties

[4–6]. Cellulose fibers also have some disadvantages such as moisture absorption, quality variations, low thermal stability, and poor compatibility with the hydrophobic polymer matrix [7, 8].

2.1. Chemistry of Cellulose. Cellulose is the most abundant form of living terrestrial biomass [9] and finds applications in many spheres of modern industry. Existence of cellulose as the common material of plant cell walls was first recognized by Anselm Payen in 1838 [10]. Cellulose has been shown to be a long-chain polymer with repeating units of D-glucose, a simple sugar. It occurs in almost pure form in cotton fiber. However, in wood, plant leaves and stalks, it is found in combination with other materials, such as lignin and hemicelluloses. Although, generally considered a plant material, but some bacteria are also found to produce cellulose.

Cellulose is a natural polymer, a long chain made by the linking of smaller molecules. The links in the cellulose chain consist of sugar, β-D-glucose [11]. The sugar units are linked when water is eliminated by combining the H and –OH group. Linking just two of these sugars produces a disaccharide called cellobiose [12]. In the cellulose chain, the glucose units are in 6-membered rings, called pyranoses. They are joined by single oxygen atoms (acetal linkages) between the C-1 of one pyranose ring and the C-4 of the next ring. Since a molecule of water is lost due to the reaction of an alcohol and a hemiacetal to form an acetal, the glucose units in the cellulose polymer are referred to as anhydroglucose units.

The spatial arrangement or stereochemistries of these acetal linkages is very important. The pyranose rings of the cellulose molecule have all the groups larger than hydrogen sticking-out from the periphery of the rings (equitorial positions). The stereochemistry at carbons 2, 3, 4 and 5 of the glucose molecule are fixed, but in pyranose form, the hydroxyl at C-4 can approach the carbonyl at C-1 from either side, resulting in two different stereochemistry at C-1. When the hydroxyl group at C-1 is on the same side of the ring as the C-6 carbon, it is said to be in the α configuration. In cellulose, the C-1 oxygen is in the opposite or β configuration (i.e., cellulose is poly[β-1,4-D-anhydroglucopyranose]). This β configuration, with all functional groups in equatorial positions, causes the molecular chain of cellulose to extend in a more or less straight line, making it a good fiber-forming polymer [13].

Because of the equatorial positions of the hydroxyls on the cellulose chain, they protrude laterally along the extended molecule and are readily available for hydrogen bonding. These hydrogen bonds cause the chains to group together in a highly ordered structure. Since the chains are usually longer than the crystalline regions, they are thought to pass through several different crystalline regions, with areas of disorder in between ("fringed-micelle" model) [14]. The interchain hydrogen bonds in the crystalline regions are strong, giving the resultant fiber good strength and insolubility in most solvents. They also prevent cellulose from melting (non-thermoplastic). In the less-ordered regions, the chains are further apart and more available for hydrogen bonding with other molecules, such as water. Most cellulose structures can absorb large quantities of water (hygroscopic). Thus, cellulose swells but does not dissolve in water [13].

The cellulose molecule contains three different kinds of anhydroglucose units, the reducing end with a free hemiacetal (or aldehyde) group at C-1, the nonreducing end with a free hydroxyl at C-4 and the internal rings joined at C-1 and C-4. But because of long-chain length, the chemistry of the alcohol groups of the internal units predominates, so long as the chains are not cleaved by the reaction conditions. However, unlike simple alcohols, cellulose reactions are usually controlled by steric factors than would be expected on the basis of the inherent reactivity of the different hydroxyl groups. C-2, C-3, and C-6 hydroxyls and C-H groups are active sites in cellulose for the incorporation of polymeric chains through grafting. In grafting, it has been reported that the reactivity of hydroxyl group at C-6 is far less than those at C-2 and C-3 [13].

2.2. Chemical Composition, Structure, and Properties of Cellulose Fibers. Cellulose fibers can be classified according to their origin and grouped into leaf: abaca, cantala, curaua, date palm, henequen, pineapple, sisal, banana; seed: cotton; bast: flax, hemp, jute, ramie; fruit: coir, kapok, oil palm; grass: alfa, bagasse, bamboo; stalk: straw (cereal). The bast and leaf (the hard fibers) types are the most commonly used in composite applications [15, 16]. Commonly used plant fibers are cotton, jute, hemp, flax, ramie, sisal, coir, henequen, and kapok. The largest producers of sisal in the world are Tanzania and Brazil. Henequen is produced in Mexico whereas abaca and hemp in Philippines. The largest producers of jute are India, China, and Bangladesh [1].

Plant fibers are constitutes of cellulose fibers, consisting of helically wound cellulose microfibrils, bound together by an amorphous lignin matrix. Lignin keeps the water in fibers, acts as a protection against biological attack and as a stiffener to give stem its resistance against gravity forces and wind. Hemicellulose found in the natural fibers is believed to be a compatibilizer between cellulose and lignin [1]. The cell wall in a fiber is not a homogenous membrane (Figure 1) [17]. Each fiber has a complex, layered structure consisting of a thin primary wall which is the first layer deposited during cell growth encircling a secondary wall. The secondary wall is made up of three layers and the thick middle layer determines the mechanical properties of the fiber. The middle layer consists of a series of helically wound cellular microfibrils formed from long-chain cellulose molecules. The angle between the fiber axis and the microfibrils is called the microfibrillar angle. The characteristic value of microfibrillar angle varies from one fiber to another. These microfibrils have typically a diameter of about 10–30 nm and are made up of 30–100 cellulose molecules in extended chain conformation and provide mechanical strength to the fiber.

The properties of cellulose fibers are affected by many factors such as variety, climate, harvest, maturity, retting degree, decortications, disintegration (mechanical, steam explosion treatment), fiber modification, textile, and technical processes (spinning and carding) [18]. In order to understand the properties of natural fiber-reinforced composite materials, it becomes necessary to know the mechanical,

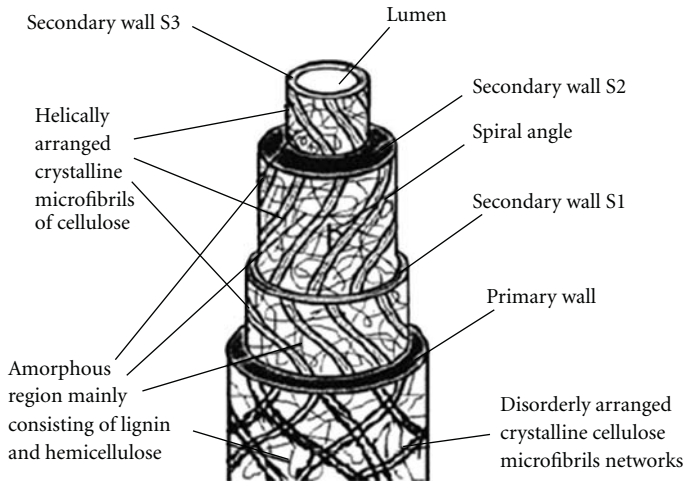

Figure 1: Structural constitution of natural fiber cell [17].

physical, and chemical properties of natural fibers. Flax fibers are relatively strong fibers as compared to other natural fibers. The tensile strength of elementary fibers is in the region of 1500 MPa and for technical fibers a value of circa 800 MPa was observed at 3 mm clamp length [19]. Baley [20] and Lamy and Baley [21] investigated the modulus of flax fibers. The modulus of elementary fibers is dependent on the diameter of fiber and it ranges from 39 GPa for fibers having diameter approximately 35 μm to 78 GPa for fibers having 5 μm diameter. This variation is related to the variation in relative lumen size between fibers having different diameter. An average Young's modulus of 54 GPa was observed after numerous tensile tests on single flax fibers and the results are within the range of moduli measured on technical fibers. The mechanical, chemical, and physical properties of plant fibers are strongly harvest dependent, influenced by climate, location, weather conditions, and soil characteristics. These properties are also affected during the processing of fiber such as retting, scotching, bleaching, and spinning [22].

Cellulose fibers have relatively high strength, high stiffness, and low density [23]. The characteristic value for soft-wood-Kraft-fibers and flax has been found close to the value for E-glass fibers. Different mechanical properties can be incorporated in natural fibers during processing period. The fiber properties and structure are influenced by several conditions and varies with area of growth, its climate and age of the plant [24]. Technical digestion of the fiber is another important factor which determines the structure as well as characteristic value of fiber. The elastic modulus of the bulk natural fibers such as wood is about 10 GPa. Cellulose fibers with moduli up to 40 GPa can be separated from wood by chemical-pulping process. Such fibers can be further subdivided into microfibrils within elastic modulus of 70 GPa. Theoretical calculations of elastic moduli of cellulose chain have been given values up to 250 GPa. However, no technology is available to separate these from microfibrils [25]. The tensile strength of natural fibers depends upon the test length of the specimen which is of main importance with respect to reinforcing efficiency. Mieck et al. [26] and Mukherjee and Satyanarayana [27] reported that tensile strength of flax fiber is significantly more dependent on the length of the fiber. In comparison to this, the tensile strength of pineapple fiber is less dependent on the length, while the scatter of the measured values for both is located mainly in the range of the standard deviation. The properties of flax fiber are controlled by the molecular fine structure of the fiber which is affected by growing conditions and the fiber processing techniques used. Flax fibers possess moderately high-specific strength and stiffness.

Quality and other properties of fibers depend on factors such as size, maturity, and processing methods adopted for the extraction of fibers. Properties such as density, electrical resistivity, ultimate tensile strength, and initial modulus are related to the internal structure and chemical composition of fibers [23]. Desirable properties for fibers include excellent tensile strength and modulus, high durability, low bulk density, good moldability, and recyclability.

3. Cellulose Nanofibers

Cellulose nanofibers have a high potential to be used in many different area particularly as reinforcement in development of nanocomposites. Many studies have been done on isolation and characterization of cellulose nanofibers from various sources. Cellulose nanofibers can be extracted from the cell walls by simple mechanical methods or a combination of both chemical and mechanical methods.

3.1. Synthesis of Cellulose Nanofibers. Alemdar and Sain [28] have extracted cellulose nanofibers from wheat straw by a chemical treatment, resulting to purified cellulose. To individualize the nanofibers from the cell walls a mechanical treatment (cryocrushing, disintegration, and defibrillation steps) was applied to the chemically treated fibers. Cellulose nanofibers were extracted from the agricultural residues, wheat straw and soy hulls, by a chemomechanical technique [29]. The wheat straw nanofibers were determined to have diameters in the range of 10–80 nm and lengths of a few

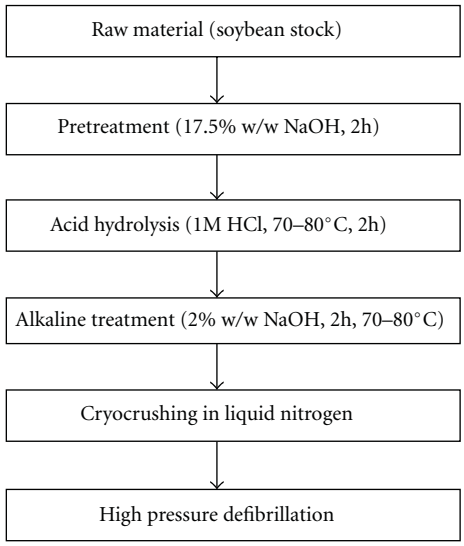

Figure 2: Isolation of nanofibers by chemomechanical treatment [31].

thousand nanometers. By comparison, the soy hull nanofibers had diameter 20–120 nm and shorter lengths than the wheat straw nanofibers. Zimmermann et al. [30] separated nanofibrillated cellulose (NFC) at the greatest possible lengths and diameters below 100 nm from different starting cellulose materials by mechanical dispersion and high pressure (up to 1500 bar) homogenization processes. The treatment resulted in nanoscaled fibril networks. Two commercial fibrous celluloses showed bigger cellulose aggregates with micrometer dimensions and a less homogeneous network structure.

The cellulose nanofibers were extracted by Wang and Sain [31] from soybean stock by chemomechanical treatments (Figure 2). These are bundles of cellulose nanofibers with a diameter ranging between 50 and 100 nm and lengths of thousands of nanometers.

The cellulose nanofibrils were extracted from wheat straw using steam explosion, acidic treatment, and high shear mechanical treatment. Alkaline-treated pulp was soaked in 8% solution of H_2O_2 (v/v) overnight. Bleached pulp was then rinsed with abundant distilled water. Bleached pulp was then treated with 10% HCl (1 N) solution and mixed using ultrasonicator at temperature around $60 \pm 1^\circ$C for 5 h. Finally, the fibers were taken out and washed several times with distilled water in order to neutralize the final pH and then dried. Fibers were suspended in water and continuously stirred with a high shear homogenizer for 15 min. High-shearing action breaks down the fiber agglomerates and result in nanofibrils [32].

3.2. Structure and Properties of Cellulose Nanofibers. Transmission electron microscopy (TEM), scanning electron microscopy (SEM), field-emission scanning electron microscopy (FE-SEM), atomic force microscopy (AFM), wide-angle X-ray scattering (WAXS), and NMR spectroscopy have been used to study the structure of cellulose nanofibers [33]. A combination of microscopic techniques with image analysis can provide information about widths of cellulose nanofiber but it is very difficult to find out the lengths of nanofiber because of entanglements and difficulties in identifying both ends of individual nanofibers. It is often reported that MFC suspensions are not homogeneous and that they consist of cellulose nanofibers and nanofiber bundles [2].

Teixeira et al. [34] obtained the suspensions of white and colored nanofibers by the acid hydrolysis of white and naturally colored cotton fibers. Possible differences among them in morphology and other characteristics were investigated. Morphological study of cotton nanofibers showed a length of 85–225 nm and diameter of 6–18 nm. It was found that there were no significant morphological differences among the nanostructures from different cotton fibers. The main differences found were the slightly higher yield, sulfonation effectiveness, and thermal stability under dynamic temperature conditions of the white nanofiber. On the other hand, the colored nanofibers showed a better thermal stability than the white in isothermal conditions at 180°C.

The structure of the cellulose nanofibers from agricultural residues was investigated by Alemdar and Sain [29]. FTIR spectroscopic analysis demonstrated that chemical treatment also led to partial removal of hemicelluloses and lignin from the structure of the fibers. PXRD results revealed that this resulted in improved crystallinity of the fibers. Thermal properties of the nanofibers were studied by the TGA technique and were found to increase dramatically.

Stelte and Sanadi [35] have studied the mechanical fibrillation process for the preparation of cellulose nanofibers from two commercial hard- and softwood cellulose pulps. The degree of fibrillation was studied using light microscopy (LM), scanning electron microscopy (SEM), and atomic force microscopy (AFM). LM and SEM images (Figure 3) of hard- and softwood fibers showed that the hardwood fibers that were fibrillated only on the surface during the refining step are now disintegrated into a network of small fibers. AFM images (Figure 4) of the final products after high-pressure homogenization showed that the size distribution of the hard- and softwood nanofibers is in the range of 10–25 nm in diameter.

Wang and Sain [31] synthesized soybean stock-based nanofibers having a diameter in the range 50–100 nm by chemomechanical isolation. X-ray crystallography (Figure 5) was carried out to investigate the percentage crystallinity after various stages of the chemomechanical treatment. It has been found that crystallinity of the samples increased after each stage of nanofiber development.

Figure 6 shows the network of cellulose nanofibers. The nanofiber suspension obtained after the high pressure defibrillation was analyzed to determine diameters using AFM. The AFM image (Figure 6) shows the surface of air-dried soybean stock nanofiber. It is seen that the fibers are indeed nanosized and the diameter of nanofibers is within the range 50–100 nm.

4. Surface Modification of Cellulose Fibers

In order to develop composites with better mechanical properties and environmental performance, it becomes necessary

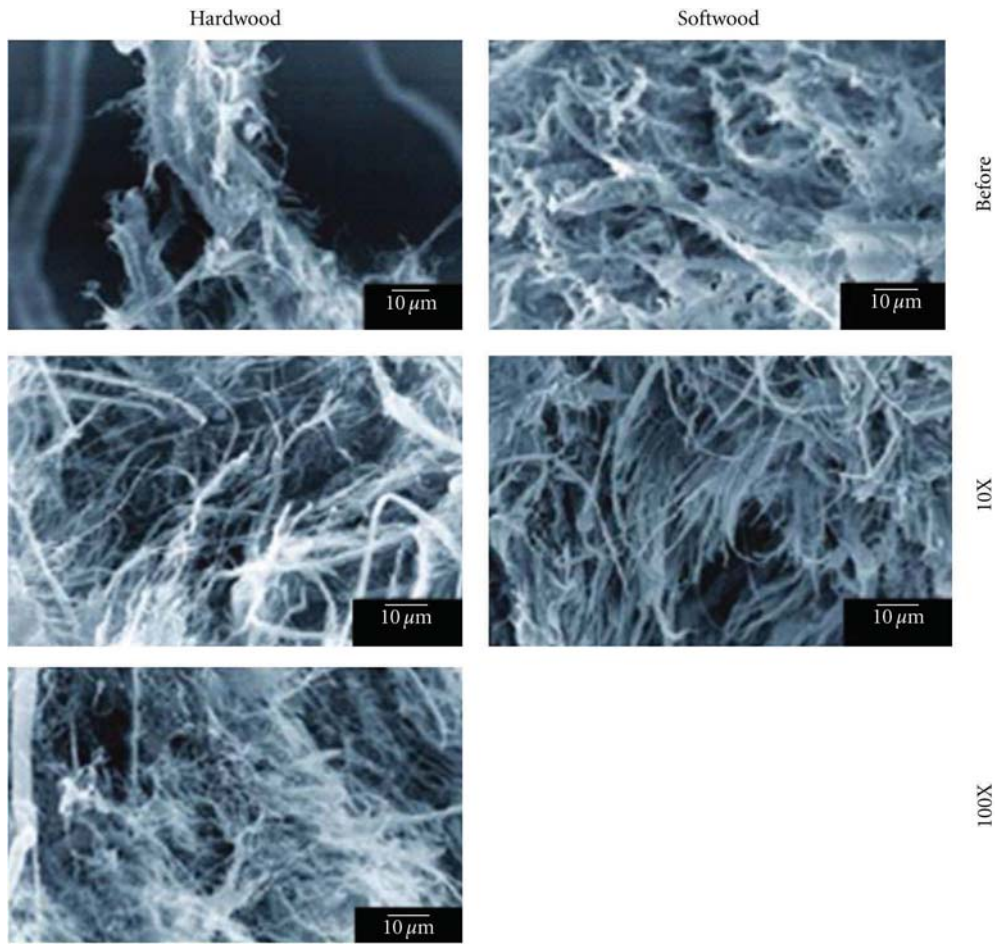

Figure 3: Scanning electron micrographs of hard- and softwood cellulose fibers, before and after 10 passes through the homogenizer [35].

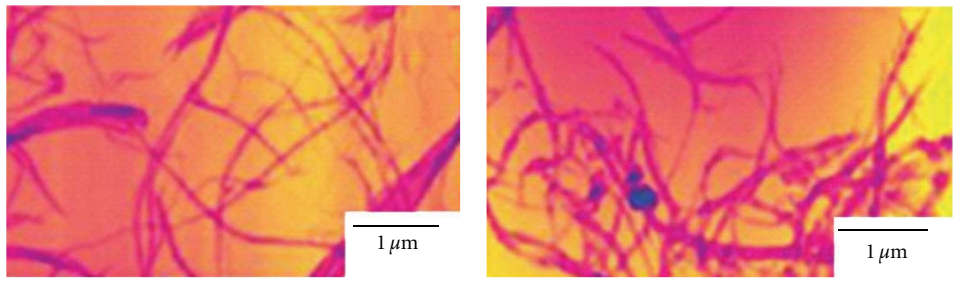

Figure 4: AFM images (a) hard- and (b) softwood cellulose nanofibers at process equilibrium [35].

to increase the hydrophobicity of the cellulose fibers and to improve the interface between matrix and fibers. Lack of good interfacial adhesion, low melting point, and poor resistance towards moisture make the use of plant cellulose fiber-reinforced composites less attractive. Pretreatments of the cellulose fiber can clean the fiber surface, chemically modify the surface, stop the moisture absorption process, and increase the surface roughness [1, 36]. Among the various pretreatment techniques, silylation, mercerization, peroxide, benzoylation, graft copolymerization, and bacterial cellulose treatment are the best methods for surface modification of natural fibers.

4.1. Silylation, Mercerization, and Other Surface Chemical Modifications. Silane-coupling agents usually improve the degree of cross-linking in the interface region and offer a perfect bonding. Among the various coupling agents, silane-coupling agents were found to be effective in modifying the natural fiber-matrix interface. Efficiency of silane treatment was high for the alkaline-treated fiber than for the untreated

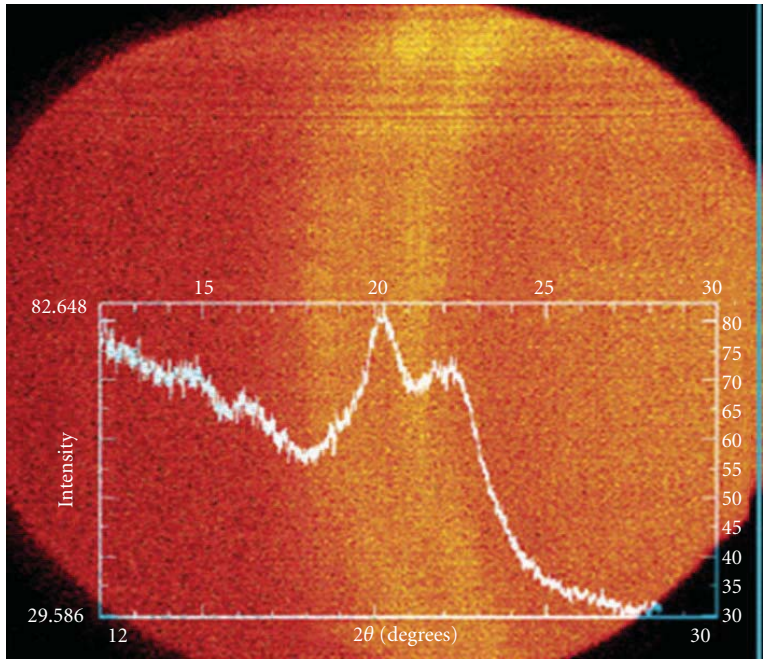

Figure 5: X-ray pattern to demonstrate the crystallinity of soybean stock nanofibers [31].

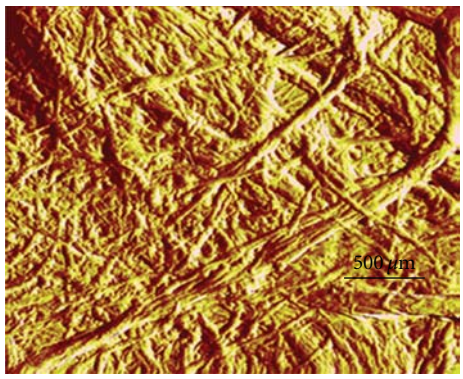

Figure 6: Atomic force micrograph of soybean stock nanofibers [31].

fiber because more reactive site can be generated for silane reaction. Therefore, fibers were pretreated with NaOH for about half an hour prior to its coupling with silane. Fibers were then washed many times in distilled water and finally dried. Silane-coupling agents may reduce the number of cellulose hydroxyl groups in the fiber–matrix interface. In the presence of moisture, hydrolyzable alkoxy group leads to the formation of silanols. The silanol then reacts with the hydroxyl group of the fiber, forming stable covalent bonds to the cell wall that are chemisorbed onto the fiber surface [37]. Therefore, the hydrocarbon chains provided by the application of silane restrain the swelling of the fiber by creating a crosslinked network due to covalent bonding between the matrix and the fiber [1].

Silanes were effective in improving the interface properties [38–41]. Alkoxy silanes are able to form bonds with hydroxyl groups. Fiber treatment with toluene dissocyanate and triethoxyvinyl silane could improve the interfacial properties. Silanes after hydrolysis undergo condensation and bond formation stage and can form polysiloxane structures by reaction with hydroxyl group of the fibers. The reactions are given in Schemes 1 and 2 [1, 42].

In the presence of moisture, hydrolysable alkoxy group leads to the formation of silanols. Hydrogen and covalent-bonding mechanisms could be found in the natural fiber-silane system. It is understood that the hydrocarbon chains provided by the silane application influenced the wetability of the fibers, thus improving the chemical affinity to polyethylene. 1% solution of three aminopropyl trimethoxy silane in a solution of acetone and water (50/50 by volume) for 2 h was reportedly used to modify the flax surface [43]. Rong et al. [17] soaked sisal fiber in a solution of 2% aminosilane in 95% alcohol for 5 min at a pH value of 4.5–5.5 followed by 30 min air drying for hydrolyzing the coupling agent. Silane solution in water and ethanol mixture with concentration of 0.033% and 1% was also carried by Valadez-Gonzalez et al. [44] and Agrawal et al. [37] to treat henequen and oil-palm fibers. They modified the short henequén fibers with a silane coupling agent in order to find out its deposition mechanism on the fiber surface and the influence of this chemical treatment on the mechanical properties of the composite. It was shown that the partial removal of lignin and other alkali soluble compounds from the fiber surface increases the adsorption of the silane coupling-agent whereas the formation of polysiloxanes inhibits this process.

Mercerization is the common method to produce high-quality fibers [45]. Scheme 3 shows the probable mechanism of mercerization of cellulose fibers. Mercerization leads to fibrillation which causes the breaking down of the composite fiber bundle into smaller fibers. Mercerization reduces fiber

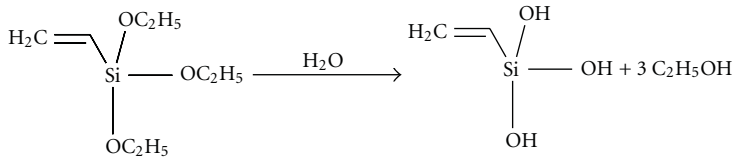

Scheme 1

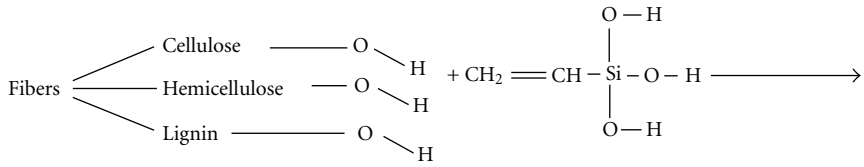

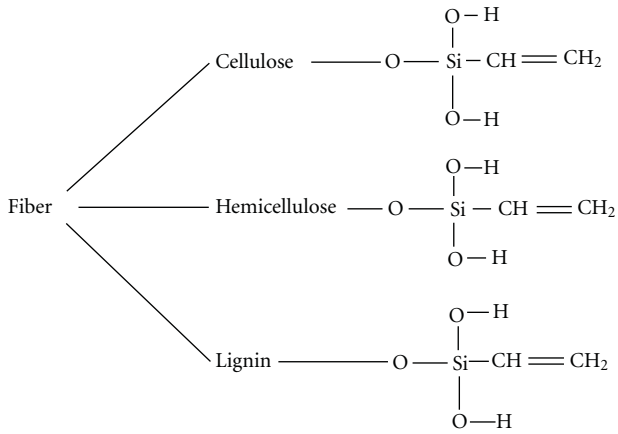

Scheme 2

diameter, thereby increases the aspect ratio which leads to the development of a rough surface topography that results in better fiber-matrix interface adhesion and an increase in mechanical properties [46]. Moreover, mercerization increases the number of possible reactive sites and allows better fiber wetting. Mercerization has an effect on the chemical composition of the flax fibers, degree of polymerization, and molecular orientation of the cellulose crystallites due to cementing substances like lignin and hemicellulose which were removed during the mercerization process. As a result, mercerization had a long-lasting effect on the mechanical properties of flax fibers, mainly on fiber strength and stiffness [47]. Sreekala et al. [42] indicated that a 10–30% sodium hydroxide solution produced the best effects on natural fiber properties. Flax fibers were soaked into 2.5, 5, 10, 13, 15, 18, 20, 25, or 30% NaOH solutions, and it was found that 5%, 18%, or 10% of sodium hydroxide solution was the appropriate concentration for mercerization. Jute fibers were treated with 5% alkali solution for 0, 2, 4, 6, and 8 h at 30°C by Ray et al. [45]. The fibers were then dried at room temperature for 48 h followed by oven drying at 100°C for 6 h. It has been reported by Garcia-Jaldon et al. [48] that 2% alkali solution at 200°C and 1.5 MPa pressure for 90 s was suitable for degumming and defibrillation to individual fibers. Several workers have carried out work on alkali treatment and reported that mercerization leads to an increase in the amount of amorphous cellulose at the cost of crystalline cellulose and the removal of hydrogen bonding in the network structure [42, 46]. The jute fibers were washed with detergent (2 vol.% in aqueous solution, 15% active matter) and then immersed in beakers with a solution of 5 wt. % NaOH for 24 h at room temperature. After that, the fibers were washed thoroughly with distilled water to remove the excess of NaOH and dried at 70°C for 24 h under vacuum [49]. The banana fibers were cleaned and refluxed in 0.25% solution of NaOH for 1 h and then washed in very dilute acid to remove the nonreacted alkali. Washing was continued until the fibers were alkali free. The washed fibers were then dried in an oven at 70°C for 3 h [50].

Peroxide treatment of cellulose fiber has attracted the attention of various researchers due to easy processability and improvement in mechanical properties. Organic peroxides tend to decompose easily to free radicals (RO), which further react with the hydrogen group of the matrix and cellulose fibers. Schemes 4 and 5 show the peroxide treatment reaction onto cellulose fibers [42].

In peroxide treatment, fibers are treated with 6% benzoyl peroxide or dicumyl peroxide in acetone solution for about 30 min after alkali pretreatment [42, 51, 52]. Flax fibers were coated with dicumyl peroxide from acetone solution

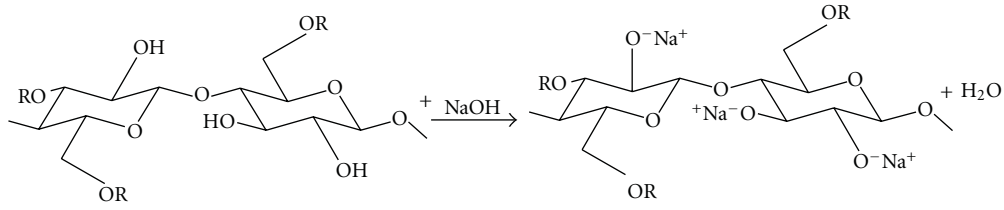

Cellulose Mercerized cellulose

Scheme 3

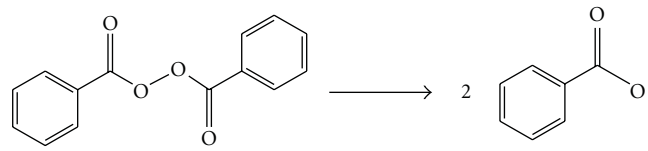

Benzoyl peroxide

Scheme 4

after alkali pretreatments. Saturated solution of the peroxide in acetone was used. Soaking of the fibers in the solution was conducted at a temperature of 70°C for 30 min. High temperatures were favored for decomposition with the peroxide. The chemically treated fibers were washed with distilled water and placed in an oven at 80°C for 24 h [53].

In benzoylation treatment, benzoyl chloride is most often used in fiber pretreatment and inclusion of benzoyl ($C_6H_5C{=}O$) group in the fiber is responsible for the decreased hydrophilic nature of the treated fiber [46]. A known amount of washed fibers (35 g) were soaked in 18% NaOH solution for 30 minutes followed by filtration and washing with water. The treated fiber was suspended in 10% NaOH solution and agitated with 50 mL benzoyl chloride. The reaction between the cellulosic –OH group of sisal fiber and benzoyl chloride is shown in Scheme 6 [46, 54].

Joseph et al. [46] and Kalia et al. [54] used NaOH and benzoyl chloride (C_6H_5COCl) solution for surface treatment of sisal fibers. The fiber was initially alkaline pretreated in order to activate the hydroxyl groups of the cellulose and lignin in the fiber; then the fiber was suspended in 10% NaOH and benzoyl chloride solution for 15 min. The isolated fibers were then soaked in ethanol for 1 h to remove the benzoyl chloride and finally was washed with water and dried in the oven at 80°C for 24 h [55].

4.2. Polymer Grafting. Desirable and targeted properties can be imparted to the cellulose fibers through graft copolymerization in order to meet out the requirement of specialized applications. Graft copolymerization is one of the best methods for modifying the properties of cellulose fibers. Different binary vinyl monomers and their mixtures have been graft-copolymerized onto cellulosic material for modifying the properties of numerous polymer backbones [1, 56].

During last decades, several methods have been suggested for the preparation of graft copolymers by conventional chemical techniques. Creation of an active site on the preexisting polymeric backbone is the common feature of most methods for the synthesis of graft copolymers. The active site may be either a free-radical or a chemical group which may get involved in an ionic polymerization or in a condensation process. Polymerization of an appropriate monomer onto this activated backbone polymer leads to the formation of a graft copolymer. Ionic polymerization has to be carried-out in presence of anhydrous medium and/or in the presence of considerable quantity of alkali metal hydroxide. Another disadvantage with the ionic grafting is that low molecular weight graft copolymers are obtained while in case of free radical grafting high molecular weight polymers can be prepared. C_2, C_3, and C_6 hydroxyls and C-H groups are the active cites for grafting in cellulosics (Figure 7) [57].

The conventional technique of grafting and chemical modification of natural fibers requires significant time and energy. The use of MWR technique to modify the properties of natural fibers within the textile industry, although somewhat slow and still rather limited, is finding its way into numerous uses in production plants. Microwave radiation technique reduces the extent of physicochemical stresses to which the fibers are exposed during the conventional techniques. Microwave technology uses electromagnetic waves, which passes through material and causes its molecules to oscillate. Microwave energy is not observed by nonpolar materials to any degree while polar water molecules held within a polymer matrix do absorb energy very proficiently, thus becoming heated [58, 59].

Graft copolymerization of methyl methacrylate onto flax fiber was carried out under three different reaction methods, in air, under pressure, and under the influence of microwave radiations. Grafting through microwave-radiation technique is an effective method in terms of time consumption and cost effectiveness. Maximum percentage grafting has been observed in case of grafting carried out in air followed by grafting under pressure and under the influence

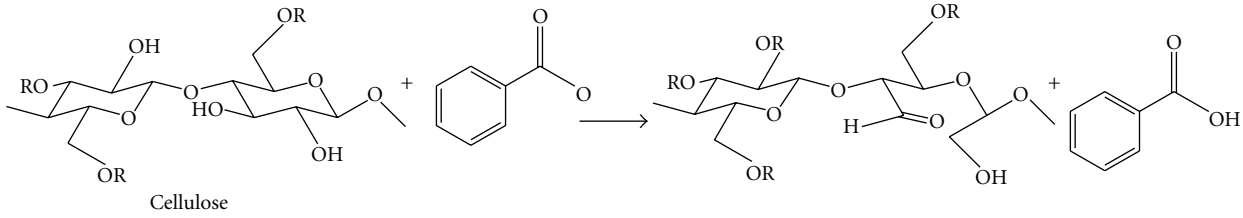

Scheme 5

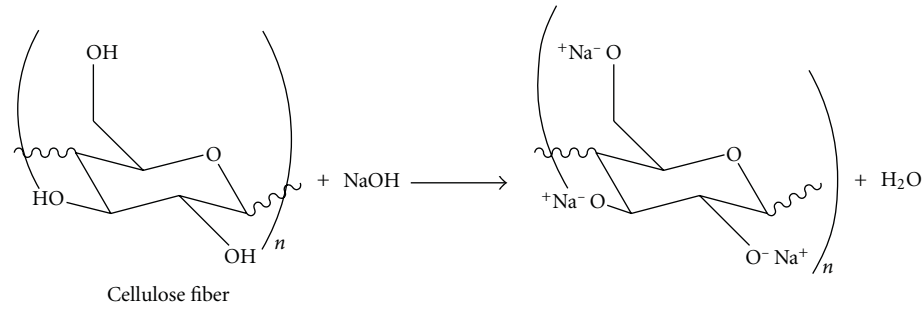

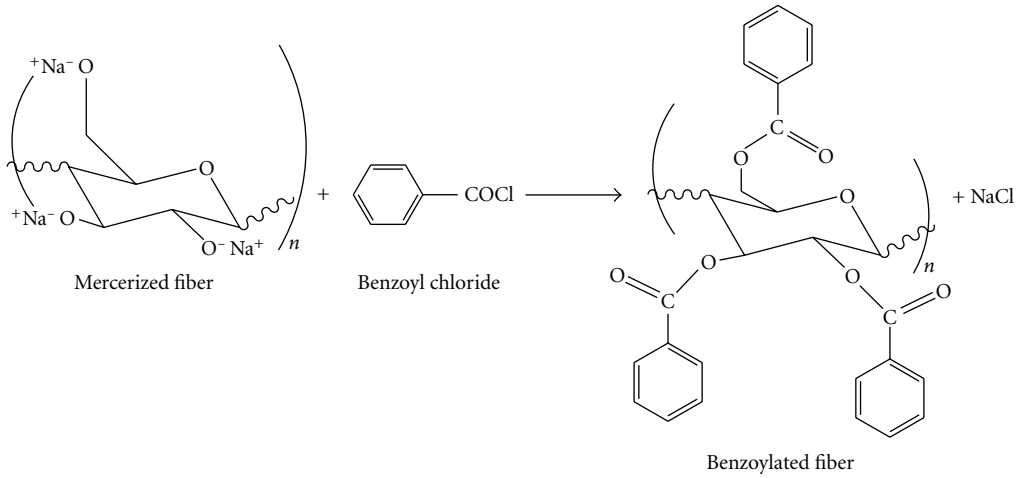

Scheme 6

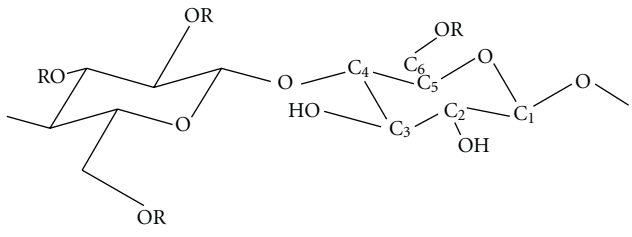

Figure 7: Structure of cellulose [57].

of microwave radiations. Flax fiber faces less surface deformations during grafting process under the influence of microwave radiations as compared to grafting in air and under pressure, thereby retaining better crystalline structure. Morphological and thermal studies showed that surface of sunn hemp fibers becomes rough through graft copolymerization and thermal stability has been found to be increased. Microwave radiation-induced grafting showed a diminutive effect on the crystalline behavior of the sunn hemp fibers as optimum time to get maximum grafting is very less (40 minutes) in comparison to conventional grafting [60].

4.3. Bacterial Modification. The coating of bacterial cellulose onto cellulose fibers provides new means of controlling the interaction between fibers and polymer matrices. Coating of fibers with bacterial cellulose does not only facilitate good distribution of bacterial cellulose within the matrix, but also results in an improved interfacial adhesion between the fibers and the matrix. This enhances the interaction between the fibers and the polymer matrix through mechanical interlocking [3, 61]. Surface modification of cellulose fibers using bacterial cellulose is one of the best methods for greener surface treatment of fibers. Bacterial Cellulose has

gained attention in the research area for the encouraging properties it possesses; such as its significant mechanical properties in both dry and wet states, porosity, water absorbency, moldability, biodegradability, and excellent biological affinity [62]. Because of these properties, BC has a wide range of potential applications.

Acetobacter xylinum (or *Gluconacetobacter xylinus*) is the most efficient producer of bacterial cellulose. BC is secreted as a ribbon-shaped fibril, less than 100 nm wide, which is composed of much finer 2–4 nm nanofibrils. In comparison to the methods for obtaining nanocellulose through mechanical or chemomechanical processes, it is produced by bacteria through cellulose biosynthesis and the building up of bundles of microfibrils [63–65].

The cultivation of the cellulose producing bacteria in the presence of natural fibers, such as sisal and hemp, results in the coating of natural fiber surfaces by bacterial nanocellulose (Figure 8) [61]. Strong and highly crystalline nanocellulosic fibrils preferentially attached to the surface of natural fibers thereby creating "hairy fibers" (Figure 9), leading to a nanostructured natural fiber surface. Simply weighing the fibers before and after the BC fermentation process confirmed that between 5 and 6 wt% of bacterial cellulose adhered to the fibers after the surface modification. The strength of attachment of the nanocellulose coating to the fibers can be attributed to strong hydrogen bonding between the hydroxyl groups present in bacterial cellulose and the lignocellulose in natural fibers [66]. The modification process did not affect the mechanical properties of sisal fibers but it significantly reduced the mechanical properties of hemp fibers. Figure 10 shows the coating of bacterial nanocellulose onto hemp fibers [61].

To improve the compatibility between natural fibers and hydrophobic polymer matrices, various greener methods have been explored such as fungi, enzymes and bacterial treatments. Kalia and Sheoran [67] have reported cellulase enzyme assisted biopolishing of ramie fibers using bacteria *Streptomyces albaduncus.* Biopolishing of ramie fibers by utilizing cellulase from bacteria *Streptomyces albaduncus* was observed for 5 days, at the pH 7.4 and 2.0 g glucose, which results in enhanced brightness due to the removal of gum materials and small fibrils protruding from the fiber surface. Bacterial treatment has diminutive effect on thermal stability and crystalline structure of ramie fibers.

5. Cellulose-Fiber-Reinforced Biocomposites

5.1. Processing Method. Natural fiber composites are prepared using various composites manufacturing methods such as compression molding, injection molding, resin transfer molding (RTM), and vacuum bagging. The preforms are mostly fibers, fabrics, or nonwovens. Prepregs are also widely used to prepare composites [68]. Equation (1) is commonly used in the preparation of composites

$$V_f = \frac{W_f/\rho_f}{\left(W_f/\rho_f\right) + \left(W_m/\rho_m\right)}, \quad (1)$$

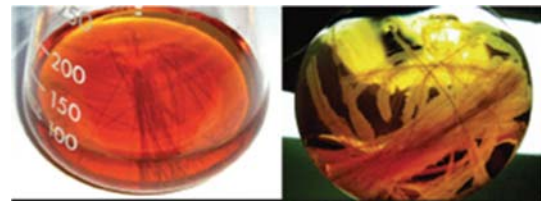

Figure 8: Photographs of sisal fibers before and after bacterial culture [61].

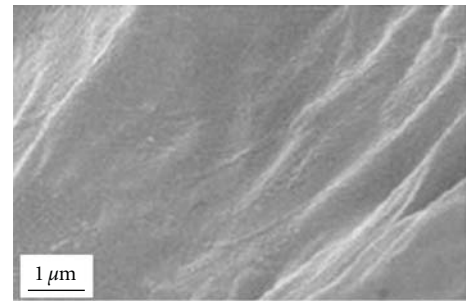

(a)

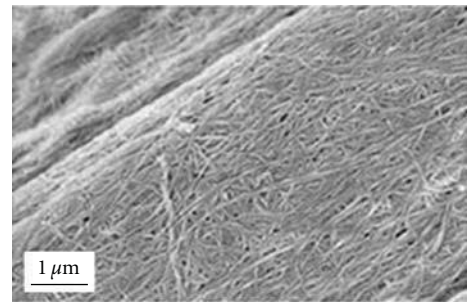

(b)

Figure 9: SEM micrographs (a) sisal fiber and (b) bacterial cellulose-coated sisal fiber [61].

where V_f is the fiber-volume fraction, W_f is the weight of fiber, and W_m is the weight of matrix. r_f and r_m are the densities of the fiber and matrix, respectively.

The production of the composites is optimized in relation to temperature, pressure, and molding time. It is often necessary to preheat the natural fibers to reduce the moisture before processing the composites. High temperatures degrade the cellulose; thus, negatively affecting the mechanical properties of the composites. Inefficient fiber dispersion in the matrix causes fiber agglomeration which decreases the tensile strength [68]. Most of the previous research on natural fiber composites has focused on reinforcements such as flax, hemp, sisal and jute, and thermoplastic and thermoset matrices. Some of these composites have been produced using matrices made of derivatives from cellulose, starch, and lactic acid to develop fully biodegradable composites or biocomposites [69]. The emerging diversity of applications of natural fiber composites has seen the production of sandwich structures based on natural-fiber composite skins. In some cases, these sandwich composites have been produced from paper honeycomb and natural fiber-reinforced thermoplastic or thermoset skins, depending on the applications.

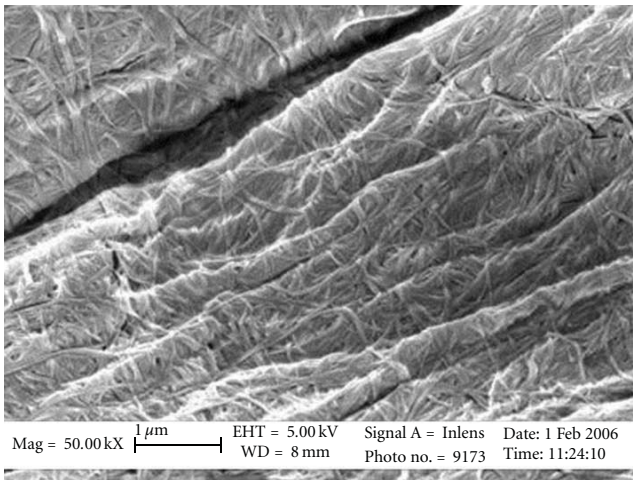

Figure 10: Hemp fiber after bacterial cellulose modification [61].

The main criteria for the selection of the appropriate process technology for natural-fiber composite manufacture include the desired product geometry, the performance needed, and the cost and the ease of manufacture. The fabrication methods for natural fiber composites are similar to those used for glass fibers. The most commonly used manufacturing processes are introduced in the following. Although many variants on these techniques exist, this overview gives a good indication of the production possibilities.

5.1.1. Hand Laminating. The fibers are placed in a mould and the resin is later applied by rollers. One option is to cure using a vacuum bag, as then excess air is removed and the atmospheric pressure exerts pressure to compact the part. The simplicity, low cost of tooling, and flexibility of design are the main advantages of the procedure. On the other end, the long production time, intensive labour, and low automation potential, consist some of the disadvantages.

5.1.2. Resin Transfer Molding (RTM). The resin transfer molding technique requires the fibers to be placed inside a mould consisting of two solid parts (close mould technique). A tube connects the mould with a supply of liquid resin, which is injected at low pressure through the mould, impregnating the fibers. The resulting part is cured at room temperature or above until the end of the curing reaction, when the mould is opened and the product removed. Parameters such as injection pressure, fiber content, and mould temperature have a great influence on the development of the temperature profiles and the thermal boundary layers, especially for thin cavities. This technique has the advantage of rapid manufacturing of large, complex, and high performance parts. Several types of resins (epoxy, polyester, phenolic, and acrylic) can be used for RTM as long as their viscosity is low enough to ensure a proper wetting of the fibers. Parameters such as injection pressure, fiber content, and mould temperature have a great influence on the development of the temperature profiles and the thermal boundary layers, especially for thin cavities. Good knowledge of all the operating steps is very important to obtain high-quality parts [68].

An alternative variant of this process is the vacuum injection or vacuum-assisted resin transfer molding (VARTM), where a single solid mould and a foil (polymeric film) are used. The VARTM process is a very clean and low cost manufacturing method: resin is processed into a dry reinforcement on a vacuum-bagged tool, using only the partial vacuum to drive the resin. As one of the tool faces is flexible, the moulded laminate thickness depends partially on the compressibility of the fiber-resin composite before curing and the vacuum negative pressure.

5.1.3. Compression Molding. Compression molding is another major technique for the construction of fiber-reinforced polymers, which involves a semifinished composite sheet widely known as sheet molding compound (SMC) that is later moulded into the final parts by compression. For the SMC the process consists of a rolling film of resin on which fibers are added. A second film of resin is then added, so as to later be compressed in a composite sheet that may be stored for few days. To get the final product the reinforced sheet is then placed into a press to take its desired shape.

Advantages of compression molding are the very high volume production ability, the excellent part reproducibility and the short cycle times. Processing times of <2 min are reached during the compression molding of three-dimensional components with a high forming degree. It has also been shown that the adhesion of natural fibers and matrix resin is important in order to obtain good mechanical properties of natural fiber composites, and the mechanical properties were improved by the molding condition, the molding pressure and temperature. A big concern with compression molding that needs always to be considered is the maximum pressure before the damage of the fibers and the structure.

5.1.4. Injection Molding. Injection molding process is suitable to form complex shapes and fine details with excellent surface finish and good dimensional accuracy for high production rate and low labour cost. In the injection molding resin granules and short fibers are mixed into a heated barrel and transported to the mould cavity by a spindle. Injection molding is another process among the most important for the manufacturing of plastics/composites and can produce from very small products such as bottle tops to very large car body parts.

5.1.5. Pultrusion. Pultrusion is a continuous process to manufacture composite profiles at any length. The impregnated fibers are pulled through a die, which is shaped according to the desired cross-section of the product. The resulting profile is shaped until the resin is dry. Advantages of this process are the ability to build thin wall structures, the large variety of cross-sectional shapes and the possibility for high degree of automation.

5.2. Interfacial Interactions. All natural fibers are (in different extent) hydrophilic in nature. This is attributed mainly to the lignocellulose into their structure, which contain strongly polarized hydroxyl groups [68]. These fibers, therefore, are inherently incompatible with many well known and popular

in composite manufacturing resins. Only some thermosets such as the phenol-formaldehyde and related polymers are less hydrophilic and thus less problematic.

This discrepancy leads often to the formation of ineffective interface between the fibers and the matrix. The major limitations of using these fibers as reinforcements in such matrices include poor interfacial adhesion between polar-hydrophilic fibers and nonpolar-hydrophobic matrix, and difficulties in mixing due to poor wetting of the fibers with the matrix. The role of the matrix in a fiber-reinforced composite is to transfer the load to the stiff fibers through shear stresses at the interface. This process requires a good bond between the polymeric matrix and the fibers [70].

Poor adhesion at the interface means that the full capabilities of the composite cannot be exploited and leaves it vulnerable to environmental attacks that may weaken it, thus reducing its life span. Insufficient adhesion between the polymer and the fibers results in poor mechanical properties of the natural fiber-reinforced polymer composites.

Pretreatments of the fibers can clean the fiber surface, chemically modify the surface, stop the moisture absorption process, and increase the surface roughness [71, 72]. These properties may be improved by both physical treatments like cold plasma treatment or corona treatment, and chemical treatment such as maleic anhydride, organosilanes, isocyanates, sodium hydroxide, permanganate, and peroxide.

5.2.1. Physical Treatment. Physical treatments change the structural and surface properties of the fibers and thereby influence the mechanical bonding to polymers. Corona treatment is one of the most popular techniques for surface oxidation activation through electric discharge that changes the surface energy of the cellulose fibers. Cold plasma treatment is another electric discharge technique and can have the same surface effects and increase the fiber matrix adhesion [72]. A traditional physical method is mercerization. In this process, the fibers are treated with an aqueous solution of a strong base (alkali treatment) so as to produce great swelling that results in changes of their structure, dimensions, morphology, and mechanical properties [72].

5.2.2. Chemical Treatment. Among the most effective methods of chemical treatment is graft copolymerization [68, 72]. The cellulose is treated with an aqueous solution with selected ions and is exposed to a high energy radiation. Under the radiation, the cellulose molecule cracks and radicals are formed. Using then a suitable (compatible with the matrix) solution it is possible to create a copolymer with properties and characteristics of both the fibers and the matrix. Graft copolymers of natural fibers with vinyl monomers provide better adhesion between matrix and fiber. Gauthier et al. [73] reported that adhesion may be improved by using coupling agents like maleic anhydride to incorporate hydroxyl groups on the matrix through hydrophilization and consequently enhancing the wetting effect of the resin on the fibers. The hydroxyl groups then interact with –OH molecules on the lignocellulosic fibers via hydrogen bonding, thus producing stronger bond. George et al. [74] reviewed the physical and chemical treatments that may improve the fiber-matrix adhesion and manufactured biocomposites by applying an alkaline solution to the fibers. Natural fibers are mainly composed of cellulose, whose elementary unit, anhydro d-glucose, contains three hydroxyl (OH) groups. These hydroxyl groups form intra- and intermolecular bonds, causing all vegetable fibers to be hydrophilic. The alkaline solution regenerated the lost cellulose and dissolved unwanted microscopic pits or cracks on the fibers resulting in better fiber-matrix adhesion.

Coupling agents are based on the concept that when two materials are incompatible, a third material with intermediate properties can bring the compatibility to the mixture [72]. The coupling agents have two functions: to react with OH groups of the cellulose and to react with the functional groups of the matrix with the goal of facilitating stress transfer between the fibers and the matrix. Numerous studies [68, 72] have been conducted on the use of coupling agents including organosilanes, triazine, and maleic-anhydride (MAH). For instance, Xie et al. [75] used silane-coupling agents in natural fiber/polymer composites and concluded that proper treatment of fibers with silanes can increase the interfacial adhesion and improve the mechanical performance of the resulting composites. Gassan and Bledzki [76] improved the tensile and flexural strength and stiffness of jute/epoxy composites by treating the fibers with silane. Acetylation, isocyanate treatment, and treatment with stearic acid are some more chemical methods for modification and preparation of the fiber/matrix adhesion.

5.3. Characterization. Plant fibers are basically composite materials designed by nature and consist of a collection of long and thin cells made up of hollow cellulose fibrils held together by a lignin and hemicellulose matrix [77]. The strength and stiffness of the fibers are provided by hydrogen bonds and other linkages. The overall properties of the fibers depend on the individual properties of each of its components. Hemicellulose is responsible for the biodegradation, moisture absorption, and thermal degradation of the fiber. On the other hand, lignin (or pectin) is thermally stable but is responsible for UV degradation of the fiber. On average, natural fibers contain 60–80% cellulose, 5–20% lignin (or pectin), and up to 20% moisture.

On a composite, the properties of the fibers are combined with those of the matrix, which is responsible to transfer the external loads to the stiff fibers through shear stresses at the interface as well as keep the fibers together in a specific structural form. Thus, the properties of the composite are a combination of the properties of the ingredients and their prediction and estimation becomes a difficult job.

5.3.1. Stiffness and Strength. The mechanical properties of natural fiber composites are much lower than those of glass fibers. However, their specific properties, especially stiffness, are comparable to the stated values of glass fibers. Moreover, natural fibers are about 50% lighter than glass, and in general cheaper. It is widely acknowledged that natural fiber composites combine good mechanical properties with a low specific mass and offer an alternative material to glass fiber-reinforced plastics in some technical applications.

For example, Bledzki and Gassan [72] observed that the characteristic values of natural fibers are comparable to those of glass fibers. Experimental data giving the tensile strength, flexural strength, modulus, impact force, and compressive force are available in the literature for different types of natural-fiber composites.

The ultimate strength of any composite depends on several factors, most important of which are the properties of the components and the volume fraction. Wambua et al. [70] studied the importance and effect of the volume fraction on the tensile strength of natural fiber composites. They reported that an increase in the fiber weight fraction produces an increase in the tensile strength. Testing different fiber reinforcement, they also found that hemp/polypropylene (PP) composites with a 30% volume fraction displayed a tensile strength of 52 MPa, higher than equivalent glass-reinforced composites with the same volume fraction. Further, hemp and kenaf-polypropylene composites registered a high tensile modulus of 6.8 GPa compared to 6.2 GPa of equivalent glass composites. The increase of the modulus and the tensile strength with increase of the volume or weight fraction was also showed by Bos et al. [78, 79] on flax/PP composites with maleic-anhydride grafted polypropylene for improved adhesion.

Studies and results of tensile tests on flax-fiber-reinforced PP composites were conducted by Garkhail et al. [80] which concluded that fiber length affect the strength and modulus of the composites for small fiber lengths whilst after a specific value for the length the two parameters are constant. The stiffness of a flax/PP composite was shown to be comparable to E-glass-based composite, especially when the specific properties are concerned due to the very low density of flax. However, the results also depicted a relatively low tensile strength.

Nishino [81] studied the mechanical properties of kenaf/poly-L-lactide (PLLA) composites. He concluded that the modulus of the composites increases with the increase of the volume fraction, but only up to a certain level. When this threshold is achieved, further increase of the fiber fraction leads to a dramatic reduction of the composite properties.

Water content has also a dramatic effect on the properties of natural-fiber composites. Espert et al. [82] showed this effect on cellulose/PP composites by submerging samples into distilled water under different temperatures. The samples were removed from the water at certain times and the water absorption was measured. The results of tensile tests showed a significant effect of the water content to the young's modulus of the samples, and an even bigger effect on the tensile strength. The studies also concluded that the effect of the water to the properties is highly influenced by the fiber content, the matrix and mainly the temperature. Thwe and Liao [83] investigated the same effect on bamboo-fiber composites and resulted that both the tensile strength and modulus have decreased after aging in water at 25 and 75°C for prolonged period. The extent of strength and stiffness loss depends upon aging time and temperature. They also concluded that tensile strength and stiffness are enhanced by inclusion of a coupling agent, maleic anhydride polypropylene (MAPP), in matrix material as a result of improved interfacial bonding.

5.3.2. Impact Performance. There are only few studies known about the impact behaviour of natural-fiber reinforced-composites. The impact performance of several natural fiber composites was compared and reviewed by Wambua et al. [70]. Using kenaf-, coir-, sisal-, hemp-, and jute-reinforced polypropylene the study concluded that natural fiber composites display low impact strengths compared to glass composites, whereas their specific impact strength can be comparable with those of glass mat composites. Among the materials studied, sisal and hemp showed the higher impact strength.

Pavithran et al. [84] determined the fracture energies for sisal, pineapple, banana, and coconut fiber-polyester composites in a Charpy impact test. They concluded that increased fiber toughness results in increased fracture energy and found that fibers with higher fibril angles have higher fracture-toughness than those with small spiral angle.

Fiber content and fiber length have also a contribution to the impact performance of the composite. Tobias [85] examined this influence with banana-fiber composites and concluded that smaller fiber lengths have higher impact strength which also increases for higher fiber content. Contradictorily, the fiber length was also studied by Garkhail et al. [80] on flax/PP composites. The results showed that (as in glass fiber composites) the impact strength increases with increasing fiber length until a plateau level is reached. After that level, the impact performance drops depending on the pretreatment of the fibers and the adhesion of the fiber/matrix interface.

Mueller [86] investigated the effect of several material parameters on the impact strength of compression-molding components of hemp-, flax- and kenaf-polypropylene composites. The studies showed a strong influence of the thermal process conditions during the molding. He concluded that for every material studied there is an optimum temperature that results to a peak of the impact strength. Higher and lower processing temperature resulted in lower mechanical values that could be explained by a thermal decomposition of the fibers. Strong impact of the fiber fineness was also proved, with the impact performance getting higher from composites with fiber of higher fineness.

The effect of temperature and water on the impact properties of natural-fiber thermoplastics were reviewed by De Bruijn [87] and showed not significant effect on the impact properties of the composites. However, the results showed that the impact strength was 20 to 25% to that of glass-reinforced thermoplastics.

A significant contribution of coupling agents on the impact strength has also been reported. When the composites have no coupling agent, a part of the energy is lost in the interface, by for example debonding and friction effects. Maleic-anhydride-treated jute composites showed higher impact strength than untreated samples made out of the same process.

5.3.3. Fatigue Behaviour. The cyclic loading of natural fiber composites is still poorly investigated. Gassan [88] investigated the fatigue behaviour of flax and jute epoxy resin composites. Fiber type, textile architecture, interphase properties, and fiber properties and content were found to affect the fatigue behaviour strongly. It was also found that natural fiber-reinforced plastics with higher fiber strength and modulus, stronger fiber-matrix adhesion, or higher fiber fractions possess higher critical loads for damage initiation and higher failure loads. In addition, damage propagation rates were reduced. Furthermore, unidirectional composites were less sensitive to fatigue-induced damage than woven reinforced ones.

Savastano et al. [89] presented the results of experimental studies of resistance-curve behaviour and fatigue crack growth in cementitious matrices reinforced with natural fibers such as sisal, banana, and bleached eucalyptus pulp. Fatigue crack growth was observed to occur in three stages: an initial decelerated growth, a steady-state growth, and a final catastrophic crack growth. In the case of the composites reinforced with sisal and banana fibers, most of fatigue life was spent in the second stage of steady-state crack growth. The results showed that fatigue crack growth in the composites occurred via matrix cracking, crack deflection around fibers, and crack-bridging by uncracked fibers and ligaments, whilst fiber pullout was also observed.

The fatigue performance of sisal/epoxy composites was also studied by Towo and Ansell [90, 91] which looked into the effect of surface modification on the fatigue performance of the composite. The results show that an NaOH surface treatment has a significant effect on the tensile modulus and strength of the material, but the fatigue life is not highly influenced, especially in low stress levels. Their conclusion states that the behaviour of sisal fiber composites is similar to that of conventional synthetic fiber composites and static and fatigue strengths are suitably high for many commercial applications. Towo et al. also studied the fatigue properties of flax/polyester with alkali-treated and untreated fibers. In this case they observed a high influence of the treatment on the fatigue life of the components and they also underlined that the polyester matrix samples had lower life than the epoxy samples.

A comparison between hemp- and flax-reinforced polyester composites with focus on the fatigue behaviour was conducted by Yuanjian and Isaac [92]. A steeper gradient of the S-N curve for the hemp-fiber composite was indicative of a higher rate of reduction in fatigue strength. However, the fatigue performance levels of this hemp mat composite were comparable and slightly greater than those of the glass fiber composite.

6. Cellulose Nanofiber-Reinforced Nanocomposites

The potential of nanocomposites in various sectors of research and application is promising and attracting increasing investments. In the nanocomposite industry, a reinforcing particle is usually considered as a nanoparticle when at least one of its linear dimensions is smaller than 100 nm. Owing to the hierarchical structure and semicrystalline nature of cellulose, nanoparticles can be extracted from this naturally occurring polymer. Native cellulose fibers are built up by smaller and mechanically stronger long thin filaments, the microfibrils consisting of alternating crystalline and noncrystalline domains. Multiple mechanical shearing actions can be used to release more or less individually these microfibrils. This material is usually called microfibrillated cellulose (MFC). Figure 11 [93–96] shows transmission electron micrographs from dilute suspensions of MFC obtained from different sources.

Longitudinal cutting of these microfibrils can be performed by submitting the biomass to a strong acid hydrolysis treatment, allowing dissolution of amorphous domains. The ensuing nanoparticles occur as rod-like nanocrystals or whiskers with dimensions depending on the source of cellulose and preparation procedure. Examples are shown in Figure 12 [97–104]. The typical geometrical characteristics for nanocrystals derived from different species and reported in the literature are collected in Table 1 [105–139].

Impressive mechanical properties and reinforcing capability, abundance, low weight, and biodegradability of cellulose nanocrystals make them ideal candidates for the processing of polymer nanocomposites [140–143]. With a Young's modulus around 150 GPa and a surface area of several hundred $m^2 \cdot g^{-1}$ [144], they have the potential to significantly reinforce polymers at low filler loadings. A broad range of applications of nanocellulose exists even if a high number of unknown remains at date. Tens of scientific publications and experts show its potential even if most of the studies focus on their mechanical properties as reinforcing phase and their liquid crystal self-ordering properties. However, as for any nanoparticle, the main challenge is related to their homogeneous dispersion within a polymeric matrix.

6.1. Nanocomposite Processing. Cellulose nanoparticles are obtained as stable aqueous suspensions and most investigations focused on hydrosoluble (or at least hydrodispersible) or latex-form polymers. The main advantage is that the dispersion state of the nanoparticles is kept when using an aqueous medium for the processing.

After dissolution of the hydrosoluble or hydrodispersible polymer, the aqueous solution can be mixed with the aqueous suspension of cellulosic nanoparticles. The ensuing mixture is generally cast and evaporated to obtain a solid nanocomposite film. It can also be freeze-dried and hot-pressed. The preparation of cellulose nanofiber reinforced starch [145–150], silk fibroin [151], poly(oxyethylene) (POE) [152–156], polyvinyl alcohol (PVA) [157–161], hydroxypropyl cellulose (HPC) [157, 158], carboxymethyl cellulose (CMC) [162], or soy protein isolate (SPI) [163] has been reported in the literature.

The first publication reporting the preparation of cellulose nanocrystals-reinforced polymer nanocomposites was carried out using a latex obtained by the copolymerization of styrene and butyl acrylate (poly(S-co-BuA)) and tunicin (the cellulose extracted from tunicate—a sea animal) whiskers [137]. The same copolymer was used in association

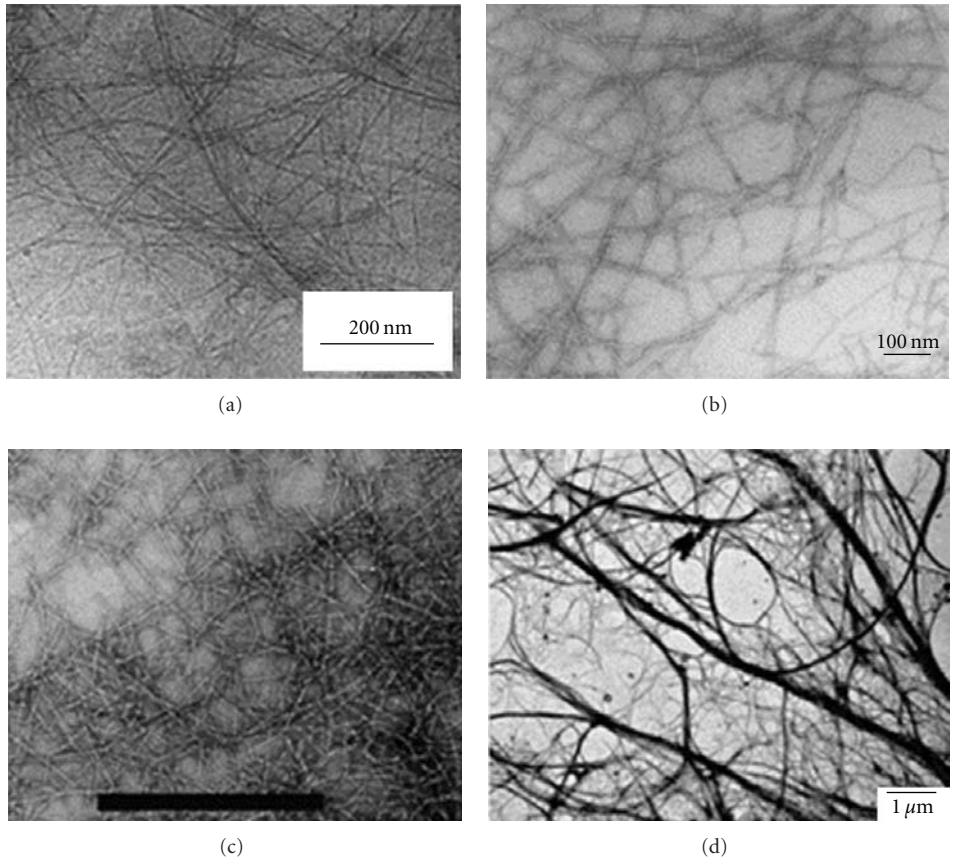

Figure 11: Transmission electron micrographs from dilute suspension of MFC obtained from wood fibers by mechanical processing combined to (a) enzymatic [93], (b) TEMPO-mediated oxidation [94], (c) carboxylmethylation pretreatment [95], and (d) extracted from Opuntia ficus-indica [96].

with wheat straw [103, 164] or sugar beet [101] cellulose nanocrystals. Other latexes such as poly(β-hydroxyoctanoate) (PHO) [165–167], polyvinylchloride (PVC) [168–171], waterborne epoxy [172], natural rubber (NR) [122, 173, 174], and polyvinyl acetate (PVAc) [99] were also used as matrix. Recently, stable aqueous nanocomposite dispersions-containing cellulose whiskers and a poly(styrene-co-hexylacrylate) matrix were prepared via miniemulsion polymerization [106]. Addition of a reactive silane was used to stabilize the dispersion. Solid nanocomposite films can be obtained by mixing and casting the two aqueous suspensions followed by water evaporation.

The possibility of dispersing cellulosic nanofibers in nonaqueous media has been investigated using surfactants or chemical grafting and it opens other possibilities for nanocomposites processing. Cellulose nanoparticles possess a reactive surface covered with hydroxyl groups, providing the possibility to extensive chemical modification. Although this strategy decreases the surface energy and polar character of the nanoparticles, improving by the way the adhesion with nonpolar polymeric matrix, a detrimental effect is generally reported for the mechanical performances of the composite. This unusual behavior is ascribed to the originality of the reinforcing phenomenon of polysaccharide nanocrystals resulting from the formation of a percolating network thanks to hydrogen bonding forces. Therefore, grafting of long chains instead of small molecules can be used to preserve the mechanical properties of the material.

Very few studies have been reported concerning the processing of cellulose nanofibers-reinforced nanocomposites by extrusion methods. The hydrophilic nature of cellulose causes irreversible agglomeration during drying and aggregation in nonpolar matrices because of the formation of additional hydrogen bonds between amorphous parts of the nanoparticles. Therefore, the preparation of cellulose whiskers-reinforced PLA nanocomposites by melt extrusion was carried out by pumping the suspension of nanocrystals into the polymer melt during the extrusion process [175]. An attempt to use PVA as a compatibilizer to promote the dispersion of cellulose whiskers within the PLA matrix was reported [176]. Organic acid chlorides-grafted cellulose whiskers were extruded with LDPE [177]. The homogeneity of the ensuing nanocomposite was found to increase with the length of the grafted chains. Polycaprolactone-grafted cellulose nanocrystals obtained by ring-opening polymerization (ROP) of the corresponding lactone were also used as "masterbatches" by melt blending with a PCL matrix [178].

An attempt to use a recently patented concept (Dispersed nanoobjects protective encapsulation—DOPE process) intended to disperse carbon nanotubes in polymeric

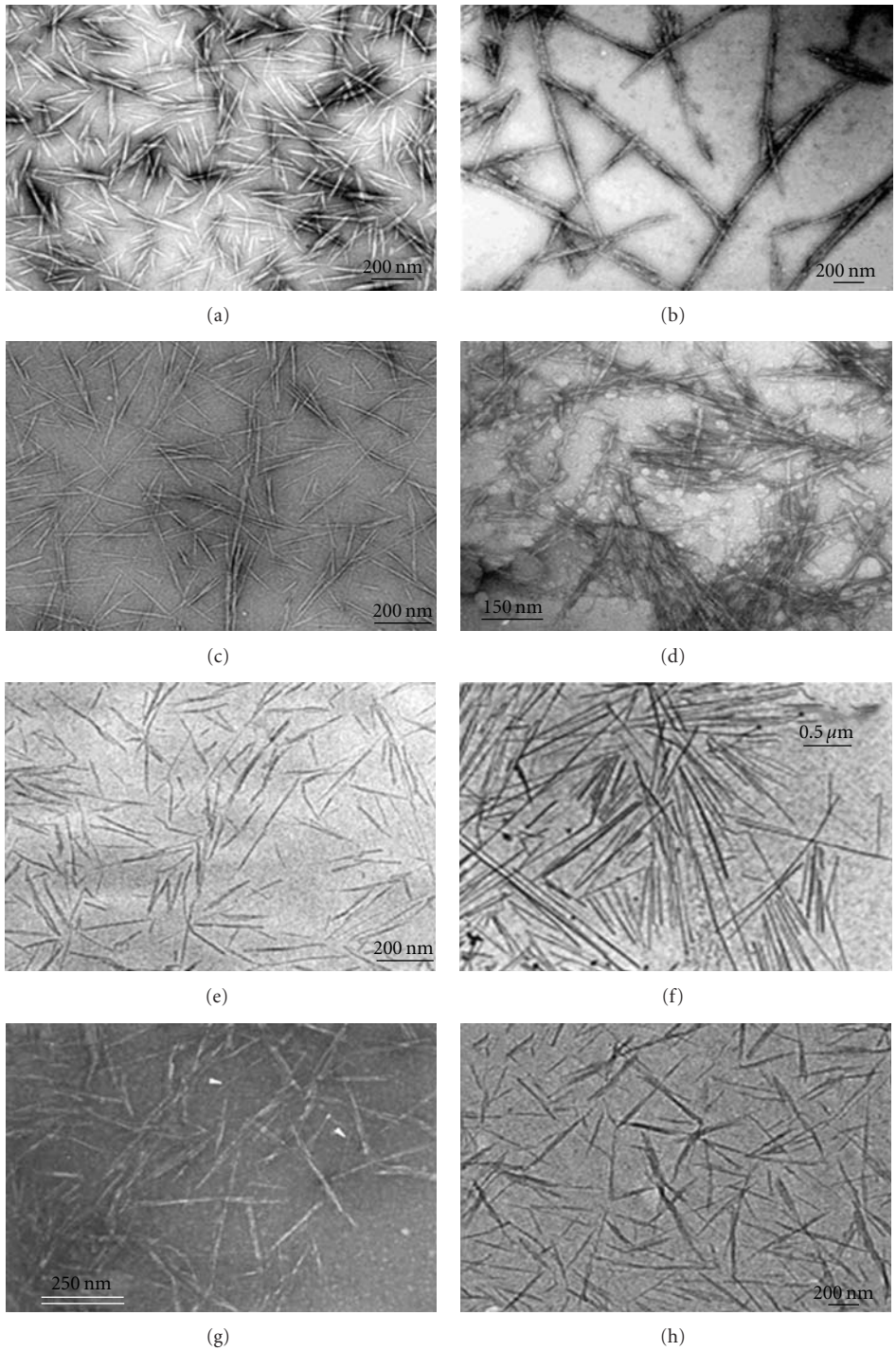

Figure 12: Transmission electron micrographs from dilute suspension of cellulose nanocrystals from: (a) ramie [97], (b) bacterial [98], (c) sisal [99], (d) microcrystalline cellulose [100], (e) sugar beet pulp [101], (f) tunicin [102], (g) wheat straw [103], and (h) cotton [104].

matrices was reported. Physically cross-linked alginate capsules were successfully formed in the presence of either cellulose whiskers or microfibrillated cellulose [179]. The ensuing capsules have been extruded with a thermoplastic material.

6.2. Interfacial Interactions. Strong interactions between cellulose nanofibers prepared from cottonseed linters and between the filler and the glycerol-plasticized starch matrix were reported to play a key role in reinforcing properties [120]. In nonpercolating systems, for instance for materials processed from freeze-dried cellulose nanocrystals, strong matrix/filler interactions enhance the reinforcing effect of the filler. This observation was reported using EVA matrices with different vinyl acetate contents and then different

Table 1: Geometrical characteristics of cellulose nanocrystals from various sources: length (L), cross section (D), and aspect ratio (L/d).

Source	L (nm)	D (nm)	L/D	Reference
Acacia pulp	100–250	5–15	—	[105]
Alfa	200	10	20	[106]
Algal (*Valonia*)	>1,000	10–20	∞	[107, 108]
Bacterial	100–several 1,000	5–10 × 30–50	—	[98, 109, 110]
Banana rachis	500–1,000	5	—	[111]
Bioresidue from wood bioethanol production	several 100	10–20	—	[112]
Capim dourado	300	4.5	67	[113]
Cassava bagasse	360–1,700	2–11	—	[114]
Cladophora	—	20 × 20	—	[115]
Coconut husk fibers	80–500	6	39	[116]
Cotton	100–300	5–15	10	[117–119]
Cottonseed linter	170–490	40–60	—	[120]
Curaúa	80–170	6–10	13-17	[121]
Date palm tree (rachis/leaflets)	260/180	6.1	43/30	[122]
Eucalyptus wood pulp	145	6	24	[123]
Flax	100–500	10–30	15	[124]
Grass Zoysia	200–700	10–60	—	[125, 126]
Hemp	several 1,000	30–100	—	[127]
Luffa cylindrica	242	5.2	47	[128]
MCC	150-300	3–7	—	[100]
Mulberry	400–500	20–40	—	[129]
Pea hull	240–400	7–12	34	[130]
Ramie	350–700 150–250	70–120 6–8	[97, 131, 132]	
Recycled pulp	100–1,800	30–80	—	[133]
Sisal	100–500 215	3–5 5	60/43	[99, 134, 135]
Sugar beet pulp	210	5	42	[101]
Sugarcane bagasse	200–310	2–6	64	[136]
Tunicin	100–several 1,000	10–20	67	[137]
Wheat straw	150–300	5	45	[103]
Wood	100–300	3–5	50	[115, 138, 139]

polarities [180]. Improvement of matrix/filler interactions by using cellulose whiskers coated with a surfactant was shown to play a major role on the nonlinear mechanical properties, especially on the elongation at break [181]. Grunert and Winter [98] founded a higher reinforcing effect for unmodified cellulose whiskers than for trimethylsilylated whiskers. Apart from the fact that 18% of the weight of the silylated crystals was due to the silyl groups, they attributed this difference to restricted filler/filler interactions.

6.3. Mechanical Performance. The first demonstration of the reinforcing effect of cellulose nanocrystals in a poly(S-co-BuA) matrix was reported by Favier et al. [137]. The authors measured by DMA in the shear mode a spectacular improvement in the storage modulus after adding tunicin whiskers even at low content into the host polymer. This increase was especially significant above the glass-rubber transition temperature of the thermoplastic matrix because of its poor mechanical properties in this temperature range. Figure 13 shows the isochronal evolution of the logarithm of the relative storage shear modulus ($\log G'_T/G'_{200}$, where G'_{200} corresponds to the experimental value measured at 200 K) at 1 Hz as a function of temperature for such composites prepared by water evaporation.

In the rubbery state of the thermoplastic matrix, the modulus of the composite with a loading level as low as 6 wt% is more than two orders of magnitude higher than the one of the unfilled matrix. Moreover, the introduction of 3 wt% or more cellulosic whiskers provides an outstanding thermal stability of the matrix modulus up to the temperature at which cellulose starts to degrade (500 K).

The macroscopic behavior of cellulose nanofibers-based nanocomposites depends as for any heterogeneous materials, on the specific behavior of each phase, the composition (volume fraction of each phase), the morphology (spatial arrangement of the phases) and the interfacial properties.

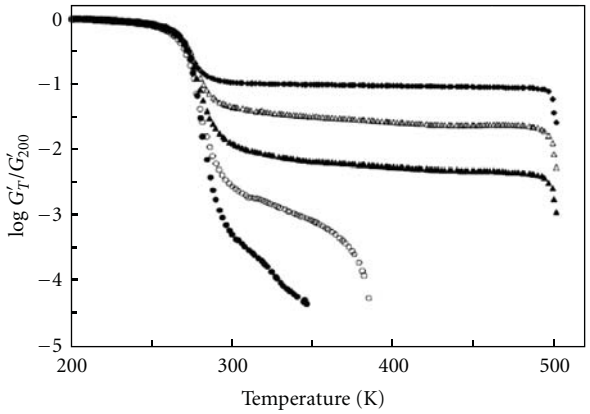

Figure 13: Logarithm of the normalized storage shear modulus (log G'_T/G'_{200}, where G'_{200} corresponds to the experimental value measured at 200 K) versus temperature at 1 Hz for tunicin whiskers reinforced poly(S-co-BuA) nanocomposite films obtained by water evaporation and filled with 0 (●), 1 (○), 3 (▲), 6 (△) and 14 wt% (♦) of cellulose whiskers [140].

The outstanding properties observed for these systems were ascribed to a mechanical percolation phenomenon [137]. A good agreement between experimental and predicted data was reported when using the series-parallel model of Takayanagi modified to include a percolation approach. Therefore, the mechanical performances of these systems were not only due to the high mechanical properties of the reinforcing nanoparticles. It was suspected that the stiffness of the material was due to infinite aggregates of cellulose whiskers. Above the percolation threshold, the cellulosic nanoparticles can connect and form a 3D continuous pathway through the nanocomposite film. For rod-like particles such as tunicin whiskers with an aspect ratio of 67, the percolation threshold is close to 1 vol%. The formation of this cellulose network was supposed to result from strong interactions between nanofibers, like hydrogen bonds. This phenomenon is similar to the high mechanical properties observed for a paper sheet, which result from the hydrogen-bonding forces that hold the percolating network of fibers. This mechanical percolation effect allows explaining both the high reinforcing effect and the thermal stabilization of the composite modulus for evaporated films.

Any factor that affects the formation of the percolating whiskers network or interferes with it changes the mechanical performances of the composite [141]. Three main parameters were reported to affect the mechanical properties of such materials, namely, the morphology and dimensions of the nanoparticles, the processing method, and the microstructure of the matrix and matrix/filler interactions.

6.4. Thermal Stability. Thermogravimetric analysis (TGA) experiments were performed to investigate the thermal stability of tunicin whiskers/POE nanocomposites [152, 153]. No significant influence of the cellulosic filler on the degradation temperature of the POE matrix was reported. Cotton cellulose nanocrystals content appeared to have an effect on the thermal behavior of CMC plasticized with lycerin suggesting a close association between the filler and the matrix [162]. The thermal degradation of unfilled CMC was observed from its melting point (270°C) and had a very narrow temperature range of degradation. Cellulose nanocrystals were found to degrade at a lower temperature (230°C) than CMC, but shown a very broad degradation temperature range. The degradation of cellulose whiskers-reinforced CMC was observed between these two limits, but of interest was the lack of steps. Composites were reported to degrade as a unit.

7. Applications of Polymer Composites

7.1. Biocomposites. The charm of the use of synthetic fibres in polymer composites is fading, because these are expensive, nonbiodegradable, and pollute the environment. There is an increasing movement of scientists and engineers who are dedicated to minimizing the environmental impact of polymer composite production. Environmental footprints must be diminished at every stage of the life cycle of the polymer composite. Using natural fibers with polymers based on renewable resources will allow many environmental issues to be solved. By embedding biofibers with renewable resource-based biopolymers such as cellulosic plastics; polylactides; starch plastics; polyhydroxyalkanoates (bacterial polyesters); soy-based plastics, the so-called green biocomposites could soon be the future.

Nowadays, biocomposites have been the subject of extensive research, specifically in construction and building industry due to their many advantages such as lower weight, and lower manufacturing costs. Currently, not only builders, but also many home owners are interested in using biocomposites for different products such as decking, fencing, and so on. Biocomposites may be classified, with respect to their applications in building industry into two main groups: structural and nonstructural biocomposites [182, 183].

7.1.1. Structural Application. A structural Biocomposite can be defined as one that is needed to carry a load in use. For instance, building industry, load-bearing walls, stairs, roof systems, and subflooring are examples of structural biocomposites. Structural biocomposites can range broadly in performance, from high performance to low performance materials. Biobased composite materials have been tested for suitability in roof structure (Figure 14) [184]. Structural beams have been designed, manufactured, and tested, yielding good results. Soy oil-based resin and cellulose fibers, in the form of paper sheets made from recycled cardboard boxes may be used for the manufacture of the composite structures.

Figure 15 represents, stay-in-place bridge forms (SIP) are utilized to span the distance between bridge girders. The SIP forms made from biocomposites have many benefits in comparison to steel forms. Biocomposite-based SIP forms are porous or breathable. Therefore, this lets water to evaporate through the form and to avoid any rebar corrosion. The form is also biodegradable; a biobased form has the potential to break down in the future, allowing underside inspection of the bridge deck. In addition, the form is

Figure 14: Biobased composite roof panels; one of them is mounted on a demonstration house made of timber [184].

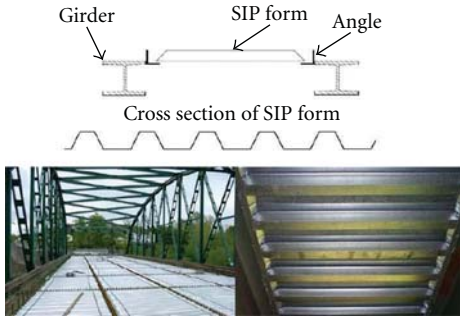

Figure 15: Stay-in-place bridge form.

lighter compared to a steel form, allowing faster and cheaper installations.

7.1.2. Nonstructural Application. A nonstructural biocomposite can be defined as one that need not carry a load during service. Materials such as thermoplastics, wood particles, and textiles are used to make this kind of Biocomposites. Nonstructural biocomposites are used for products such as ceiling tiles, furniture, windows, and doors.

Wood fiber plastic composites are made in standard lumber profile cross-section dimensions in exterior construction. These bioproducts are utilized as dock surface boards, deck, picnic tables, landscape timbers, and industrial flooring. Many manufacturers recommend that biocomposites need gaps on both edges and ends for their thermal expansion. Furthermore, wood-based bioproducts are gapped for expansion due to the moisture absorption.

Clear ponderosa pine is utilized in clad components. Currently, it is becoming limited and expensive. In addition, ponderosa pine needs broad cutting, edge gluing, and finger jointing to get clear sections for window and door fabrication. Also, the glued up material have to be milled to the accurate cross section to be used in the assembly which results in increasing cost and waste wood. Therefore, manufacturers use wood fiber plastic composites as an alternative for solid wood in clad components.

Biocomposites are utilized for the construction of composite panels. There are three types of panels: fiberboard, particleboard, and mineral-bonded panels. Bagasse fibers are used for particleboards, fiberboards, and composition panel production. Cereal straw is the second most usual agrobased fiber in panel production. The high percentages of silica in cereal straw make them naturally fire resistant. Also, the low density of straw panels has made them resilient. Results show that houses built by these panels are resistant to earthquake. Straw is also used in particleboards. Rice husks are also fibrous and need little energy input to make the husks ready for use. Rice husks or their ash are used in fiber cement blocks and other cement products. The presence of rice husks in building products helps to increase acoustic and thermal properties. A stress-skin panel-type product has been made by using polyurethane or polyester foam in the core and ply-bamboo in the faces [185]. Figure 16 indicates performance of cellular biocomposite panels against conventional slab and panel systems for commercial and residential construction [186].

7.2. Nanocomposites. The potential applicability of nanocellulose is widely extended. Applications of nanocellulose are mainly considered to be in paper and packaging products, although construction, automotive, furniture, electronics, pharmacy, and cosmetics are also being considered. For companies producing electroacoustic devices, nanocellulose is used as a membrane for high quality sound. Additionally, nanocellulose is applied in membrane for combustible cells (hydrogen); additives for high quality electronic paper (e-paper); ultrafiltrating membranes (water purification); membranes used to retrieve mineral and oils [187], and nowadays, nanocellulose has been greatly discussed and researched a huge variety of applications. The high strength and stiffness as well as the small dimensions of nanocellulose may well impart useful properties to composite materials reinforced with these fibers, which could subsequently be used in wide range of applications.

7.2.1. Electronic Industry

Diaphragms. Among various applications studied so far, which has already reached the level of practical use is related to acoustic diaphragms, nanocellulose has been found to bear two essential properties: high sonic velocity and low dynamic loss. In fact, the sonic velocity of pure film was almost equivalent to those of aluminium and titanium [63]. Jonas and Farah [188] stated that SONY had already been using it in headphones diaphragm (Figure 17).

The nanocellulose diaphragms are developed by dehydration and compressed to a thickness of 20 microns in a diaphragm die. The advantage of the ultrathin nanocellulose diaphragm is that it can produce the same sound velocity as an aluminum or titanium diaphragm, along with the warm, delicate sound that a paper diaphragm provides. Trebles are sparkling clear, and bass notes are remarkably deep and rich in these types of headphones.

Digital Displays. Cellulose has always been the prime medium for displaying information in our society; nowadays, efforts have been made to find dynamic display technology, for

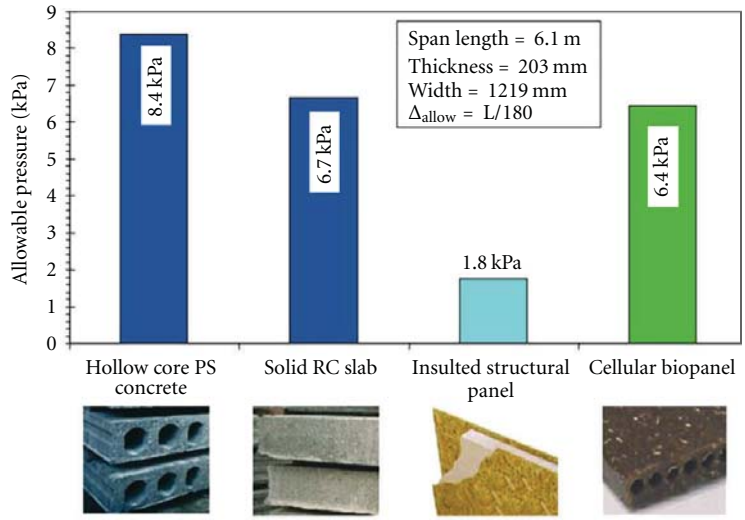

Figure 16: Performance of cellular biocomposite panels against conventional slab and panel systems for commercial and residential construction [186].

Figure 17: Nanocellulose diaphragm used in SONY headphones.

example in electronic paper. Nanocellulose is dimensionally stable and has a paper-like appearance which puts it into the leading role for the electronic paper's basic structure [189]. Shah and Brown [189] proved the concept in a device that holds many advantages such as high paper-like reflectivity, flexibility, contrast, and biodegradability. Figures 18 and 19 show the fabrication process of display device using nanocellulose. Summarizing, the whole idea is to integrate an electronic dye into the nanostructure of the microbial cellulose, and when integrated, a simple pixel can reversibly switch from the ON to the OFF state. The pixel size is controlled by the minimum addressing resolution of backplane drive circuits [189]. Yano et al. [190] have shown nanocellulose extraordinary potential as a reinforcement material in optically transparent plastics, for instance, as a substrate for bendable displays. According to the author, the composite remained optically transparent even at high fiber contents.

Legnani et al. [191] developed biodegradable and biocompatible flexible organic light emitting diode (FOLED) (Figure 20) based on nanocellulose (NC) membrane as substrate. Nanocomposite substrates based on nanocellulose (NC) and Boehmite-siloxane systems with improved optical transmittance in the visible region were used as flexible substrate for OLED applications. The nanocomposites formations improve the optical transmittance in visible range. Transmittance of 66% at 550 nm was found for the NC-nanocomposite/ITO (Indium Tin Oxide) substrate when compared to the 40% value at the same wavelength for the NC/ITO substrate. ITO film was deposited at room temperature onto membranes and glass using rf magnetron sputtering with a r_f power of 60 W and at pressure of 1 mtorr in Ar atmosphere.

Other Electronic Usages. Evans et al. [192] found that nanocellulose catalyzed the deposition of metals within its structure, thus a finely divided homogeneous catalyst layer is generated. Experimental data suggested that nanocellulose possessed reducing groups capable of initiating the precipitation of palladium, gold, and silver from aqueous solution. Thus, the structure is suitable for the construction of membrane electrode assemblies. Olson et al. [193] showed that freeze-dried cellulose nanofibril aerogels can be used as templates for making lightweight porous magnetic aerogels, which can be compacted into a stiff magnetic nanopaper.

7.2.2. Pharmaceutical. Cellulose has a long history of use in the pharmaceutical industry. The material has excellent compaction properties when blended with other pharmaceutical excipients so that drug-loaded tablets form dense matrices suitable for the oral administration of drugs. Polysaccharides, natural polymers, fabricated into hydrophilic matrices remain popular biomaterials for controlled-release dosage forms and uses of a hydrophilic polymer matrix is one of the most popular approaches in formulating an extended

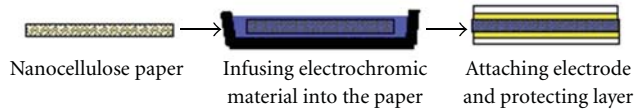

Figure 18: Fabrication process of the display using nanocellulose.

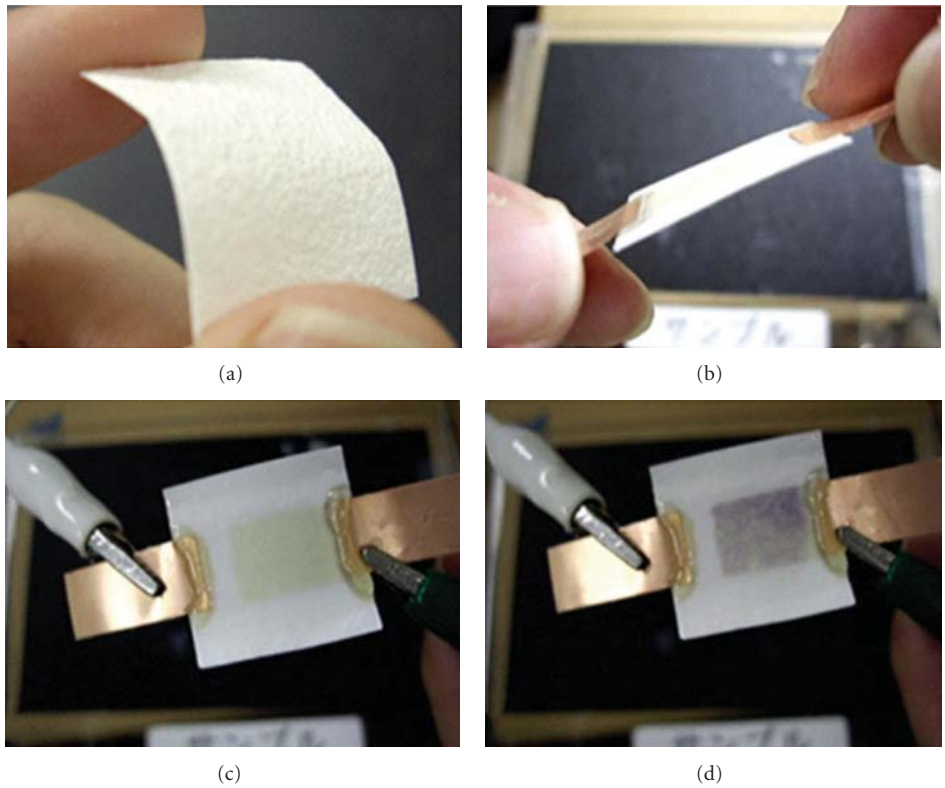

Figure 19: (a) The paper made of nanocellulose; (b) display device; (c) and (d) show the result of the chromogenic testing [189].

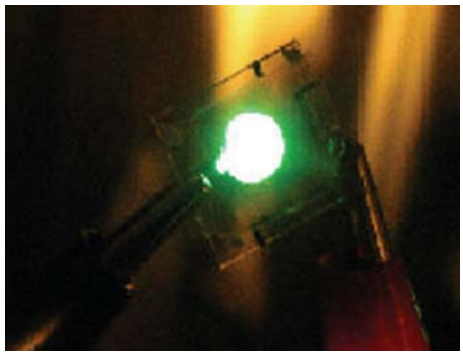

Figure 20: Cellulose Nanocomposite based Flexible Organic Light Emitting Diode (FOLED).

release dosage forms [194–196]. This is due to the fact that these formulations are relatively flexible, and a well-designed system usually gives reproducible release profiles. Drug release is the process by which a drug leaves a drug product and is subjected to absorption, distribution, metabolism, and excretion (ADME), eventually becoming available for pharmacologic action. Crystalline nanocellulose offers several potential advantages as a drug delivery excipient. Crystalline nanocellulose and other types of cellulose in advanced pelleting systems whereby the rate of tablet disintegration and drug release may be controlled by microparticle inclusion, excipient layering or tablet coating [197, 198].

The very large surface area and negative charge of crystalline nanocellulose suggest that large amounts of drugs might be bound to the surface of this material with the potential for high payloads and optimal control of dosing. Other nanocrystalline materials, such as nanocrystalline clays, have been shown to bind and subsequently release drugs in a controlled manner via ion exchange mechanisms and are being investigated for use in pharmaceutical formulations [199]. The established biocompatibility of cellulose supports the use of nanocellulose for a similar purpose. The abundant surface hydroxyl groups on crystalline nanocellulose provide a site for the surface modification of the material with a range of chemical groups by a variety of methods. Surface modification may be used to modulate the loading and release of drugs that would not normally bind to nanocellulose, such as nonionized and hydrophobic

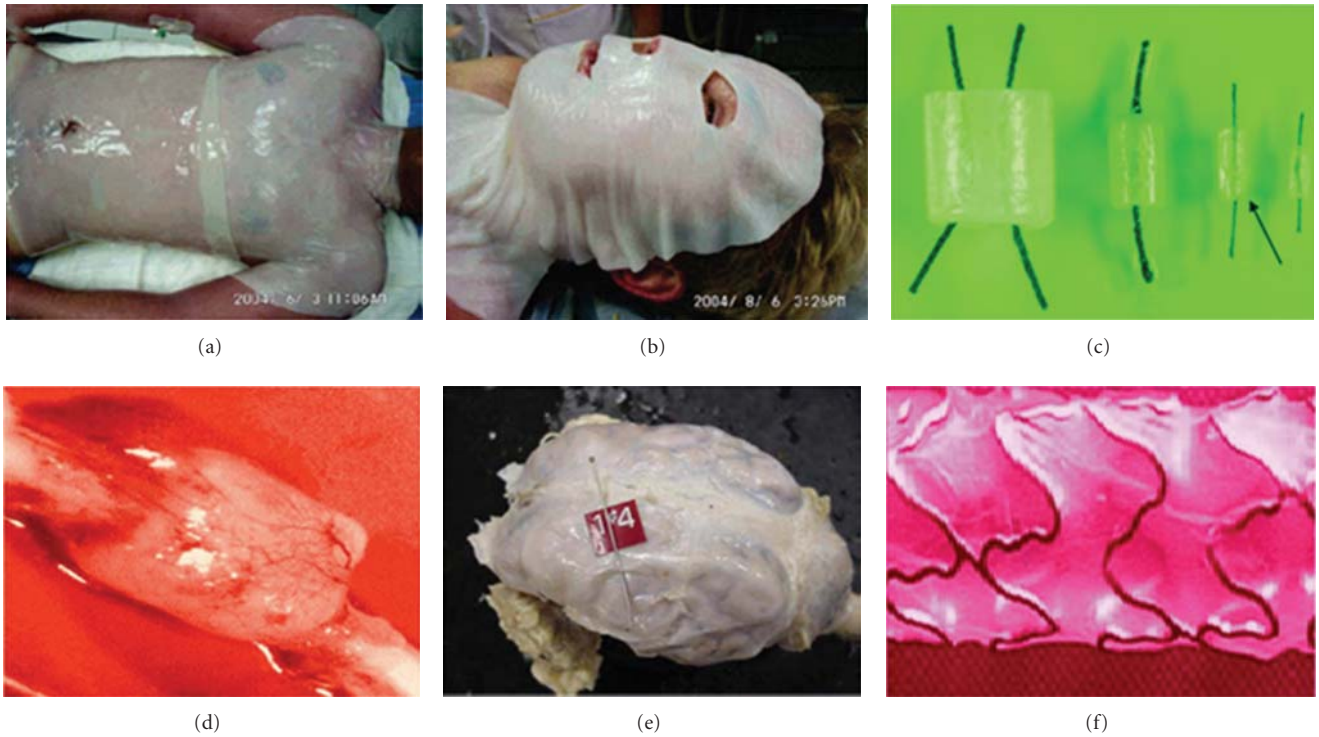

Figure 21: Biomedical applications of nanocellulose (a) and (b) never dried nanocellulose membrane [203]; (c) and (d) artificial blood vessels [205]; (e) dura mater reconstruction [202] (f) covering Stents [204].

drugs. For example, Lönnberg et al. suggested that poly(caprolactone) chains might be conjugated onto nanocrystalline cellulose for such a purpose [200].

Additionally, since crystalline nanocellulose is a low-cost, readily abundant material from a renewable and sustainable resource, its use provides a substantial environmental advantage compared with other nanomaterials.

7.2.3. Medical. Recently, nanocellulose has been called as the eyes of biomaterial highly applicable to biomedical industry which includes skins replacements for burnings and wounds; drugs releasing system; blood vessel growth; nerves, gum and duramater reconstruction; scaffolds for tissue engineering; stent covering and bone reconstruction [201–205]. Figure 21 shows some applications for nanocellulose within biomedical field.

Tissue engineering looks for new material and devices which could interact positively with biological tissues [206], either working as an in vitro basis for cell growth or rearranging and developing tissue about to be implanted. They also aim new classes of degradable biopolymers that are biocompatible and whose activities are controllable and specific [207], more likely to be used as cell scaffolds [208] or in vitro tissue reconstruction.

As described above, a great variety of biomaterials have been developed recently. They have all sorts of properties (physical,chemical, and mechanical) depending mostly in the final application (tissue regeneration, medication holding and releasing, tissue grafting, or scaffolding) [203]. The scaffold's success depends much on the cellular adhesion and growth onto the surface, thus biopolymer's chemical surface can dictates cellular response by interfering in cellular adhesion, proliferation, migration, and functioning.

The surface-cell interaction is extremely important in implant effectiveness, including its rejection. Since the interaction is fully understood in a cell level, new biomaterials and products can be easily developed [209]. The problems still arise due to some methods inefficiency such as cell seeds and sources, scaffolding, ambient, extracellular matrix producing, and analysis and appropriate models [210].

On the other hand, to regenerate tissues, three specific foundations are taken: cells, support, and growth factors. Cells synthesize the matrix for the new tissues, support holds and keeps the ambient proper for the growth, while the growth factors facilitate and promote the cell regeneration [210]. Material used for implants cannot be either rejected or causes inflammatory response, in others, it should be biocompatible. Furthermore, it should promote regeneration and if necessary, be absorbed after a while or biodegradable [211]. Studies on support-cell interactions are crucial to implants viability. Many cell responses are observed out of different materials, so the cell ability to discriminate and adapt to it whether adhere or not to its surface [212]. This is crucial as it will direct further responses as cell proliferation, migration, and viability.

Due to the clinical importance of skin lesions, many laboratories had been aroused to the search for healing products having benefits including immediate pain relief, close adhesion to the wound bed, and reduced infection rate. The nanocellulose developed having huge superficial area that

Figure 22: Nanocellulose and propolis-based bandage [213].

gives great water absorption capacity and elasticity. These are characteristics from an ideal healing bandage. On the other hand, it holds no microbial activity. Nanocellulose mats are very effective in promoting autolytic debridement, reducing pain, and accelerating granulation, all of which are important for proper wound healing. These nanobiocellulose membranes can be created in any shape and size, which is beneficial for the treatment of large and difficult to cover areas of the body.

Barud [213] has developed a biological membrane with bacterial cellulose and standardized extract of propolis. Propolis has many biological properties including antimicrobial and anti-inflammatory activities. All the above mentioned characteristics present, which make the membrane (Figure 22) a good treatment for burns and chronic wounds.

Odontology is challenged to find ideal materials to replace the bones in several procedures, as bones malformation, maxillary, and facial deformities. The biggest challenge is the loss of alveolar bone. Nanocellulose having suitable porosity which gives the mat an infection barrier, loss of fluids, painkiller effect, allows medicines to be easily applied and it also absorbs the purulent fluids during all inflammatory stages, expelling it later on in a controlled and painless manner [214].

Polyvinyl alcohol (PVA) is a hydrophilic biocompatible polymer with various characteristics desired for biomedical applications. PVA can be transformed into a solid hydrogel with good mechanical properties by physical crosslinking, using freeze-thaw cycles. Hydrophilic nanocellulose fibers of an average diameter of 50 nm are used in combination with PVA to form biocompatible nanocomposites. According to Millon and Wan [215], the resulting nanocomposites possess a broad range of mechanical properties and can be made with mechanical properties similar to that of cardiovascular tissues, such as aorta and heart valve leaflets. On their studies, the stress-strain properties for porcine aorta are matched by at least one type of PVA-nanocellulose nanocomposite in both the circumferential and the axial tissue directions. A PVA-nanocellulose nanocomposite with similar properties as heart valve tissue is also developed. Relaxation properties of all samples, which are important for cardiovascular applications, were also studied and found to relax at a faster rate and to a lower residual stress than the tissues they might replace. So, finally the new PVA-nanocellulose composite is a promising material for cardiovascular soft-tissue replacement applications.

Cai and Kim [216] have three different methods to prepare nanocellulose/PEG composite. In the method I, PEG was incorporated in nanocellulose hydrogels by adding PEG solution to the culture medium for Gluconacetobacter xylinus. In the method II, suspensions of microbial cellulose nanofibers are mixed with PEG solution with mechanical stirring followed by freezing-thawing process. The composite is a hydrogel and can be used for soft tissue replacement devices. In the method III, a previously produced nanocellulose hydrogel was soaked with PEG solution, allowing the PEG molecules to penetrate the nanocellulose [217]. The third method seems simple and effective. It has also been used to prepare other nanocellulose-based composite. For instance, nanocellulose has been soaked into hydroxyapatite to develop a composite scaffold for bone regeneration [218]. Nanocellulose has also been augmented by immersion in solutions of polyacrylamide and gelatin, yielding hydrogels with improved toughness [219]. Similarly, immersion of nanocellulose into poly (vinyl alcohol) has yielded hydrogels having a wide range of mechanical properties of interest for cardiovascular implants [215]. In this study, authors reported method III. SEM images showed that PEG molecules were not only coated on the nanocellulose fibrils surface but also penetrated into the nanocellulose fiber networks. The prepared scaffold has very well-interconnected porous network structure and large aspect surface. The TGA results prove the improved thermal stability. Tensile test results indicated that Young's Modulus and tensile strength tended to decrease while the elongation at break had a slight increase. It showed much better biocompatibility compared with the pure nanocellulose. Thus, the prepared Nanocellulose/PEG composite scaffolds are suitable for cell adhesion/attachment, suggesting that these scaffolds can be used for wound dressing or tissue-engineering applications.

Lin et al. [220] used gelatin and its enzymatically modified form (EMG) to prepare nanocellulose nanocomposites in an attempt to enhance the property of rehydration ability of nanocellulose. Referencing SEM photographs of the low gelatin/nanocellulose composites (LG/NC), gelatin is shown to lodge in nanocellulose networks and wrap up parts of cellulose ribbons (Figure 23(a)). As gelatin content in this sample was around 50% (less than in high gelatin/nanocellulose composites (HG/NC)), a certain quantity of cellulose ribbons emerged. EMG filled up some of the space in the nanocellulose network and some thickened cellulose ribbons could be observed in EMG/NC composites (Figure 23(b)). Film-like structures were observed only less in nonpolar EMG/nanocellulose (NPEMG/NC) and polar (PEMG/NC) composites. Porous networks and thickened cellulose ribbons could be found in these two composites (Figures 23(c) and 23(d)).

It appears that NPEMG and PEMG permeated into the network and adsorbed on the cellulose ribbons, allowing the continuance of porous structures in these composites. According to the results, they concluded that gelatin and its hydrolysates in combination with nanocellulose can effectively improve the rehydration properties of composites.

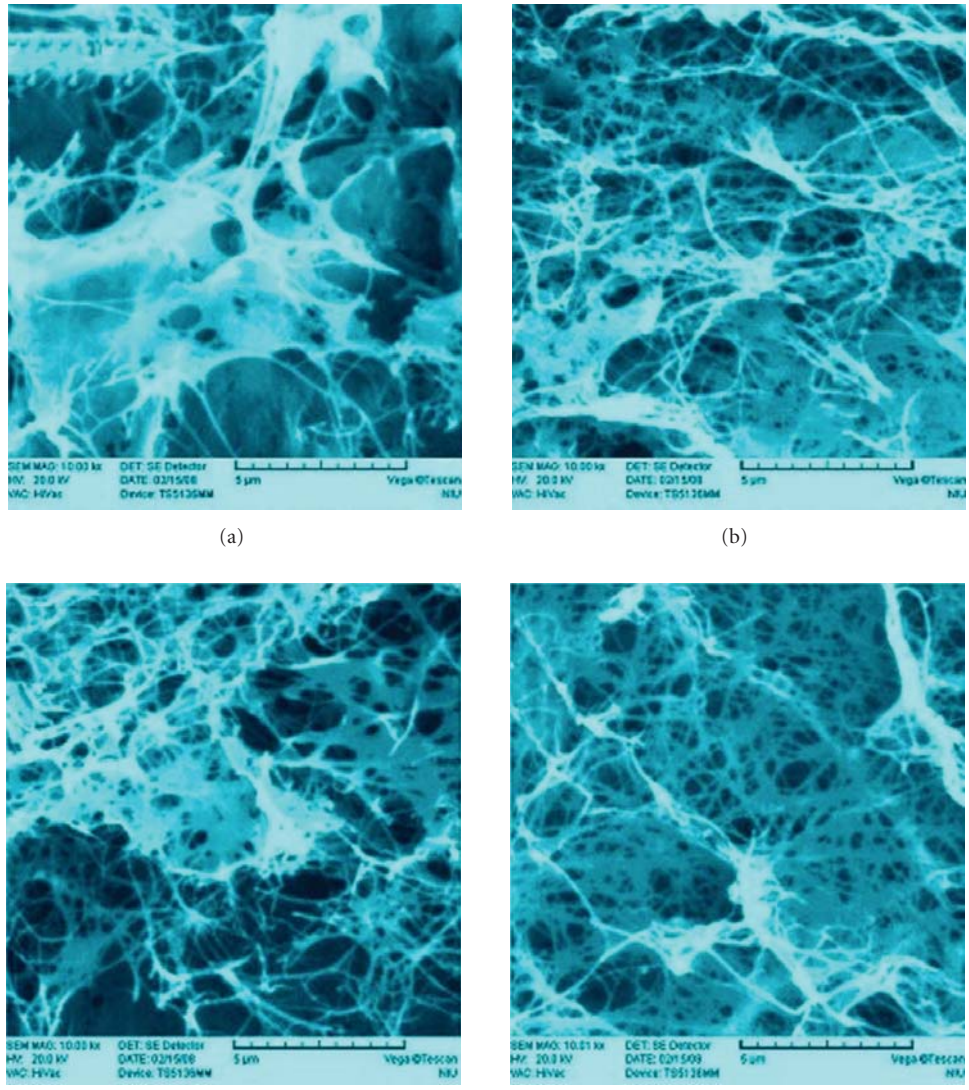

(a) (b)

(c) (d)

Figure 23: SEM photographs (10000X) of LG/NC (a) Gelatin/NC (b) EMG/NC (c) NPEMG/NC (d) PEMG/NC [220].

The polar functional groups of gelatin and EMG as well as nanocellulose porous networks with lower level of crystallinity contributed to the rehydration ability of composites. Nanocellulose immersed in 0.5% EMG solution was sufficient to prepare the desirable composites and may be applied in a rehydratable membrane.

In ophthalmologist area, Huia et al. [221] explored the potentiality of nanocellulose applied as the scaffold of tissue engineering cornea. They studied the growth of human corneal stromal cells on nanocellulose. The ingrowth of corneal stromal cells into the scaffold was verified by laser-scanning confocal microscope. The results suggest the potentiality for this biomaterial as a scaffold for tissue engineering of artificial cornea. The surface of nanocellulose is lumpy with rills. In Figures 24(a) and 24(b), the red regions are corneal stromal cells immunofluorescent stained by Vim and the blue region is the nanocellulose scaffold. It is clearly illustrated that corneal stromal cells ingrew into the scaffold.

For otorhinolaryngologist, surgery of the lateral wall of the nose is common procedure in the ENT specialty and was recommended for resection of soft lush, removal of tumors, or to promote aeration of the sinuses. The evolution of surgical techniques provided increased safety to patients, drastically reducing the complications and postoperative morbidity. The nasal bleeding, surgical wound infections, local pain, and the presence of adhesions are the major complicating factors related to nasal surgery. Several types of materials have been developed in order to prevent these complications. Nasal packing has been used in these postsurgical procedures and, although effective in preventing bleeding, requires removal causing great discomfort to the patient. Moreover, their presence has been associated with systemic infections graves.

The use of a material that, in addition to preventing bleeding, could provide more rapid healing without the formation of crusts and prevent infection without the need

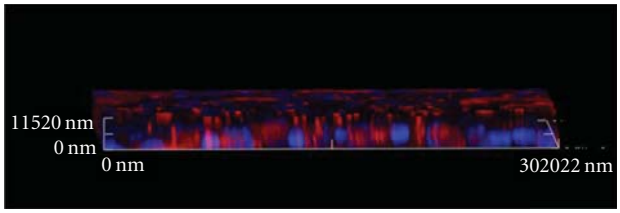

(a)

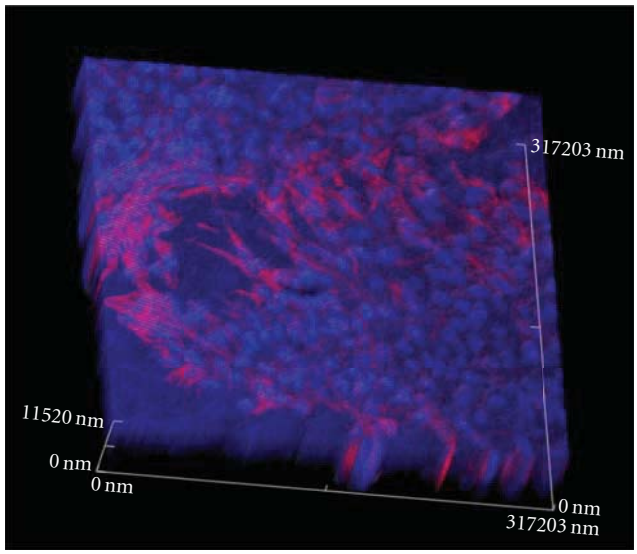

(b)

Figure 24: Growth of Vim immune fluorescent stained human corneal stromal cells in nanocellulose scaffold, observed by LSCM (400X) [221].

for removal would be of great aid in the postoperative period of patients undergoing resection of the lower nasal concha and other nasal surgeries. In 1984, microbiologist Louis Farah Fernando Xavier was able, through the fermentation of bacteria of the genus Acetobacter, to produce bacterial cellulose. The resulting film of this synthesis, after processing, is endowed with selective permeability, allowing passage of water vapour but preventing the passage of microorganisms. It is semitransparent, homogeneous, with an average thickness of 0.05 mm and visually very similar to human skin. Schumann et al. [222] studied the artificial vascular implants from nanocellulose by two studies. In a first microsurgical study, the nanocellulose implants were attached in an artificial defect of the carotid artery of rats for 1 year. These long-term results show the incorporation of the nanocellulose under formation of neointima and ingrowth of active fibroblasts. In a second study, the grafts were used to replace the carotid arteries of pigs. After 3 months, these grafts were removed and analyzed both macro- and microscopically. Seven grafts (87.5%) were patent whereas one graft was found occluded. These data indicate that the innovative nanocellulose engineering technique results in the production of stable vascular conduits and confirm a highly attractive approach to in vivo tissue-engineered blood vessels as part of programs in cardiovascular surgery. The Figure 25 shows the untreated segment of carotid artery revealing a homogeneous endothelialization inside the grafts with an almost smooth transition to the artery.

Another use of nanocellulose is for nasal reconstruction. The desire for an ideal shape has always been part of mankind. Nose, centrally located in the face, is better susceptible to traumas, deformities, thus social disorders. Even since having a major breathing function, it has a great esthetic function, highlighting face's genetics. Amorim et al. [223] evaluated the tissue response to the presence of nanocellulose in the nose bone (Figure 26). It had been used 22 rabbits, being that, in 20 a cellulose blanket was implanted in the nasal dorsum, 2 were kept as control group. After three and six months, the back bone was extirpated for further histopathological study, parameter, were such as blood vessels clogging, inflammation intensity, and presence of purulent fluids.

Inflammation was found to be stable, which is probably due to the surgical procedure itself and not to the cellulosic blanket. For the other parameters, there was no statistical significance. Nanocellulosic blanket showed good biocompatibility and did not change over time, thus an excellent material to elevate the nose bone.

7.2.4. Veterinary. Hart et al. [224] studied the pellicle and its ability to promote fibroblast migration and cellular proliferation in diabetic rats. The treatment accelerated the wound healing for the diabetic rats and improved histological outcome. Diabetic rat is a recognized model for chronic wounds, thus sharing some features with the chronic human wound. So they could predict the applicability in humans.

Helenius et al. [225] studied for the first time the in vivo biocompatibility of nanocellulose systematically. Thus, in the development nanocellulose membrane was implanted into the subcutaneous space of rats for 1, 4, and 12 weeks. The implants were evaluated in aspects of chronic inflammation, foreign body responses, cell ingrowth, and angiogenesis, using histology, immunohistochemistry, and electron microscopy. There were no macroscopic signs of inflammation around the implants (redness, edema or exudates) (Figure 27). There were no microscopic signs of inflammation either (i.e., a high number of small cells around the implants or the blood vessels). No fibrotic capsule or giant cells were present. Fibroblasts infiltrated nanocellulose (Figure 28), which was well integrated into the host tissue and did not elicit any chronic inflammatory reactions, so the biocompatibility of nanocellulose is proved and the material has potential to be used as a scaffold in tissue engineering.

Helenius et al. [225] brought up more knowledge on biomaterial and its interaction with the cell. In their study, membranes of nanocellulose had been implanted into rats and the biocompatibility was evaluated in vivo. Implants did not cause "foreign body reaction," fibrosis or encapsulation, and the rat's conjunctive tissues were well integrated to nanocellulose. Some weeks after the implantation, the rearrangement kept on happening and fibroblasts were fully integrated to the cellulosic structure, they had started to synthesize collagen.

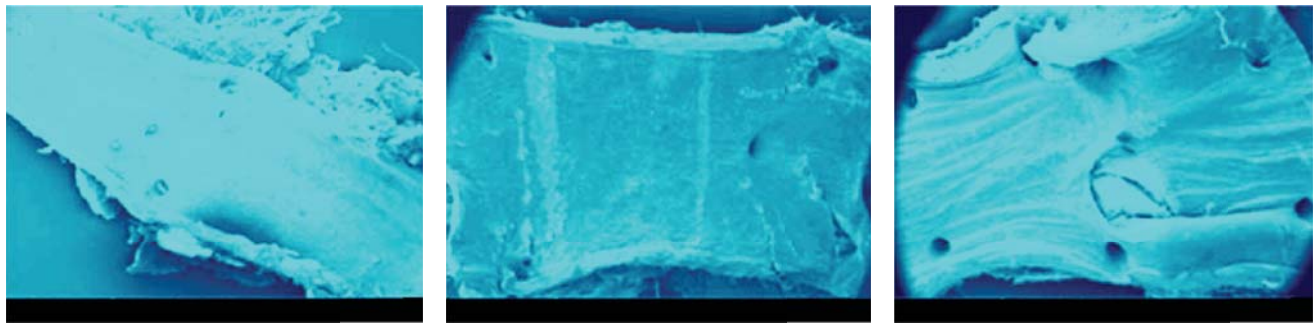

(a) (b) (c)

Figure 25: SEM (magnification 169× to 199×): (a) untreated segment of the carotid artery, (b) and (c) good endothelialization of nanocellulose grafts [222].

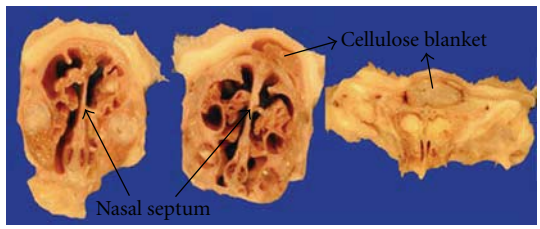

Figure 26: Serial cut from the nasal septum and front part of the nose showing the cellulose blanket in the nose bone structure.

Figure 27: Explantation of implants after 1 week [225].

Helenius et al. [225] had also shown that the density influenciates the morphology and cell penetration such as density increased, cell migration lowed. It was observed that nucleus morphology depends on the direction taken by the cellulosic nanofiber, blood flow was also observed.

Fewer cells are present compared to that after 1 and 4 weeks and the fibroblasts inside the nanocellulose have synthesized collagen (B) high magnification of the interface area at the porous side of nanocellulose after 12 weeks. Arrow heads show collagen synthesized by the fibroblasts

Silva [226] had evaluated the biological behavior of synthetic hydroxyapatite (HAP-91) when implanted in the dental cavities and covered by nanocellulose. Membranes were shaped into triangles fully covering the cavities avoiding the contact between hydroxyapatite and the oral cavity (a source of contaminants, Figure 29). Silva found that nanocellulose associated to the HAP promoted faster bone regeneration if compared with the control group. 8 days after procedure and a delay of 30 days, although after 50 days they had tissues alike.

Costa and de Souza [227] studied the skin healing in white swines; they underwent thermal abrasion, (metal temperature at 100°C). Comparing Bionext to the daily healing bandage, all the animals had the healing process completed equally. No differences were seen between the daily bandage and the cellulose pellicle (Bionext®).

For dogs whose peritoneum had been replaced, it was observed that 45 days after the implant, fibroblasts and blood vessels numbers increased. After 90 days, collagen and fibroblasts penetrated into nanocellulose and 180 days after implantation nanocellulose formed a net along the conjunctive tissue, little evidence of neovascularization was found [228].

7.2.5. Dental. Nanocellulose was tested in dental tissue regeneration. Microbial cellulose, produced by the Glucanacetobacter xylinus strain, can be used to regenerate dental tissues in humans (Figure 30).

Nanocellulose product Gengiflex and Gore-Tex has intended applications within the dental industry. It was developed to aid periodontal tissue recovery [229]. A description was given of a complete restoration of an osseus defect around an IMZ implant in association with a Gengiflex therapy. The benefits included the reestablishment of aesthetics and function of the mouth and that a reduced number of surgical steps were required.

The bandage, called Gengiflex, consists of two layers: the inner layer is composed of microbial cellulose, which offers rigidity to the membrane, and the outer alkali-cellulose layer is chemically modified [230]. Salata et al. [231] compared the biological performance of Gengiflex and Gore-Tex membranes using the in vivo nonhealing bone-defect model proposed by Dahlin et al. [232].

The study showed that Gore-Tex membranes (a composite with polytetrafluoroethylene, urethane, and nylon) were associated with significantly less inflammation and both membranes promoted the same amount of bone formation

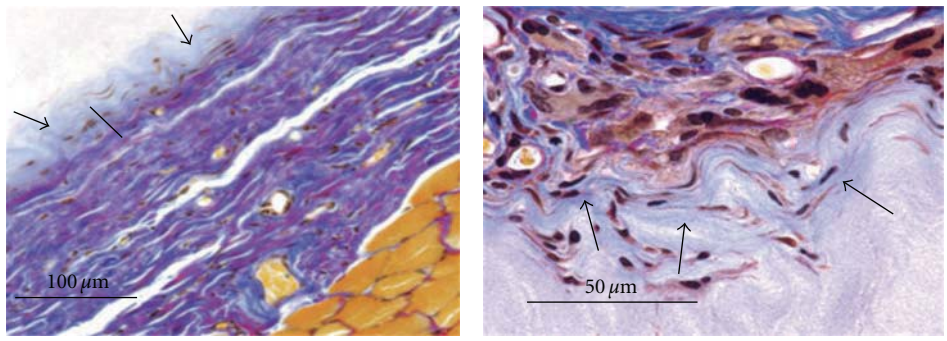

(a) (b)

Figure 28: Ladewig's trichrome staining. (a) The compact side after 12 weeks showing the fibroblasts inside the nanocellulose have synthesized collagen (seen as blue staining; indicated with arrow heads), (b) High magnification of the interface area at the porous side of nanocellulose after 12 weeks (Arrow heads show collagen synthesized by the fibroblasts) [225].

Figure 29: Cellulosic membranes used as dental cavities covering in cats [226].

Figure 30: Nanocellulose used in dental tissue regeneration in 39-year-old female patient.

during the same period of time. A greater amount of bone formation was present in bone defects protected by either Gore-Tex or microbial cellulose membrane, when compared to the control sites. Gore-Tex is better tolerated by the tissues than Gengiflex. Recently, in a similar vein, Macedo et al. [233] also compared bacterial cellulose and polytetrafluoroethylene (PTFE) as physical barriers used to treat bone defects in guided tissue regeneration. In this study, two osseous defects (8 mm in diameter) were performed in each hind-foot of four adult rabbits, using surgical burs with constant sterile saline solution irrigation. The effects obtained on the right hind-feet were protected with PTFE barriers, while Gengiflex membranes were used over wounds created in the left hind-feet. After 3 months, the histological evaluation of the treatments revealed that the defects covered with PTFE barriers were completely repaired with bone tissue, whereas incomplete lamellar bone formation was detected in defects treated with Gengiflex membranes, resulting in voids and lack of continuity of bone deposition.

Nanocellulose with its characteristics like nanofibers size and distribution, mechanical properties, compatibility, and ability to mold create it has a unique biomaterial indispensable in health area. The nanocellulose composite scaffolds are biocompatible with less rejection with cellular contact and

blood contact cells interaction to be a promissory biomaterial and may be suitable for cell adhesion/attachment suggesting that these scaffolds can be used for wound-dressing or tissue-engineering scaffolds.

8. Conclusions

The potential applicability of cellulose-based biocomposites and nanocomposites is widely extended. Due to a great number of properties, applications of nanocellulose-based materials are mainly considered to be in a wide range of applications such as paper and packaging products, construction, automotive, furniture, and electronics. Pharmacy, cosmetics, and biomedical applications are also being considered. The mechanical properties such as high strength and stiffness, the surface reactivity (with numerous hydroxyl groups), the specific organization as well as the small dimensions of nanocellulose may well impart useful properties to (nano)composite materials reinforced with these fibers.

References

[1] S. Kalia, B. S. Kaith, and I. Kaur, "Pretreatments of natural fibers and their application as reinforcing material in polymer composites-a review," *Polymer Engineering and Science*, vol. 49, no. 7, pp. 1253–1272, 2009.

[2] I. Siro and D. Plackett, "Microfibrillated cellulose and new nanocomposite materials: a review," *Cellulose*, vol. 17, no. 3, pp. 459–494, 2010.

[3] S. J. Eichhorn, A. Dufresne, M. Aranguren et al., "Review: current international research into cellulose nanofibres and nanocomposites," *Journal of Materials Science*, vol. 45, no. 1, pp. 1–33, 2010.

[4] A. K. Bledzki, S. Reihmane, and J. Gassan, "Properties and modification methods for vegetable fibers for natural fiber composites," *Journal of Applied Polymer Science*, vol. 59, no. 8, pp. 1329–1336, 1996.

[5] P. R. Hornsby, E. Hinrichsen, and K. Tarverdi, "Preparation and properties of polypropylene composites reinforced with wheat and flax straw fibres: part II analysis of composite microstructure and mechanical properties," *Journal of Materials Science*, vol. 32, no. 4, pp. 1009–1015, 1997.

[6] K. Oksman, L. Wallstrom, L. A. Berglund, and R. D. T. Filho, "Morphology and mechanical properties of unidirectional sisal-epoxy composites," *Journal of Applied Polymer Science*, vol. 84, no. 13, pp. 2358–2365, 2002.

[7] D. N. Saheb and J. P. Jog, "Natural fiber polymer composites: a review," *Advances in Polymer Technology*, vol. 18, no. 4, pp. 351–363, 1999.

[8] S. T. Georgopoulos, P. A. Tarantili, E. Avgerinos, A. G. Andreopoulos, and E. G. Koukios, "Thermoplastic polymers reinforced with fibrous agricultural residues," *Polymer Degradation and Stability*, vol. 90, no. 2, pp. 303–312, 2005.

[9] R. L. Crawford, *Lignin Biodegradation and Transformation*, John Wiley & Sons, New York, NY, USA, 1981.

[10] A. Payen, "Mémoire sur la composition du tissu propre des plantes et du ligneux," *Comptes Rendus*, vol. 7, pp. 1052–1056, 1838.

[11] Dorée, *The Methods of Cellulose Chemistry*, Chapman & Hall, London, UK, 1947.

[12] *The Merck Index*, Merck & Co, Rahway, NJ, USA, 8th edition, 1968.

[13] http://www.fibersource.com/f-tutor/cellulose.htm.

[14] P. M. Visakh and S. Thomas, "Preparation of bionanomaterials and their polymer nanocomposites from waste and biomass," *Waste and Biomass Valorization*, vol. 1, no. 1, pp. 121–134, 2010.

[15] G. I. Williams and R. P. Wool, "Composites from natural fibers and soy oil resins," *Applied Composite Materials*, vol. 7, no. 5-6, pp. 421–432, 2000.

[16] F. G. Torres and R. M. Diaz, "Morphological characterisation of natural fibre reinforced thermoplastics (NFRTP) processed by extrusion, compression and rotational moulding," *Polymers & Polymer Composites*, vol. 12, no. 8, pp. 705–718, 2004.

[17] M. Z. Rong, M. Q. Zhang, Y. Liu, G. C. Yang, and H. M. Zeng, "The effect of fiber treatment on the mechanical properties of unidirectional sisal-reinforced epoxy composites," *Composites Science and Technology*, vol. 61, Article ID 10.1016/S0266-3538(01)00046-X, pp. 1437–1447, 2001.

[18] K. Van de Velde and P. Kiekens, "Thermoplastic pultrusion of natural fibre reinforced composites," *Composite Structures*, vol. 54, no. 2-3, pp. 355–360, 2001.

[19] H. L. Bos, M. J. A. van den Oever, and O. C. J. J. Peters, "Tensile and compressive properties of flax fibres for natural fibre reinforced composites," *Journal of Materials Science*, vol. 37, no. 8, pp. 1683–1692, 2002.

[20] C. Baley, "Analysis of the flax fibres tensile behaviour and analysis of the tensile stiffness increase," *Composites Part A*, vol. 33, no. 7, pp. 939–948, 2002.

[21] B. Lamy and C. Baley, "Stiffness prediction of flax fibers-epoxy composite materials," *Journal of Materials Science Letters*, vol. 19, no. 11, pp. 979–980, 2000.

[22] A. Jähn, M. W. Schröder, M. Füting, K. Schenzel, and W. Diepenbrock, "Characterization of alkali treated flax fibres by means of FT Raman spectroscopy and environmental scanning electron microscopy," *Spectrochimica Acta Part A*, vol. 58, no. 10, pp. 2271–2279, 2002.

[23] J. Gassan and A. K. Bledzki, "Einfluß von haftvermittlern auf das feuchteverhalten naturfaserverstärkter kunststoffe," *Die Angewandte Makromolekulare Chemie*, vol. 236, pp. 129–138, 1996.

[24] A. J. Michell, "Wood cellulose-organic polymer composites," in *Composite Asia Pacific*, vol. 89, p. 19, Institute of Australia, Adelaide, Australia, 1989.

[25] T. M. Maloney, in *International Encyclopedia of Composites*, S. M. Lee and R. M. Rowell, Eds., p. 656, VCH Publishers, New York, USA, 1995.

[26] K. P. Mieck, A. Nechwatal, and C. Knobelsdorf, "Potential applications of natural fibres in composite materials," *Melliand Textilberichte*, vol. 75, no. 11, p. 892, 1994.

[27] P. S. Mukherjee and K. G. Satyanarayana, "An empirical evaluation of structure-property relationships in natural fibres and their fracture behaviour," *Journal of Materials Science*, vol. 21, no. 12, pp. 4162—4168, 1986.

[28] A. Alemdar and M. Sain, "Biocomposites from wheat straw nanofibers: morphology, thermal and mechanical properties," *Composites Science and Technology*, vol. 68, no. 2, pp. 557–565, 2008.

[29] A. Alemdar and M. Sain, "Isolation and characterization of nanofibers from agricultural residues—wheat straw and soy hulls," *Bioresource Technology*, vol. 99, no. 6, pp. 1664–1671, 2008.

[30] T. Zimmermann, N. Bordeanu, and E. Strub, "Properties of nanofibrillated cellulose from different raw materials and its

reinforcement potential," *Carbohydrate Polymers*, vol. 79, no. 4, pp. 1086–1093, 2010.

[31] B. Wang and M. Sain, "Dispersion of soybean stock-based nanofiber in a plastic matrix," *Polymer International*, vol. 56, no. 4, pp. 538–546, 2007.

[32] A. Kaushik, M. Singh, and G. Verma, "Green nanocomposites based on thermoplastic starch and steam exploded cellulose nanofibrils from wheat straw," *Carbohydrate Polymers*, vol. 82, no. 2, pp. 337–345, 2010.

[33] S. Kalia, S. Vashistha, and B. S. Kaith, "Cellulose nanofibers reinforced bioplastics and their applications," in *Handbook of Bioplastics and Biocomposites Engineering Applications*, S. Pilla, Ed., chapter 16, Wiley-Scrivener Publishing, New York, NY, USA, 2011.

[34] E. M. Teixeira, A. C. Corrêa, C. R. de Oliveira et al., "Cellulose nanofibers from white and naturally colored cotton fibers," *Cellulose*, vol. 17, no. 3, pp. 595–606, 2010.

[35] W. Stelte and A. R. Sanadi, "Preparation and characterization of cellulose nanofibers from two commercial hardwood and softwood pulps," *Industrial and Engineering Chemistry Research*, vol. 48, no. 24, pp. 11211–11219, 2009.

[36] S. Kalia, B. S. Kaith, S. Sharma, and B. Bhardwaj, "Mechanical properties of flax-g-poly(methyl acrylate) reinforced phenolic composites," *Fibers and Polymers*, vol. 9, no. 4, pp. 416–422, 2008.

[37] R. Agrawal, N. S. Saxena, K. B. Sharma, S. Thomas, and M. S. Sreekala, "Activation energy and crystallization kinetics of untreated and treated oil palm fibre reinforced phenol formaldehyde composites," *Materials Science and Engineering A*, vol. 277, no. 1-2, pp. 77–82, 2000.

[38] F. M. B. Coutinho, T. H. S. Costa, and D. L. Carvalho, "Polypropylene-wood fiber composites: effect of treatment and mixing conditions on mechanical properties," *Journal of Applied Polymer Science*, vol. 65, no. 6, pp. 1227–1235, 1997.

[39] L. González, A. Rodríguez, J. L. de Benito, and A. Marcos-Fernández, "Applications of an azide sulfonyl silane as elastomer crosslinking and coupling agent," *Journal of Applied Polymer Science*, vol. 63, no. 10, pp. 1353–1359, 1997.

[40] S. R. Culler, H. Ishida, and J. L. Koenig, "silane interphase of composites: effect of process conditions on gamma - aminopropyltriethoxysilane," *Polymer Composites*, vol. 7, no. 4, pp. 231–238, 1986.

[41] N. D. Ghatge and R. S. Khisti, "Performance of new silane coupling agents along with phenolic nobake binder for sand core," *Journal of Polymer Materials*, vol. 6, no. 3, pp. 145–149, 1989.

[42] M. S. Sreekala, M. G. Kumaran, S. Joseph, M. Jacob, and S. Thomas, "Oil palm fibre reinforced phenol formaldehyde composites: influence of fibre surface modifications on the mechanical performance," *Applied Composite Materials*, vol. 7, no. 5-6, pp. 295–329, 2000.

[43] I. Van De Weyenberg, J. Ivens, A. De Coster, B. Kino, E. Baetens, and I. Verpoest, "Influence of processing and chemical treatment of flax fibres on their composites," *Composites Science and Technology*, vol. 63, no. 9, pp. 1241–1246, 2003.

[44] A. Valadez-Gonzalez, J. M. Cervantes-Uc, R. Olayo, and P. J. Herrera-Franco, "Chemical modification of henequen fibers with an organosilane coupling agent," *Composites Part B*, vol. 30, no. 3, pp. 321–331, 1999.

[45] D. Ray, B. K. Sarkar, A. K. Rana, and N. R. Bose, "Effect of alkali treated jute fibres on composite properties," *Bulletin of Materials Science*, vol. 24, no. 2, pp. 129–135, 2001.

[46] K. Joseph, L. H. C. Mattoso, R. D. Toledo et al., "Natural fiber reinforced thermoplastic composites," in *Natural Polymers and Agrofibers Composites*, E. Frollini, A. L. Leão, and L. H. C. Mattoso, Eds., chapter 4, pp. 159–201, Embrapa, Sãn Carlos, Brazil, 2000.

[47] J. Gassan and A. K. Bledzki, "Alkali treatment of jute fibers: relationship between structure and mechanical properties," *Journal of Applied Polymer Science*, vol. 71, no. 4, pp. 623–629, 1999.

[48] C. Garcia-Jaldon, D. Dupeyre, and M. R. Vignon, "Fibres from semi-retted hemp bundles by steam explosion treatment," *Biomass and Bioenergy*, vol. 14, no. 3, pp. 251–260, 1998.

[49] E. S. Rodriguez, P. M. Stefani, and A. Vazquez, "Effects of fibers' alkali treatment on the resin transfer molding processing and mechanical properties of Jute—Vinylester composites," *Journal of Composite Materials*, vol. 41, no. 14, pp. 1729–1741, 2007.

[50] L. A. Pothan, C. N. George, M. Jacob, and S. Thomas, "Effect of chemical modification on the mechanical and electrical properties of banana fiber polyester composites," *Journal of Composite Materials*, vol. 41, no. 19, pp. 2371–2386, 2007.

[51] A. Paul, S. Joseph, and S. Thomas, "A study of the influence of interfacial damage on stress concentrations in unidirectional composites," *Composites Science and Technology*, vol. 57, p. 67, 1997.

[52] M. S. Sreekala, M. G. Kumaran, and S. Thomas, "Water sorption in oil palm fiber reinforced phenol formaldehyde composites," *Composites Part A*, vol. 33, no. 6, pp. 763–777, 2002.

[53] B. Wang, S. Panigrahi, L. Tabil, and W. Crerar, "Pre-treatment of flax fibers for use in rotationally molded biocomposites," *Journal of Reinforced Plastics and Composites*, vol. 26, no. 5, pp. 447–463, 2007.

[54] S. Kalia, V. K. Kaushik, and R. K. Sharma, "Effect of benzoylation and graft copolymerization on morphology, thermal stability, and crystallinity of sisal fibers," *Journal of Natural Fibers*, vol. 8, no. 1, p. 27, 2011.

[55] B. Wang, "Pre-treatment of flax fibers for use in rotationally molded biocomposites," M.S. thesis, University of Saskatchewan, Saskatoon, Canada, 2004.

[56] B. S. Kaith, A. S. Singha, S. Kumar, and B. N. Misra, "FAS-H2O2 initiated graft copolymerization of methylmethacrylate onto flax and evaluation of some physical and chemical properties," *Journal of Polymer Materials*, vol. 22, no. 4, pp. 425–432, 2005.

[57] S. Kalia, A. Kumar, and B. S. Kaith, *Advanced Materials Letters*, vol. 2, p. 17, 2011.

[58] M. Tsukada, S. Islam, T. Arai, A. Boschi, and G. Freddi, "Microwave irradiation technique to enhance protein fibre properties," *Autex Research Journal*, vol. 5, no. 1, pp. 40–48, 2005.

[59] B. S. Kaith and S. Kalia, "Preparation of microwave radiation induced graft copolymers and their applications as reinforcing material in phenolic composites," *Polymer Composites*, vol. 29, no. 7, pp. 791–797, 2008.

[60] B. S. Kaith and S. Kalia, "Graft copolymerization of MMA onto flax under different reaction conditions: a comparative study," *Express Polymer Letters*, vol. 2, no. 2, pp. 93–100, 2008.

[61] M. Pommet, J. Juntaro, J. Y. Y. Heng et al., "Surface modification of natural fibers using bacteria: depositing bacterial cellulose onto natural fibers to create hierarchical fiber reinforced nanocomposites," *Biomacromolecules*, vol. 9, no. 6, pp. 1643–1651, 2008.

[62] M. Shoda and Y. Sugano, "Recent advances in bacterial cellulose production," *Biotechnology and Bioprocess Engineering*, vol. 10, no. 1, pp. 1–8, 2005.

[63] M. Iguchi, S. Yamanaka, and A. Budhiono, "Bacterial cellulose—a masterpiece of nature's arts," *Journal of Materials Science*, vol. 35, no. 2, pp. 261–270, 2000.

[64] E. E. Brown and M. P. G. Laborie, "Bioengineering bacterial cellulose/poly(ethylene oxide) nanocomposites," *Biomacromolecules*, vol. 8, no. 10, pp. 3074–3081, 2007.

[65] A. N. Nakagaito and H. Yano, "Novel high-strength biocomposites based on microfibrillated cellulose having nano-order-unit web-like network structure," *Applied Physics A*, vol. 80, no. 1, pp. 155–159, 2005.

[66] D. J. Gardner, G. S. Oporto, R. Mills, and M. Samir, "Adhesion and surface issues in cellulose and nanocellulose," *Journal of Adhesion Science and Technology*, vol. 22, pp. 545–545, 2008.

[67] S. Kalia and R. Sheoran, "Modification of ramie fibers using microwave-assisted grafting and cellulase enzyme—assisted biopolishing: a comparative study of morphology, thermal stability, and crystallinity," *International Journal of Polymer Analysis and Characterization*, vol. 16, no. 5, pp. 307–318, 2011.

[68] J. Njuguna, P. Wambua, K. Pielichowski, and K. Kayvantash, "Natural Fiber-reinforced polymer composites and nanocomposites for automotive applications," in *Cellulose Fibers: Bio- and Nano-Polymer Composites*, S. Kalia, B. S. Kaith, and I. Kaur, Eds., Springer, Heidelberg, Germany, 2011.

[69] S. Mishra, A. K. Mohanty, L. T. Drzal, M. Misra, and G. Hinrichsen, "A review on pineapple leaf fibers, sisal fibers and their biocomposites," *Macromolecular Materials and Engineering*, vol. 289, no. 11, pp. 955–974, 2004.

[70] P. Wambua, J. Ivens, and I. Verpoest, "Natural fibres: can they replace glass in fibre reinforced plastics?" *Composites Science and Technology*, vol. 63, no. 9, pp. 1259–1264, 2003.

[71] J. Summerscales, N. Dissanayake, A. Virk, and W. Hall, "A review of bast fibres and their composites. Part 2—composites," *Composites Part A*, vol. 41, no. 10, pp. 1336–1344, 2010.

[72] A. K. Bledzki and J. Gassan, "Composites reinforced with cellulose based fibres," *Progress in Polymer Science*, vol. 24, no. 2, pp. 221–274, 1999.

[73] R. Gauthier, C. Joly, A. C. Coupas, H. Gauthier, and M. Escoubes, "Interfaces in polyolefin/cellulosic fiber composites: chemical coupling, morphology, correlation with adhesion and aging in moisture," *Polymer Composites*, vol. 19, no. 3, pp. 287–300, 1998.

[74] J. George, M. S. Sreekala, and S. Thomas, "A review on interface modification and characterization of natural fiber reinforced plastic composites," *Polymer Engineering & Science*, vol. 41, no. 9, pp. 1471–1485, 2001.

[75] Y. Xie, C. A. S. Hill, Z. Xiao, H. Militz, and C. Mai, "Silane coupling agents used for natural fiber/polymer composites: a review," *Composites Part A*, vol. 41, no. 7, pp. 806–819, 2010.

[76] J. Gassan and A. K. Bledzki, "Effect of cyclic moisture absorption desorption on the mechanical properties of silanized jute-epoxy composites," *Polymer Composites*, vol. 20, no. 4, pp. 604–611, 1999.

[77] A. K. Mohanty, M. Misra, and L. T. Drzal, Eds., *Natural Fibers, Biopolymers, and Biocomposites*, CRC Press, Boca Raton, Fla, USA, 2005.

[78] H. L. Bos, J. Müssig, and M. J. A. van den Oever, "Mechanical properties of short-flax-fibre reinforced compounds," *Composites Part A*, vol. 37, no. 10, pp. 1591–1604, 2006.

[79] H. L. Bos, *The potential of flax fibers as reinforcement for composite materials*, Ph.D. thesis, Technische Universiteit Eindhoven, Eindhoven, The Netherlands, 2004.

[80] S. K. Garkhail, R. W. H. Heijenrath, and T. Peijs, "Mechanical properties of natural-fibre-mat-reinforced thermoplastics based on flax fibres and polypropylene," *Applied Composite Materials*, vol. 7, no. 5-6, pp. 351–372, 2000.

[81] T. Nishino, "Natural fiber sources," in *Green Composites: Polymer Composites and the Environment*, CRC Press, Boca Raton, Fla, USA, 2004.

[82] A. Espert, F. Vilaplana, and S. Karlsson, "Comparison of water absorption in natural cellulosic fibres from wood and one-year crops in polypropylene composites and its influence on their mechanical properties," *Composites Part A*, vol. 35, no. 11, pp. 1267–1276, 2004.

[83] M. M. Thwe and K. Liao, "Durability of bamboo-glass fiber reinforced polymer matrix hybrid composites," *Composites Science and Technology*, vol. 63, no. 3-4, pp. 375–387, 2003.

[84] C. Pavithran, P. S. Mukherjee, and M. Brahmakumar, "Coir-glass intermingled fibre hybrid composites," *Journal of Reinforced Plastics and Composites*, vol. 10, no. 1, pp. 91–101, 1991.

[85] B. C. Tobias, "Tensile and Impact behaviour of natural fiber-reinforced composite materials," in *Proceedings of the International Conference on Advanced Composite Materials*, T. D. A. K. Chandra, Ed., The Minerals, Metals and Materials Society, 1993.

[86] H. D. Mueller, "Improving the impact strength of natural fiber reinforced composites by specifically designed material and process parameters," *IJN Winter*, 2004.

[87] J. C. M. De Bruijn, "Natural fibre mat thermoplastic products from a processor's point of view," *Applied Composite Materials*, vol. 7, no. 5-6, pp. 415–420, 2000.

[88] J. Gassan, "A study of fibre and interface parameters affecting the fatigue behaviour of natural fibre composites," *Composites Part A*, vol. 33, no. 3, pp. 369–374, 2002.

[89] H. Savastano Jr., S. F. Santos, M. Radonjic, and W. O. Soboyejo, "Fracture and fatigue of natural fiber-reinforced cementitious composites," *Cement and Concrete Composites*, vol. 31, no. 4, pp. 232–243, 2009.

[90] A. N. Towo and M. P. Ansell, "Fatigue of sisal fibre reinforced composites: constant-life diagrams and hysteresis loop capture," *Composites Science and Technology*, vol. 68, no. 3-4, pp. 915–924, 2008.

[91] A. N. Towo and M. P. Ansell, "Fatigue evaluation and dynamic mechanical thermal analysis of sisal fibre-thermosetting resin composites," *Composites Science and Technology*, vol. 68, no. 3-4, pp. 925–932, 2008.

[92] T. Yuanjian and D. H. Isaac, "Impact and fatigue behaviour of hemp fibre composites," *Composites Science and Technology*, vol. 67, no. 15-16, pp. 3300–3307, 2007.

[93] M. Henriksson, G. Henriksson, L. A. Berglund, and T. Lindström, "An environmentally friendly method for enzyme-assisted preparation of microfibrillated cellulose (MFC) nanofibers," *European Polymer Journal*, vol. 43, no. 8, pp. 3434–3441, 2007.

[94] T. Saito, S. Kimura, Y. Nishiyama, and A. Isogai, "Cellulose nanofibers prepared by TEMPO-mediated oxidation of native cellulose," *Biomacromolecules*, vol. 8, no. 8, pp. 2485–2491, 2007.

[95] L. Wågberg, G. Decher, M. Norgren, T. Lindström, M. Ankerfors, and K. Axnäs, "The build-up of polyelectrolyte multilayers of microfibrillated cellulose and cationic polyelectrolytes," *Langmuir*, vol. 24, no. 3, pp. 784–795, 2008.

[96] M. E. Malainine, M. Mahrouz, and A. Dufresne, "Thermoplastic nanocomposites based on cellulose microfibrils from opuntia ficus-indica parenchyma cell," *Composites Science and Technology*, vol. 65, no. 10, pp. 1520–1526, 2005.

[97] Y. Habibi, A. L. Goffin, N. Schiltz, E. Duquesne, P. Dubois, and A. Dufresne, "Bionanocomposites based on poly(ε-caprolactone)-grafted cellulose nanocrystals by ring-opening polymerization," *Journal of Materials Chemistry*, vol. 18, no. 41, pp. 5002–5010, 2008.

[98] M. Grunert and W. T. Winter, "Nanocomposites of cellulose acetate butyrate reinforced with cellulose nanocrystals," *Journal of Polymers and the Environment*, vol. 10, no. 1-2, pp. 27–30, 2002.

[99] N. L. Garcia de Rodriguez, W. Thielemans, and A. Dufresne, "Sisal cellulose whiskers reinforced polyvinyl acetate nanocomposites," *Cellulose*, vol. 13, no. 3, pp. 261–270, 2006.

[100] I. Kvien, B. S. Tanem, and K. Oksman, "Characterization of cellulose whiskers and their nanocomposites by atomic force and electron microscopy," *Biomacromolecules*, vol. 6, no. 6, pp. 3160–3165, 2005.

[101] M. A. S. A. Samir, F. Alloin, M. Paillet, and A. Dufresne, "Tangling effect in fibrillated cellulose reinforced nanocomposites," *Macromolecules*, vol. 37, no. 11, pp. 4313–4316, 2004.

[102] M. N. Anglès and A. Dufresne, "Plasticized starch/tuniein whiskers nanocomposites. 1. Structural analysis," *Macromolecules*, vol. 33, no. 22, pp. 8344–8353, 2000.

[103] W. Helbert, J. Y. Cavaillé, and A. Dufresne, "Thermoplastic nanocomposites filled with wheat straw cellulose whiskers. Part I: processing and mechanical behavior," *Polymer Composites*, vol. 17, no. 4, pp. 604–611, 1996.

[104] K. Fleming, D. Gray, S. Prasannan, and S. Matthews, "Cellulose crystallites: a new and robust liquid crystalline medium for the measurement of residual dipolar couplings," *Journal of the American Chemical Society*, vol. 122, no. 21, pp. 5224–5225, 2000.

[105] Y. Pu, J. Zhang, T. Elder, Y. Deng, P. Gatenholm, and A. J. Ragauskas, "Investigation into nanocellulosics versus acacia reinforced acrylic films," *Composites Part B*, vol. 38, no. 3, pp. 360–366, 2007.

[106] A. B. Elmabrouk, T. Wim, A. Dufresne, and S. Boufi, "Preparation of poly(styrene-co-hexylacrylate)/cellulose whiskers nanocomposites via miniemulsion polymerization," *Journal of Applied Polymer Science*, vol. 114, no. 5, pp. 2946–2955, 2009.

[107] J. F. Revol, "On the cross-sectional shape of cellulose crystallites in valonia ventricosa," *Carbohydrate Polymers*, vol. 2, no. 2, pp. 123–134, 1982.

[108] S. J. Hanley, J. Giasson, J. F. Revol, and D. G. Gray, "Atomic force microscopy of cellulose microfibrils: comparison with transmission electron microscopy," *Polymer*, vol. 33, no. 21, pp. 4639–4642, 1992.

[109] C. Tokoh, K. Takabe, M. Fujita, and H. Saiki, "Cellulose synthesized by acetobacter xylinum in the presence of acetyl glucomannan," *Cellulose*, vol. 5, no. 4, pp. 249–261, 1998.

[110] M. Roman and W. T. Winter, "Effect of sulfate groups from sulfuric acid hydrolysis on the thermal degradation behavior of bacterial cellulose," *Biomacromolecules*, vol. 5, no. 5, pp. 1671–1677, 2004.

[111] R. Zuluaga, J. L. Putaux, A. Restrepo, I. Mondragón, and P. Ganan, "Cellulose microfibrils from banana farming residues: isolation and characterization," *Cellulose*, vol. 14, no. 6, pp. 585–592, 2007.

[112] K. Oksman, J. A. Etang, A. P. Mathew, and M. Jonoobi, "Cellulose nanowhiskers separated from a bio-residue from wood bioethanol production," *Biomass & Bioenergy*, vol. 35, no. 1, pp. 146–152, 2011.

[113] G. Siqueira, H. Abdillahi, J. Bras, and A. Dufresne, "High reinforcing capability cellulose nanocrystals extracted from Syngonanthus nitens (Capim Dourado)," *Cellulose*, vol. 17, no. 2, pp. 289–298, 2010.

[114] E. D. M. Teixeira, D. Pasquini, A. A. S. Curvelo, E. Corradini, M. N. Belgacem, and A. Dufresne, "Cassava bagasse cellulose nanofibrils reinforced thermoplastic cassava starch," *Carbohydrate Polymers*, vol. 78, no. 3, pp. 422–431, 2009.

[115] U. J. Kim, S. Kuga, M. Wada, T. Okano, and T. Kondo, "Periodate oxidation of crystalline cellulose," *Biomacromolecules*, vol. 1, no. 3, pp. 488–492, 2000.

[116] M. F. Rosa, E. S. Medeiros, J. A. Malmonge et al., "Cellulose nanowhiskers from coconut husk fibers: effect of preparation conditions on their thermal and morphological behavior," *Carbohydrate Polymers*, vol. 81, no. 1, pp. 83–92, 2010.

[117] X. M. Dong, J. F. Revol, and D. G. Gray, "Effect of microcrystallite preparation conditions on the formation of colloid crystals of cellulose," *Cellulose*, vol. 5, no. 1, pp. 19–32, 1998.

[118] T. Ebeling, M. Paillet, R. Borsali et al., "Shear-induced orientation phenomena in suspensions of cellulose microcrystals, revealed by small angle X-ray scattering," *Langmuir*, vol. 15, no. 19, pp. 6123–6126, 1999.

[119] J. Araki, M. Wada, and S. Kuga, "Steric Stabilization of a Cellulose Microcrystal Suspension by Poly(ethylene glycol) Grafting," *Langmuir*, vol. 17, no. 1, pp. 21–27, 2001.

[120] Y. Lu, L. Weng, and X. Cao, "Biocomposites of plasticized starch reinforced with cellulose crystallites from cottonseed linter," *Macromolecular Bioscience*, vol. 5, no. 11, pp. 1101–1107, 2005.

[121] A. C. Corrêa, E. M. Teixeira, L. A. Pessan, and L. H. C. Mattoso, "Cellulose nanofibers from curaua fibers," *Cellulose*, vol. 17, no. 6, pp. 1183–1192, 2010.

[122] A. Bendahou, Y. Habibi, H. Kaddami, and A. Dufresne, "Physico-chemical characterization of palm from Phoenix Dactylifera-L, preparation of cellulose whiskers and natural rubber-based nanocomposites," *Journal of Biobased Materials and Bioenergy*, vol. 3, no. 1, pp. 81–90, 2009.

[123] J. P. De Mesquita, C. L. Donnici, and F. V. Pereira, "Biobased nanocomposites from layer-by-layer assembly of cellulose nanowhiskers with chitosan," *Biomacromolecules*, vol. 11, no. 2, pp. 473–480, 2010.

[124] X. Cao, H. Dong, and C. M. Li, "New nanocomposite materials reinforced with flax cellulose nanocrystals in waterborne polyurethane," *Biomacromolecules*, vol. 8, no. 3, pp. 899–904, 2007.

[125] J. K. Pandey, J. W. Lee, W. S. Chu, C. S. Kim, C. S. Lee, and S. H. Ahn, "Cellulose nanowhiskers from grass of Korea," *Macromolecular Research*, vol. 16, no. 5, pp. 396–498, 2008.

[126] J. K. Pandey, W. S. Chu, C. S. Kim, C. S. Lee, and S. H. Ahn, "Bio-nano reinforcement of environmentally degradable polymer matrix by cellulose whiskers from grass," *Composites Part B*, vol. 40, no. 7, pp. 676–680, 2009.

[127] B. Wang, M. Sain, and K. Oksman, "Study of structural morphology of hemp fiber from the micro to the nanoscale," *Applied Composite Materials*, vol. 14, no. 2, pp. 89–103, 2007.

[128] G. Siqueira, J. Bras, and A. Dufresne, "Luffa cylindrica as a lignocellulosic source of fiber, microfibrillated cellulose, and cellulose nanocrystals," *BioResources*, vol. 5, no. 2, pp. 727–740, 2010.

[129] R. Li, J. Fei, Y. Cai, Y. Li, J. Feng, and J. Yao, "Cellulose whiskers extracted from mulberry: a novel biomass production," *Carbohydrate Polymers*, vol. 76, no. 1, pp. 94–99, 2009.

[130] G. Chen, A. Dufresne, J. Huang, and P. R. Chang, "A novel thermoformable bionanocomposite based on cellulose nanocrystal-graft-poly(ε-caprolactone)," *Macromolecular Materials and Engineering*, vol. 294, pp. 59–67, 2009.

[131] Y. Lu, L. Weng, and X. Cao, "Morphological, thermal and mechanical properties of ramie crystallites—reinforced plasticized starch biocomposites," *Carbohydrate Polymers*, vol. 63, no. 2, pp. 198–204, 2006.

[132] Y. Habibi and A. Dufresne, "Highly filled bionanocomposites from functionalized polysaccharide nanocrystals," *Biomacromolecules*, vol. 9, no. 7, pp. 1974–1980, 2008.

[133] P. B. Filson, B. E. Dawson-Andoh, and D. Schwegler-Berry, "Enzymatic-mediated production of cellulose nanocrystals from recycled pulp," *Green Chemistry*, vol. 11, no. 11, pp. 1808–1814, 2009.

[134] G. Siaueira, J. Bras, and A. Dufresne, "Cellulose whiskers versus microfibrils: influence of the nature of the nanoparticle and its surface functionalization on the thermal and mechanical properties of nanocomposites," *Biomacromolecules*, vol. 10, no. 2, pp. 425–432, 2009.

[135] G. Siqueira, J. Bras, and A. Dufresne, "New process of chemical grafting of cellulose nanoparticles with a long chain isocyanate," *Langmuir*, vol. 26, no. 1, pp. 402–411, 2010.

[136] E. M. Teixeira, T. J. Bondancia, K. B. R. Teodoro, A. C. Corrêa, J. M. Marconcini, and L. H. C. Mattoso, "Sugarcane bagasse whiskers: extraction and characterizations," *Industrial Crops and Products*, vol. 33, no. 1, pp. 63–66, 2011.

[137] V. Favier, G. R. Canova, J. Y. Cavaillé, H. Chanzy, A. Dufresne, and C. Gauthier, "Nanocomposite materials from latex and cellulose whiskers," *Polymers for Advanced Technologies*, vol. 6, no. 5, pp. 351–355, 1995.

[138] J. Araki, M. Wada, S. Kuga, and T. Okano, "Influence of surface charge on viscosity behavior of cellulose microcrystal suspension," *Journal of Wood Science*, vol. 45, no. 3, pp. 258–261, 1999.

[139] S. Beck-Candanedo, M. Roman, and D. G. Gray, "Effect of reaction conditions on the properties and behavior of wood cellulose nanocrystal suspensions," *Biomacromolecules*, vol. 6, no. 2, pp. 1048–1054, 2005.

[140] M. A. S. A. Samir, F. Alloin, and A. Dufresne, "Review of recent research into cellulosic whiskers, their properties and their application in nanocomposite field," *Biomacromolecules*, vol. 6, no. 2, pp. 612–626, 2005.

[141] A. Dufresne, "Comparing the mechanical properties of high performances polymer nanocomposites from biological sources," *Journal of Nanoscience and Nanotechnology*, vol. 6, no. 2, pp. 322–330, 2006.

[142] A. Dufresne, "Polysaccharide nanocrystals reinforced nanocomposites," *Canadian Journal of Chemistry*, vol. 86, pp. 484–494, 2008.

[143] M. A. Hubbe, O. J. Rojas, L. A. Lucia, and M. Sain, "Cellulosic nanocomposites: a review," *Bioresources*, vol. 3, pp. 929–980, 2008.

[144] A. Šturcova, G. R. Davies, and S. J. Eichhorn, "Elastic modulus and stress-transfer properties of tunicate cellulose whiskers," *Biomacromolecules*, vol. 6, no. 2, pp. 1055–1061, 2005.

[145] Liu Dagang, Zhong Tuhua, R. Chang Peter, Li Kaifu, and Wu Qinglin, "Starch composites reinforced by bamboo cellulosic crystals," *Bioresource Technology*, vol. 101, no. 7, pp. 2529–2536, 2010.

[146] M. N. Anglès and A. Dufresne, "Plasticized starch/tunicin whiskers nanocomposite materials. 2. Mechanical behavior," *Macromolecules*, vol. 34, no. 9, pp. 2921–2931, 2001.

[147] A. P. Mathew and A. Dufresne, "Morphological investigation of nanocomposites from sorbitol plasticized starch and tunicin whiskers," *Biomacromolecules*, vol. 3, no. 3, pp. 609–617, 2002.

[148] W. J. Orts, J. Shey, S. H. Imam, G. M. Glenn, M. E. Guttman, and J. F. Revol, "Application of cellulose microfibrils in polymer nanocomposites," *Journal of Polymers and the Environment*, vol. 13, no. 4, pp. 301–306, 2005.

[149] A. P. Mathew, W. Thielemans, and A. Dufresne, "Mechanical properties of nanocomposites from sorbitol plasticized starch and tunicin whiskers," *Journal of Applied Polymer Science*, vol. 109, no. 6, pp. 4065–4074, 2008.

[150] A. J. Svagan, M. S. Hedenqvist, and L. Berglund, "Reduced water vapour sorption in cellulose nanocomposites with starch matrix," *Composites Science and Technology*, vol. 69, no. 3-4, Article ID 10.1016/j.compscitech.2008.11.016, pp. 500–506, 2009.

[151] Y. Noishiki, Y. Nishiyama, M. Wada, S. Kuga, and J. Magoshi, "Mechanical properties of silk fibroin-microcrystalline cellulose composite films," *Journal of Applied Polymer Science*, vol. 86, no. 13, pp. 3425–3429, 2002.

[152] M. A. S. A. Samir, F. Alloin, J. Y. Sanchez, and A. Dufresne, "Cellulose nanocrystals reinforced poly(oxyethylene)," *Polymer*, vol. 45, no. 12, pp. 4149–4157, 2004.

[153] M. A. S. A. Samir, F. Alloin, W. Gorecki, J. Y. Sanchez, and A. Dufresne, "Nanocomposite polymer electrolytes based on poly(oxyethylene) and cellulose nanocrystals," *The Journal of Physical Chemistry B*, vol. 108, no. 30, pp. 10845–10852, 2004.

[154] M. A. S. A. Samir, A. M. Mateos, F. Alloin, J. Y. Sanchez, and A. Dufresne, "Plasticized nanocomposite polymer electrolytes based on poly(oxyethylene) and cellulose whiskers," *Electrochimica Acta*, vol. 49, no. 26, pp. 4667–4677, 2004.

[155] M. A. S. A. Samir, L. Chazeau, F. Alloin, J. Y. Cavaillé, A. Dufresne, and J. Y. Sanchez, "POE-based nanocomposite polymer electrolytes reinforced with cellulose whiskers," *Electrochimica Acta*, vol. 50, no. 19, pp. 3897–3903, 2005.

[156] M. A. S. A. Samir, F. Alloin, and A. Dufresne, "High performance nanocomposite polymer electrolytes," *Composite Interfaces*, vol. 13, no. 4–6, pp. 545–559, 2006.

[157] T. Zimmermann, E. Pöhler, and T. Geiger, "Cellulose fibrils for polymer reinforcement," *Advanced Engineering Materials*, vol. 6, no. 9, pp. 754–761, 2004.

[158] T. Zimmermann, E. Pöhler, and P. Schwaller, "Mechanical and morphological properties of cellulose fibril reinforced nanocomposites," *Advanced Engineering Materials*, vol. 7, no. 12, pp. 1156–1161, 2005.

[159] M. Roohani, Y. Habibi, N. M. Belgacem, G. Ebrahim, A. N. Karimi, and A. Dufresne, "Cellulose whiskers reinforced polyvinyl alcohol copolymers nanocomposites," *European Polymer Journal*, vol. 44, no. 8, pp. 2489–2498, 2008.

[160] S. A. Paralikar, J. Simonsen, and J. Lombardi, "Poly(vinyl alcohol)/cellulose nanocrystal barrier membranes," *Journal of Membrane Science*, vol. 320, no. 1-2, pp. 248–258, 2008.

[161] J. Lu, T. Wang, and L. T. Drzal, "Preparation and properties of microfibrillated cellulose polyvinyl alcohol composite materials," *Composites Part A*, vol. 39, no. 5, pp. 738–746, 2008.

[162] Y. Choi and J. Simonsen, "Cellulose nanocrystal-filled carboxymethyl cellulose nanocomposites," *Journal of Nanoscience and Nanotechnology*, vol. 6, no. 3, pp. 633–639, 2006.

[163] Y. Wang, X. Cao, and L. Zhang, "Effects of cellulose whiskers on properties of soy protein thermoplastics," *Macromolecular Bioscience*, vol. 6, no. 7, pp. 524–531, 2006.

[164] A. Dufresne, J. Y. Cavaillé, and W. Helbert, "Thermoplastic nanocomposites filled with wheat straw cellulose whiskers. Part II: effect of processing and modeling," *Polymer Composites*, vol. 18, no. 2, pp. 198–210, 1997.

[165] D. Dubief, E. Samain, and A. Dufresne, "Polysaccharide microcrystals keinforced amorphous poly(/3-hydroxyoctanoate) nanocomposite materials," *Macromolecules*, vol. 32, no. 18, pp. 5765–5771, 1999.

[166] A. Dufresne, M. B. Kellerhals, and B. Witholt, "Transcrystallization in Mcl-PHAs/cellulose whiskers composites," *Macromolecules*, vol. 32, no. 22, pp. 7396–7401, 1999.

[167] A. Dufresne, "Dynamic mechanical analysis of the interphase in bacterial polyester/cellulose whiskers natural composites," *Composite Interfaces*, vol. 7, no. 1, pp. 53–67, 2000.

[168] L. Chazeau, J. Y. Cavaillé, G. Canova, R. Dendievel, and B. Boutherin, "Viscoelastic properties of plasticized PVC reinforced with cellulose whiskers," *Journal of Applied Polymer Science*, vol. 71, no. 11, pp. 1797–1808, 1999.

[169] L. Chazeau, J. Y. Cavaillé, and P. Terech, "Mechanical behaviour above T(g) of a plasticised PVC reinforced with cellulose whiskers; a SANS structural study," *Polymer*, vol. 40, no. 19, pp. 5333–5344, 1999.

[170] L. Chazeau, M. Paillet, and J. Y. Cavaillé, "Plasticized PVC reinforced with cellulose whiskers. I. Linear viscoelastic behavior analyzed through the quasi-point defect theory," *Journal of Polymer Science Part B*, vol. 37, no. 16, pp. 2151–2164, 1999.

[171] L. Chazeau, J. Y. Cavaillé, and J. Perez, "Plasticized PVC reinforced with cellulose whiskers. II. Plastic behavior," *Journal of Polymer Science Part B*, vol. 38, no. 3, pp. 383–392, 2000.

[172] M. M. Ruiz, J. Y. Cavaillé, A. Dufresne, C. Graillat, and J. F. Gérard, "New waterborne epoxy coatings based on cellulose nanofillers," *Macromolecular Symposia*, vol. 169, pp. 211–222, 2001.

[173] A. Bendahou, H. Kaddami, and A. Dufresne, "Investigation on the effect of cellulosic nanoparticles' morphology on the properties of natural rubber based nanocomposites," *European Polymer Journal*, vol. 46, no. 4, pp. 609–620, 2010.

[174] M. F. Rosa, E. S. Medeiros, J. A. Malmonge et al., "Nanocomposites based on natural rubber and cellulose nanocrystals from coconut fibers," in *Proceedings of the 11th International Conference on Advanced Materials (ICAM '09)*, Rio de Janeiro, Brazil, September 2009.

[175] K. Oksman, A. P. Mathew, D. Bondeson, and I. Kvien, "Manufacturing process of cellulose whiskers/polylactic acid nanocomposites," *Composites Science and Technology*, vol. 66, no. 15, pp. 2776–2784, 2006.

[176] D. Bondeson and K. Oksman, "Polylactic acid/cellulose whisker nanocomposites modified by polyvinyl alcohol," *Composites Part A*, vol. 38, no. 12, pp. 2486–2492, 2007.

[177] A. J. de Menezes, G. Siqueira, A. A. S. Curvelo, and A. Dufresne, "Extrusion and characterization of functionalized cellulose whiskers reinforced polyethylene nanocomposites," *Polymer*, vol. 50, no. 19, pp. 4552–4563, 2009.

[178] A. L. Goffin, J. M. Raquez, E. Duquesne, Y. Habibi, A. Dufresne, and P. Dubois, "Poly(ε-caprolactone) based nanocomposites reinforced by surface-grafted cellulose nanowhiskers via extrusion processing: morphology, rheology, and thermo-mechanical properties," *Polymer*, vol. 52, no. 7, Article ID 10.1016/j.polymer.2011.02.004, pp. 1532–1538, 2011.

[179] L. Lemahieu, L. Bras, P. Tiquet, S. Augier, and A. Dufresne, "Extrusion of nanocellulose-reinforced nanocomposites using the dispersed nano-objects protective encapsulation (DOPE) process ," Macromolecular Materials and Engineerin*journal name*. In press.

[180] G. Chauve, L. Heux, R. Arouini, and K. Mazeau, "Cellulose poly(ethylene-co-vinyl acetate) nanocomposites studied by molecular modelling and mechanical spectroscopy," *Biomacromolecules*, vol. 6, no. 4, pp. 2025–2031, 2005.

[181] N. Ljungberg, C. Bonini, F. Bortolussi, C. Boisson, L. Heux, and J. Y. Cavaillé, "New nanocomposite materials reinforced with cellulose whiskers in atactic polypropylene: Effect of surface and dispersion characteristics," *Biomacromolecules*, vol. 6, no. 5, pp. 2732–2739, 2005.

[182] R. N. Rowell, "A new generationof composite materials from agro-based fibers," in *Polymers and Other Advanced Materials: Emerging Technologies and Business Opportunity*, P. N. Prasas, M. E. James, and T. F. Joo, Eds., pp. 66–69, Plenum Press, New York, NY, USA, 1995.

[183] R. N. Rowell, "A new generation of composite materials from agro-based fibers," in *Proceedings of the Third International Conference on Frontiers of Polymers and Advanced Materials*, Kuala Lumpur, Malaysia, January 1995.

[184] M. A. Dweib, B. Hu, H. W. Shenton, and R. P. Wool, "Bio-based composite roof structure: manufacturing and processing issues," *Composite Structures*, vol. 74, no. 4, pp. 379–388, 2006.

[185] V. M. H. Govindarao, "Utilization of rice husk—a preliminary analysis," *Journal of Scientific & Industrial Research*, vol. 39, no. 9, pp. 495–515, 1980.

[186] R. Burgueño, M. J. Quagliata, G. M. Mehta, A. K. Mohanty, M. Misra, and L. T. Drzal, "Sustainable cellular biocomposites from natural fibers and unsaturated polyester resin for housing panel applications," *Journal of Polymers and the Environment*, vol. 13, no. 2, pp. 139–149, 2005.

[187] R. M. Brown, "Microbial Cellulose: a new resource for wood, paper, textiles, food and specialty products," Position Paper, 1998, http://www.botany.utexas.edu/facstaff/facpages/mbrown/position1.htm.

[188] R. Jonas and L. F. Farah, "Production and application of microbial cellulose," *Polymer Degradation and Stability*, vol. 59, no. 1–3, pp. 101–106, 1998.

[189] J. Shah and R. M. Brown Jr., "Towards electronic paper displays made from microbial cellulose," *Applied Microbiology and Biotechnology*, vol. 66, no. 4, pp. 352–355, 2005.

[190] H. Yano, J. Sugiyama, A. N. Nakagaito et al., "Optically transparent composites reinforced with networks of bacterial nanofibers," *Advanced Materials*, vol. 17, no. 2, pp. 153–155, 2005.

[191] C. Legnani, H. S. Barud, W. G. Quirino et al., "Transparent nanocomposite bacterial cellulose used as flexible substrate for OLED," in *Proceedings of the 11th International Conference on Advanced Materials*, Rio de Janeiro, Brazil, September 2009.

[192] B. R. Evans, H. M. O'Neill, V. P. Malyvanh, I. Lee, and J. Woodward, "Palladium-bacterial cellulose membranes for fuel cells," *Biosensors and Bioelectronics*, vol. 18, no. 7, pp. 917–923, 2003.

[193] D. G. Olson, S. A. Tripathi, R. J. Giannone et al., "Deletion of the Cel48S cellulase from Clostridium thermocellum,"

Proceedings of the National Academy of Sciences of the United States of America, vol. 107, no. 41, pp. 17727–17732, 2010.

[194] D. A. A. Alderman, "A review of cellulose ethers in hydrophilic matrices for oral controlled-release dosage forms," *International Journal of Pharmaceutical Technology and Product Manufacture*, vol. 5, no. 3, pp. 1–9, 1984.

[195] J. Heller, "Use of polymers in controlled release of active agents in controlled drug delivery," in *Fundamentals and Applications*, J. R. Robinson and V. H. L. Lee, Eds., pp. 210–180, Marcel Dekker, New York, NY, USA, 2nd edition, 1987.

[196] M. A. Longer and J. R. Robinson, "Sustained-release drug delivery systems," in *Remington's Pharmaceutical Sciences*, J. P. Remington, Ed., pp. 1676–1693, Mack Publishing, Easton, Pa, USA, 18th edition, 1990.

[197] M. D. Baumann, C. E. Kang, J. C. Stanwick et al., "An injectable drug delivery platform for sustained combination therapy," *Journal of Controlled Release*, vol. 138, no. 3, pp. 205–213, 2009.

[198] Y. Watanabe, B. Mukai, K. I. Kawamura et al., "Preparation and evaluation of press-coated aminophylline tablet using crystalline cellulose and polyethylene glycol in the outer shell for timed-release dosage forms," *Yakugaku Zasshi*, vol. 122, no. 2, pp. 157–162, 2002.

[199] S. Shaikh, A. Birdi, S. Qutubuddin, E. Lakatosh, and H. Baskaran, "Controlled release in transdermal pressure sensitive adhesives using organosilicate nanocomposites," *Annals of Biomedical Engineering*, vol. 35, no. 12, pp. 2130–2137, 2007.

[200] H. Lönnberg, L. Fogelström, M. A. S. A. Samir, L. Berglund, E. Malmström, and A. Hult, "Surface grafting of microfibrillated cellulose with poly(ε-caprolactone)—synthesis and characterization," *European Polymer Journal*, vol. 44, no. 9, pp. 2991–2997, 2008.

[201] J. D. Fontana, A. M. de Souza, C. K. Fontana et al., "Acetobacter cellulose pellicle as a temporary skin substitute," *Applied Biochemistry and Biotechnology*, vol. 24-25, pp. 253–264, 1990.

[202] L. R. Mello, Y. Feltrin, R. Selbach, G. Macedo Jr., C. Spautz, and L. J. Haas, "Use of lyophilized cellulose in peripheral nerve lesions with loss of substance," *Arquivos de Neuro-Psiquiatria*, vol. 59, no. 2, pp. 372–379, 2001.

[203] W. K. Czaja, D. J. Young, M. Kawecki, and R. M. Brown Jr., "The future prospects of microbial cellulose in biomedical applications," *Biomacromolecules*, vol. 8, no. 1, pp. 1–12, 2007.

[204] S. W. Negrão, R. R. L. Bueno, E. E. Guérios et al., "A Eficácia do stent recoberto com celulose biossintética comparado ao stent convencional em angioplastia em coelhos," *Revista Brasileira de Cardiologia Invasiva*, vol. 14, no. 1, pp. 10–19, 2006.

[205] D. Klemm, D. Schumann, U. Udhardt, and S. Marsch, "Bacterial synthesized cellulose—artificial blood vessels for microsurgery," *Progress in Polymer Science*, vol. 26, no. 9, pp. 1561–1603, 2001.

[206] M. A. Croce, C. Silvestri, D. Guerra et al., "Adhesion and proliferation of human dermal fibroblasts on collagen matrix," *Journal of Biomaterials Applications*, vol. 18, no. 3, pp. 209–222, 2004.

[207] S. V. Madihally and H. W. T. Matthew, "Porous chitosan scaffolds for tissue engineering," *Biomaterials*, vol. 20, no. 12, pp. 1133–1142, 1999.

[208] S. Nehrer, H. A. Breinan, A. Ramappa et al., "Canine chondrocytes seeded in type I and type II collagen implants investigated in vitro," *Journal of Biomedical Materials Research*, vol. 38, no. 2, pp. 95–104, 1997.

[209] T. V. Kumari, U. Vasudev, A. Kumar, and B. Menon, "Cell surface interactions in the study of biocompatibility," *Trends in Biomaterials and Artificial Organs*, vol. 15, no. 2, pp. 37–41, 2001.

[210] Y. Ikada, "Challenges in tissue engineering," *Journal of the Royal Society Interface*, vol. 3, no. 10, pp. 589–601, 2006.

[211] G. Q. Chen and Q. Wu, "The application of polyhydroxyalkanoates as tissue engineering materials," *Biomaterials*, vol. 26, no. 33, pp. 6565–6578, 2005.

[212] K. Anselme, "Osteoblast adhesion on biomaterials," *Biomaterials*, vol. 21, no. 7, pp. 667–681, 2000.

[213] H. S. Barud, "Development and evaluation of Biocure obtained from bacterial cellulose and standardized extract of propolis (EPP-AF) for the treatment of burns and / or skin lesions," São Paulo Research Foundation—FAPESP, Brazil, 2009.

[214] W. Czaja, A. Krystynowicz, S. Bielecki, and R. M. Brown Jr., "Microbial cellulose—the natural power to heal wounds," *Biomaterials*, vol. 27, no. 2, pp. 145–151, 2006.

[215] L. E. Millon and W. K. Wan, "The polyvinyl alcohol-bacterial cellulose system as a new nanocomposite for biomedical applications," *Journal of Biomedical Materials Research Part B*, vol. 79, no. 2, pp. 245–253, 2006.

[216] Z. Cai and J. Kim, "Bacterial cellulose/poly(ethylene glycol) composite: characterization and first evaluation of biocompatibility," *Cellulose*, vol. 17, no. 1, pp. 83–91, 2010.

[217] A. Seves, G. Testa, A. M. Bonfatti, E. D. Paglia, E. Selli, and B. Marcandalli, "Characterization of native cellulose/poly(ethylene glycol) films," *Macromolecular Materials and Engineering*, vol. 286, no. 9, pp. 524–528, 2001.

[218] Y. Z. Wan, L. Hong, S. R. Jia et al., "Synthesis and characterization of hydroxyapatite-bacterial cellulose nanocomposites," *Composites Science and Technology*, vol. 66, no. 11-12, pp. 1825–1832, 2006.

[219] K. Yasuda, J. P. Gong, Y. Katsuyama et al., "Biomechanical properties of high-toughness double network hydrogels," *Biomaterials*, vol. 26, no. 21, pp. 4468–4475, 2005.

[220] S. B. Lin, C. P. Hsu, L. C. Chen, and H. H. Chen, "Adding enzymatically modified gelatin to enhance the rehydration abilities and mechanical properties of bacterial cellulose," *Food Hydrocolloids*, vol. 23, no. 8, pp. 2195–2203, 2009.

[221] J. Huia, J. Yuanyuan, W. Jiao, H. Yuan, Z. Yuan, and J. Shiru, "Potentiality of bacterial cellulose as the scaffold of tissue engineering of cornea," in *Proceedings of the 2nd International Conference on Biomedical Engineering and Informatics, (BMEI '09)*, China, October 2009.

[222] D. A. Schumann, J. Wippermann, D. O. Klemm et al., "Artificial vascular implants from bacterial cellulose: preliminary results of small arterial substitutes," *Cellulose*, vol. 16, no. 5, pp. 877–885, 2009.

[223] W. L. Amorim, H. O. Costa, F. C. Souza, M. G. Castro, and L. Silva, "Experimental study of the tissue reaction caused by the presence of cellulose produced," *Brazilian Journal of Otorhinolaryngology*, vol. 75, no. 2, pp. 200–207, 2009.

[224] J. Hart, D. Silcock, S. Gunnigle, B. Cullen, N. D. Light, and P. W. Watt, "The role of oxidised regenerated cellulose/collagen in wound repair: effects in vitro on fibroblast biology and in vivo in a model of compromised healing," *International Journal of Biochemistry and Cell Biology*, vol. 34, no. 12, pp. 1557–1570, 2002.

[225] G. Helenius, H. Backdahl, A. Bodin, U. Nannmark, P. Gatenholm, and B. Risberg, "In vivo biocompatibility of

bacterial cellulose," *Journal of Biomedical Materials Research Part A*, vol. 76, no. 2, pp. 431–438, 2006.

[226] E. C. Silva, *Hidroxiapatita Sintética em alvéolo dentário após exodontia em Felis catus: estudo clínico, radiológico e histomorfométrico*, M.S. Dissertation, Universidade Federal de Viçosa, Viçosa, Brazil, 2009.

[227] H. O. Costa and F. C. de Souza, "Evaluation of the tissue regeneration of the burned pigś skin followed by Biotissue^{TM} grafting," *Acta ORL/Técnicas em Otorrinolaringologia*, vol. 23, no. 4, pp. 192–196, 2005.

[228] A. P. Nemetz, D. R. R. Loures, J. C. U. Coelho et al., "Efeito estrutural da utilização de celulose biossintética e politetrafluoroetileno expandido como substitutos do peritônio em cães," *Arquivos Brasileiros De Cirugia Digestiva*, vol. 14, no. 2, pp. 139–142, 2001.

[229] A. B. Novaes Jr. and A. B. Novaes, "Soft tissue management for primary closure in guided bone regeneration: sugical technique and case report," *The International Journal of Oral and Maxillofacial Implants*, vol. 12, no. 1, pp. 84–87, 1997.

[230] A. B. Novaes Jr. and A. B. Novaes, "IMZ implants placed into extraction sockets in association with membrane therapy (Gengiflex) and porous hydroxyapatite: a case report," *The International Journal of Oral and Maxillofacial Implants*, vol. 7, no. 4, pp. 536–540, 1992.

[231] L. A. Salata, G. T. Craig, and I. M. Brook, "*In vivo* evaluation of a new memnbrane (Gengiflex) for guided bone regeneratien (GBR)," *Journal of Dental Research*, vol. 74, no. 3, p. 825, 1995.

[232] C. Dahlin, A. Linde, J. Gottlow, and S. Nyman, "Healing of bone defects by guided tissue regeneration," *Plastic and Reconstructive Surgery*, vol. 81, no. 5, pp. 672–676, 1988.

[233] N. L. Macedo, F. S. Matuda, L. G. S. Macedo, A. S. F. Monteiro, M. C. Valera, and Y. R. Carvalho, "Evaluation of two membranes in guided bone tissue regeneration: histological study in rabbits," *Brazilian Journal of Oral Sciences*, vol. 3, no. 8, pp. 395–400, 2004.

Hindawi Publishing Corporation
International Journal of Polymer Science
Volume 2011, Article ID 212047, 8 pages
doi:10.1155/2011/212047

Research Article

Kenaf Bast Fibers—Part I: Hermetical Alkali Digestion

Jinshu Shi,[1] Sheldon Q. Shi,[1] H. Michael Barnes,[1] Mark Horstemeyer,[2] Jinwu Wang,[1] and El-Barbary M. Hassan[1]

[1] *Forest Products Department (FPD), Mississippi State University (MSU), Box 9820, Starkville, MS 39762-9601, USA*
[2] *Center for Advanced Vehicular Systems (CAVS), Box 5405, Starkville, MS 39762-5405, USA*

Correspondence should be addressed to Sheldon Q. Shi, sshi@cfr.msstate.edu

Received 1 April 2011; Accepted 16 May 2011

Academic Editor: Susheel Kalia

The objective of this study was to develop a hermetical alkali digestion process to obtain single cellulosic fibers from kenaf bast. Kenaf bast were hermetically digested into single fiber using a 5% sodium hydroxide solution for one hour at four different temperatures (80°C, 110°C, 130°C, and 160°C). The hermetical digestion process used in this study produced fibers with high cellulose content (84.2–92.3%) due to the removal of lignin and hemicelluloses. The surface hardness and elastic modulus of the fibers digested at 130°C and 160°C were improved significantly compared with those digested at 80°C. The tensile modulus and tensile strength of the individual fibers reduced as the digestion temperature increased from 110°C to 160°C. Micropores were generated in fiber cell wall when the fibers were digested at 130°C and 160°C. The studies on the composites that were made from polypropylene reinforced with the digested fibers indicated that the compatibility between the digested fibers and polypropylene matrix was poor.

1. Introduction

Kenaf (*Hibiscus cannabinus*) an agricultural crop, is in the Malvaceae family, belonging to the division of *Magnoliophyta*. The history of kenaf cultivation can be traced back to ancient Africa [1]. Kenaf grows very quickly, rising to the heights of 12 to 14 feet in 4 to 5 months. In the United States, kenaf is mainly cultivated in Mississippi, Texas, and California, and so forth. Kenaf yields six to eight metric tons of bast and core per acre annually [1].

Kenaf bast fiber is a lignocellulosic fiber that has been used for pulp, paper, and textiles [2]. It is a good potential reinforcement material for polymer composites [3–8]. The lignocellulosic fiber mainly consists of cellulose, hemicelluloses, and lignin. Noncellulosic substances such as lignin, hemicelluloses, and pectins hold the cellulose fibrils together. The reinforcement effect for the lignocellulosic fiber is influenced by its cellulose content. Usually, high cellulose content can be obtained from the chemical retting [2, 9–14]. Retting is a term to describe a process to digest wood and agricultural stalks, especially bast crop stalks, into fibers. Alkali treatment is a standard procedure used in pulp and paper industries to remove lignin [15]. Through the alkali digestion process, individual fibers can be obtained by separating the fiber bundles. A uniform fiber distribution in the polymer composites may be easily achieved by using the individual fibers as reinforcements. In addition, micropores in the fiber can be created [16], which provide spaces for downstream fiber treatment such as nanoparticle impregnation, and so forth.

In a hermetically alkali digestion process, the temperature is the most influential factor affecting fiber quality and determines the pressure level of the autogneous vapor. High vapor pressure improves the penetration of digesting agents and accelerates the digestion process. The objective of this study was to investigate the effect of four digestion temperatures on the characteristics of kenaf bast fibers in hermetical alkali digestion process and to evaluate the reinforcement effects of the digested fibers in polymer composites.

2. Materials and Methods

2.1. Materials. Kenaf stalks were obtained from MSU North Farm. After the separation of the kenaf core and bast, the bast was cut into 50.8 mm lengths and dried to a moisture content of 7.4% at 103°C. Sodium hydroxide (NaOH) solution (5%, w/v) prepared with NaOH beads (Lab grade,

Thermo Fisher Scientific Inc.) and distilled water was used as digestion agent. Glacial acetic acid (17.4 N, Regent grade, Thermo Fisher Scientific Inc.) was used as a pH neutralizer. Polypropylene (PP) film (CO-EX Oriented Polypropylene), provided by Plastic Suppliers, Inc. Dallas, TX, was used to fabricate the laminated kenaf fiber-PP composites.

2.2. Hermetical Alkali Digestion. Kenaf bast fiber was digested with 5% NaOH solution (fiber: NaOH solution = 1 : 30 g/mL) in a hermetical reactor (Parr Instrument Co. 251 M) for one hour at four temperatures (80°C, 110°C, 130°C, and 160°C). The autogenous vapor pressures were 0.05 MPa at 80°C, 0.15 MPa at 110°C, 0.27 MPa at 130°C, and 0.60 MPa at 160°C. After digestion, the pH value of the fiber suspension was adjusted to 7.0 using acetic acid. The neutralized fibers were washed with tap water in order to remove the chemicals. Finally, the digested fibers were freeze dried for further analysis or oven dried for composites fabrication.

2.3. Digested Fiber/PP Composites Fabrication. The fibers digested at 80°C, 110°C, and 130°C were long fiber bundles. These fiber bundles were mechanically separated using a blender (Oster 6791) for five minutes. The disintegrated fibers could be dispersed in water and made into uniform fiber sheets. The fibers digested at 160°C had a better dispersion in water and could be made into uniform fiber sheets directly without further mechanical separation. For the fiber sheet forming, the fibers were first dispersed in water by vigorous stirring. The suspension was then passed through a screen (mesh 35), on which the fiber sheets were formed. The fiber sheets were dried at 80°C. The fiber sheets and polypropylene films were cut into 15.2 cm × 15.2 cm and layered in alternate fiber directions. The weight ratio of fiber to polypropylene was 50 : 50. The laminated mats were hot pressed at a temperature of 200°C and a pressure of 0.7 MPa for 2.5 minutes. The pressure was not released until the platen was cooled down to the room temperature. The laminated kenaf fiber/PP panels were removed from the press and stored in a desiccator for two days before the specimen preparation for mechanical testing. Three panels were fabricated for each digested fiber type.

2.4. Chemical Components and Yields. Chemical components, including holocellulose, α-cellulose, Klason lignin, and ash content were determined for both the raw kenaf bast fibers and the digested fibers. The ash contents were measured following the procedure described in TAPPI standard T 211-om. 93 [17]. The determination of Klason lignin was based on the constituent insoluble in 72% sulfuric acid, which was estimated in accordance with the method #482 from the Institute of Paper Chemistry [18]. Holocellulose is the total polysaccharide fraction (cellulose and hemicelluloses) of the fibers and was estimated according to the method of Wise et al. [19]. Alpha cellulose is the part of cellulose which does not dissolve in 17.5% sodium hydroxide solution. The alpha cellulose was determined in accordance with the method from German Association of Cellulose Chemists and Engineers [20]. The yields of the digested fibers were obtained based on the ratio of the oven-dry weights of the resultant fibers to the original weight of the raw kenaf bast fibers.

2.5. Fiber Surface Morphology. A Zeiss SupraTM 40-Gemini Scanning Electron Microscope (SEM) with an accelerating voltage of 15 kV was used for studying the morphology of the digested fibers. The fibers were treated with 15 nm gold sputter coating before being scanned in SEM. Seventy fibers from each digestion temperature were randomly selected, and the images were taken with the SEM. The dimensions of the fibers were measured by the image analysis. The distributions of their length, diameter, and aspect ratio were statistically analyzed.

2.6. Fiber Surface Hardness and Elastic Modulus. A Hysitron TriboIndenter with a Berkovich diamond tip was used to test the surface hardness and elastic modulus at a 400 μN peak force and a 40 μN/s loading rate using a 10-second segment time. The single fibers were mounted in a hardened epoxy matrix, and the load was perpendicular to the longitudinal direction of the fibers. According to the elastic punch theory and the method of Oliver and Pharr [21], the reduced elastic modulus was obtained based on the elastic contact stiffness.

2.7. Tensile Properties of Single Fibers. The single-fiber tests were conducted at the International Center for bamboo and Rattan (ICBR), Beijing, China, using a newly developed microtester (SF-I) [22]. Thirty individual kenaf fibers chemically digested at 110°C and 160°C were tested for tensile modulus and strength. The nominal gauge length was 0.7 mm, and the cross-head speed was 0.8 m/s. A multiple comparison with Fisher's least significance difference (LSD) method at $\alpha = 0.05$ was carried out with SAS software (SAS Institute Inc. NC, USA).

2.8. Mechanical Properties of the Composites. Dog bone-shaped samples were cut from kenaf fiber/PP panels in accordance with ASTM 1037 [23] for the tension testing. The samples were stored in the desiccators with silica gel at the bottom for one week before they were used for mechanical tests. Tensile modulus and tensile strength of kenaf fiber/PP composites were tested using Instron 5869 (50 kN load cell) according to ASTM 1037. Nine replicates of each composite formulation were used. Multiple comparison of the results was conducted with Fisher's Least Square method at $\alpha = 0.05$ using SAS 9.2 software (SAS Institute Inc. NC, USA). The fracture surfaces of the samples were observed using scanning electron microscopy (SEM, Zeiss Supra TM 40).

3. Results and Discussion

3.1. Fiber Yields and Chemical Compositions. Table 1 shows the yields and chemical composition of digested fibers and control fibers. It is shown that the fiber yield is gradually decreased as the digestion temperature increased. This result can be attributed to the removal of lignin and low molecular weight compounds as well as solubilization of hemicelluloses in hot alkali solution.

Table 1: Yields and chemical compositions of the digested fibers.

Digestion temperature (°C)	Yield (%)	Chemical composition (%)				
		Holocellulose	α-cellulose	Hemicellulose*	Lignin	Ash
(Control fiber)		75.8	46.0	29.8	19.1	5.1
80	56.8	84.1	81.4	2.7	10.5	3.0
110	57.3	85.8	84.0	1.8	10.0	3.2
130	53.2	87.8	86.6	1.2	8.1	2.8
160	44.6	94.2	92.3	0.9	0.24	2.7

* Hemicellulose content is calculated from the difference between holocellulose and α-cellulose content.

(a) (b) (c) (d)

Figure 1: Images of the fibers digested at (a) 80°C, (b) 110°C, (c) 130°C, and (d) 160°C.

Table 2: Average and standard deviation of the fiber dimensions.

		Length (μm)	Diameter (μm)	Aspect ratio
Digested at 80°C, 110°C, and 130°C with mechanical disintegration	Ave.*	1578.8	20.3	89.0
	Stdev.*	524.8	9.4	41.7
Digested at 160°C	Ave.	468.0	18.2	16.0
	Stdev.	575.5	6.4	15.1

* Ave.: average of 70 samples. *Stdev.: standard deviation.

The total amount of holocelluloses is gradually increased as the increase of the digestion temperature. The holocellulose content increased from 75.8% for the control fibers to 94.2 % for the digested fibers at 160°C. This increase in the total holocellulose content is probably related to the decrease of the lignin content. The total amount of pure cellulose in the fibers expressed by α-cellulose is remarkably increased as the increase of digestion temperature. The amount of hemicelluloses remained in the digested fibers were significantly decreased as the increase of digestion temperature. The above results indicate that the alkali digestion process used in the study solubilized most of hemicelluloses and removed most of lignin from the fibers by increasing the digestion temperature.

3.2. Morphology. From the appearance of the fibers, those digested at 80°C, 110°C, and 130°C were fiber bundles, which were bigger and longer compared with those digested at 160°C (Figure 1). The fiber bundles obtained at 80°C, 110°C, and 130°C were separated mechanically and made into fine fibers. Having been mechanically separated, these fibers have the same distribution in length, diameter, and aspect ratio, because they went through the same mechanical disintegration process. The fibers digested at 160°C were

Table 3: Surface hardness and elastic modulus of digested fibers.

	80°C	110°C	130°C	160°C
		Surface hardness (MPa)		
Ave.*	64.25	179.50	224.74	287.91
Stdev.*	45.23	124.07	31.88	113.75
LSD test	A	B	B	B
		Elastic modulus (GPa)		
Ave.	2.48	3.19	4.98	5.24
Stdev.	1.15	1.68	0.25	1.59
LSD test	A	A, B	B, C	C

* Ave.: average of four samples. Stdev.: standard deviation. Means with the different letter are significantly different at $\alpha = 0.05$.

Table 4: Tensile properties of individual digested fibers.

Temperatures (°C)	Modulus (GPa)	LSD test	Strength (MPa)	LSD test	Elongation (%)	LSD test
110	23.6	A	1051	A	4.5	A
160	13.5	B	810	B	5.6	B

Average of 30 samples. Means with the different letter are significantly different a $\alpha = 0.05$.

fine individual fibers and were not subjected to mechanical separation. The distributions of the dimensions are shown in Figure 2. The average and its standard deviation of the dimensions are shown in Table 2.

After the mechanical separation, the lengths of the fibers digested at 80°C, 110°C, and 130°C ranged from 0.5 and 2.6 mm. The lengths of the fibers digested at 160°C were between 0.05 to 0.87 mm, which was much smaller compared to the other fibers. However, the fibers digested at 80°C, 110°C, and 130°C had aspect ratios ranging from 24 to 148, which were higher than those digested at 160°C.

Figure 3 shows the SEM images of the digested fibers. The micropores were seen in Figure 3 in cell wall structures of the fibers digested at 130°C and 160°C. The generated micropores are due to the removal of hemicelluloses and lignin. The size of the micropores was about 50 nm.

3.3. Surface Hardness and Elastic Modulus. Table 3 shows the results of surface hardness and elastic modulus of digested fibers tested by nanoindentation.

The higher the digestion temperature, the higher the hardness and elastic modulus were. The elastic modulus of the fibers digested at 160°C was two times higher than those digested at 80°C, while the hardness of the fibers digested at 160°C was four times higher than those digested at 80°C. This might be due to the increase of cellulose content and the decrease of lignin and hemicelluloses. Cellulose has more ordered crystalline structure than lignin and hemicelluloses, while lignin and hemicelluloses are in amorphous arrangement. The crystalline arrangement of the cellulose molecular chain may result in high surface hardness and elastic modulus [24]. However, cellulose also contains amorphous regions. Crystalline regions and amorphous regions alternately exist in a cellulose chain. Therefore, cellulose structure is not homogeneous. Moreover, the micropore distribution in the digested fibers is not uniform, known from the SEM images. The nonuniform structure of cellulose and the micropore distribution in the fibers resulted in big variations of the indentation results.

3.4. Tensile Properties of Individual Fibers. The tensile properties of the individual fibers digested at 100°C and 160°C are shown in Table 4.

Significant differences were observed between the tensile modulus, tensile strength, and elongation of the fibers digested at 110°C and 160°C. The tensile modulus of the fibers digested at 110°C was 10.1 GPa higher than that of the fibers digested at 160°C. The fiber tensile strength reduced from 1,051 MPa to 810 MPa as the digestion temperature increased from 110°C to 160°C. However, the elongation of the fibers digested at 160°C was 1.1% higher than that digested at 110°C. The decrease in the tensile modulus and strength may be due to the removal of lignin and hemicelluloses. In the control kenaf fibers, lignin filled the spaces in the cell wall between cellulose and hemicelluloses. It is covalently linked to the hemicelluloses and thereby cross-linked the different polysaccharides. Thus, lignin conferred mechanical strength to the single fibers as a whole [25]. The removal of lignin and hemicelluloses resulted in a microporosity structure in the fiber cell wall and a loose connection between individual cellulose microfibrils in an individual fiber. Therefore, a lower tensile modulus and strength were obtained.

3.5. Mechanical Properties of Composites. The results of tensile modulus and tensile strength of the composites are shown in Table 5. Statistical analysis indicated that there was no significant difference in tensile modulus and tensile strength at the 95% significance level among the four types of composites.

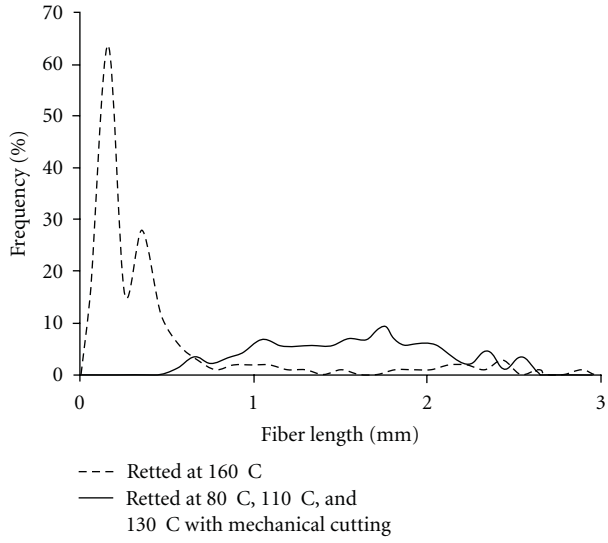

(a)

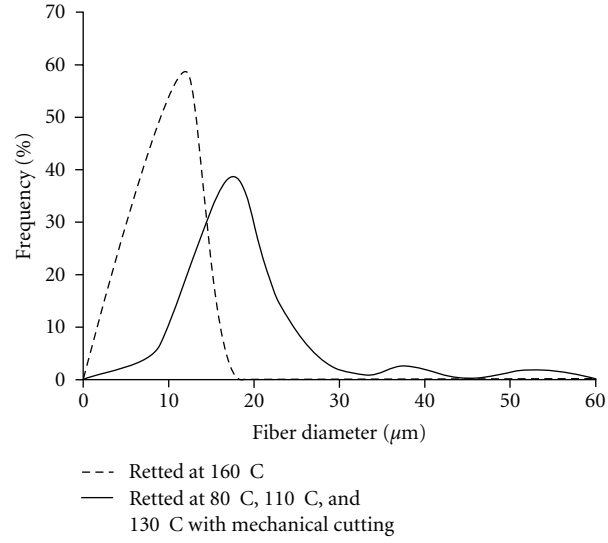

(b)

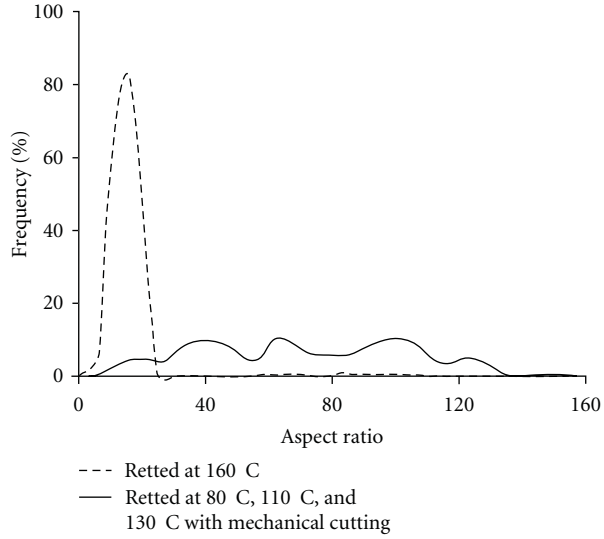

(c)

Figure 2: Dimensional distribution of the digested fibers. (a) length distribution, (b) diameter distribution, (c) aspect ratio distribution.

Table 5: Tensile properties of the kenaf fiber/PP composites.

Digestion temperatures (°C)	Tensile strength (MPa)			Tensile modulus (GPa)		
	Ave.*	Stdev.*	LSD Test	Ave.	Stdev.	LSD Test
80°C	42.44	7.12	A	1.57	0.11	A
110°C	47.35	2.20	A	1.53	0.09	A
130°C	45.20	3.57	A	1.67	0.12	A
160°C	46.77	3.43	A	1.70	0.20	A

* Ave.: average of four samples. Stdev.: standard deviation. Means with the different letter are significantly different at $\alpha = 0.05$. Average of 27 samples. Means with the same letter are not significantly different at $\alpha = 0.05$.

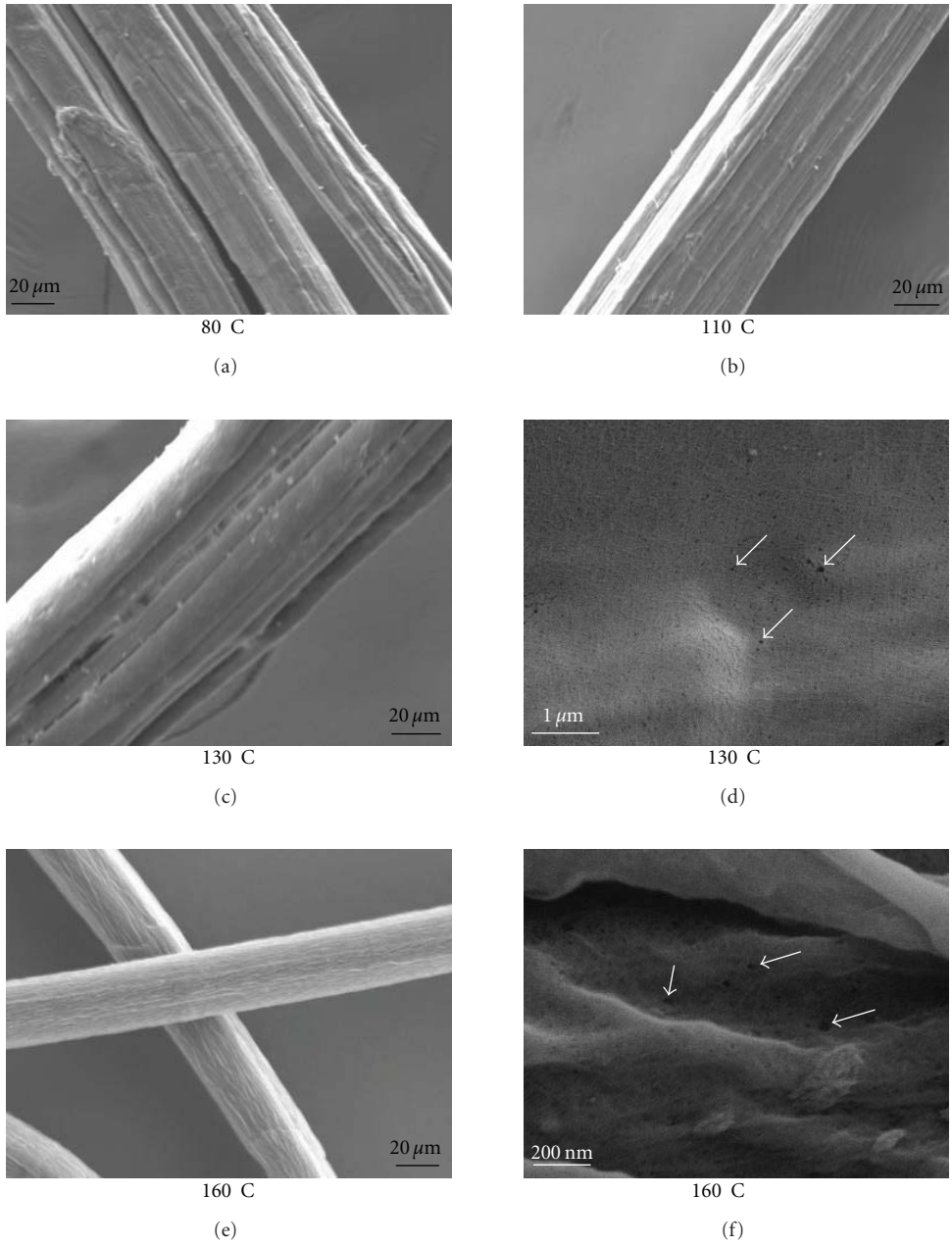

Figure 3: SEM images of the digested fibers. (The arrows designate the micropores).

Many factors may influence the reinforcement efficiency of the fibers including aspect ratio, chemical component, and surface characterization. Although the fibers digested at 160°C had a smaller aspect ratio than the other fibers, the resulting composites did not show a lower tensile modulus or tensile strength. This may be due to its higher cellulose content, which compensated the lower aspect ratio. The high cellulose content of the fibers resulted in a high fiber tensile modulus. More severe breakage of the fibers in the composite made from fibers digested at 160°C (Figure 4(a)) indicates a slightly better bondage between the fibers and the PP matrix but also probably resulted in their low strength at 160°C (Table 4). Generally, the fracture surface images (Figure 4) illuminated that the compatibility between the digested fibers and polypropylene was poor as evidenced by the complete separation between the fibers and polypropylene matrix. Therefore, surface modification for the digested fibers is necessary in order to improve the compatibility between the fibers and the PP matrix

4. Conclusions

Hermetical alkali digestion process effectively removed the lignin and hemicelluloses from kenaf bast fibers at 160°C.

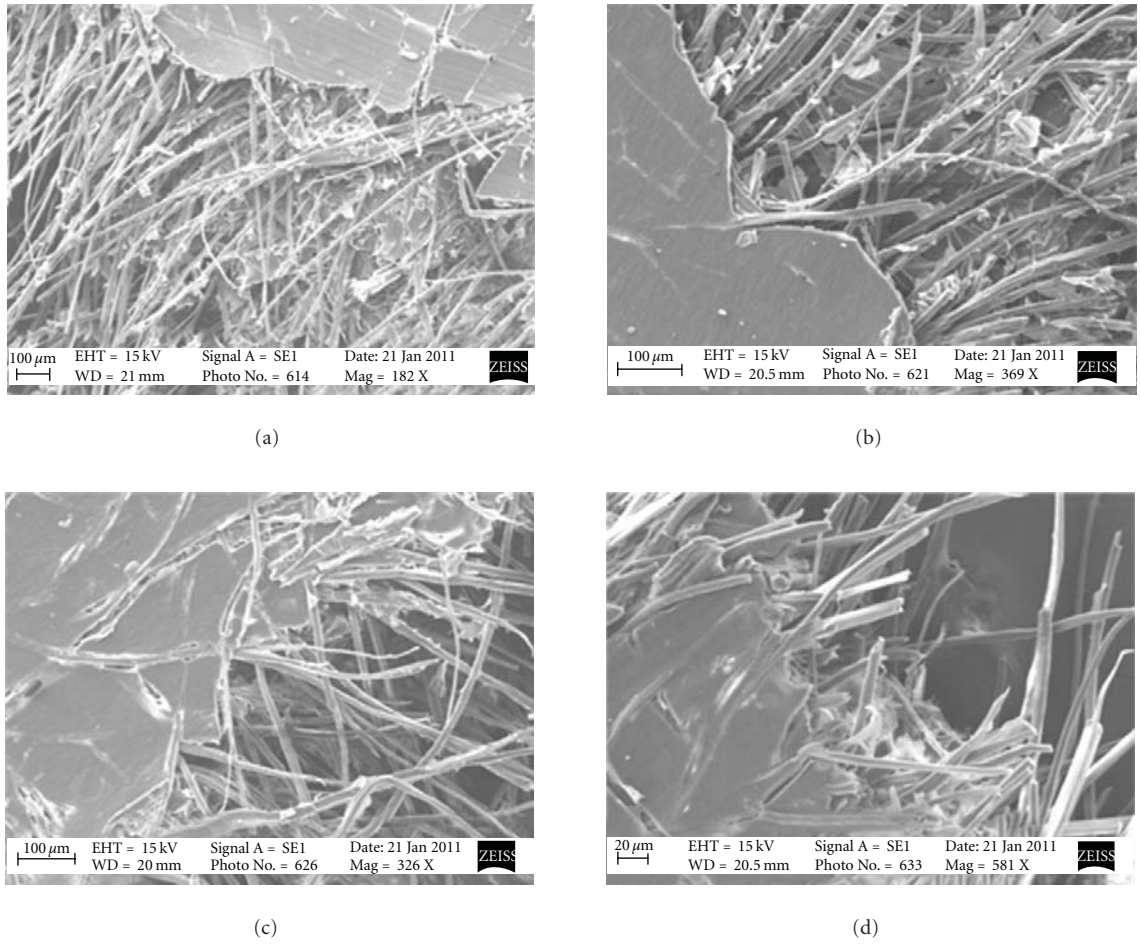

Figure 4: SEM images of the fracture surface of the PP composites reinforced with kenaf fibers digested at (a) 80°C, (b) 110°C, (c) 130°C, and (d) 160°C.

The α-cellulose content of the fibers was 92%. The average surface hardness and elastic modulus of the fiber digested at 160°C yielded improvement of 348.1% and 111.3%, respectively, compared with those digested at 80°C. The increase of cellulose content of the digested fibers resulted in an improved fiber surface hardness and elastic modulus. The digestion temperature had a significant effect on tensile modulus and tensile strength properties of the fiber. When the digestion temperature increased from 110°C to 160°C, the tensile modulus and tensile strength of individual fibers were reduced by 42.8% and 22.9%, respectively, while the elongation increased by 1.1%. The SEM images showed that the micropores were generated in cell wall structures for the fibers digested at 130°C and 160°C, providing the possibility to anchor nanoparticles into the cell wall. The digested fibers without surface modification had a poor interfacial compatibility with the polypropylene matrix.

Acknowledgments

The research work was supported by Department of Energy (DOE), funding # 362000-060803 through Center for Advanced Vehicular System (CAVs) at Mississippi State University and National Science Foundation (NSF), fund # CMMI0928641 09080796. Acknowledgments are given to Dr. Sangyeob Lee for the involvement of the project when he worked as a postdoc at Mississippi State University, the USDA-Forest Service Southern Research Station, Pineville, LA, and the International Center for Bamboo and Rattan, Beijing, China for the instrumental support. The manuscript is approved for publication by Forest and Wildlife Research Center (FWRC), Mississippi State University. The FWRC Publication No.: FP610.

References

[1] A. F. Kaldor, C. Karlgren, and H. Verwest, "Kenaf-a fast growing fiber source for papermaking," *Tappi Journal*, vol. 73, no. 11, pp. 205–208, 1990.

[2] K. H. Song and S. K. Obendorf, "Chemical and biological retting of kenaf fibers," *Textile Research Journal*, vol. 76, no. 10, pp. 751–756, 2006.

[3] B. Aleksandra, B. G. Gordana, A. Grozdanov, M. Avella, G. Gentile, and M. Errico, "Crystallization behavior of poly(hydroxybytyrate-co-valerate) in model and bulk PHBV/kenaf fiber composites," *Journal of Materials Science*, vol. 42, no. 16, pp. 6501–6509, 2007.

[4] T. A. Bullions, D. Hoffman, R. A. Gillespie, J. P. Brien, and A. C. Loos, "Contributions of feather fibers and various cellulose fibers to the mechanical properties of polypropylene matrix composites," *Composites Science and Technology*, vol. 66, no. 1, pp. 102–114, 2006.

[5] C. Clemons and A. R. Sanadi, "Instrumented impact testing of kenaf fiber reinforced polypropylene composites: effects of temperature and composition," *Journal of Reinforced Plastics and Composites*, vol. 26, no. 15, pp. 1587–1602, 2007.

[6] J. M. Park, T. Q. Son, J. G. Jung, and B. S. Hwang, "Interfacial evaluation of single ramie and kenaf fiber/epoxy resin composites using micromechanical test and nondestructive acoustic emission," *Composite Interfaces*, vol. 13, no. 2-3, pp. 105–129, 2006.

[7] T. Nishino, K. Hirao, M. Kotera, K. Nakamae, and H. Inagaki, "Kenaf reinforced biodegradable composite," *Composites Science and Technology*, vol. 63, no. 9, pp. 1281–1286, 2003.

[8] S. H. Aziz, M. P. Ansell, S. J. Clarke, and S. R. Panteny, "Modified polyester resins for natural fibre composites," *Composites Science and Technology*, vol. 65, no. 3-4, pp. 525–535, 2005.

[9] S. Keshk, W. Suwinarti, and K. Sameshima, "Physicochemical characterization of different treatment sequences on kenaf bast fiber," *Carbohydrate Polymers*, vol. 65, no. 2, pp. 202–206, 2006.

[10] H. J. Lee, Y. S. Han, H. J. Yoo, J. H. Kim, K. H. Song, and C. S. Ahn, "Effect of chemical retting on the fiber separation of kenaf bast," *Journal of the Korean Society of Clothing and Textiles*, vol. 27, no. 9-10, pp. 1144–1152, 2003.

[11] W. H. Morrison, D. E. Akin, G. Ramaswamy, and B. Baldwin, "Evaluating chemically retted kenaf using chemical, histochemical, and microspectrophotometric analyses," *Textile Research Journal*, vol. 66, no. 10, pp. 651–656, 1996.

[12] D. V. Parikh, T. A. Calamari, A. P. S. Sawhney et al., "Improved chemical retting of kenaf fibers," *Textile Research Journal*, vol. 72, no. 7, pp. 618–624, 2002.

[13] J. Wang and G. N. Ramaswamy, "Physical and chemical properties of wet processed hemp and kenaf," *AATCC Review*, vol. 5, no. 1, pp. 22–26, 2005.

[14] G. N. Ramaswamy, C. G. Ruff, and C. R. Boyd, "Effect of bacterial and chemical retting on kenaf fiber quality," *Textile Research Journal*, vol. 64, no. 5, pp. 305–308, 1994.

[15] A. P. Deshpande, M. B. Rao, and C. L. Rao, "Extraction of bamboo fibers and their use as reinforcement in polymeric composites," *Journal of Applied Polymer Science*, vol. 76, no. 1, pp. 83–92, 2000.

[16] G. G. Allan, J. P. Carroll, A. R. Negri, M. Raghuraman, P. Ritzenthaler, and A. Yahiaoui, "The microporosity of pulp: the precipitation of inorganic fillers within the micropores of the cell wall," *Tappi Journal*, vol. 75, no. 1, pp. 175–178, 1992.

[17] TAPPI T 211 om-93, "Ash in wood, pulp, paper and paperboard: combustion at 525 degrees Celsius," Tappi Standards, 1993.

[18] The Institute of Paper Chemistry, Method no. 428, The Institute of Paper Chemistry, Appleton, Wis, USA, 1951.

[19] L. E. Wise, M. Murphy, and A. D. Addieco, "Chlorite holocellulose, its fractionation and bearing on summative wood analysis and on studies on the hemicelluloses," *Paper Trade Journal*, vol. 122, no. 2, pp. 35–43, 1946.

[20] Markblatt (IV/29 Zellcheming), "Bestimmung der Alphacellulose und de langeunloslichen Anteils von Zellstoffen," German Association of Cellulose Chemists and Engineers,1951.

[21] W. C. Oliver and G. M. Pharr, "Improved technique for determining hardness and elastic modulus using load and displacement sensing indentation experiments," *Journal of Materials Research*, vol. 7, no. 6, pp. 1564–1580, 1992.

[22] G. Wang, Y. Yu, S. Q. Shi, J. Wang, S. Cao, and H. Cheng, "A micro-tension test method for measuring tensile properties of individual cellulosic fibers," *Wood and Fiber Science*. In press.

[23] ASTM D1037-06a, "Standard test methods for evaluating properties of wood-base fiber and particle panel materials," ASTM International, 2006.

[24] P. Zadorecki and A. J. Michell, "Future prospects for wood cellulose as reinforcement in organic polymer composites," *Polymer Composites*, vol. 10, no. 2, pp. 69–77, 1989.

[25] M. Chabannes, K. Ruel, A. Yoshinaga et al., "In situ analysis of lignins in transgenic tobacco reveals a differential impact of individual transformations on the spatial patterns of lignin deposition at the cellular and subcellular levels," *The Plant Journal*, vol. 28, no. 3, pp. 271–282, 2001.

Hindawi Publishing Corporation
International Journal of Polymer Science
Volume 2011, Article ID 279610, 6 pages
doi:10.1155/2011/279610

Research Article

Isolation of Cellulose Nanofibers: Effect of Biotreatment on Hydrogen Bonding Network in Wood Fibers

Sreekumar Janardhnan and Mohini Sain

Department of Chemical Engineering & Applied Chemistry, University of Toronto, 200 College Street, Toronto, ON, Canada M5S 3E5

Correspondence should be addressed to Sreekumar Janardhnan, s.janardhnan@utoronto.ca

Received 10 March 2011; Accepted 3 May 2011

Academic Editor: Susheel Kalia

The use of cellulose nanofibres as high-strength reinforcement in nano-biocomposites is very enthusiastically being explored due to their biodegradability, renewability, and high specific strength properties. Cellulose, through a regular network of inter- and intramolecular hydrogen bonds, is organized into perfect stereoregular configuration called microfibrils which further aggregate to different levels to form the fibre. Intermolecular hydrogen bonding at various levels, especially at the elementary level, is the major binding force that one need to overcome to reverse engineer these fibres into their microfibrillar level. This paper briefly describes a novel enzymatic fibre pretreatment developed to facilitate the isolation of cellulose microfibrils and explores effectiveness of biotreatment on the intermolecular and intramolecular hydrogen bonding in the fiber. Bleached Kraft Softwood Pulp was treated with a fungus (OS1) isolated from elm tree infected with Dutch elm disease. Cellulose microfibrils were isolated from these treated fibers by high-shear refining. The % yield of nanofibres and their diameter distribution (<50 nm) isolated from the bio-treated fibers indicated a substantial increase compared to those isolated from untreated fibers. FT-IR spectral analysis indicated a reduction in the density of intermolecular and intramolecular hydrogen bonding within the fiber. X-ray spectrometry indicated a reduction in the crystallinity. Hydrogen bond-specific enzyme and its application in the isolation of new generation cellulose nano-fibers can be a huge leap forward in the field of nano-biocomposites.

1. Introduction

Cellulose is the most important constituent of the cell wall and forms a framework around which all other cell wall polysaccharides like hemicellulose, lignin, and pectin are deposited during the plant cell growth [1].

1.1. Cellulose Microfibrils. Cellulose microfibrils are a self-assembly of cellulose chains that are synthesized by plasma membrane, which through a regular network of inter- and intramolecular hydrogen bonds are organized into perfect stereoregular configuration called microfibrils. Each chain is stabilized by intrachain hydrogen bonds formed between the pyranose ring oxygen in one residue and the hydrogen of the OH group on C3 in the next residue (O5$\cdots$H-O3′) and between the hydroxyls on C2 and C6 in the next residue (O2-H$\cdots$O6′) [2].

Microfibrils are generated in the laboratory through a combination of high-energy refining in a PFI mill and subsequent cryocrushing under the presence of liquid nitrogen [3].

The elementarization of natural fibres into thier elementary cellulosic constituents like microfibrils is gaining wider attention due to their high strength and stiffness [4], high reinforcing potential [5], and their biodegradability and renewability.

1.2. Application. Numerous high-end potential applications for cellulose microfibrils are currently being explored. Cellulose microfibrils can be used to make ultralight composite materials (e.g., film). Microfibrils are being used to reinforce biopolymers like polylactic acid and starch-based polymers for packaging materials that are 100% biodegradable. Cellulose-based nano-biocomposites are also gaining considerable attention in various structural application in auto- and aerospace industry. Cellulose microfibrils give considerable toughness and strength to traditional paper products even in small quantities.

1.3. Challenges. Utilization of cellulose nano-fibers in composites is faced with three major challenges—isolation (high energy requirement), interfacial compatibility, and chemistry and dispersion of cellulose nano-fibers in polymer matrix.

The very first approach to utilizing hydroxyl chemistry-specific enzymes to facilitate the isolation of cellulose microfibrils from wood plant cell wall was successfully demonstrated in [6]. Hydrogen bond cleaving enzymes from a specific fungus was used to bring about internal defibrillation in the fibre. This paper briefly explores the mechanism behind the action of a specific enzyme in bringing about internal defibrillation in the fibre cell wall which is important in addressing the high-energy requirement associated with cellulose nanofibre isolation from plant fibres.

1.4. Enzyme Technology in Isolation of Cellulose Microfibrils. Although enzymes have been widely used to modify cellulosic fibres for various applications enhancement [7–9] and drainage [10–13], there has not been any research effort to understand and utilize the enzyme-fiber interaction at the fiber molecular level. An understanding of the chemistry at this level and its exploitation to isolate high-strength nanofibers from plant cell wall in an economical manner will be a huge step towards their commercial scale utilization in various applications.

2. Materials and Methods

2.1. Materials

2.1.1. Wood Fibre. Bleached Kraft Softwood Pulp, northern black spruce, was used as the starting material for the isolation of microfibrils. The fiber has a cellulose content of 86% and hemicellulose content of 14%.

2.1.2. Fungus. OS1, a fungus isolated in our laboratory from elm tree infected with Dutch Elm disease, was used as the source of enzyme for the fibre treatment.

2.2. Methods

2.2.1. Biotreatment. Bleached kraft fibre was soaked overnight and thoroughly disintegrated in 2 liters of water and autoclaved for 20 minutes. 200 mL of OS1 fungal culture was added to a 2-liter fibre suspension (containing 24 g dry fibre) in a sterile flask with 10 g/L of sucrose and 2 g/L of yeast extract to support the fungal growth. The fungus was left to grow on the fibres at room temperature for a period of three to four days with slow agitation. The fibres are autoclaved after their respective treatment time and washed for further processing to cellulose nano-fibers.

2.2.2. High-Shear Refining. The biotreated fibres were passed through a PFI (Paperindustriens Forkninginstitutt, Oslo, Norway) high-shear refiner to further affect internal defibrillation. 24 grams of fiber at 10% consistency was charged into the PFI mill and sheared for 100,000 revolutions to affect internal defibrillation in the fibre.

2.3. Fiber Characterization

2.3.1. Transmission Electron Microscopy (TEM). Phillips CM 201 model was used for this study. The transmission electron microscopy (TEM) images were used to understand the surface morphology and diameter distribution of the treated fibres and cellulose microfibrils isolated.

2.3.2. FI-IR Spectroscopy. The hydrogen bond type and density associated with the fibre were investigated using FT-IR spectroscopy.

Dried cellulose samples over phosphorus pentoxide in a desiccator were made into a pellet with Potassium Bromide (KBr) powder (1 : 5, cellulose: KBr) and analyzed by FT-IR spectroscopy. The FT-IR spectra (256 scans, 4 cm^{-1}) were determined by the diffuse reflectance method (DRIFT) using a Bruker Tensor 27 spectrometer.

There are many powerful tools which may be used to investigate cellulose chemistry and its structure: X-ray, electron diffraction and microscopy, FTIR, FT-Raman and solid-state MNR of which FT-IR is one of the most versatile techniques to study the hydrogen bond formation. Using FT-IR, Fengel [14, 15] analyzed the hydroxyl absorption bands by deconvoluting the spectra of cellulose. Michell [16, 17] used the 2nd derivative mode of the FT-IR spectra to improve its resolution considerably. Sugiyama et al. [18] and Michell [19] used FT-IR spectral data to establish and confirm the findings of Wiley and Atalla [20], that the crystalline dimorphism of native cellulose, cellulose I_α and I_β were considered to differ in their hydrogen bonding rather than in their conformation. Tashiro and Kobayashi used IR spectra to determine the O-H stretching frequencies due to intra- and intermolecular hydrogen bonds in cellulose I and II.

Fourier Self-Deconvolution. All FT-IR spectra are baseline corrected and compensated for CO_2 and H_2O before any manipulation.

The aim of Fourier self-deconvolution is to enhance the apparent resolution of a spectrum or to decrease the line width. Fourier self-deconvolution (FDS) assumes that the spectrum to be measured consists of well-resolved lines which have been convoluted by the same type of line broadening function (LBF). If the shape and width of the LBF are known, its effects can be arithmetically excluded from the spectra. In general, the deconvolution corresponds to a multiplication of the interferogram $I\ (x)$ using the exp $(a*x)$ deconvolution function for Lorentzian and exp $(a*x*x)$ for Gaussian shapes. The deconvolution factor is the maximum value of these functions at the end of the interferogram. To avoid the increase of noise caused by the deconvolution, a Blackman-Harris apodization is simultaneously performed on the spectra.

Curve Fit. Curve fitting procedure was used to calculate single components in a system of overlapping bands. A model consisting of an estimated number of bands is essen-tial before the fitting calculation is started. The IR absorption bands for the OH stretchingregions were

deconvoluted before the curve fitting procedure. To improve the calculation, the peaks need to be resolved and their number, position, and areas determined. The number of peaks and their position were determined by the point at which the second derivative of the spectrum contained peaks of interest. The position of the deconvoluted bands can give us information about the nature and type of OH functionality.

3. Results and Discussion

3.1. Effect of OS1 Pretreatment of Fibres on Cellulose Nanofibres Yield and Fibre Diameter Distribution. As mentioned earlier, one of the major challenges impeding the isolation of cellulose nanofibres on a sizable scale for any application is the high-energy requirement associated with neutralizing the predominating hydrogen bonds between the cellulose microfibrils and also between microfibrils and hemicellulose. The interfibrillar hydrogen bonding energy has to be overcome in order to separate the microfibres into individual entities. This association energy for cellulose ranges between 19 and 21 MJ/kg moL, with 20 MJ/kg·moL being used as an average value in most cases.

OS1 fungus was used for the fibre treatment and is based on our prior knowledge of their effect on hemp fibres—its capacity to degrade and probably hydrolyze the cellulose [21].

3.1.1. Yield and Diameter Distribution of Cellulose Nanofibres. The effect of bio-treatment on the yield of cellulose nanofibres and their diameter distribution is detailed in an earlier publication by Janardhnan and Sain [6].

Fibres treated with OS1 were PFI refined and the number average diameter distribution of these refined fibres for 4-day treatment is detailed in Figure 1. Cellulose nanofibre diameter distribution showed a significant shift towards the lower diameter range with the maximum yield of fibres occurring between 50 and 75 nm for the 4-day biotreated fibres while the maximum yield for the untreated fibre occurred between 100 and 250 nm.

The separation of elementary fibres takes place to a good extent with biotreated fibres while PFI refining seems to have a less fibril separation effect on untreated fibers. The isolated nano-fibers from biotreated and untreated fibers showed distinct morphological differences. There is a distinct separation of elementary fibers into individualized nanofibres for biotreated fibers compared to limited microfibrillation and separation for the untreated fibres after high-shear refining.

3.2. Effect of Enzymatic Pretreatment on the Hydroxyl Chemistry of Cellulose Fibre. Having established the fact that the biotreatment can bring about a certain degree of internal defibrillation in the treated wood fibre, it is important to substantiate and validate the possible mechanism in this effect. It is assumed that the internal defibrillation is a result of the cleavage of hydrogen bonds between elementary cellulose fibrils. Analysis of the FTIR spectra of biotreated and untreated fibers is done here to support and validate this assumption.

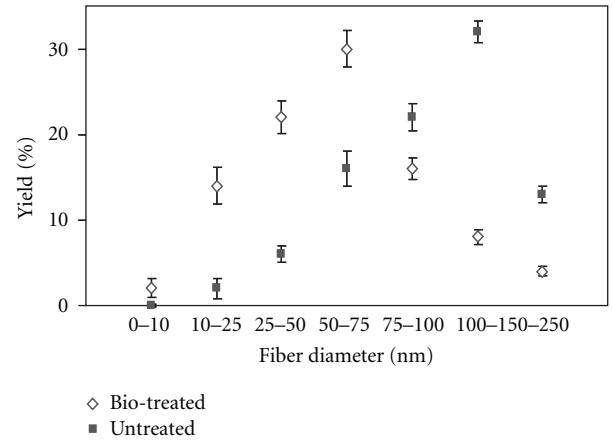

Figure 1: Effect of OS1 fungal treatments on number average diameter distribution of nanofibres after PFI refining for a 4-day treatment.

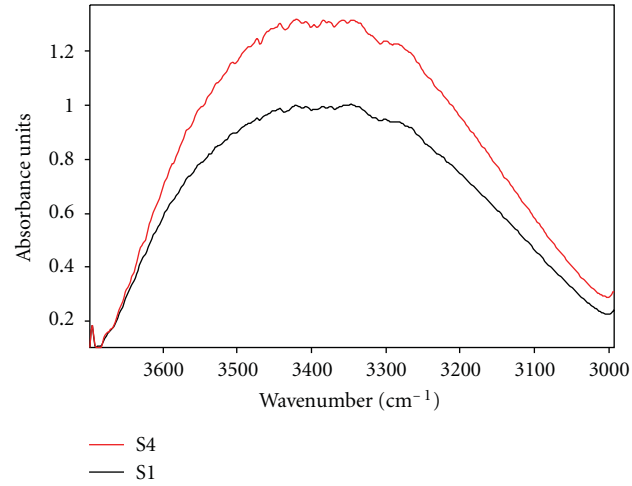

Figure 2: FT-deconvoluted OH bands (3600 to 3200 cm^{-1}); S1: biotreated; S4: untreated wood fiber.

FT-IR spectra of the untreated fibres and the biotreated fibres are FT-deconvoluted to improve the resolution of the OH stretching band and evaluated by curve fitting to determine the contributions of the integral intensities of each of the components to the total intensity of the whole band. Normalized FT-IR spectra of 4-day biotreated and untreated cellulose fibres are shown in Figure 2. The spectrum was obtained with equal amount of cellulose fibres and KBr to contain relative quantitative information about the OH functionality and their interaction in the sample.

The band at 2900/cm, which corresponds to C–H stretching vibration, is relatively unaffected by the degree of bio-treatment or other variables. Area under the peak 2900/cm is identified in Table 1. Thus, the area under this 2900/cm band was selected to serve as an internal standard for comparison.

Table 1: Change in IR Index of wood fire with enzymatic treatment.*

Enzyme treatment	OH peak area 2997–3742/cm	2900/cm Peak area	*Hydrogen bonds
S1	624.958	69.92	8.94
S4	681.227	70.52	9.66

S1: 4-day OS1 treatment; S4: untreated.
*Calculated by relative peak area with 2900/cm as internal standard.

3.2.1. Relative Intensity of Hydrogen Bond Network. Hydroxyl (OH^-) is the main functional group in cellulose, having various hydrogen bonding acceptors for the formation of hydrogen bonds. The untreated wood fibre sample, S4, shows 1.3 IR absorption units compared to the IR absorption unit of 0.7 with biotreated fibers as shown in Figure 2. A comparison of areas under the respective peaks is shown in Table 1. The absorption bands associated with OH stretching vibration in the cellulose samples indicate a difference in their absorption level suggesting a difference in the relative availability of OH in the samples analyzed. The difference in this IR absorption levels between the biotreated and untreated cellulose could be attributed to the difference in the density of hydrogen bonding in the fibre. Internal defibrillation that is happening in the fibres due to bio-treatment can be due to cleavage of hydrogen bonding that exists between the elementary cellulose fibres within the fibre.

3.2.2. Nature of Hydrogen Bonds. To better understand the effect of bio-treatment on the OH functionality and the hydrogen bonding type and pattern in the cellulose fibre, the OH bands associated with S1 and S4 are deconvoluted and curve fitted to individual bands that have a major contribution to the overall intensity of the OH band. To resolve this thought further, the peaks need to be resolved and their number and positions accurately determined. The major 2nd derivative peak in the region of interest (3600 to 3200 cm^{-1}) associated with FT-deconvoluted OH band was used for this purpose.

The peaks of interest are picked from the FT-deconvoluted bands of S1 and S4, and a model is set up to run the curve fitting procedure. Calculations were repeated until a best fit was obtained with rms error less than 0.01.

Investigators have established that the two bands between 3500 and 3400/cm are derived from the intramolecular hydrogen bonds between OH(3) and O(5) and that the bands between 3400 and 3100/cm are derived from intermolecular hydrogen bonds.

Curve-fitted OH bands (Figures 3 and 4) based on the peaks of interest picked, were found to provide more insight into the individual peaks that contributed to the broad OH band. FT-IR absorption characteristic bands associated with S4-untreated fibre in the OH stretching region demonstrated a marked difference from that of the peaks for S1 4-day OS-treated fibres.

Intermolecular Hydrogen Bonds. A careful observation of the IR absorption characteristic curves for biotreated fibre and untreated fibre in the 3400 to 3100/cm region which is due to the intermolecular hydrogen bonds that exist between the elementary cellulose fibres showed an apparent difference in the IR absorption intensity—0.9 IR absorption units for untreated fibre compared to 0.48 IR absorption unit for biotreated fibre. This observation can be considered as a direct validation of the supposition—OS1 treatment of wood fibres can facilitate the isolation of nanofibres by reducing the intermolecular hydrogen bond density. As discussed above, the increase in internal defibrillation of the biotreated fibre can be attributed to the decrease in the intermolecular hydrogen bonds between the elementary cellulose fibres.

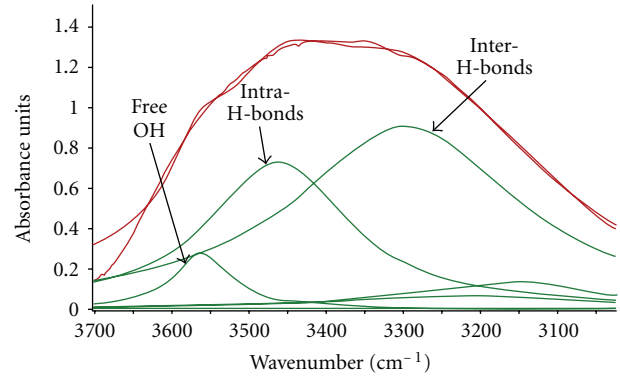

Figure 3: Curve fitting and peak assignments for OH stretching regions: S4: untreated wood fibre.

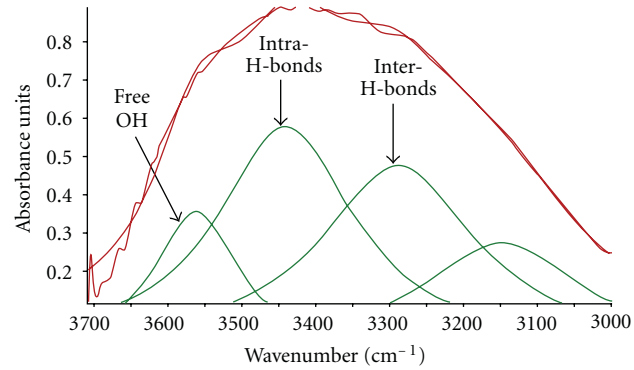

Figure 4: Curve fitting and peak assignments for OH stretching regions: S4: untreated wood fibre.

Intramolecular Hydrogen Bonds. The characteristic band of intramolecular hydrogen bonds in a cellulosic fibre peaks in the 3500 to 3400/cm region. The IR absorption intensity of the intramolecular hydrogen bond for enzyme-treated fibre showed a slight decrease compared to absorption intensity of the band for untreated fibre—0.71 IR absorption units for untreated fibre versus 0.58 IR absorption units for enzyme-treated fibres.

Free Hydroxyl Functionality. It is interesting to note that the peak 3560/cm, characteristic of the free hydroxyl groups in the cellulose fibre, showed a slight increase in the band

Table 2: Change in IR Index of D_2O-saturated wood fire with enzymatic treatment: OH peak from 2997 to 3724/cm.

Enzyme treatment	OH peak area 2997–3742/cm	2900 / cm Peak area	*Hydrogen bonds
S1	601.958	69.90	8.59
S4	652.227	70.50	9.24

S1: biotreated fibre; S4: untreated,
*Calculated by relative peak area with 2900/cm as internal standard.

intensity—0.28 IR absorption units for the untreated fibre compared to 0.35 IR absorption units for the enzyme-treated fibres. This increase may be a result of the reduction in the intermolecular and the intramolecular hydrogen bonds in the cellulose fibre. The increase in free OH groups in cellulose fibers may not be of benefit in the context of this research as the increased hydrophilicity of these fibers can reduce their interfacial compatibility (fibre-matrix interaction) in a hydrophobic polymer matrix.

Hydrogen Bonds and Their Association. The discussion above with respect to the effect of bio-treatment on hydrogen bond density in the fiber points to the fact that the extracellular enzyme produced by the fungus OS1 has the ability to interact with the OH chemistry, indeed reducing the intermolecular and intramolecular hydrogen bonding.

The hydrogen bonds in a fiber may be associated with either the amorphous region or the crystalline region. In order to differentiate and understand the contribution of hydrogen bonds associated with the crystalline and the amorphous regions to the IR absorption, the biotreated and untreated fibers were saturated with deuterium (D_2O), and the FT-IR absorption spectra were taken and analyzed. The hydrogen bond density, as shown in Table 2, showed a similar trend indicating the fact that the impact of bio-treatment was primarily on the hydrogen bonds associated with the crystalline region of the cellulose. When the fiber is placed in an environment saturated with D_2O, the OH group associated with amorphous region will be preferentially replaced with the D_2O. The OH associated with the crystalline region of the fiber will remain unaffected due to very limited accessibility.

4. Conclusion

The bio-treatment of fibres has shown to have a significant positive impact on the internal defibrillation characteristics of the fibre.

(a) FT-IR absorption characteristic of the biotreated fibres has shown a marked decrease in the intermolecular hydrogen-bond OH functionality, while only a marginal change in intramolecular hydrogen-bonded OH group and free OH groups.

(b) The fungus OS1 during its growth on fiber substrate potentially secretes enzymes capable of interacting with the hydroxyl chemistry of the fibers thereby disrupting the hydrogen bonding network.

(c) The bio-treatment of fibers has the potential of being developed into an energy efficient approach for the isolation of cellulose nanofibres from plant cell wall.

Acknowledgment

The authors are grateful for the support of Natural Science and Engineering Research Council of Canada.

References

[1] F. A. L. Clowes and B. E. Juniper, *Plant Cells*, Blackwell Scientific Publications, 1968.
[2] C. Y. Liang and R. H. Marchessault, "Infrared spectra of crystalline polysaccharides. I. Hydrogen bonds in native celluloses," *Journal of Polymer Science*, vol. 37, pp. 385–395, 1959.
[3] A. Chakraborty, M. Sain, and M. Kortschot, "Cellulose microfibrils: a novel method of preparation using high shear refining and cryocrushing," *Holzforschung*, vol. 59, no. 1, pp. 102–107, 2005.
[4] K. Tashiro and M. Kobayashi, "Theoretical evaluation of three-dimensional elastic constants of native and regenerated celluloses: role of hydrogen bonds," *Polymer*, vol. 32, no. 8, pp. 1516–1526, 1991.
[5] L. A. Burglund, *Cellulose Based Nanobiocomposites*, CRC Press LLC, 2004.
[6] S. Janardhnan and M. Sain, "Isolation of cellulose microfibrils—an enzymatic approach," *Bio-Resources*, vol. 1, no. 2, pp. 176–188, 2006.
[7] W. Bolaski, A. Gallatin, and J. C. Gallatin, "Enzymatic Conversion of Cellulosic Fibers," United States Patent no. 3, 041,246, 1959.
[8] W. D. Yerkes, "Process for the digestion of cellulosic materials by enzymatic action of Trametes suaveolens," United States Patent 3, 406,089, 1985.
[9] Y. Nomura, "Digestion of pulp," 1985, Japanese Patent no. 126, 395/85.
[10] J. L. Fuentes and M. Robert, "Process of treatment of a paper pulp by an enzymic solution," European Patent 262040, 1988.
[11] I. Uchimoto, K. Endo, and Y. Yamagishi, "Improvement of deciduous tree pulp," Japanese Patent no. 135, 1988.
[12] M. G. Paice and L. Jurasek, "Removing hemicellulose from pulps by specific enzymic hydrolysis," *Journal of Wood Chemistry and Technology*, vol. 4, no. 2, pp. 187–198, 1984.
[13] L. Jurasek and M. G. Paice, "Biological treatments of pulps," *Biomass*, vol. 15, no. 2, pp. 103–108, 1988.
[14] D. Fengel, "Characterization of cellulose by deconvoluting the OH valency range in the FTIR spectra," *Holzforschung*, vol. 46, no. 4, pp. 283–288, 1992.
[15] D. Fengel, "Influence of water on the OH valency range in deconvoluted FT-IR spectra of cellulose," *Holzforschung*, vol. 47, pp. 103–108, 1993.
[16] A. J. Michell, "Second derivative F.t.-i.r. spectra of celluloses I and II and related mono- and oligo-saccharides," *Carbohydrate Research*, vol. 173, no. 2, pp. 185–195, 1988.
[17] A. J. Michell, "Second-derivative F.t.-i.r. spectra of native celluloses," *Carbohydrate Research*, vol. 197, no. C, pp. 53–60, 1990.
[18] J. Sugiyama, J. Persson, and H. Chanzy, "Combined infrared and electron diffraction study of the polymorphism of native celluloses," *Macromolecules*, vol. 24, no. 9, pp. 2461–2466, 1991.

[19] A. J. Michell, "Second-derivative FTIR spectra of native celluloses from Valonia and tunicin," *Carbohydrate Research*, vol. 241, pp. 47–54, 1993.
[20] J. H. Wiley and R. H. Atalla, "Band assignments in the raman spectra of celluloses," *Carbohydrate Research*, vol. 160, no. C, pp. 113–129, 1987.
[21] D. Gulati, *Modification of interface in natural fiber reinforced composites*, M.A.Sc thesis, University of Toronto, 2006.

Hindawi Publishing Corporation
International Journal of Polymer Science
Volume 2011, Article ID 803428, 7 pages
doi:10.1155/2011/803428

Research Article

Effect of Sisal Fiber Surface Treatment on Properties of Sisal Fiber Reinforced Polylactide Composites

Zhaoqian Li,[1,2] Xiaodong Zhou,[1] and Chonghua Pei[2]

[1] *State Key Laboratory of Chemical Engineering, East China University of Science and Technology, Shanghai 200237, China*
[2] *State Key Laboratory Cultivation Base for Nonmetal Composites and Functional Materials, Southwest University of Science and Technology, Mianyang 621010, China*

Correspondence should be addressed to Xiaodong Zhou, xdzhou@ecust.edu.cn and Chonghua Pei, peichonghua@swust.edu.cn

Received 30 March 2011; Accepted 10 June 2011

Academic Editor: James Njuguna

Mechanical properties of composites are strongly influenced by the quality of the fiber/matrix interface. The objective of this study was to evaluate the mechanical properties of polylactide (PLA) composites as a function of modification of sisal fiber with two different macromolecular coupling agents. Sisal fiber reinforced polylactide composites were prepared by injection molding, and the properties of composites were studied by static/dynamic mechanical analysis (DMA). The results from mechanical testing revealed that surface-treated sisal fiber reinforced composite offered superior mechanical properties compared to untreated fiber reinforced polylactide composite, which indicated that better adhesion between sisal fiber and PLA matrix was achieved. Scanning electron microscopy (SEM) investigations also showed that surface modifications improved the adhesion of the sisal fiber/polylactide matrix.

1. Introduction

With the increasing of environmental protection consciousness, natural fibers as a group of environmental friendly reinforcements are in considerable demand in composites [1, 2]. Natural fibers such as flax, hemp, sisal, nettle and jute were the most common reinforced elements [2, 3]. Of course, natural fiber reinforced degradable polymers composite is likely more ecofriendly because that the reinforcement and the matrix (e.g., polylactide (PLA)) are readily biodegradable and such biocomposites are sometimes termed "green composites" [4, 5].

Natural fibers as reinforcement are familiar. However, there is also a major drawback associated with its application for reinforcement of polymeric matrices. The presence of hydroxyl and other polar groups in natural fibers constituents makes them exhibit high hydrophilic nature, which leads to incompatibility and poor wettability in a hydrophobic polymer matrix, and weak bonding in the fiber/matrix interface [6]. Herewith, there are many problems in dealing with the interface of natural fiber and polylactide.

Several approaches have been studied, such as surface modification of cellulose (e.g., esterification of cellulose and graft copolymerization onto cellulose substrates) and the use of some compatibilizers (e.g., maleated polylactide and isocyanate [7–11]). Nevertheless, only a limited number of studies had achieved good results. And there is no commercial sale of such interfacial compatibilizers in the market.

Among the various natural fibers, sisal fiber is fairly coarse and inflexible. It possesses moderately high specific strength and stiffness, durability, ability to stretch, and resistance to deterioration in saltwater [12, 13]. Therefore, it can be used as a reinforcing material in polymeric resin matrices to make useful structural composite materials [14–16].

In our recent work, we have synthesized two different macromolecular coupling agents: MPS-g-PLA (Polylactide-graft-γ-methacryloxypropyltrimethoxysilane) and PLA-co-PGMA (Polylactide-co- glycidyl methacrylate) [17, 18]. And the results of the former research suggested that they were efficient in modifying natural fiber surface and in improving the compatibility of PLA/cellulose composites. In this study,

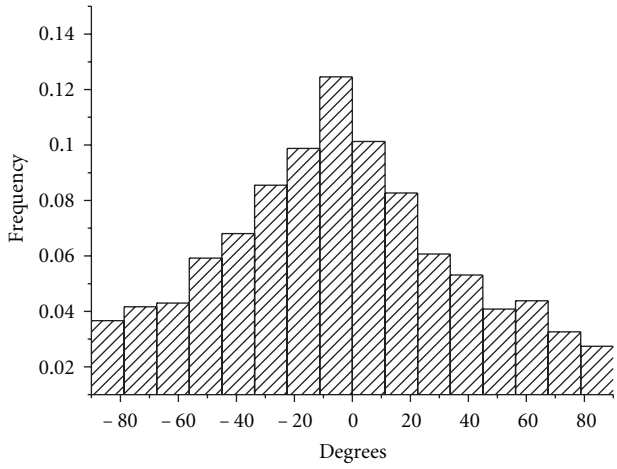

Figure 1: Fiber orientation distribution of PLA composite (PLA/sisal 30%).

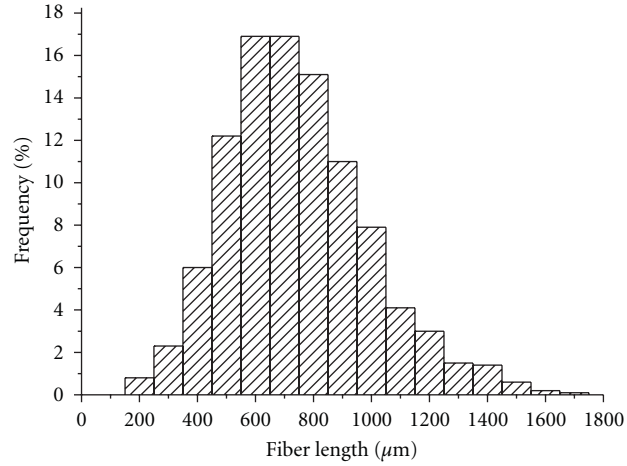

Figure 2: Fiber length distribution of PLA composite (sisal fiber content of 30%).

we attempt to use these two macromolecular coupling agents to improve the interfacial adhesion of PLA matrix and sisal fibers and solve the poor compatibility of natural fiber and PLA matrix. The effect of surface treatment of sisal fiber with MPS-g-PLA and PLA-co-PGMA on the mechanical properties was also evaluated.

2. Experimental

2.1. Materials. Commercial PLA (2002D, extrusion/thermoforming grade) from NatureWorks LLC was used in this work. It has a density of 1.24 g/cm^3, melt flow index of 5–7 g/10 min (210 C/2.16 Kg). Before use, it was dried at 80 C under vacuum for 24 h. Sisal fibers were supplied by Dongfang Sisal Group Co. Ltd., China. MPS-g-PLA and PLA-co-PGMA were prepared by us according to the literatures [17, 18].

2.2. Fiber Surface Modification. The MPS-g-PLA treatment of sisal fiber was carried out by immersing fibers in the dioxane solution of MPS-g-PLA at the concentration of 1 wt% for 48 h used acetic acid to adjust pH. Sisal fibers were taken out of the solution and dried for 2 days at room temperature, then sisal fibers reacted with MPS-g-PLA at 120 C for 2 h.

For PLA-co-PGMA treatment, sisal fibers were immersed in the dioxane solution of PLA-co-PGMA at the concentration of 1 wt% for 48 h. After dried at room temperature, the products were Soxhlet extracted with THF for 24 h and then dried.

2.3. Fabrication of Composites. PLA and the treated sisal fibers were compounded with a twin screw extruder (self-made, conical screw 110 mm in length), at 75 rpm and 190 C for 10 min. In order to obtain the desired specimens for various measurements and analysis, the molten composite samples were transferred, after extrusion through a pre-heated cylinder, to a mini-injection molder, which was preset

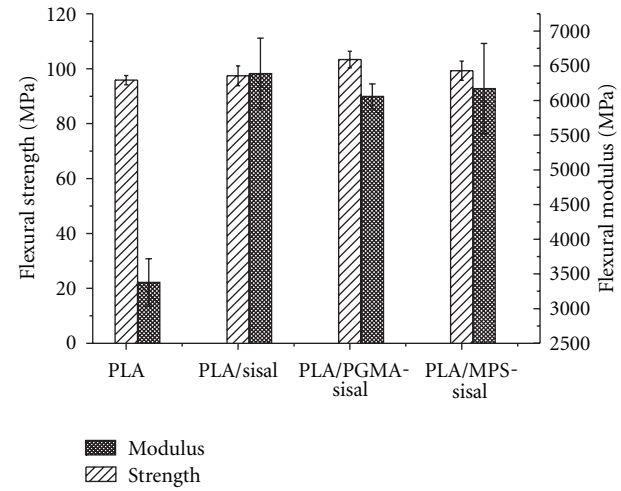

Figure 3: Flexural properties of 30 wt.% surface-treated Sisal fibers compared to untreated Sisal fibers reinforced composites.

the desired temperature (injection temperature at 190 C) and cooling system (mold temperature at 50 C).

2.4. Mechanical Properties. The tensile properties of the composites were measured on a CMT4204 universal testing machine (Shenzhen SANS testing machine co., ltd., China) according to ASTM D630. The cross-head speed was 1 mm/min, and the gauge length was 30 mm. The universal testing machine was also used to measure the flexural properties according to ASTM D790. The notched Izod impact strength was tested on an impact tester (Chengde, China), according to ASTM D256.

2.5. Dynamic Mechanical Analysis. The storage modulus, loss modulus, and loss factor (tan delta) of the composites were measured as a function of temperature (from 30 to 90 C) using a TA Q800 DMA, equipped with a

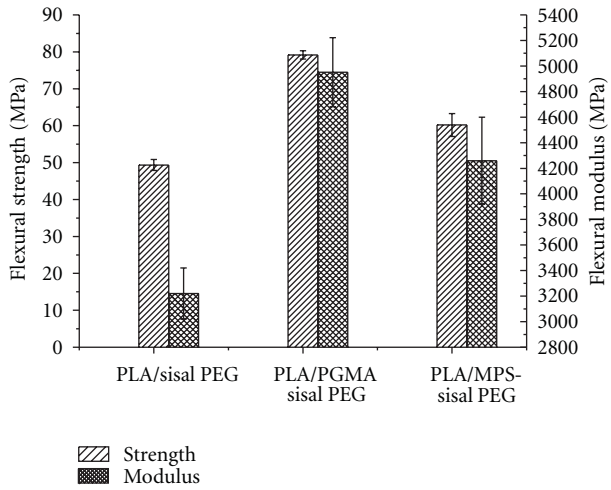

Figure 4: Flexural properties of PEG-Plasticized PLA and 30 wt.% sisal fiber composites.

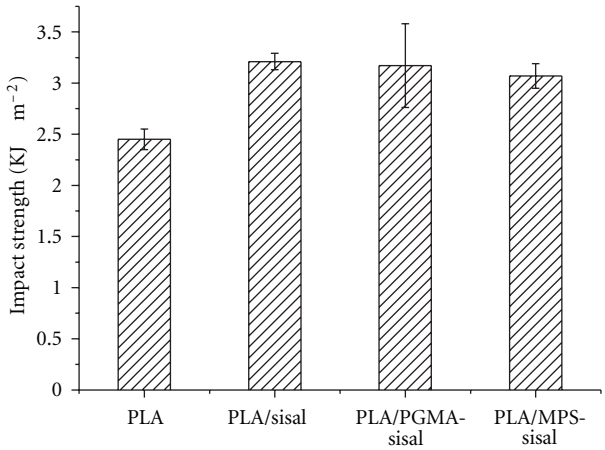

Figure 5: Notched Izod impact strength of Sisal fibers reinforced PLA composites.

dual-cantilever clamp at a frequency of 1 Hz and a heating constant rate of 3 C/min.

2.6. Scanning Electron Microscopy (SEM). Scanning electron microscopy (JSM-6360, FEI) was used to characterize the fractured surface of the composites. The samples were coated with a thin layer of gold before observation under the microscope mark, in order to increase the sample conductivity.

3. Results and Discussion

3.1. Fiber Orientation and Length Distribution. The fiber orientation and length distribution of the composites with unmodified sisal fiber is presented in Figures 1 and 2, respectively. The data were obtained from an analysis of a large number of micrographs. This composite shows a clear orientation with more than 30% of the fibers in the ± 20 interval. In addition, the visible length distribution

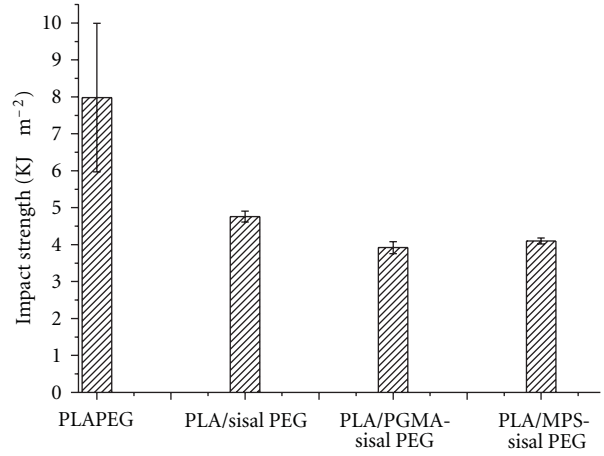

Figure 6: Notched Izod impact properties of PEG Plasticized PLA and their composites.

was measured from the micrographs, as shown in Figure 2. It was observed that most of the fibers had a length range of 600–800 μm, and the average fiber length was less than 1 mm, as a result of the shear stress imposed on fibers during compounding in the twin screw extruder.

3.2. Static Mechanical Properties

3.2.1. Tensile Properties. Mechanical properties of composites were strongly determined by the fiber-matrix interface. The tensile strengths of sisal/PLA composites at maximum load were shown in Table 1. Compared to the composites made with untreated fibers, the tensile strengths of composites were an improvement of 6.77% for PLA-co-PGMA treated fibers and 5.35% for MPS-g-PLA-treated sisal fibers. This was an indication that surface modification promoted good wettability and better fiber-matrix adhesion, allowing efficient stress transfer between the matrix and the fibers. This could be due to the better dispersion of fibers and the interaction of PLA and modified sisal fibers, and the reaction mechanism of the coupling agents and natural fiber has been explained in former paper [17, 18].

Table 1 also showed the properties of PLA plasticized with PEG and their composites with sisal fibers. The tensile strength of PEG-plasticized PLA reduced 50%, and the elongation at break was improved. In the treated fiber composites with PEG, the improvement of tensile strength was more obviously with respect to the samples without the plasticizer. This is likely because the increase of elongation at break optimizes the reinforcing effect of the fiber, and the interfacial adhesion play a key role in the transfer of the stress. Therefore, the results suggested that the surface treatment of sisal fibers significantly increased the interfacial adhesion.

3.2.2. Flexural Properties. Flexural properties of PLA and its composites were shown in Figure 3. According to the results, the introduction of sisal fibers significantly improved flexural modulus compared to the neat PLA matrix. The

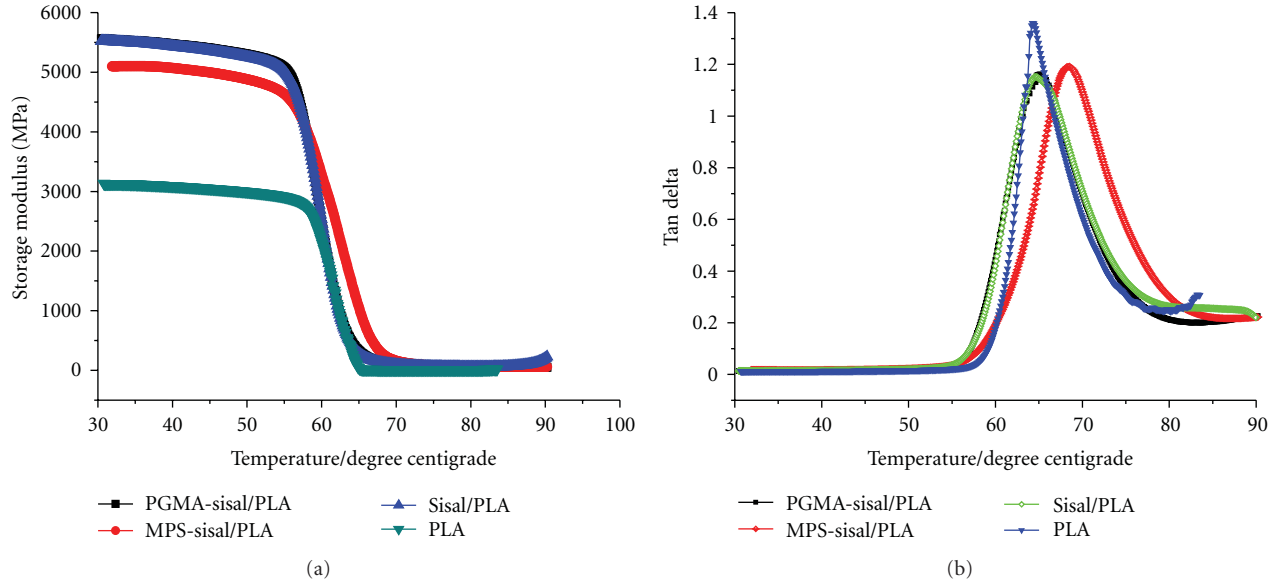

Figure 7: The storage modulus as a function of temperature for PLA and its composites. (a) Storage modulus; (b) The loss factor.

Table 1: Tensile properties of PLA and their composites with 30 wt.% sisal fibers.

Sample	Tensile strength (MPa)	Improvement (%)
PLA	56.97 ± 1.25	—
PLA/sisal 30%	56.68 ± 3.51	—
PLA/PLA-co-PGMA treatment sisal 30%	60.52 ± 1.43	6.23 (6.77)
PLA/MPS-g-PLA treatment sisal 30%	59.71 ± 1.57	4.81 (5.35)
PEG-plasticized PLA	27.88 ± 2.14	—
PEG-plasticized PLA/sisal 30%	33.96 ± 2.17	21.81
PEG-plasticized PLA/PLA-co-PGMA treatment sisal 30%	39.08 ± 1.48	40.17
PEG-plasticized PLA/MPS-g-PLA treatment sisal 30%	34.99 ± 2.94	25.50

Note: the figure in brackets was compared with that of PLA/sisal 30%.

two surface-treated sisal fibers composites improved the flexural strength compared to unmodified fibers. The best results were observed when the reinforcement surface had been treated with PLA-PGMA. This was due to improving the bonding between the fiber and the matrix. However, the flexural modulus of the PLA composites with the treated fibers decreases, which was paradoxical that good interfacial adhesion should improve the flexural modulus of composites. It is probable that the treatments have a lasting effect on natural fibers, such as the removal of amorphous components of fibers, especially on fiber stiffness [19, 20]. All the treatments decreased the strength and modulus of sisal fibers and influenced the modulus of the composite.

Flexural properties of PEG-plasticized PLA composites were shown in Figure 4. It can be noticed that the surface modification of fiber caused marked changes in the flexural strength and modulus of the composites. This also indicates that surface treatment enhances the interfacial adhesion of fibers and matrix.

3.2.3. Impact Strength of Composites. The notched Izod impact strength of the surface-treated sisal fiber reinforced composite results can supply information of the fiber-matrix interactions. Figure 5 showed the impact strength of the untreated and surface-treated sisal fibers reinforced composites. The impact strength of surface-treated composites was higher than those of the PLA matrix. Surface-treated composites decreased slightly compared to the untreated fiber composite. The negative impact of the treated composites is attributed to the fact that the surface treatment improves the fiber-matrix adhesion, which leads to the fracture of fibers rather than their pullout when they receive a mechanical shock.

The impact strength for PEG-plasticized PLA and their composites were shown in Figure 6. The same tendency is seen there. That is, surface modification reduces the impact strength of composites, which is in agreement with the report made by Huda et al. [21].

3.3. Dynamic Mechanical Analysis. Figure 7 showed the temperature dependence of dynamic storage modulus and tan delta of the PLA and its composites. As seen in Figure 7(a), the storage modulus increased with the addition of sisal

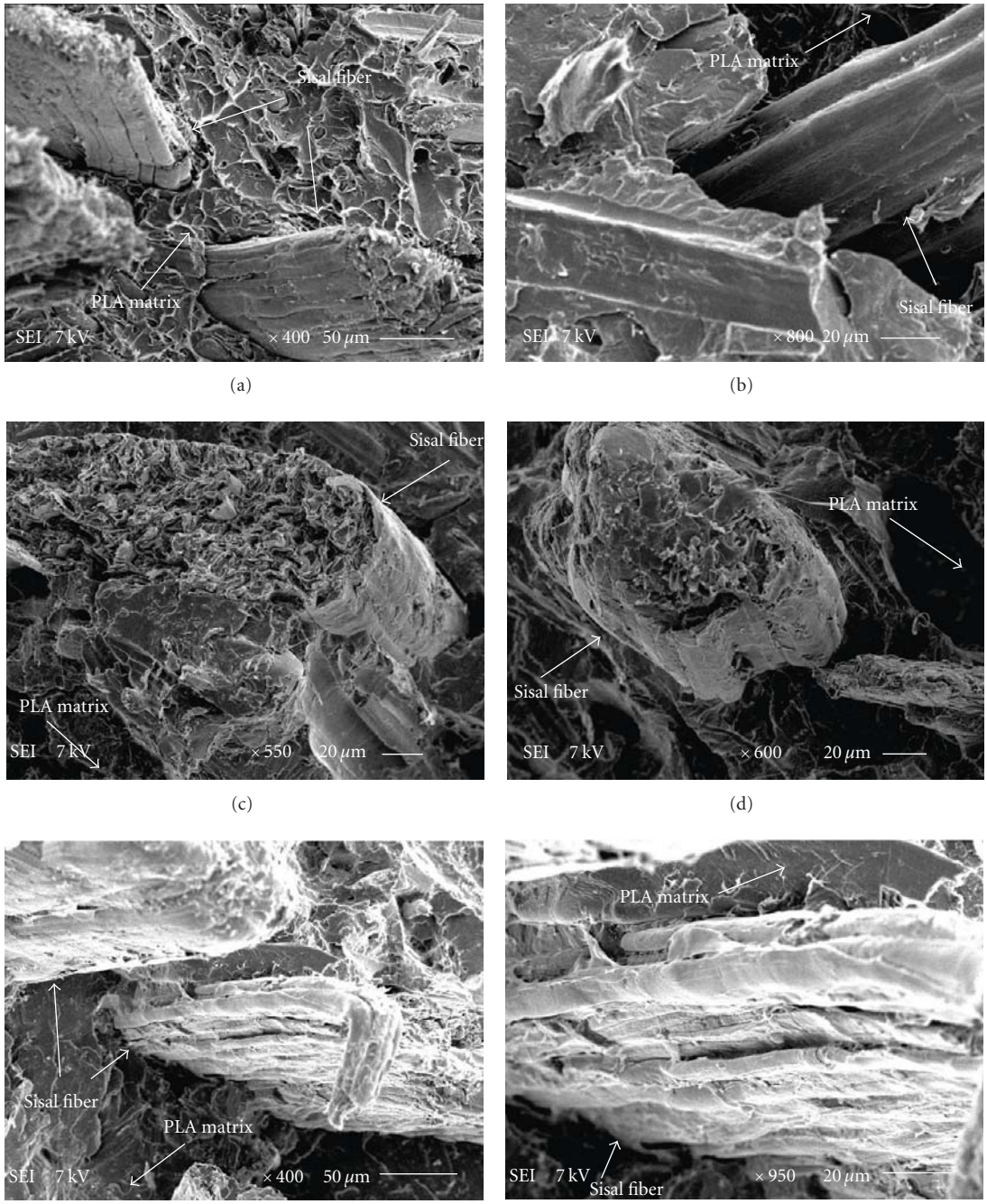

Figure 8: Morphology of a fractured surface of 30 wt.% sisal fiber/PLA composites. (a, b) Unmodified sisal fiber; (c, d) sisal fiber modified with PLA-co-PGMA; (e, f) sisal fiber modified with MPS-g-PLA.

fibers compared to that of PLA, which indicated that stress could be effectively transferred from the matrix to the fiber. The effect of surface treatment on the storage modulus of composites can be observed by comparing sisal/PLA with MPS-Sisal/PLA and PLGA-Sisal/PLA. Compared to unmodified fiber, the storage modulus of composites has a slight increase with PLA-co-PGMA treatment and a decline with MPS-g-PLA treatment. The chemical treatment of sisal fibers will bring about a positive effect as well as a negative one upon properties of fibers. Surface treatments of sisal fiber decreased its surface energy and the interfacial tension of fibers/PLA, which improved the dispersion of sisal fiber in PLA matrix and the compatibility of fiber and PLA [17, 18]. On the other hand, the strength and modulus of natural fiber reduced because of chemical treatment. When the two effects considered together, the modulus of PLA composites didn't get a significant rise, which was accorded with the result of flexural properties of the composites.

As can be seen in Figure 7(b), the addition of sisal fiber made the loss factor of PLA matrix diminish, which resulted from the impeding of sisal fibers on the movement of PLA molecular chain. The treatment with MPS-g-PLA enhanced the glass transition temperature of the composite. There was relatively little difference in their peak value of the loss factor of composites, which indicated that the composites possessed similar damping properties. The $\tan\delta$ of composites with MPS-g-PLA treatment was high compared to unmodified fiber, which agreed with Sreekumar et al.'s research result, and they thought this was for the decrease of the compactness and rigidity of natural fiber after the treatment [22]. Other researchers suggested that the increase of loss factor attributed to well-interfacial adhesion, which limited the movement of polymer molecular chains and increased the molecular segmental friction [23].

3.4. Morphology of Fractured Surface. SEM micrographs of the fractured surface of the treated and untreated sisal fiber composites can be seen in Figure 8. Figures 8(a) and 8(b) showed that no PLA matrix adhered to the fibers which were pulled out to a large extent. The fiber pullout in micrographs was an indication of weak fiber/matrix adhesion. In Figures 8(c), 8(d), 8(e), and 8(f), it was noted that sisal fibers were tightly connected with PLA matrix, which suggested interfacial bonding between sisal fiber and PLA was improved by the treatment with coupling agent. This indicated the improvement in the adhesion between fiber surface, and matrix and this well adhesion also led to an increase in mechanical properties. Therefore, surface modification has improved the compatibility of sisal fiber/PLA.

4. Conclusions

This study demonstrated that surface modification of sisal fiber had slightly increased tensile strength of composites and decreased its impact strength, which suggested that surface treatment improved the compatibility of sisal fiber and PLA matrix and effective stress transferred between fibers and matrix. In the case of PEG-plasticized polylactide, surface modification of sisal fiber made efficiency of reinforcement more obvious. This further revealed the interfacial binding strength of PLA, and fiber with PLA-co-PGMA and MPS-g-PLA was higher compared to unmodified fiber. From the DMA results, the storage modulus of composites has a slight increase with PLA-co-PGMA treatment and a decline with MPS-g-PLA treatment in contrast with that of unmodified fiber/PLA composites. SEM micrographs of the fracture surface of the impact specimen indicated that the adhesion between fiber and matrix could be improved after surface treatment of sisal fiber with coupling agents.

Acknowledgment

The authors acknowledge the financial support of the Open Project Program of the State Key Laboratory of Chemical Engineering, East China, University of Science and Technology.

References

[1] A. K. Bledzki, W. Zhang, and A. Chate, "Natural-fibre-reinforced polyurethane microfoams," *Composites Science and Technology*, vol. 61, no. 16, pp. 2405–2411, 2001.

[2] A. Ashori, "Wood—plastic composites as promising green-composites for automotive industries!," *Bioresource Technology*, vol. 99, no. 11, pp. 4661–4667, 2008.

[3] J. Ganster and H.-P. Fink, "Novel cellulose fibre reinforced thermoplastic materials," *Cellulose*, vol. 13, no. 3, pp. 271–280, 2006.

[4] M. S. Huda, A. K. Mohanty, L. T. Drzal, E. Schut, and M. Misra, "'Green' composites from recycled cellulose and poly(lactic acid): physico-mechanical and morphological properties evaluation," *Journal of Materials Science*, vol. 40, no. 16, pp. 4221–4229, 2005.

[5] A. Iwatake, M. Nogi, and H. Yano, "Cellulose nanofiber-reinforced polylactic acid," *Composites Science and Technology*, vol. 68, no. 9, pp. 2103–2106, 2008.

[6] X. Li, L. G. Tabil, and S. Panigrahi, "Chemical treatments of natural fiber for use in natural fiber-reinforced composites: a review," *Journal of Polymers and the Environment*, vol. 15, no. 1, pp. 25–33, 2007.

[7] H. Lönnberg, Q. Zhou, H. Brumer III, T. T. Teeri, E. Malmström, and A. Hult, "Grafting of cellulose fibers with poly(ε-caprolactone) and poly(L-lactic acid) via ring-opening polymerization," *Biomacromolecules*, vol. 7, no. 7, pp. 2178–2185, 2006.

[8] M. Takatani, K. Ikeda, K. Sakamoto, and T. Okamoto, "Cellulose esters as compatibilizers in wood/poly(lactic acid) composite," *Journal of Wood Science*, vol. 54, no. 1, pp. 54–61, 2008.

[9] N. Teramoto, K. Urata, K. Ozawa, and M. Shibata, "Biodegradation of aliphatic polyester composites reinforced by abaca fiber," *Polymer Degradation and Stability*, vol. 86, no. 3, pp. 401–409, 2004.

[10] D. Plackett, "Maleated polylactide as an interfacial compatibilizer in biocomposites," *Journal of Polymers and the Environment*, vol. 12, no. 3, pp. 131–138, 2004.

[11] S. H. Lee and S. Wang, "Biodegradable polymers/bamboo fiber biocomposite with bio-based coupling agent," *Composites Part A*, vol. 37, no. 1, pp. 80–91, 2006.

[12] S. M. Sapuan, M. Harimi, and M. A. Maleque, "Mechanical properties of epoxy/coconut shell filler particle composites," *Arabian Journal for Science and Engineering*, vol. 28, no. 2B, pp. 171–181, 2003.

[13] P. V. Joseph, K. Joseph, and S. Thomas, "Effect of processing variables on the mechanical properties of sisal-fiber-reinforced polypropylene composites," *Composites Science and Technology*, vol. 59, no. 11, pp. 1625–1640, 1999.

[14] F. A. Silva, D. Zhu, B. Mobasher, C. Soranakom, and R. D. Toledo Filho, "High speed tensile behavior of sisal fiber cement composites," *Materials Science and Engineering A*, vol. 527, no. 3, pp. 544–552, 2010.

[15] J. T. Kim and A. N. Netravali, "Mercerization of sisal fibers: effect of tension on mechanical properties of sisal fiber and fiber-reinforced composites," *Composites Part A*, vol. 41, no. 9, pp. 1245–1252, 2010.

[16] I. Singh, P. K. Bajpai, D. Malik, A. K. Sharma, and P. Kumar, "Feasibility Study on Microwave Joining of 'green composites'," *Akademeia*, vol. 1, no. 1, pp. 1–6, 2011.

[17] Z. Li, X. Zhou, and C. Pei, "Synthesis and characterization of mps-g-pla copolymer and its application in surface modification of bacterial cellulose," *International Journal of Polymer*

Analysis and Characterization, vol. 15, no. 4, pp. 199–209, 2010.

[18] Z. Q. Li, X. D. Zhou, and C. H. Pei, "Synthesis of PLA-co-PGMA copolymer and its application in the surface modification of bacterial cellulose," *International Journal of Polymeric Materials*, vol. 59, no. 9, pp. 725–737, 2010.

[19] M. Z. Rong, M. Q. Zhang, Y. Liu, G. C. Yang, and H. M. Zeng, "The effect of fiber treatment on the mechanical properties of unidirectional sisal-reinforced epoxy composites," *Composites Science and Technology*, vol. 61, no. 10, pp. 1437–1447, 2001.

[20] M. S. Huda, L. T. Drzal, A. K. Mohanty, and M. Misra, "Effect of chemical modifications of the pineapple leaf fiber surfaces on the interfacial and mechanical properties of laminated biocomposites," *Composite Interfaces*, vol. 15, no. 2-3, pp. 169–191, 2008.

[21] M. S. Huda, L. T. Drzal, A. K. Mohanty, and M. Misra, "Effect of fiber surface-treatments on the properties of laminated biocomposites from poly(lactic acid) (PLA) and kenaf fibers," *Composites Science and Technology*, vol. 68, no. 2, pp. 424–432, 2008.

[22] P. A. Sreekumar, R. Saiah, J. M. Saiter et al., "Effect of chemical treatment on dynamic mechanical properties of sisal fiber-reinforced polyester composites fabricated by resin transfer molding," *Composite Interfaces*, vol. 15, no. 2-3, pp. 263–279, 2008.

[23] I. C. Finegan and R. F. Gibson, "Recent research on enhancement of damping in polymer composites," *Composite Structures*, vol. 44, no. 2-3, pp. 89–98, 1999.

Hindawi Publishing Corporation
International Journal of Polymer Science
Volume 2011, Article ID 192865, 9 pages
doi:10.1155/2011/192865

Research Article

Time Effects on Morphology and Bonding Ability in Mercerized Natural Fibers for Composite Reinforcement

T. Williams,[1] M. Hosur,[1] M. Theodore,[2,3] A. Netravali,[4] V. Rangari,[1] and S. Jeelani[1]

[1] *Tuskegee Center for Advanced Materials, Tuskegee University, Tuskegee, AL 36088, USA*
[2] *Universal Technologies Corporation (UTC), 1270 N. Fairfield Rd., Dayton, OH 45432, USA*
[3] *Materials & Manufacturing Directorate, Air Force Research Laboratory, WPAFB 2941 Hobson Way, Dyton, OH 45433, USA*
[4] *Department of Fiber Science and Apparel Design, Cornell University, Ithaca, NY 14853, USA*

Correspondence should be addressed to M. Hosur, hosur@mytu.tuskegee.edu

Received 29 March 2011; Accepted 3 May 2011

Academic Editor: Susheel Kalia

Properties of cellulose-derived fibers are extremely sensitive to surface treatment. Many studies have investigated the effects of varying surface treatment parameters in natural fibers to improve fiber-matrix bonding; however, work is still needed to assist with developing better quality control methods to use these fibers in more load-bearing composites. Kenaf fibers were alkali treated, and the surface and morphology were analyzed to determine how treatment time affected the bonding sites in natural fibers. The mechanical behavior was also characterized, and tensile testing reported a 61% increase in strength and a 25% increase in modulus in fibers treated for 16 hours. The increase in tensile properties was assumed to result from increased intermolecular interaction and increased crystallinity in cellulose, which was supported by XRD. On the other hand, FTIR spectroscopy and XPS showed that the amount of hydroxyl groups needed for fiber-matrix bonding decreased at longer treatment times.

1. Introduction

Many plant-based fibers are known to exhibit high mechanical properties and are thought to have the potential to possibly replace some synthetic composite reinforcement [1–4]. Unlike synthetic fibers, natural fibers are inexpensive, lower in density, yearly renewable, carbon neutral, and are known to pose no health hazard to workers [5, 6]. However, many factors can prevent natural fibers from displaying their full potential due to resin-reinforcement incompatibility and the presence of surface impurities.

Hydrophobic layers found in natural fibers, such as lignin, are not favored for interaction with most hydrophilic resins. Lignin, being mostly hydrophobic, shows poor adhesion between the fibers and the resin resulting in low mechanical properties in biocomposites. Typical structures of the most common components in natural fibers, pectin, cellulose, hemicelluloses, and lignin, are shown in Figures 1, 2, 3, and 4, respectively.

Chemical treatment has been a well-known method employed to clean the surfaces of fibers and remove unwanted components, such as waxes, pectin, hemicellulose, and lignin. The removal of these materials has been observed to help with improving interfacial bonding with the commonly used industrial resins [7]. In addition, since the cellulose content increases, the fiber tensile properties also improve. However, the success of treatment in cellulose-based fibers depends not only on the type of treatment, but also on treatment parameters, such as time, concentration, and temperature.

Previous studies have revealed how various methods such as silane, alkali, peroxide, and isocyanate treatments affect the properties of natural fibers [8, 9]. Out of these methods, it has been observed that one of the simplest, most economical and effective forms of treatments with least environmental impact, is alkali treatment particularly mercerization using NaOH [10]. Much work has been done with alkali treating natural fibers for use in composites [11, 12]. Temperature-dependent alkali treatment studies have shown how fibrillation is affected with increased treatment temperatures [13]. At higher temperatures, it was discovered that fibrillation and the removal of noncellulose components

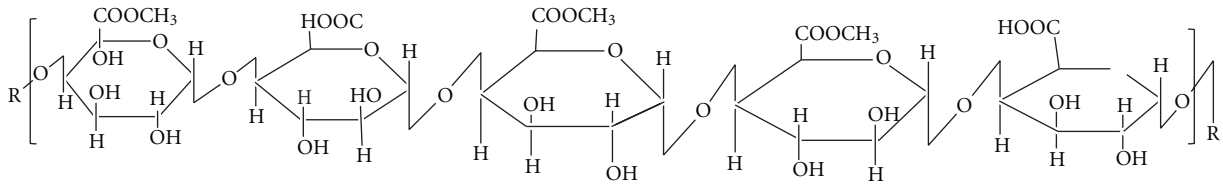

Figure 1: Structure of pectin.

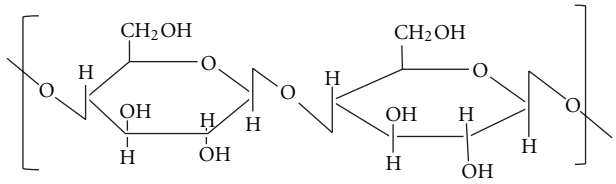

Figure 2: Cellulose structure.

occurred at a faster rate [13]. On the other hand, if the treatment temperature is too high, it is possible to deteriorate cellulose, resulting in lower mechanical properties of the fibers.

Literature has also shown the effect of varying alkali concentrations and times during natural fiber mercerization [14]. In one study, jute fibers were treated with multiple alkali solutions at two different times. The authors reported a 79% increase in modulus in jute fibers [15]. Another group of authors investigated how different alkali treatment times and concentrations affected properties of Indian grass fibers [16]. SEM showed that fibers were finer in size after mercerization, which could have been evidence of increased fiber fibrillation. On the other hand, plant-based fibers are fairly difficult to measure due to the inconsistencies with varying fiber diameters.

A 40% increase in tensile and impact properties was reported in alkali-treated Indian grass-reinforced biocomposites. The increase in mechanical properties was believed to be caused from better dispersion of finer fibers, which improved reinforcement ability in the composites. Increased mechanical properties were also believed to result from the presence of increased hydroxyl groups at different treatment times and concentrations. The effects of alkali treatment on the tensile and impact properties of natural fiber-reinforced biocomposites were also studied by Suizu et al. [11]. Suiza et al. alkali treated unidirectional ramie yarns for 2 hours with a 15 wt% NaOH solution. After fabricating the biocomposites using a biodegradable thermoplastic resin, an increase in mechanical properties of ramie-reinforced biocomposites was observed. It was assumed that the increase in impact and tensile properties were caused by enhanced interfacial bonding between the fibers and resin [11].

In another study, curaua fibers were alkali treated for 2 hours with a 10 wt% or 15 wt% NaOH solution and used as reinforcement in a thermoplastic matrix [12]. Although several different composite processing methods were studied, biocomposites that contained alkali-treated curaua fibers showed superior tensile properties compared to untreated curaua biocomposites. Once again, the increase in tensile properties was assumed to be the result of an increase in interfacial bonding between the fibers and matrix, which was caused from the removal of lignin and other incompatible ingredients [12].

Most time-based studies have generally shown that longer treatment times lead to better mechanical properties and enhanced cellulose exposure [17]. However, fibers can also exhibit lower mechanical properties if treated too long. As previously stated, the mechanical performance and composition of natural fibers can be influenced significantly by alkali treatment parameters. Unfortunately, treatment times in many natural fibers have not been extensively analyzed to determine how the duration of treatment affects the morphology, surface chemistry, and fiber bonding for later use with common resins, such as epoxies and polyesters.

The objective of this study, therefore, is to investigate how treatment times influence the surface changes, morphology, and, hence, bonding ability in natural fibers. All of these factors can severely influence the effectiveness of using natural fibers in composites. For example, if a certain type of fibers has high mechanical properties, but the amount of sites available for bonding is low, treatment would prove to be ineffective. Since the overall mechanical properties of composites are heavily dependent upon fiber-matrix adhesion, providing means to enhance interfacial bonding is crucial.

In the present study, bast kenaf fibers were alkali treated with sodium hydroxide (NaOH) solution, and the fibers were characterized using FTIR spectroscopy and XPS, XRD, SEM, and Instron tensile testing to characterize the structural changes, crystallinity, surface, and tensile properties, respectively. Kenaf plant is considered as a weed and, hence, does not need much care before or during its growth. It is also fairly disease resistant. As a result, kenaf is one of the least expensive natural fibers and, if processed properly, expansion in its use as reinforcement in "green" and other composites is possible. The fibers are extracted from the stem of the plants and are also known as bast fibers. This type of fiber has been used in paper, furniture, and textile applications, and, with treatment, it can also be used as reinforcement in some composite structures.

2. Materials and Methods

2.1. Treatment of Kenaf Fibers. Kenaf fibers (Kenaf Industries of South Texas, Raymondville, TX, USA) were treated using NaOH. The NaOH solution was prepared by dissolving

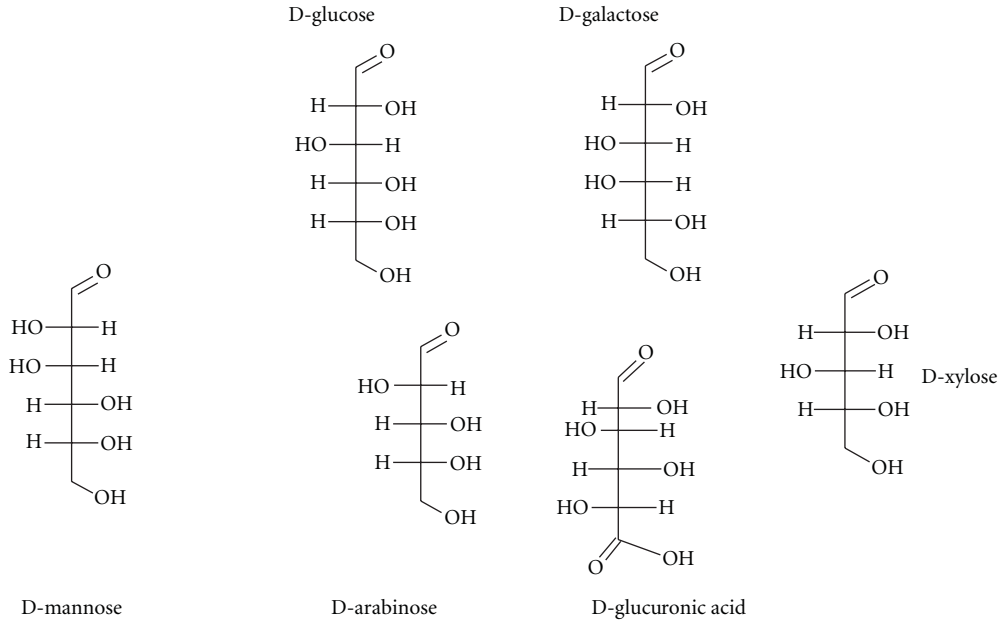

Figure 3: Various sugars of hemicelluloses.

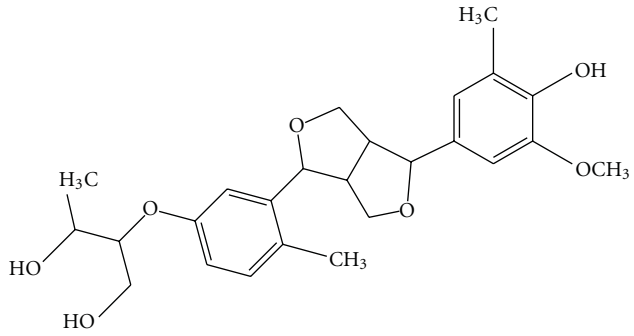

Figure 4: Proposed structure of lignin.

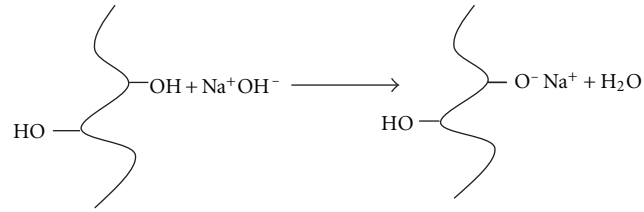

Figure 5: Alkali treatment reaction of cellulose-based fibers with NaOH.

NaOH pellets (Fisher Scientific) in deionized water to make up a 7 wt% of NaOH solution. Small bundles of kenaf fibers were cut approximately 44 mm in length and were soaked in alkali solution. The fibers made up 0.35 wt% of the NaOH solution. The fibers were alkali treated for 0.5, 1, 2, 4, 8, 16, and 24 hours at room temperature. After the treatment was complete, the fibers were rinsed thoroughly in distilled water until a neutral pH was obtained. The fibers were later dried in a vacuum oven at 80°C for 24 hours to ensure that all residual moisture was removed. An example of the alkali treatment reaction is shown in Figure 5.

2.2. Attenuated Total Reflectance-Fourier Transform Infrared (ATR-FTIR) Spectroscopy. The effect of alkali treatment on the surface of kenaf was studied using a Nicolet IR spectrometer in attenuated total reflectance (ATR) mode. This technique was used to study how alkali treatment times affected the surface properties of bast kenaf fibers. Generally, this method is carried out by placing a sample on a small crystal of a certain refractive index. The energy from the IR beam protrudes a few micrometers from the crystal and onto the sample surface. The absorbed energy from the surface of the sample is then passed to the IR detector. A diamond crystal was used, and 64 scans with a resolution of 4 cm^{-1} were collected for each spectrum. Additionally, ATR-FTIR spectroscopy was used to determine the effect of alkali treatment time on the mean hydrogen bond strength (MHBS) in kenaf. The MHBS was calculated by the use of the following equation:

$$\text{MHBS} = \frac{A_{(\text{OH})}}{A_{(\text{CH})}}, \tag{1}$$

where $A_{(\text{OH})}$ denoted the absorption of the hydroxyl stretching vibration in the region located at ~3300 cm^{-1} wavenumber, and $A_{(\text{CH})}$ corresponded to the absorption activity occurring in alkyl groups at 2980 cm^{-1} wavenumber [18].

2.3. X-Ray Photoelectron Spectroscopy (XPS). XPS was used to study the elemental compositions on the surfaces of kenaf following alkali treatment. This technique was carried out

using surface science instruments (SSI) M-Probe spectrometer using an incidence angle of 55°, where 95% of the signal comes from a depth of 3x (inelastic mean free path)x sin (55°). The samples were subjected to both low- and high-resolution scans. A survey scan was carried out to determine which elements were present. The peaks of interest were carbon and oxygen whose binding energies appeared in the ~290–270 and ~540–520 eV ranges, respectively. With this particular method, changes in the levels of the oxygen to carbon ratio (O : C) was assumed to be an indication of the presence or removal of hemicellulose and lignin. Casa software was used to analyze the peaks of interest. Casa processing software offers analysis techniques for both spectral and imaging data.

2.4. Scanning Electron Microscopy. The surfaces of untreated and alkali-treated kenaf were studied using a Jeol JSM 5800 scanning electron microscope with an accelerating voltage of 15 kV. The fibers were sputtered with Au/Pd for 5 minutes prior to imaging. The samples were sputtered using a Hummer 6.2 sputter coater by Anatech Ltd. to help eliminate charging on the samples during imaging.

2.5. Tensile Testing of Kenaf Fibril Bundles. The mechanical behavior of kenaf fibril bundles was characterized using an Instron Model 5566 materials testing system. Treated and untreated kenaf fibers were placed in a chamber maintained at ASTM conditions of 71°F (21°C) and 65% RH for 72 hours prior to testing. Specimens were prepared by mounting the bundles on paper tabs and securing the tips of the bundles with tape and glue. The kenaf bundles were tested using an effective gauge length of 30 mm. The diameters of the fibril bundles were determined using an optical microscope. A 100N load cell was used, and the fibers were strained at a rate of 4%/min. Bluehill software (version 1.2.) was used to analyze the data. At least 20 specimens were tested for each treatment times.

2.6. X-Ray Diffraction. X-ray diffraction was used to determine the effects of alkali treatment on the morphology of kenaf. XRD was carried out using a Rigaku Ultima diffractometer with a Cu Kα detector to determine if there was any effect on the crystallographic order in the fibers at various treatment times following alkali treatment. Samples were scanned at 5°/min across the range of 10–80° (2θ) using a step size of 0.2°, a voltage of 20 kV, and a current of 20 mA.

3. Results and Discussion

3.1. Effect of Alkali Treatment on Fiber Surface Functionality. Figure 6 shows the changes in chemical functionality in the ATR-FTIR spectra in untreated and alkali-treated kenaf fibers for all treatment times. It was observed that the absorption peak at ~1730 cm^{-1} wavenumber in as-received kenaf disappeared in as short as 30 minutes following treatment. The removal of this carbonyl peak corresponded to its removal from either carboxylate (–COOH) groups or (COO) ester linkages in pectin [19]. It is assumed that this peak belonged

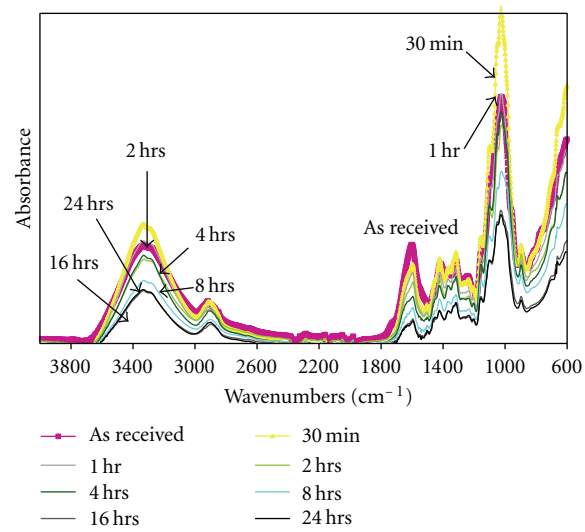

Figure 6: Effect of alkali treatment on surface functionality of kenaf fibers.

to carboxylate or ester linkages in pectin, because room temperature treatment using a 7 wt% NaOH solution may have been incapable of removing significant amounts of hemicelluloses in 30 minutes. The absorption peak located at ~1600 cm^{-1} wavenumber appeared to decrease as alkali treatment time increased. This absorption was believed to belong to the C=C bonds or aromatic bonds from lignin and was an indication that more lignin was removed as the length of mercerization increased [20].

The intensity in the absorption peaks located at ~1040 cm^{-1} wavenumber was also observed to decrease as treatment time increased. This change was possibly an indication of a decrease in absorption from C–OH or C–C stretching groups primarily found in hemicelluloses and/or cellulose [19]. The absorption band found at ~3300 cm^{-1} wavenumber was believed to belong to the hydroxyl-stretching vibration in hemicellulose and/or cellulose as well as absorbed moisture.

According to the spectra, the peak for the hydroxyl (–OH) groups at ~3300 cm^{-1} wavenumber was highest in fibers treated for 30 minutes. This was expected due to some of lignin being removed. It was believed that after lignin was removed, the exposure of hydroxyl groups in hemicellulose and cellulose increased. The intensity of the hydroxyl groups eventually decreased with longer alkali treatment times. Results showed that the hydroxyl stretching vibration continued to decrease as the treatment time increased to 16 hours, which was expected due to the increased degradation of hemicellulose. After 16 hours of treatment, very little changes were observed for the –OH peak. Since cellulose is fairly resistant to alkali solution, the minimum amount of activity taking place during these times was possibly an indication that mostly cellulose was present on the surface.

The mean hydrogen bond strength (MHBS) was calculated for the fibers at all treatment times. Figure 7 shows the effect of alkali treatment time on MHBS. According to the plot in Figure 7, the MHBS was highest for untreated

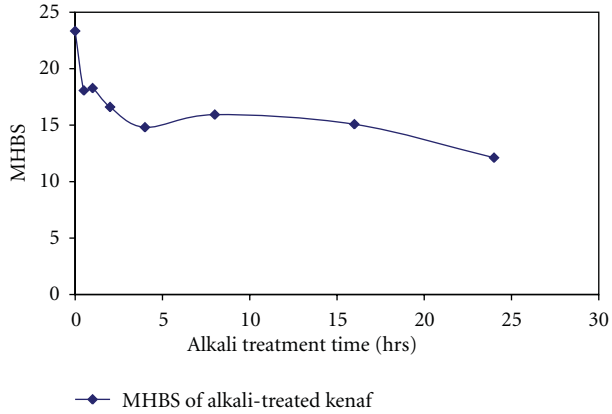

Figure 7: Effect of time on MHBS of alkali-treated kenaf fibers.

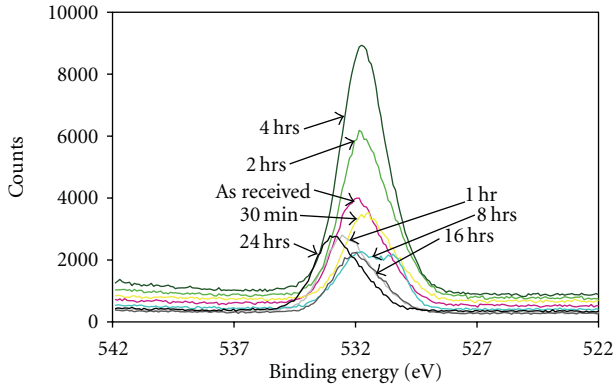

Figure 8: Oxygen region of XPS spectra in untreated and treated bast kenaf fibers.

kenaf. As the treatment time increased, the MHBS strength decreased, with the most significant decrease occurring between 30 minutes and 4 hours. Between 8 and 24 hours, the MHBS continued to gradually decrease. The sharp decrease in MHBS for kenaf alkali treated at shorter treatment times, confirm that the most significant changes taken place are a result of the removal of lignin and hemicellulose. The fact that the MHBS was highest for the untreated fibers was expected. Lignin has been known to form strong hydrogen bonds with hemicellulose, cellulose, and pectin, which was an indication why the MHBS was highest for untreated kenaf [21]. However, as mentioned earlier, the alkali treatment is capable of removing lignin and hemicellulose by disrupting the hydrogen bonding formed with cellulose by swelling the fiber cells [22]. As the hydrogen bonding was disrupted, a decrease in MHBS was observed in kenaf with increased treatment time.

3.2. XPS Surface Analysis of Alkali-Treated Fibers. In the XPS surface analysis scans, oxygen and carbon were the main elements of interest. As discussed, all natural fibers consist of hemicellulose, cellulose, pectin, and lignin. However, the major differences in properties of natural fibers are a result of varying concentrations of these constituents. Hemicellulose and pectin are both polysaccharides, while cellulose is a sugar

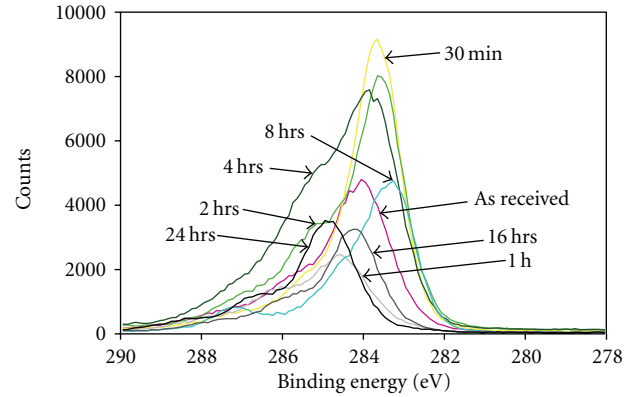

Figure 9: Carbon region of XPS spectra in untreated and alkali-treated kenaf fibers.

molecule as well. As a result, carbon and oxygen primarily make up the structures of these particular fiber layers. In some cases, however, it has been reported that hemicellulose may contain some nitrogen atoms in its structure [23]. Another point to note is that lignin is mostly made of hydrocarbons and is known to be either highly aromatic or highly unsaturated. For this reason, lignin is expected to possess a very low O : C ratio.

The changes in the oxygen and carbon regions associated with these elements are shown in Figures 8 and 9, respectively, for all alkali treatments. According to the data in Figures 8 and 9, the peaks that corresponded to the presence of oxygen and carbon fluctuated considerably in both intensity and broadness. Because of the variance, the peak ratios were studied to gather quantitative information in regards to how the length of treatment affected the surface chemistry of kenaf fibers.

Analysis of the data was carried out by measuring the areas under the curves and calculating the O : C ratios at each treatment time. These data are presented in Table 1. According to the data in Table 1, the as-received fibers contained an O : C ratio of ~0.87. After the first 30 minutes of treatment, the O : C ratio showed a noticeable decrease to 0.49 followed by an increase to almost a 1 : 1 O : C ratio for 1 hour treatment. The low O : C ratio observed at 30 minutes after treatment could be attributed to the removal of pectin and increased exposure of lignin on the fiber surface. Pectin is a complex structure that contains many hydroxyl and carboxyl groups. When NaOH is added to pectin, the sugars were possibly broken down and removed, leading to exposure of lignin. The O : C ratios between 1 and 4 hours were higher than at 30 minutes, but eventually decreased and appeared somewhat constant at 0.79 for treatments between 16 and 24 hours. This constant trend could have signified the increased exposure of cellulose, which is fairly resistant to NaOH treatment.

3.3. Scanning Electron Microscopy of Untreated and Alkali-Treated Kenaf Fibers. The effect of alkali treatment on the surfaces of kenaf fibers is shown as SEM photomicrographs in Figures 10(a) and 10(f). According to Figure 10(a),

Table 1: Oxygen to carbon ratio for untreated and alkali-treated kenaf fibers.

	0 hr	0.5 hr	1 hr	2 hrs	4 hrs	8 hrs	16 hrs	24 hrs
Oxygen	2155.9	1749.3	1551.1	1896.2	2321.8	1528.3	1513.1	1598.0
Carbon	2475.0	3550.0	1552.0	2031.0	2393.0	2451.0	1924.0	2035.3
O : C ratio	0.87	0.49	1.00	0.93	0.97	0.62	0.79	0.79

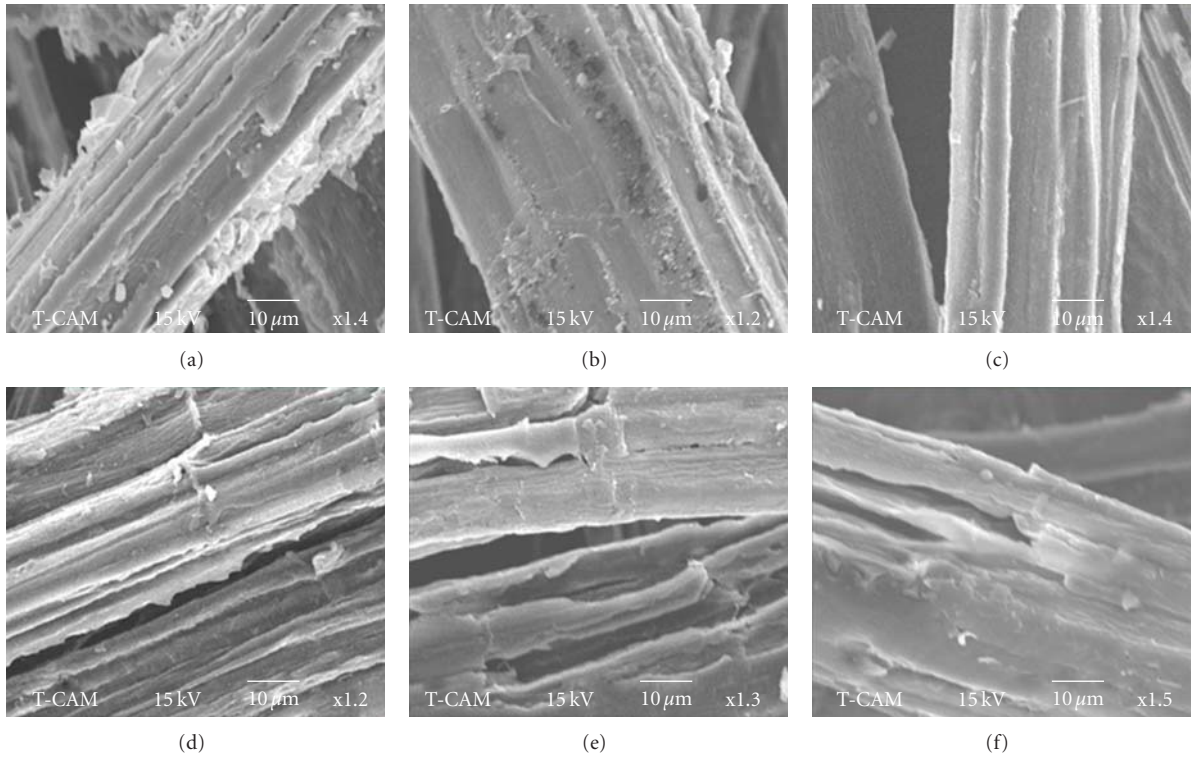

Figure 10: SEM of kenaf fibril bundles for (a) untreated fibers and kenaf fibril bundles treated for (b) 30 minutes, (c) 2 hours, (d) 4 hours, (e) 16 hours, and (f) 24 hours.

untreated kenaf contained considerable amounts of unwanted impurities on the kenaf surface. At 30 minutes (Figure 10(b)), it appeared that alkali treatment was successful with removing the surface contaminants. As the treatment time increased beyond 2 hours (Figure 10(c)), an increase in surface roughness was observed. This was believed to be caused from the deterioration of lignin and hemicellulose, the components that essentially bind individual fibrils into bundles to form fibers. The reduction in the amount of fibril bundles (commonly known as fibrillation) was assumed to lead to an increase in exposure of more reactive cellulose groups on the fiber surfaces.

As the treatment time approached 16–24 hours (Figures 10(e) and 10(f)), more evidence of breakage or damage on the fiber surfaces was observed. It is quite possible that some of the fibrils that were sufficiently loosened were lost and the inner surface, which consisted of hemicellulose and lignin and bound cellulose fibrils, was exposed. According to these observations, treating kenaf for longer than 16–24 hours would damage the fibers, and a decrease in mechanical performance would be noticed. On the contrary, what may have appeared as cracks on the kenaf surfaces could have been evidence of more fiber fibrillation from the removal of more hemicellulose.

3.4. Mechanical Property Evaluation of Alkali-Treated Kenaf Fibers. Figures 11(a) and 11(b) show the effects of alkali treatment times on the tensile stress and moduli, respectively, for kenaf fibers. According to Figure 11(a), the tensile stress increased as the treatment time increased from 195.4 MPa for control to a maximum of 314.9 MPa at 16 hour. When treated for 24 hours, the tensile stress of the fiber bundles decreased to 226.2 MPa. It was confirmed from statistical analysis that the tensile strength was significantly higher after treating kenaf for 8 hours.

The effect of alkali treatment on the Young's modulus of kenaf fibers is shown in Figure 11(b). The modulus for control fibers was 21.1 GPa. However, the modulus fluctuated between 18.1 GPa and 20.9 GPa for treatments of 30 minutes and 4 hours. However, the modulus eventually increased as the treatment times increased beyond 4 hours. The decrease in stiffness observed at 30 minutes may have been caused by the removal of lignin, the rigid component on the fibers. The increased modulus in kenaf fibers treated

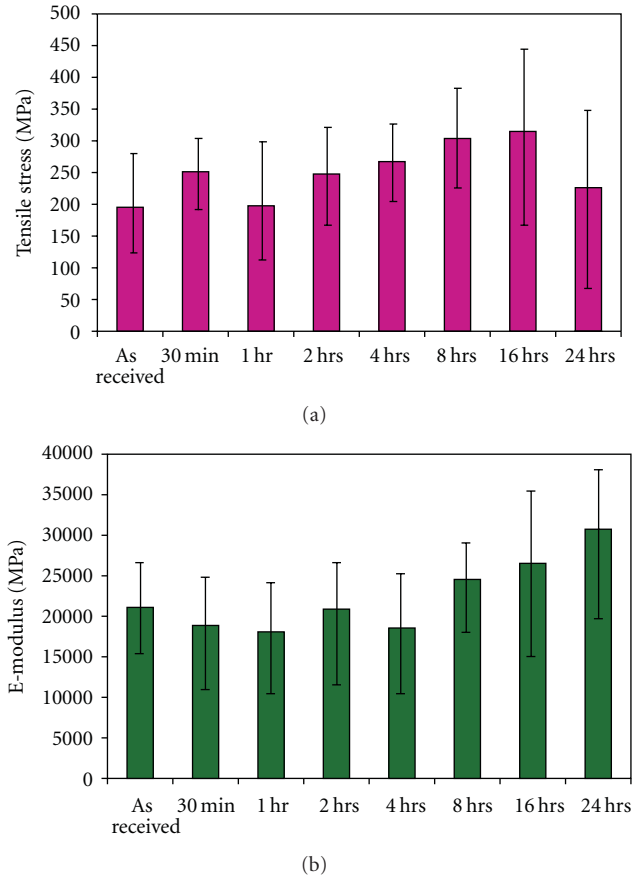

Figure 11: Effect of alkali treatment time on (a) tensile stress and (b) Young's moduli in untreated and alkali-treated kenaf fibril bundles.

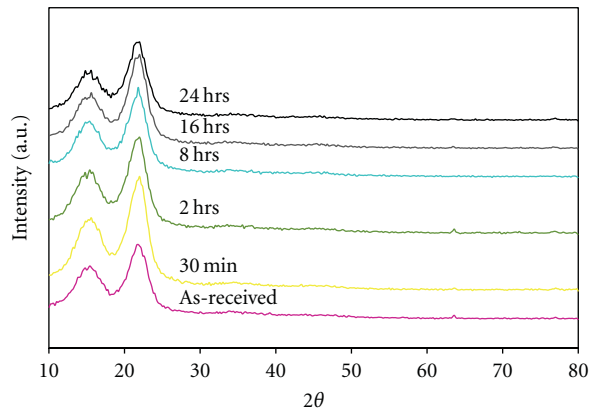

Figure 12: Effect of alkali treatment on crystallinity of as-received and alkali-treated kenaf.

beyond 4 hours was believed to be attributed to an increase in cellulose crystallinity.

3.5. Effect of Alkali Treatment Times on Morphology and Cellulose Crystallinity. Cellulose is the only constituent in the fiber that exists in crystalline form since it is the only linear and regular molecule in the fiber that is capable of crystallizing. Figure 12 shows the effect of alkali-treatment on the crystallinity of as-received and alkali treated kenaf fibers. Because kenaf fibers were assumed to be more crystalline, XRD was used to confirm the time-based effects of alkali treatment on the crystallinity of cellulose. According to Figure 12, the major peak of interest in the X-ray diffractograms was the crystalline peak for cellulose, located at ~22° 2θ. It was determined that the crystal lattice planes were located in the 002 direction. According to the diffraction patterns, the peak for crystalline cellulose did not appear to show significant changes as the treatment time varied. The full width at half maximum (FWHM) was calculated for the peaks belonging to crystalline cellulose to get a better representation of the changes taking place in order as a result of treatment.

Table 2: Effect of time on FWHM in kenaf fibers.

Treatment time (hrs)	2θ (degrees)	Average FWHM (degrees)
0	~22.0	1.20 ± 0.021
0.5	~22.0	1.22 ± 0.082
2	~22.0	1.15 ± 0.051
8	~22.0	1.06 ± 0.093
16	~22.0	1.06 ± 0.15
24	~22.0	1.00 ± 0.084

Typically, smaller FWHM values observed in fibers represent materials with higher crystalline contents as this means sharper or narrower peaks. Previous work has shown that the FWHM could provide information about the crystallite sizes of cellulose as well [24, 25]. According to Table 2, the FWHM values decreased as the treatment time increased. This suggested that the amount of crystalline content in cellulose increased as treatment time increased and supported evidence of the tensile property improvements in kenaf. Previous work has reported that an increase in crystallinity could be caused by an increase in van der Waals and hydrogen bonding between neighboring molecules as a result of the increased interaction of hydroxyl groups found in cellulose [26]. On the other hand, the increase in crystallinity could have been caused by the removal of the amorphous parts of the fibers from alkali treatment.

4. Conclusions

Effects of alkali treatment times on the surface chemistry, morphology, and bonding were studied in bast kenaf fibers. ATR-FTIR spectroscopy, XPS, and SEM showed that the most significant chemical changes on the surfaces occurred between 30 minutes and 4 hours of treatment; however, fibers treated for 16 hours showed the most significant increase in tensile strength.

SEM photomicrographs illustrated that alkali treatment was successful in removing waxes and unwanted surface impurities. ATR-FTIR spectroscopy showed gradual changes consistent with the removal of hemicellulose and lignin. After 16 hours of alkali treatment, the surface chemistry did not

appear to show any significant changes according to ATR-FTIR spectroscopy and XPS. With higher times, the inner surfaces were being exposed as more materials were being removed. XPS and ATR-FTIR spectroscopy also showed that the amounts of hydroxyl groups on the fiber surfaces decreased as treatment time increased. This suggested that there was a decrease in the number of sites available for hydrogen bonding in kenaf when treated between 8 and 24 hours according to XPS and between 2 and 24 hours according to the MHBS calculations from ATR-FTIR spectroscopy.

Alkali treated-kenaf fibers displayed the highest tensile properties at 16 hours of treatment; however, using this group of fibers in a composite would ultimately result in poor properties. Fiber-resin bonding is the biggest factor that affects mechanical properties in composites. Since it was observed that longer treatment times resulted in fewer surface hydroxyl groups on the kenaf surfaces, the amount of sites needed for fiber-matrix bonding were reduced and would lead to lower mechanical properties in resulting biocomposites.

It was believed that treating bast kenaf fibers for 2–4 hours would work best as reinforcement in composites, because the mechanical properties in fibers were slightly higher, and more hydroxyl groups in cellulose were available to bond with compatible functional groups in resins. To conclude, when treating natural fibers for use as composite reinforcement, it is essential to establish a proper balance among fibers that will yield increased mechanical properties and fibers that will provide optimal bonding.

Acknowledgments

The authors would like to thank NSF Alabama EPSCoR and ACHE for funding as well as Chuck Taylor at Kenaf Industries of South Texas for supplying the kenaf fibers. NSF Alabama EPSCoR Grant, Alabama Commission for Higher Education (ACHE).

References

[1] M. Pervaiz and M. M. Sain, "Sheet-molded polyolefin natural fiber composites for automotive applications," *Macromolecular Materials and Engineering*, vol. 288, no. 7, pp. 553–557, 2003.

[2] W. Liu, A. K. Mohanty, L. T. Drzal, P. Askeland, and M. Misra, "Effects of alkali treatment on the structure, morphology and thermal properties of native grass fibers as reinforcements for polymer matrix composites," *Journal of Materials Science*, vol. 39, no. 3, pp. 1051–1054, 2004.

[3] A. Mohanty, M. Misra, and L. Drzal, *Natural Fibers, Biopolymers, and Biocomposites*, Taylor & Francis Group LLC, Boca Raton, Fla, USA, 2005.

[4] A. M. M. Edeerozey, H. M. Akil, A. B. Azhar, and M. I. Z. Ariffin, "Chemical modification of kenaf fibers," *Materials Letters*, vol. 61, no. 10, pp. 2023–2025, 2007.

[5] F. Wallenberger and N. Weston, *Natural Fibers, Plastics and Composites*, Kluwer Academic Publishers, 2004.

[6] S. H. Aziz and M. P. Ansell, "The effect of alkalization and fibre alignment on the mechanical and thermal properties of kenaf and hemp bast fibre composites—part 1—polyester resin matrix," *Composites Science and Technology*, vol. 64, no. 9, pp. 1219–1230, 2004.

[7] B. C. Mitra, R. K. Basak, and M. Sarkar, "Studies on jute-reinforced composites, its limitations, and some solutions through chemical modifications of fibers," *Journal of Applied Polymer Science*, vol. 67, no. 6, pp. 1093–1100, 1998.

[8] N. Sgriccia, M. C. Hawley, and M. Misra, "Characterization of natural fiber surfaces and natural fiber composites," *Composites Part A*, vol. 39, no. 10, pp. 1632–1637, 2008.

[9] K. Joseph, S. Thomas, and C. Pavithran, "Effect of chemical treatment on the tensile properties of short sisal fibre-reinforced polyethylene composites," *Polymer*, vol. 37, no. 23, pp. 5139–5149, 1996.

[10] B. Xiao, X. F. Sun, and R. Sun, "Chemical, structural, and thermal characterizations of alkali-soluble lignins and hemicelluloses, and cellulose from maize stems, rye straw, and rice straw," *Polymer Degradation and Stability*, vol. 74, no. 2, pp. 307–319, 2001.

[11] N. Suizu, T. Uno, K. Goda, and J. Ohgi, "Tensile and impact properties of fully green composites reinforced with mercerized ramie fibers," *Journal of Materials Science*, vol. 44, no. 10, pp. 2477–2482, 2009.

[12] A. Gomes, T. Matsuo, K. Goda, and J. Ohgi, "Development and effect of alkali treatment on tensile properties of curaua fiber green composites," *Composites Part A*, vol. 38, no. 8, pp. 1811–1820, 2007.

[13] W. Zhang, S. Okubayashi, and T. Bechtold, "Fibrillation tendency of cellulosic fibers—part 2: effects of temperature," *Cellulose*, vol. 12, no. 3, pp. 275–279, 2005.

[14] J. Gassan and A. K. Bledzki, "Alkali treatment of jute fibers: relationship between structure and mechanical properties," *Journal of Applied Polymer Science*, vol. 71, no. 4, pp. 623–629, 1999.

[15] D. Ray and B. K. Sarkar, "Characterization of alkali treated jute fibres for physical and mechanical properties," *Journal of Applied Polymer Science*, vol. 80, no. 7, pp. 1013–1020, 2001.

[16] W. Liu, A. K. Mohanty, P. Askeland, L. T. Drzal, and M. Misra, "Influence of fiber surface treatment on properties of Indian grass fiber reinforced soy protein based biocomposites," *Polymer*, vol. 45, no. 22, pp. 7589–7596, 2004.

[17] D. Ray, B. K. Sarkar, A. K. Rana, and N. R. Bose, "Mechanical properties of vinylester resin matrix composites reinforced with alkali-treated jute fibres," *Composites Part A*, vol. 32, no. 1, pp. 119–127, 2001.

[18] S. Keshk, W. Suwinarti, and K. Sameshima, "Physicochemical characterization of different treatment sequences on kenaf bast fiber," *Carbohydrate Polymers*, vol. 65, no. 2, pp. 202–206, 2006.

[19] M. Akerholm, B. Hinterstoisser, and L. Salmén, "Characterization of the crystalline structure of cellulose using static and dynamic FT-IR spectroscopy," *Carbohydrate Research*, vol. 339, no. 3, pp. 569–578, 2004.

[20] G. Socrates, *Infrared and Raman Characteristic Group Frequencies: Tables and Charts*, John Wiley & Sons, New York, NY, USA, 3rd edition, 2001.

[21] K. H. Song and S. K. Obendorf, "Chemical and biological retting of kenaf fibers," *Textile Research Journal*, vol. 76, no. 10, pp. 751–756, 2006.

[22] R. Sun, J. M. Lawther, and W. B. Banks, "Influence of alkaline pre-treatments on the cell wall components of wheat straw," *Industrial Crops and Products*, vol. 4, no. 2, pp. 127–145, 1995.

[23] R. C. Sun, J. Tomkinson, P. L. Ma, and S. F. Liang, "Comparative study of hemicelluloses from rice straw by alkali and

hydrogen peroxide treatments," *Carbohydrate Polymers*, vol. 42, no. 2, pp. 111–122, 2000.

[24] N. Reddy and Y. Yang, "Structure and properties of high quality natural cellulose fibers from cornstalks," *Polymer*, vol. 46, no. 15, pp. 5494–5500, 2005.

[25] C. J. Garvey, I. H. Parker, and G. P. Simon, "On the interpretation of X-ray diffraction powder patterns in terms of the nanostructure of cellulose I fibres," *Macromolecular Chemistry and Physics*, vol. 206, no. 15, pp. 1568–1575, 2005.

[26] A. Guinier, *X-Ray Diffraction in Crystals, Imperfect Crystals, and Amorphous Bodies*, Dover Publications, New York, NY, USA, 1963.

Hindawi Publishing Corporation
International Journal of Polymer Science
Volume 2011, Article ID 503940, 11 pages
doi:10.1155/2011/503940

Research Article

Role of Polysaccharides on Mechanical and Adhesion Properties of Flax Fibres in Flax/PLA Biocomposite

Gijo Raj, Eric Balnois, Christophe Baley, and Yves Grohens

LIMATB (Laboratoire d'Ingénierie des MATériaux de Bretagne), Centre de Recherche, Université de Bretagne Sud (UBS-Ueb), Rue de Saint Maudé, 56321 Lorient Cedex, France

Correspondence should be addressed to Eric Balnois, eric.balnois@univ-ubs.fr

Received 10 January 2011; Accepted 2 March 2011

Academic Editor: Susheel Kalia

The effect of alkali and enzymatic treatments on flax fibre morphology, mechanical, and adhesion properties was investigated. The multilength scale analysis allows for the correlation of the fibre's morphological changes induced by the treatments with mechanical properties to better explain the adherence properties between flax and PLA. The atomic force microscopy (AFM) images revealed the removal of primary layers, upon treatments, down to cellulose microfibrils present in the secondary layers. The variation in mechanical properties was found to be dependent, apart from the crystalline content, on interaction between cellulose microfibrils and encrusting polysaccharides, pectins and hemicelluloses, in the secondary layers. Finally, microbond tests between the modified fibres and PLA emphasize the important role of the outer fibre's surface on the overall composite properties. It was observed here that gentle treatments of the fibres, down to the oriented microfibrils, are favourable to a better adherence with a PLA drop. This paper highlights the important role of amorphous polymers, hemicellulose and pectin, in the optimisation of the adhesion and mechanical properties of flax fibres in the biocomposite.

1. Introduction

Research for environmental friendly alternatives has led the composite community to develop new "ecobiocomposites," made from natural fibres and biodegradable polymer matrices, such as polylactic acid (PLA) [1–3]. It was reported that the specific Young's modulus of PLA/Flax biocomposite (6.52 ± 0.075 GPa for 25% fibre volume fraction) can be as close to that of glass/polyester composites (7.762 ± 0.0638 GPa) [1] and makes them suitable for interesting applications.

Even though natural fibres have ecofriendly credentials, they present some major drawbacks, such as poor thermal stability, anisotropic resistance, high moisture absorption heterogeneity, and in some cases poor incompatibility with polymer matrices [3]. These drawbacks prevent the use of natural fibre reinforcements in high performance structural composite applications and limit, up to now, their use for nonstructural parts. The complex chemical and physical structure of natural fibres [4, 5] is certainly responsible for these limitations which may be overcome using different chemical or physical surface treatments.

A detailed description of the flax fibre structure can be found in the literature [4, 5]. Briefly, a flax fibre consists of (i) a middle lamella region, principally made up of pectin, with small quantities of lignin that ensures bundle cohesion, (ii) a primary cell wall which forms ~10% of the fibre's diameter and mainly consists of cellulose microfibrils embedded in a matrix of pectin, hemicelluloses, and small quantities of lignin [5, 6], and (iii) a secondary cell wall, which makes up 90% of the cell cross section and mainly consists of three layers of cellulose microfibrils, with a mean axial orientation of 10°, bounded with pectin and hemicellulose. In this layer, pectin and hemicellulose are forming an interphase between cellulose microfibrils [5, 7] and are thus called "encrusting polymers." Cellulose microfibrils with typical diameters about 25–30 nm [4] consist of highly ordered crystalline cellulose zones (with typical Young's modulus up to 143 Gpa [8]), in which cellulose crystals are arranged periodically and longitudinally along the fibre's axis, interconnected by

amorphous cellulose zones. An important issue concerns the hierarchical organisation and structuration of different polysaccharides in the different layers of the fibre and the structural difference between primary and secondary layers. This point is very important to better understand the mechanical and surface properties of flax fibre and consequently to better understand the effect of specific treatments to improve the mechanical properties of the fibre-reinforced composite.

During the past decade, numerous works have been published in the literature concerning modifications of flax fibres to improve the interface adhesion with a polymeric matrix [9, 10]. Among the different chemical treatments, alkali treatment of flax fibres was found to be simple and efficient in improving the adhesion with polymer matrices [11, 12]. This treatment is known to remove amorphous polysaccharides such as hemicellulose, pectin [5], lignin [13], and separate fibre bundles into elementary fibres. Additionally, alkaline solution reacts not only with noncellulosic materials, but also with cellulosic components creating large cellulose lattices, which can be converted to new crystalline structures (cellulose II) [12]. Another effect of mercerisation is the possible depolymerisation of the native cellulose type I molecular structure into short-length crystallites [14]. This last effect has a direct negative effect on the fibre strength and stiffness [13].

Recently, enzymatic treatments involving the use of mainly pectinase enzymes have gained the attention of the scientific community as an environmental friendly treatment on flax fibres [15]. These treatments were found to be efficient in removing the shive and epidermal tissues of fibres, as characterized by optical and Scanning Electron Microscopy studies [16]. Commercially available enzyme preparations mainly contain pectinase, as well as some quantities of hemicellulase and cellulase enzymes. Enzymes rich in pectinase and poor in cellulase are generally more suited to avoid any cellulose alteration within the fibre. However, it has been shown in a recent work, using X-ray scattering techniques, that cellulase enzymes act only on the surface of cellulose microfibrils and are not able to penetrate into nanopores of the cellulose crystallites without affecting the degree of crystallinity [17].

Although modifications of flax fibres by both chemical and enzymatic methods result in improved mechanical properties of the biocomposite, a detailed investigation of the relation between the morphological changes of the fibre and the resulting properties, at different length scales, is necessary to better understand the complex properties of such heterogeneous fibres. Generally, the overall properties of the composites are probed by macroscopic and indirect analysis such as mechanical tests [11, 18], water sorption studies [19], or chemical analysis [20, 21]. A major limitation of such macroscopic studies comes from the fact that they do not give a direct and clear relationship between the structural modifications of the fibre and their consequence on the fibre and composite properties. Recently, nanoscale studies of flax fibre using atomic force microscopy have emphasized the relevance of a multiscale investigation on such materials and provide valuable morphological and quantitative data to characterize the fibre's surface properties [22, 23]. These works were complementary to traditional determination of interfacial energies using contact angle measurements, which is difficult to experimentally perform on heterogeneous samples such as that of flax fibres.

The aim of this paper is to highlight the significant factors acting on the interfacial adherence in biocomposites. The morphology of alkali- and enzymatic-treated fibres is investigated at different length scales, in order to better understand the relationship between the structure and the mechanical properties of the flax fibre. The adhesion properties at the fibre-polymer matrix interface are followed by microbond pull-out tests and force-volume adhesion mapping and discussed in the framework of the morphological and chemical modification induced by the treatments.

2. Materials and Methods

2.1. Alkali Treatment of the Flax Fibres. Dew-retted flax fibres (variety Hermes) grown in the Normandy region (France) were used in this study. Flax fibres were initially soaked in NaOH solutions (1%, 3%, 5%, and 10%) for 20 minutes at 23°C. The fibres were filtered and washed thoroughly in Milli-Q water before being rinsed in a very diluted solution of HCl (0.01 M) to remove excessive NaOH [12] and washed again with Milli-Q water before drying in vacuum at 65°C for 3 hours.

2.2. Enzyme Treatment of Flax Fibres. Enzyme treatments of flax fibres were carried out using a pectinase enzyme, made from *Aspergillus aculeatus*, Pectinex Ultra SPL (activity 9500 units/mL, Sigma Aldrich). The enzyme solution was diluted to a concentration of 20% in an acetate buffer solution (Sigma Aldrich) having a pH of 4.6 [22]. About 1 g of flax fibres was treated in 100 mL of the 20% enzymatic solution at 40°C. Fibres were then taken out of the treatment at intervals of 5 H and 18 H, washed at least 5 times in Milli-Q water, and dried in vacuum at 65°C for 5 hours before any analysis.

2.3. Scanning Electron Microscopy (SEM). Morphology of raw-, alkali-, and enzyme-treated flax fibres was examined using a Jeol JSM 6460 LV Scanning electron microscope. Flax fibre samples were metallised (Edwards Scancoat six metallizer) for 10 minutes prior to SEM imaging.

2.4. Atomic Force Microscopy (AFM). AFM experiments were conducted using a commercial Multimode Nanoscope IIIa atomic force microscope (Veeco, USA). Images were acquired in tapping mode (TM-AFM) under ambient conditions (23°C and RH 56%) using silicon tips (LTESP, Veeco). Samples were prepared by gluing an elementary flax fibre by their two extremities on a magnetic steel disc in order to keep it fixed during image acquisition.

Force volume (FV) mode was used to construct an adhesion force map of the various fibres. In FV mode, a contact mode image of the fibre's surface was first made using a conventional contact mode tip (spring constant 0.57 N/m).

Force maps were captured in the "relative trigger" mode to ensure that the maximum loaded force exerted on the sample is the same in every force plot. The maximum cantilever deflection was fixed at 160 nm (91 nN). The image XY resolution parameter, sample/line, was kept at 128, and the number of force/line was 64. Thus, for a scan line of 1.6 μm, force plots were recorded at every 25 nm.

2.5. Infrared (IR) Spectroscopy. Infrared (ATR-IR) spectroscopy (IR Perkin Elmer spectrometer) was performed on raw-, NaOH-, and enzyme-treated flax fibres using the attenuated total reflectance method with a mountable unit (Golden Gate). Spectra were acquired with an accumulation of 25 scans and were recorded in the transmittance mode in the range 400–4000 cm^{-1}.

2.6. Single Fibre Tension Test (SFTT). Flax single fibres were manually extracted and glued at both ends onto a piece of paper which was already punched to make a 10 mm hole (equal to the initial length L_0 of the fibre). The mean diameter of flax fibres was determined by optical microscopy and obtained by analysing at least 15 different zones on each fibre. A minimum of fifty fibres, for each sample (raw-, NaOH-, and enzymatic-treated fibres), were analysed. The longitudinal Young's modulus of the flax fibres was determined from the tensile loading of elementary flax fibres respecting the standard methods (NFT 25-704, ASTM 3379-75), that also takes into account the compliance of the system. The tension experiments were performed in a tensile testing machine (MTS Synergie 1000) equipped with a load cell capture that allows for measurements in the range of 0–2 N with an accuracy of 0.01%. Loading rate was kept constant at 1 mm/min throughout all experiments.

2.7. Wide-Angle X-Ray Scattering (WAXS). X-ray scattering experiments were performed on a custom-built SAXS/WAXS machine equipped with a Rigaku MicroMax-007 HF rotating anode generator ($\lambda = 1.54$ Å). The size of the point-like X-ray beam on the sample was approximately. 300 μm. The 2D WAXS data were collected using X-ray sensitive Fuji image plates with a pixel size of $100 \times 100\,\mu m^2$. The modulus of the scattering vector s ($s = 2\sin\theta/\lambda$, where θ is the Bragg angle) was calibrated using three diffraction orders of silver behenate. The data reduction and analysis including geometrical and background correction, visualization, and radial integration of the 2D diffractograms were performed using home-built routines designed using the IgorPro software package.

2.8. Microbond Test. The adherence strength between the flax fibres and the PLA matrix (Biomer L9000) was estimated by calculating the apparent interfacial shear stress (IFSS) values obtained from microbond tests on a minimum of ten pull-out experiments. A homogeneous PLA polymer microdroplet (<200 μm) was deposited on the surface of the flax fibre. In order to achieve this microdroplet, a microknot was made on the flax fibre with a microfilament of PLA. The setup was placed in an oven preheated at 190°C for 10 minutes. The sample was then immediately taken from the oven and quenched at room temperature. Prior to any tests, the diameter of the fibre near the PLA droplet, the embedded length of the fibre, and the drop height were measured using an optical microscope. Pull-out experiments were performed on a tensile testing machine (MTS Synergie 1000, load cell 2N). On the lower clamp, a homemade X-Y translator with two sharp knife edges was mounted. The microdroplet was brought just under these knife edges, and the knife blades were brought close together so that the blades just touch the upper end of the droplet [21]. Tensile loading was applied at the rate of 0.1 mm/min.

3. Results and Discussion

3.1. Morphology of the Flax Fibres. SEM images of raw and treated bundles (Figures 1(a), 1(b), and 1(c)) provide a macroscopic investigation of the morphology of the outer surface of the fibres. Figure 1(a) shows the bundle structure of raw flax fibres formed by elementary fibres held together mainly by pectin, lignin, and amorphous polymers found in the primary cell wall and in the middle lamellae region [5]. On the other hand, the two modified fibres, following NaOH and enzymatic treatment (Figures 1(b) and 1(c), resp.), appeared to be well separated.

Figures 1(d), 1(e), and 1(f) show SEM images of elementary fibres of raw-, NaOH-, and enzyme-treated flax respectively. The surface of the treated fibres (Figures 1(e) and 1(f)) appears free of any residual particles, homogeneous and smoother, which reveal the efficiency of both treatments in removing some large particles and entities present on the raw fibre (Figure 1(d)). This result contrasts with some earlier studies of the effect of NaOH on the structure of natural fibres, which reported a drastic change of the fibre morphology that led to a decrease of the fibre diameter and the development of a rough and irregular surface [24]. It should be mentioned that in some cases, the NaOH treatment was more severe (higher concentration) [13] and less controlled (time and temperature) [21] than in more recent studies [12].

Atomic force microscopy was used to observe the surface of the flax fibres with a nanometer resolution. Tapping mode (TM) AFM images reveal similar trends as those observed by SEM (Figure 2). Large globular entities or particles that envelop the fibre's surface can be observed on raw fibres (Figure 2(a)). Upon treatment, these particles disappeared, and the flax fibre's surface becomes relatively smooth. The alkali treatment yields a cleaning effect of the fibre's surface. For a concentration of 5%, the AFM image reveals an unidirectional orientation of microfibrils in the secondary layer (Figure 2(b)). At the highest NaOH concentration (10%), a better resolution of the oriented microfibrils is obtained, with typical diameters between 20 and 40 nm (Figure 2(c)). These oriented fibrils are all aligned within a similar direction to the main fibre axis. These entities correspond well to the description of crystalline cellulosic microfibrils within the secondary cell wall of flax fibre, both in terms of size and orientation [4].

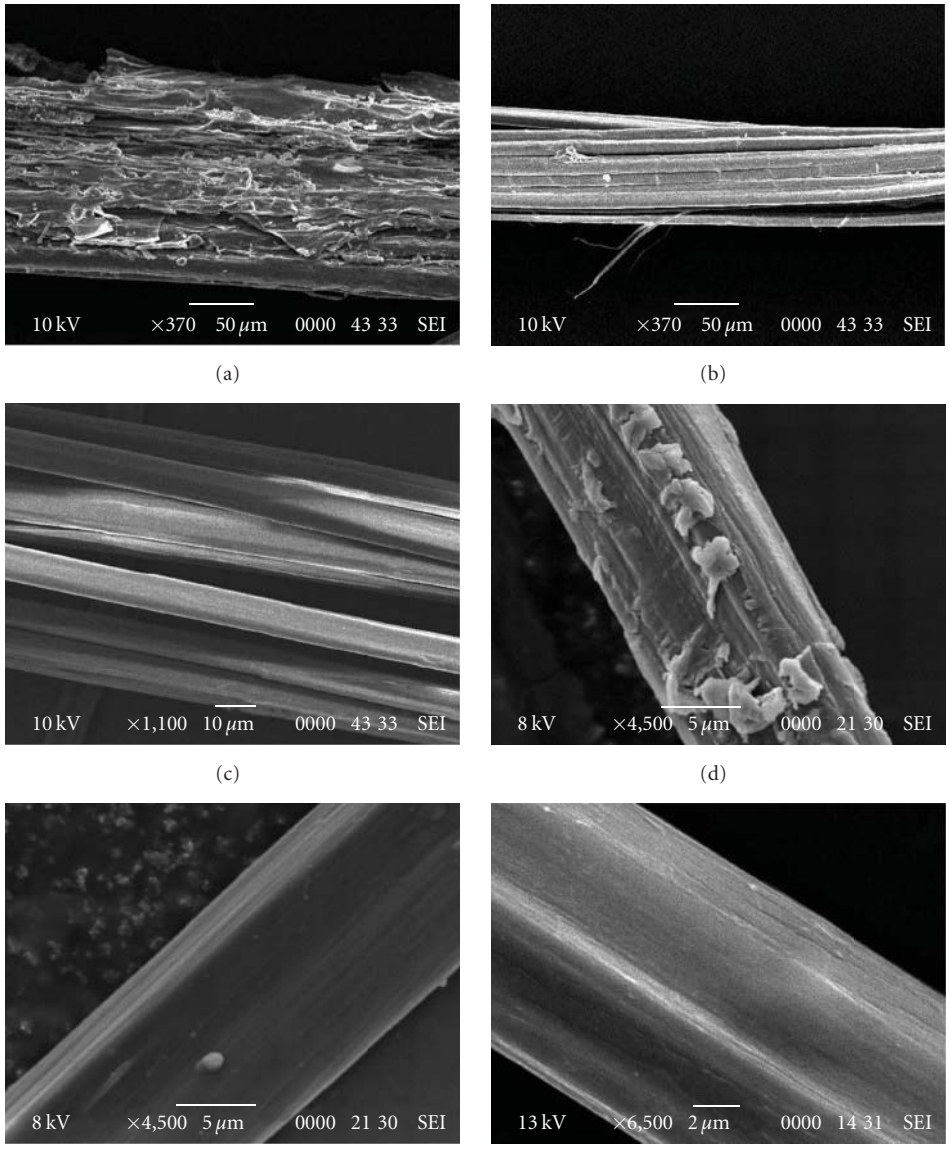

Figure 1: SEM images of flax fibres: (a) raw flax bundle, (b) 10% NaOH-treated bundle, (c) 18 H Enzyme-treated bundle, (d) raw elementary fibre, (e) 10% NaOH-treated elementary fibre, and (f) 18 H enzyme-treated elementary fibre.

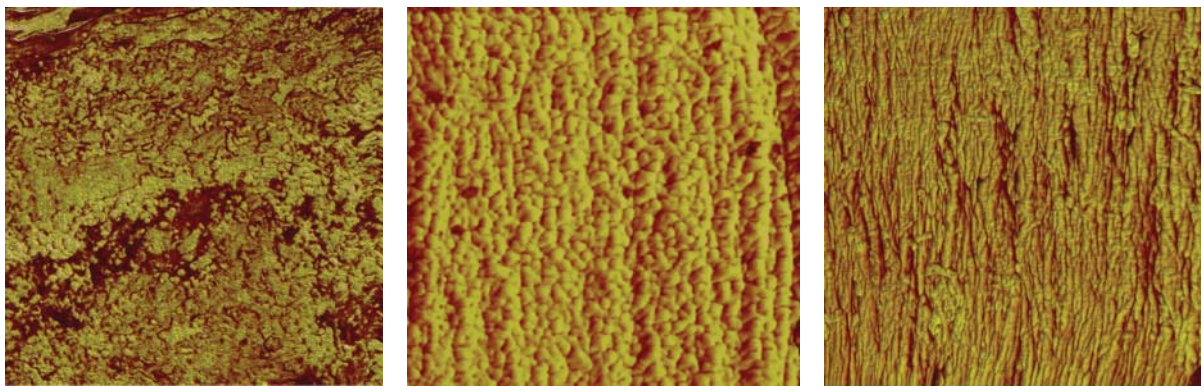

Figure 2: TM-AFM phase images (scan size of 4 μm^2) of (a) raw-, (b) 5% NaOH-, and (c) 10% NaOH-treated flax fibres.

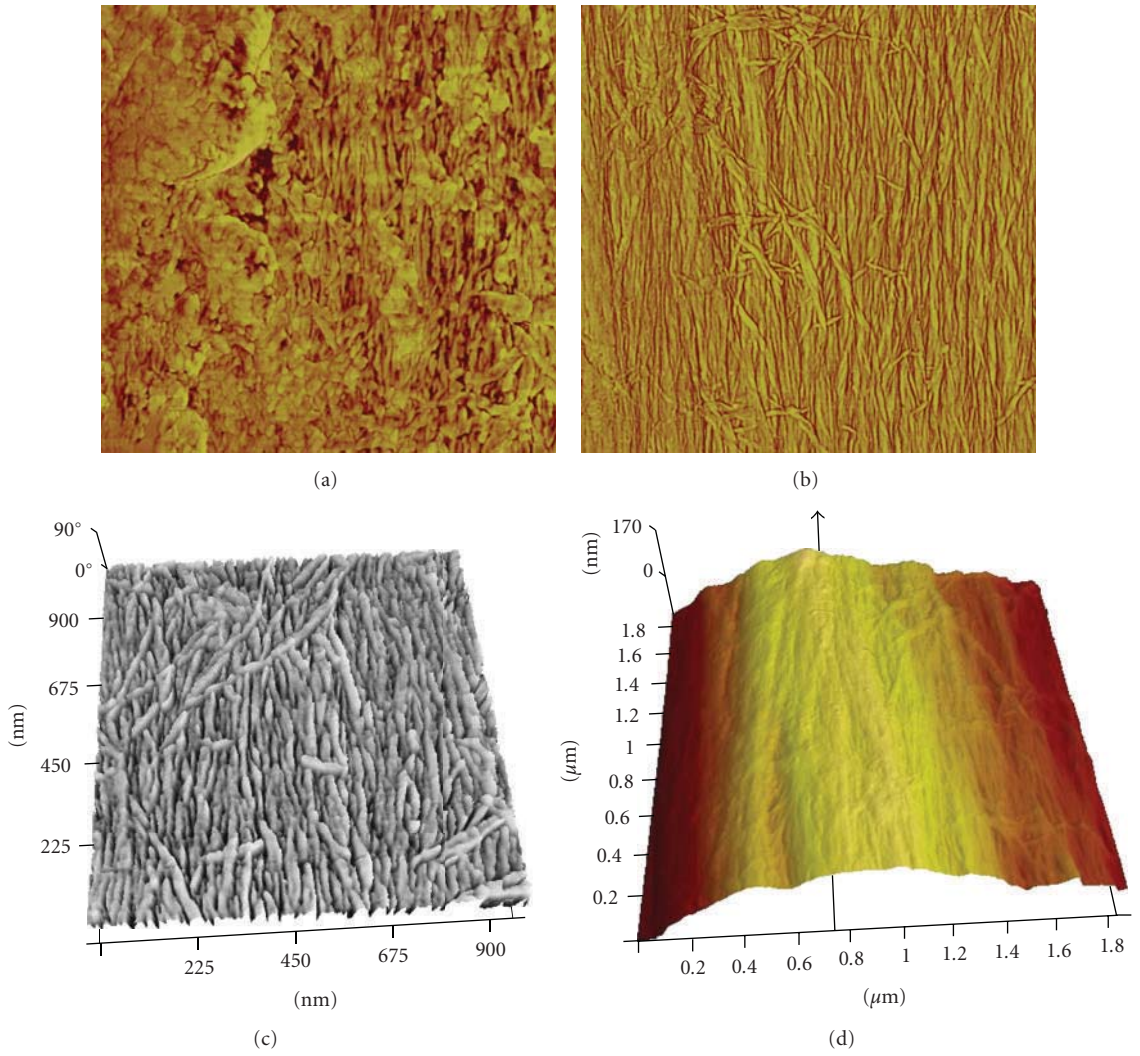

Figure 3: TM-AFM phase images (scan size of $4\,\mu m^2$) of enzyme-treated fibres of (a) 5 hours, and (b) 18 hours, (c) TM-AFM 3D phase image of the microfibrils showing their preferential orientation (scan size: $1\,\mu m^2$), (d) TM-AFM 3D height profile showing the main fibre axis going through the maximum height of the image.

The pectinase enzyme preparation, which contains pectolytic and a range of hemicellulolytic activities, has the ability to depolymerise major components of plant cell walls. After 5 H of enzymatic treatment, the flax fibre still presents some large inhomogeneous and rough areas which seem to cover, like an envelope, a more organised layer made of aligned structures (Figure 3(a)). After 18 H of treatment, a more uniform surface can be observed, showing only oriented microfibrils (Figure 3(b)). A high resolution 3D image of enzyme-treated (18 H) flax fibre (Figure 3(c)) allows for the visualisation of the oriented cellulose microfibrils (in the size range 25 to 30 nm) and indicates the preferred orientation along the fibre longitudinal axis (Figure 3(d)). In Figure 3(d), the axis of the fibre is indicated by the arrow that goes through the maximum heights of the fibre, and we can qualitatively observe that the microfibril angle is somehow quite close to the main fibre axis [4].

The multiscale complementary approach, using SEM and AFM, confirms the removal of some amorphous polysaccharides from the outermost surface of the flax fibres (middle and primary layers) to provide a clean and smooth surface with well-aligned cellulose microfibrils with an orientation angle close to the fibril's axis, typical of the secondary layer.

Surface chemical modifications induced by the treatments were investigated by ATR-IR spectroscopy, and the recorded spectra are displayed in Figure 4. When compared to raw flax fibre, ATR-IR spectra of treated fibres show a decrease of intensity of the peaks at $1615\,cm^{-1}$ (corresponding to pectin [5]), and at $2923\,cm^{-1}$ (C–H stretching vibration in hemicellulose [25]). Moreover, a shoulder peak at $1735\,cm^{-1}$, that corresponds to "C=O" stretching of carboxylic acid or ester group of hemicelluloses [26], disappeared after the treatments. These observations show that pectin and hemicelluloses are the main compounds that are removed following the treatments. However, since

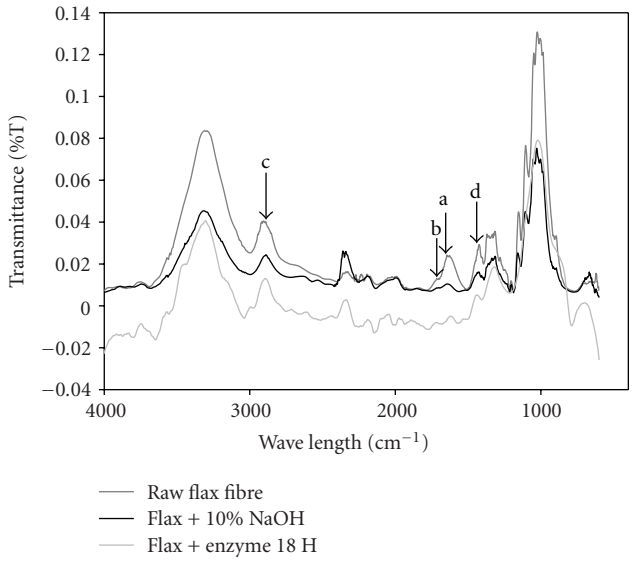

Figure 4: ATR-IR spectroscopy of raw-, NaOH-, and Enzyme-treated flax fibres: (a) peak at 1615 cm^{-1} that corresponds to pectin; (b), (c) peaks at 1735 cm^{-1} and 2923 cm^{-1}, respectively, that correspond to hemicellulose; (d) peak at 1440 cm^{-1} that corresponds to lignin.

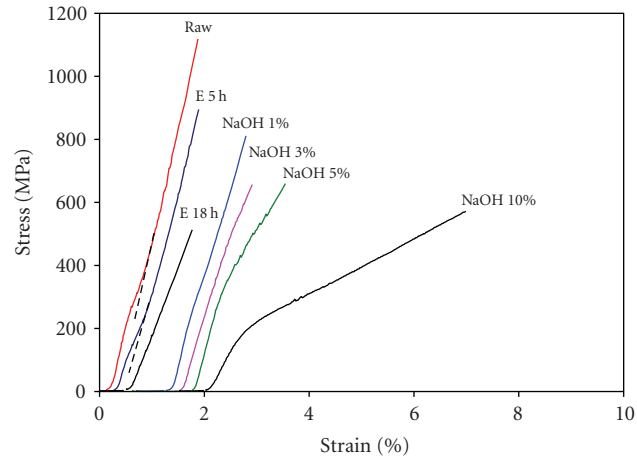

Figure 5: Comparison of stress versus strain curves of raw-, NaOH-, and Enzyme-treated elementary flax fibres under tensile loading. Shaded region corresponds to a threshold stress level bellow which fibres broke before pullout in microbonding test.

the penetration depth of the ATR-IR evanescent wave is several microns, we cannot distinguish the origin of these polymers, either coming from the primary cell wall or from the secondary one.

3.2. Mechanical Properties of Flax Fibre. The tensile mechanical properties of the raw and the treated flax fibres were evaluated by the single fibre tension test (SFTT) experiment. Figure 5 represents typical stress-strain curves of different elementary flax fibres. From the raw fibre's traction curve, two distinct regions can be identified. First, a nonlinear part, from 0 to ~350 MPa, is observed during low deformation at the initial stages of the loading curve. This first part can be associated with the global loading of the fibre, through the deformation of each cell wall structure [27] including a sliding of the microfibrils along their progressive alignment with the main fibre axis and a reorganisation of the amorphous matrix (mainly pectins and hemicelluloses) surrounding the microfibrils. The second region of the loading curve appears linear, characteristic of an elastic deformation, and corresponds to the response of the aligned microfibrils to the applied tensile strain. After reaching a maximum value of tensile stress, the fibre breaks. From the slope of the linear part of stress versus strain curve, one can extract a "global" (average) longitudinal Young's modulus of the fibre. The calculated Young's modulus for raw flax fibres from these experiments was found to be 65.3 ± 16.2 GPa (Table 1), which corresponds well with reported data [4, 27]. Taking into account the internal composite structure of flax fibres, any discontinuity that may appear in the linear part of the stress versus strain can give information regarding any internal structural changes of the different layers of the fibres during loading.

Stress-strain curves obtained for alkali- and enzymatic-treated flax fibres are significantly different from that of the raw flax fibre. For the 1% NaOH-treated fibres, the initial nonlinear part is still visible, but as the concentration of the alkali increases, the initial "nonlinear" part of the stress-strain graph disappears to give a straight and linear curve. As revealed by AFM analysis, observation of the organised and oriented microfibrils was only possible for samples treated with a 5% NaOH solution. For NaOH concentrations of 5% and 10%, the stress-strain curves present two linear regions with a transition that evolves with the increase of concentration of the sodium hydroxide solutions (up to ~400 MPa for the 5% NaOH-treated fibre, and up to 200 MPa for the 10%-treated one). This typical nonelastic behaviour can be related to the internal structural changes in the fibre, such as swelling, induced by the alkali treatment. The curves resemble a biphasic stress-strain curve which is typically observed in tensile loading of wood fibres [28], in which the first slope of the curve is due to the orientation of microfibrils in the direction of deformation. After a yield point, corresponding to a threshold stress, a second linear stage with a smaller slope evolved and can be interpreted as a consequence of plastic deformation of the polysaccharide matrix accompanied by a slippage mechanism of microfibrils under tensile loading [28]. Keckes et al. [29] proposed a simple "molecular Velcro" model to explain this deformation process in which a large number of molecular bonds, due to entangled hemicellulose chains, may disrupt upon stress transfer between cellulose fibrils and amorphous matrix.

In the case of these two NaOH treatments, traction curves observed here are likely obtained from the response of the secondary layer of the fibre, as observed by AFM. Morvan et al. [5] described the organisation of this layer and proposed a close relation between the two encrusting amorphous polymers, pectins and hemicelluloses, and crystalline cellulose microfibrils. In this system, molecular

Table 1: Comparison of Young's modulus (E_L) and tensile stress (σ) of raw-, NaOH-, and enzyme-treated flax fibres measured by single fibre tension test.

	Raw flax	1% NaOH	3% NaOH	5% NaOH	10% NaOH	Enzyme 5 h	Enzyme 18 h
Longitudinal Young's modulus E_L (Gpa)	65.3 ± 16	44.3 ± 13	40.5 ± 10	39.2 ± 6	28.5 ± 5	50.5 ± 9	43 ± 10
Tensile strength σ (MPa)	1077 ± 250	702 ± 221	649 ± 220	634 ± 200	564 ± 193	880 ± 180	527 ± 120

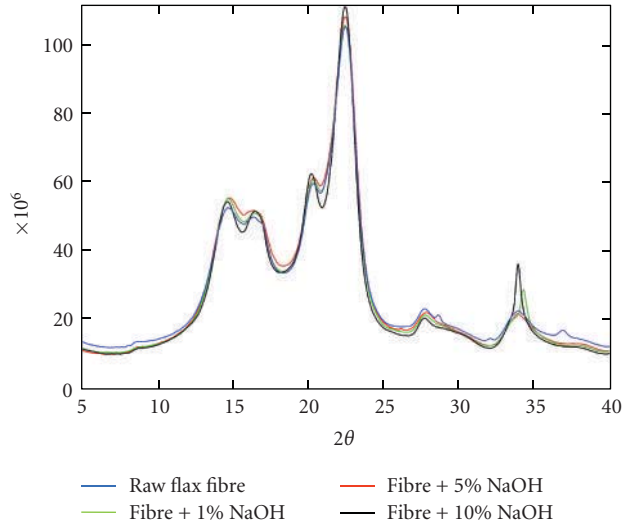

Figure 6: WAXS pattern of raw and different NaOH-treated flax fibres.

bonds between pectin and hemicellulose, including hydrogen van der Waals interactions, may break upon loading in order to dissipate the stress and could explain the "pseudoplastic" deformation observed at 10% of NaOH. Further, a linearly increasing slope after the deformation region can be attributed to the rearrangement of cellulose fibrils in the direction of strain [30]. Following this "severe" treatment, the NaOH solution may have attacked irreversibly the encrusting hemicellulose and pectin macromolecules in the secondary layer and thus weaken their ability to efficiently transfer the stress between adjacent cellulose microfibrils. The decreasing value of yield stress of fibres with increasing concentration of alkali (above 5% NaOH) is a clear indication of the severity of alkali attack on encrusting polymers, which should be avoided to conserve the good mechanical properties of the fibre. Another important feature concerns the stress at break value obtained for the different fibres. We can observe a decrease from 1100 MPa for the raw fibre to ~550 MPa, as the concentration of NaOH treatment was increased up to 10%. Wide-angle X-ray diffraction experiments, performed on raw- and alkali-treated fibres, do not show any significant difference (Figure 6) and are typical of microcrystalline cellulose [17]. Reflection peaks at 2θ = 22.4°, 16.4°, and 14.8° that correspond to native cellulose I were found, as reported in the literature [31, 32]. WAXS experiments indicate that the alkali treatment conditions used in this study did not alter the crystalline part of the fibre and confirm that a polymorphic transition of cellulose I structure to cellulose II did not occur. The decrease in the stress at break for alkali-treated flax fibres can thus be preferentially attributed to an alteration of amorphous noncellulosic polysaccharides, pectins and hemicelluloses, present in the primary and secondary cell wall layers of the fibre. Furthermore, the presence of natural defects found in flax fibres, such as kink bands, may also play an important role in the decrease of the stress since they may become more brittle after treatments, due to a favourable and rapid diffusion of the alkali solution through these defects and down to the internal structure of the fibre. It has been shown earlier that, under tensile loading, the fibre starts to break at the region near the kink band where the crack initiates [33]. It is worth noting that for alkali-treated fibres, as the concentration of NaOH increases, the area under the stress-strain curve increases considerably. This is an important property change since the total area under the curve corresponds to the energy per unit volume absorbed in the fibre until its failure and thus to a measure of toughness of the material [28] which is interesting for some applications like energy absorption or vibration damping. Our experiments show that by controlling the NaOH treatment conditions, the toughness of the fibres can be tuned for specific applications.

In the case of pectinase enzyme-treated flax fibres, after 5 hrs of treatment, the shape of the stress-stain curve was similar to that of raw flax fibres (Figure 6). It showed an initial nonlinear part followed by an increasing linear part corresponding to an elastic deformation until the fibre breaks. The nonlinear initial part of the stress-strain graph indicates the presence of a significant amount of residual amorphous polymers from the primary cell wall, as observed by the AFM images. On the other hand, flax fibres treated for 18 hours show only a single linear slope that extends until the fibre breaks, which is representative of a direct elastic response of the microfibrils under loading, in good correlation with AFM observations. Contrary to NaOH-treated flax fibres, the enzyme-treated fibres did not show biphasic stress-strain curves, even after prolonged treatment times (18 H). This result can be explained by the specificity of the pectinase enzyme treatment that largely acts on pectin and do not induces any swelling of the material. It is thus likely that encrusting hemicelluloses are not altered by the pectinase treatment and thus maintained the cohesion of the crystalline cellulose microfibrils within the secondary layer. This is an important result which shows that a specific enzymatic treatment is more suitable to keep the intrinsic stiffness of the flax fibres and emphasizes the important role of the encrusting amorphous hemicellulose in the secondary layer to maintain the cohesion between cellulose microfibrils. However, it should be also noted that the stress at break of 18 H enzyme-treated fibres was comparatively less than the 5 H-treated fibres (Table 1). This behaviour can be associated

with a possible alteration of defects such as kink bands within the fibre upon a prolonged treatment.

3.3. Adherence/Adhesion Properties. As previously discussed, another important issue in the development of biocomposites is the optimisation of the interface in order to promote a good stress transfer between the fibre and the polymer matrix. At the macroscopic scale, the microbonding pull-out test is well suited to directly determine the adherence between a reinforcement fibre and the polymer matrix [34] and was thus adapted to directly measure the adherence between an elementary flax fibre and a polylactic acid polymer drop. The apparent interfacial shear stress (IFSS), $\tau_{i.\text{mean}}$, was calculated using the following Kelly-Tyson [35] equation:

$$\tau_{i.\text{mean}} = \frac{F_{\max}}{\pi d l_e}, \quad (1)$$

where $F_{\max}$ is the maximum pull-off force at debonding, d is the fibre diameter, and l_e is the fibre-embedded length in the polymer droplet. The above equation assumes that the force $F_{\max}$ at the instant of debonding is predicted to be directly proportional to the joined surface area between the fibre and matrix, and the droplet shears off from the fibre surface when the average shear stress at the interface, $\tau_{i.\text{mean}}$, becomes large enough to break the interface. The apparent shear stress was determined from the linear regression of the plot of debonding force versus bonding area. The apparent interfacial shear stress values (IFSS), $\tau_{i.\text{mean}}$, calculated for PLA matrix and different flax fibres are summarized in Table 2. We observed that apparent IFSS values improved after both treatments. In both cases, the maximum IFSS values were obtained for the mild treatment conditions, that is, at 1% of NaOH and after 5 H of enzymatic treatment. However, for more aggressive treatment conditions, that is, at 5% NaOH, 10% NaOH, and 18 H enzyme treatments, IFSS values were not validated since the fibres break cohesively before the complete pull-out event during microbond testing. Earlier, the elastic properties of these fibres (Figure 5) were shown to be greatly reduced when the treatments reached the secondary layers and attacked the encrusting polymers. It was observed that successful fibre pull-out tests were obtained for fibres with tensile strength values above a threshold stress level of ~800 MPa. Similar observations were already reported by Pommet et al. [36] on bacterial cellulose-modified sisal fibres/PLA system where cohesive failure of the fibre occurred when interfacial adhesion exceeded the adhesion among the different constituents of the fibre.

An improved adhesion between modified fibre and the PLA polymer can be developed through different mechanisms. For example, Pommet et al. [36] suggested that the presence of cellulose microfibrils increases the roughness of the fibre's surface, that may enhance the adhesion through mechanical interlocking mechanisms. Other explanations such as the presence of hydrogen bonds between hydroxyl groups present on cellulose fibrils and carbonyl groups in PLA were also argumented [36]. The hypothesis of the fibre's roughness is not validated here since the fibre becomes smoother after the treatment, as revealed by AFM; however, we expect some strong interactions between cellulose fibrils and PLA polymer when some weakly adhering polysaccharides are removed from the fibres, through, for example, hydrogen and van der Waals interactions [37]. However, the pull-out test cannot directly distinguish the nature of these different adhesion interactions.

In a recent work [38], we demonstrate that the force volume technique provides valuable information on the adhesion properties of heterogeneous natural fibres at the nanoscopic scale. Force volume displays simultaneously a topographic image of the fibre surface and the corresponding adhesion map between the fibre surface and a standard silicon nitride AFM tip. The adhesion mapping is obtained from the measurement of force-distance curves on all the different coordinates of the fibres' scanned area (Figure 7). The topographic height image of the sample is crucial in the interpretation of adhesion force maps, since the adhesion interaction between the tip and the sample is dependent on the contact area between the tip and sample. For heterogeneous flax samples, the technique allows for a semiquantitative comparison of the changes in the topography and adhesion properties of raw and different treated fibres.

The adhesion map of raw flax fibres (Figure 7(b)) reveals a heterogeneous distribution of adhesion forces across the fibre surface. Some large aggregates can be found on the outer surface of the raw fibre, as already discussed in the first part. High values of adhesion forces were recorded on such compounds, as indicated by darker regions in the adhesion map image. Average adhesion forces measured on raw flax fibre surface ranged from 41 to 73 nN. FV images of alkali-(Figure 7(e)) and enzymatic-treated fibres (Figure 7(h)) contrast well with those of raw flax fibres. In the latter case, a more homogeneous fibre surface can be observed. The adhesion peaks of the force plots are all superposed and present a small adhesion with the AFM tip. The adhesion forces measured on the treated fibres ranged from 6.5 to 10 nN.

In the absence of electrostatic and chemical bonding forces, adhesion between an AFM tip and the fibre's surface results mainly from van der Waals interactions and capillary forces that arise from condensation of water molecules, present in ambient conditions (56% of relative humidity), between the tip and the surface [39]. Thus, under ambient humidity, adhesion forces are largely influenced by capillary forces, which in turn are dependent on the hydrophilic/hydrophobic properties of the surface and the AFM tip. The latter is known to be hydrophilic. Generally, for hydrophilic surfaces, increased relative humidity leads to an increase of the capillary forces [40]. On the other hand, if the surface is hydrophobic in nature, the contribution from the capillary forces on the adhesion force measurements is less and can even be independent of relative humidity [41]. Thus, we presume that high adhesion forces measured on raw flax fibres are mainly due to the presence of pectin materials that is known to be the more hydrophilic polysaccharide [42] in the fibre and present in the middle lamellae and the primary layer. When this polysaccharide

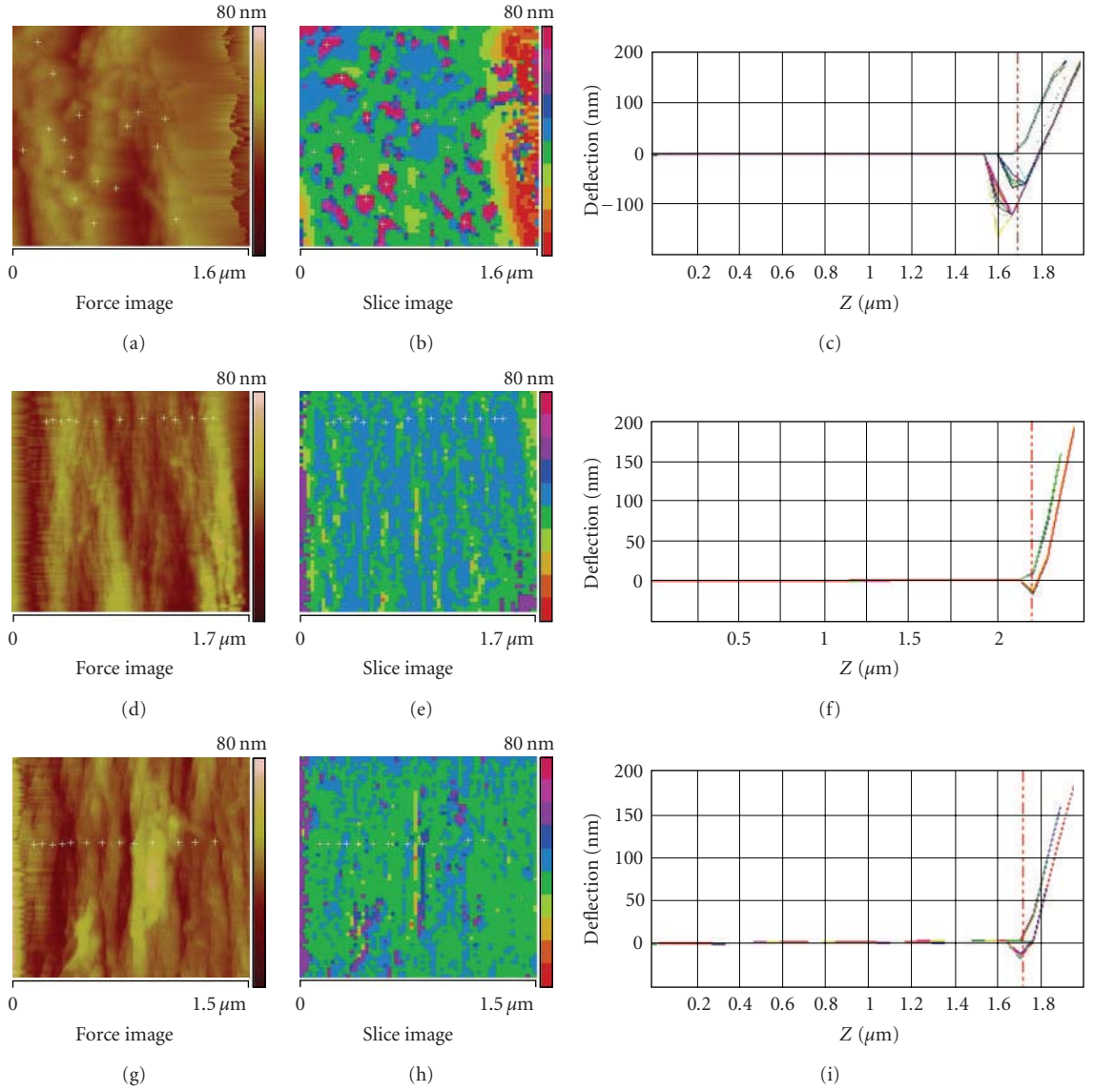

Figure 7: AFM Force-volume images: topography, FV adhesion force map, and force plots corresponding to raw flax fibres ((a), (b), and (c), resp.); NaOH-treated fibres ((d), (e), and (f), resp.); enzyme-treated flax ((g), (h), and (i), resp.).

is removed from the fibre's surface as a consequence of the treatment, as revealed by AFM, the outer surface is mainly constituted by cellulose microfibrils, which in turn gives to the fibre different chemical properties. Biermann et al. [43] studied the chemical nature of crystalline cellulose surface by dynamic molecular simulations and reported a nonhydrophilic nature. Another recent study by Zykwinska et al. [44] reported that the (1 0 0) crystal plane of cellulose is hydrophobic since CH groups are exposed at the surface, whereas the OH groups are reported to form specific types of hydrogen bonds within the crystalline regions [45]. These findings suggest that crystalline regions in cellulose are rather hydrophobic in regards of the amorphous polysaccharides which can present free hydroxyl groups and consequently may form hydrogen bonds with water molecules on the surface. This hypothesis is in good agreement with the lower adhesion forces measured on treated fibres. These results are also well correlated with the microbond test. The low adhesion forces measured by force volume are synonymous of a surface that is less hydrophilic, which may lead to a higher adhesion with the rather hydrophobic PLA matrix.

4. Conclusion

The effect of alkali and enzymatic treatments on the fibre's structure, surface composition, and adhesion properties was investigated. A major consequence of these treatments is the removal of some weakly adhering amorphous polysaccharides, mainly pectins and hemicelluloses, essentially from the middle lamellae, primary cell wall and possibly from the secondary cell wall, as observed by AFM. The organisation

Table 2: Interfacial shear stress values of raw-, NaOH-, and enzyme-treated flax fibres calculated from microbonding test with a PLA droplet.

	Raw flax	1% NaOH	5% NaOH	10% NaOH	Enzyme 5 h	Enzyme 18 h
IFSS (MPa)	14.5 ± 4	20.5 ± 3.6	Not obtained	Not obtained	19.5 ± 3.3	Not obtained

of these polymers within these layers was found to have a profound impact on the overall mechanical properties of the fibre, as revealed by traction tests on elementary fibres. We demonstrate that pectins and hemicelluloses, in the primary layer, do not significantly impact the mechanical properties of the fibre, whereas more pronounced treatments, that reach the secondary layer and attack encrusting polymers, may decrease the strength of the fibre, by reducing the interactions between amorphous and crystalline polymers. In parallel, adhesion properties of the treated fibres were examined at different scales and proved to be essential in the optimisation of a composite system. Microbond tests reveal that PLA adhesion on the flax secondary layer with oriented cellulose microfibrils was found to be the most important, through different mechanisms, mainly van der Waals interactions and H bonding. For an optimal performance of biocomposites, an improvement in interface adhesion with PLA while preserving flax fibre intrinsic mechanical properties was achieved here at gentle alkali treatments (1%, for 20 minutes) and more safely by enzymatic treatments (up to 5 Hrs). The latter ecofriendly treatment proves that this process is becoming highly attractive in the biocomposite industry.

Acknowledgments

Financial support for this work from Region Bretagne, Cap Lorient, and the Morbihan Department (France) is deeply acknowledged. The Authors thank Professor Dimitri A. Ivanov, ICSI, Mulhouse (France) for performing WAXS experiments on flax fibres.

References

[1] E. Bodros, I. Pillin, N. Montrelay, and C. Baley, "Could biopolymers reinforced by randomly scattered flax fibre be used in structural applications?" *Composites Science and Technology*, vol. 67, no. 3-4, pp. 462–470, 2007.

[2] D. Plackett, T. L. Andersen, W. B. Pedersen, and L. Nielsen, "Biodegradable composites based on L-polylactide and jute fibres," *Composites Science and Technology*, vol. 63, no. 9, pp. 1287–1296, 2003.

[3] K. Oksman, M. Skrifvars, and J. F. Selin, "Natural fibres as reinforcement in polylactic acid (PLA) composites," *Composites Science and Technology*, vol. 63, no. 9, pp. 1317–1324, 2003.

[4] C. Baley, "Analysis of the flax fibres tensile behaviour and analysis of the tensile stiffness increase," *Composites A*, vol. 33, no. 7, pp. 939–948, 2002.

[5] C. Morvan, C. Andème-Onzighi, R. Girault, D. S. Himmelsbach, A. Driouich, and D. E. Akin, "Building flax fibres: more than one brick in the walls," *Plant Physiology and Biochemistry*, vol. 41, no. 11-12, pp. 935–944, 2003.

[6] H. L. Bos, J. Müssig, and M. J. A. van den Oever, "Mechanical properties of short-flax-fibre reinforced compounds," *Composites A*, vol. 37, no. 10, pp. 1591–1604, 2006.

[7] K. Charlet, J. P. Jernot, M. Gomina, J. Bréard, C. Morvan, and C. Baley, "Influence of an Agatha flax fibre location in a stem on its mechanical, chemical and morphological properties," *Composites Science and Technology*, vol. 69, no. 9, pp. 1399–1403, 2009.

[8] A. Šturcová, G. R. Davies, and S. J. Eichhorn, "Elastic modulus and stress-transfer properties of tunicate cellulose whiskers," *Biomacromolecules*, vol. 6, no. 2, pp. 1055–1061, 2005.

[9] A. K. Mohanty, M. Misra, and L. T. Drzal, "Surface modifications of natural fibers and performance of the resulting biocomposites: an overview," *Composite Interfaces*, vol. 8, no. 5, pp. 313–343, 2001.

[10] S. Kalia, B. S. Kaith, and I. Kaur, "Pretreatments of natural fibers and their application as reinforcing material in polymer composites-a review," *Polymer Engineering and Science*, vol. 49, no. 7, pp. 1253–1272, 2009.

[11] A. Arbelaiz, G. Cantero, B. Fernández, I. Mondragon, P. Gañán, and J. M. Kenny, "Flax fiber surface modifications: effects on fiber physico mechanical and flax/polypropylene interface properties," *Polymer Composites*, vol. 26, no. 3, pp. 324–332, 2005.

[12] I. Van de Weyenberg, T. Chi Truong, B. Vangrimde, and I. Verpoest, "Improving the properties of UD flax fibre reinforced composites by applying an alkaline fibre treatment," *Composites A*, vol. 37, no. 9, pp. 1368–1376, 2006.

[13] J. Gassan and A. K. Bledzki, "Alkali treatment of jute fibers: relationship between structure and mechanical properties," *Journal of Applied Polymer Science*, vol. 71, no. 4, pp. 623–629, 1999.

[14] L. Y. Mwaikambo and M. P. Ansell, "Chemical modification of hemp, sisal, jute, and kapok fibers by alkalization," *Journal of Applied Polymer Science*, vol. 84, no. 12, pp. 2222–2234, 2002.

[15] H. S. S. Sharma, L. Whiteside, and K. Kernaghan, "Enzymatic treatment of flax fibre at the roving stage for production of wet-spun yarn," *Enzyme and Microbial Technology*, vol. 37, no. 4, pp. 386–394, 2005.

[16] D. E. Akin, J. A. Foulk, R. B. Dodd, and D. D. McAlister, "Enzyme-retting of flax and characterization of processed fibers," *Journal of Biotechnology*, vol. 89, no. 2-3, pp. 193–203, 2001.

[17] P. A. Penttilä, A. Várnai, K. Leppänen et al., "Changes in submicrometer structure of enzymatically hydrolyzed microcrystalline cellulose," *Biomacromolecules*, vol. 11, no. 4, pp. 1111–1117, 2010.

[18] M. Z. Rong, M. Q. Zhang, Y. Liu, G. C. Yang, and H. M. Zeng, "The effect of fiber treatment on the mechanical properties of unidirectional sisal-reinforced epoxy composites," *Composites Science and Technology*, vol. 61, no. 10, pp. 1437–1447, 2001.

[19] S. Marais, F. Gouanvé, A. Bonnesoeur et al., "Unsaturated polyester composites reinforced with flax fibers: effect of cold plasma and autoclave treatments on mechanical and permeation properties," *Composites A*, vol. 36, no. 7, pp. 975–986, 2005.

[20] A. Jähn, M. W. Schröder, M. Füting, K. Schenzel, and W. Diepenbrock, "Characterization of alkali treated flax fibres by means of FT Raman spectroscopy and environmental scanning electron microscopy," *Spectrochimica Acta A*, vol. 58, no. 10, pp. 2271–2279, 2002.

[21] C. Baley, F. Busnel, Y. Grohens, and O. Sire, "Influence of chemical treatments on surface properties and adhesion of flax fibre-polyester resin," *Composites A*, vol. 37, no. 10, pp. 1626–1637, 2006.

[22] A. Pietak, S. Korte, E. Tan, A. Downard, and M. P. Staiger, "Atomic force microscopy characterization of the surface wettability of natural fibres," *Applied Surface Science*, vol. 253, no. 7, pp. 3627–3635, 2007.

[23] E. Balnois, F. Busnel, C. Baley, and Y. Grohens, "An AFM study of the effect of chemical treatments on the surface microstructure and adhesion properties of flax fibres," *Composite Interfaces*, vol. 14, no. 7–10, pp. 715–731, 2007.

[24] K. Joseph, L. H. C. Mattoso, R. D. Toledo et al., "Natural fiber reinforced thermoplastic composites," in *Natural Polymers and Agrofibers Composites*, E. Frollini, A. L. Leao, and L. H. C. Mattoso, Eds., pp. 159–202, Embrapa, USP/ UNESP, San Carlos, Brazil, 2000.

[25] C. H. Chen, C. Y. Chen, Y. W. Lo, C. F. Mao, and W. T. Liao, "Characterization of alkali-treated jute fibers for physical and mechanical properties," *Journal of Applied Polymer Science*, vol. 80, no. 7, pp. 1013–1020, 2001.

[26] J. T. Kim and A. N. Netravali, "Mercerization of sisal fibers: effect of tension on mechanical properties of sisal fiber and fiber-reinforced composites," *Composites A*, vol. 41, no. 9, pp. 1245–1252, 2010.

[27] K. Charlet, C. Baley, C. Morvan, J. P. Jernot, M. Gomina, and J. Bréard, "Characteristics of Hermès flax fibres as a function of their location in the stem and properties of the derived unidirectional composites," *Composites A*, vol. 38, no. 8, pp. 1912–1921, 2007.

[28] P. Fratzl, I. Burgert, and H. S. Gupta, "On the role of interface polymers for the mechanics of natural polymeric composites," *Physical Chemistry Chemical Physics*, vol. 6, no. 24, pp. 5575–5579, 2004.

[29] J. Keckes, I. Burgert, K. Frühmann et al., "Cell-wall recovery after irreversible deformation of wood," *Nature Materials*, vol. 2, no. 12, pp. 810–814, 2003.

[30] C. M. Altaner and M. C. Jarvis, "Modelling polymer interactions of the 'molecular Velcro' type in wood under mechanical stress," *Journal of Theoretical Biology*, vol. 253, no. 3, pp. 434–445, 2008.

[31] E. Zini, M. Scandola, and P. Getenholm, "Heterogeneous acylation of flax fibers. Reaction kinetics and surface properties," *Biomacromolecules*, vol. 4, no. 3, pp. 821–827, 2003.

[32] S. Borysiak and J. Garbarczyk, "Applying the WAXS method to estimate the supermolecular structure of cellulose fibres after mercerisation," *Fibres and Textiles in Eastern Europe*, vol. 11, no. 5, pp. 104–106, 2003.

[33] C. Baley, "Influence of kink bands on the tensile strength of flax fibers," *Journal of Materials Science*, vol. 39, no. 1, pp. 331–334, 2004.

[34] A. Straub, M. Slivka, and P. Schwartz, "A study of the effects of time and temperature on the fiber/matrix interface strength using the microbond test," *Composites Science and Technology*, vol. 57, no. 8, pp. 991–994, 1997.

[35] A. Kelly and W. R. Tyson, "Tensile properties of fibre-reinforced metals: copper/tungsten and copper/molybdenum," *Journal of the Mechanics and Physics of Solids*, vol. 13, no. 6, pp. 329–338, 1965.

[36] M. Pommet, J. Juntaro, J. Y. Y. Heng et al., "Surface modification of natural fibers using bacteria: depositing bacterial cellulose onto natural fibers to create hierarchical fiber reinforced nanocomposites," *Biomacromolecules*, vol. 9, no. 6, pp. 1643–1651, 2008.

[37] G. Raj, E. Balnois, C. Baley, and Y. Grohens, "Probing cellulose/polylactic acid interactions in model biocomposite by colloidal force microscopy," *Colloids and Surfaces A*, vol. 352, no. 1-3, pp. 47–55, 2009.

[38] G. Raj, E. Balnoiso, C. Baley, and Y. Grohens, "Adhesion force mapping of raw and treated flax fibres using afm force-volume," *Journal of Scanning Probe Microscopy*, vol. 4, no. 2, pp. 66–72, 2009.

[39] H. J. Butt, B. Cappella, and M. Kappl, "Force measurements with the atomic force microscope: technique, interpretation and applications," *Surface Science Reports*, vol. 59, no. 1–6, pp. 1–152, 2005.

[40] D. L. Sedin and K. L. Rowlen, "Adhesion forces measured by atomic force microscopy in humid air," *Analytical Chemistry*, vol. 72, no. 10, pp. 2183–2189, 2000.

[41] R. Jones, H. M. Pollock, J. A. S. Cleaver, and C. S. Hodges, "Adhesion forces between glass and silicon surfaces in air studied by AFM: effects of relative humidity, particle size, roughness, and surface treatment," *Langmuir*, vol. 18, no. 21, pp. 8045–8055, 2002.

[42] R. Sun, J. M. Fang, and J. Tomkinson, "Characterization and esterification of hemicelluloses from rye straw," *Journal of Agricultural and Food Chemistry*, vol. 48, no. 4, pp. 1247–1252, 2000.

[43] O. Biermann, E. Hädicke, S. Koltzenburg, and F. Müller-Plathe, "Hydrophilicity and lipophilicity of cellulose crystal surfaces," *Angewandte Chemie—International Edition*, vol. 40, no. 20, pp. 3822–3825, 2001.

[44] A. Zykwinska, J. F. Thibault, and M. C. Ralet, "Modelling of xyloglucan, pectins and pectic side chains binding onto cellulose microfibrils," *Carbohydrate Polymers*, vol. 74, no. 1, pp. 23–30, 2008.

[45] A. J. Michell and H. G. Higgins, "The absence of free hydroxyl groups in cellulose," *Cellulose*, vol. 6, no. 1, pp. 89–91, 1999.

Hindawi Publishing Corporation
International Journal of Polymer Science
Volume 2011, Article ID 841812, 7 pages
doi:10.1155/2011/841812

Research Article

Mechanical and Thermal Behaviour of Ecofriendly Composites Reinforced by *Kenaf* and *Caroà* Fibers

P. Persico,[1] D. Acierno,[2] C. Carfagna,[1,2] and F. Cimino[2]

[1] *Institute of Chemistry and Technology of Polymers, National Research Council of Italy, Via Campi Flegrei, 34 80078 Pozzuoli (Na), Italy*
[2] *Department of Materials and Production Engineering, University of Napoli "Federico II", p.le Tecchio, 80 80125 Napoli, Italy*

Correspondence should be addressed to P. Persico, paola.persico@ictp.cnr.it

Received 31 March 2011; Accepted 12 May 2011

Academic Editor: Susheel Kalia

Two kinds of environmental friendly composites were prepared based on sustainable matrices, respectively, defatted cross-linked soy flour and thermoplastic polyhydroxybutyrate cohydroxyvalerate, reinforced by natural fibers from *Caroà* and *Kenaf* plants. The obtained composites were compared in terms of moisture tolerance, thermal and mechanical properties, and thermoregulation ability. It was found that this ecofriendly systems have suitable properties for indoor applications in housing and transportation.

1. Introduction

The transition toward a bio-based economy and sustainable developments offers high perspectives for natural fiber markets, and so-called *green* materials are increasingly being explored as substitutes to conventional plastics.

Therefore, plant-based biopolymers are fast becoming a viable alternative to petroleum-based polymers. The benefit of those sustainable resources is that they can be regrown within the foreseeable future, without negative side effects on global biodiversity [1–3].

Among biodegradable polymers, starch, wheat gluten, zein, bacterial polyesters, and soy protein have attracted much attention. The present research deals with the preparation and characterization of composites obtained by reinforcing defatted soy flour (SF) [4–8] and thermoplastic polyhydroxybutyrate cohydroxyvalerate (PHBV) resins [9–12] with two different natural fibers named, respectively, *Caroà* and *Kenaf*.

Neoglaziovia Variegata (Arruda da Camara) Mez is a species which belongs to Bromeliaceae family and is native to the lower stratum of the Brazilian Caatinga. It has striped leaves, flowers protected by bracts with bright coloration, and fruits as juicy berries. This species is known in the Northeast Region of Brazil as *Caroá* and represents the raw material most used by local craftsmanship. Natural fibers extracted from its leaves are used for manufacturing string, hats, purses, rugs, hammocks, fishing nets, and fabrics [13].

Kenaf, a species of Hibiscus, is a short-day, annual herbaceous plant cultivated for the soft bast fiber in its stem. The kenaf stalk is made up of an inner woody core and an outer fibrous bark surrounding the core. The fiber derived from the outer fibrous bark is also known as bast fiber, which has been used traditionally in the manufacture and trade of cordage products due to its superior flexural and tensile strength [14].

It is worth noting that chemical composition and cell structure of natural fibers are quite complicated. In general, they are essentially a composite in which rigid cellulose, consisting of helically wound microfibrils, is embedded in a soft matrix of lignin and hemicellulose [15, 16].

Current innovation on the markets for natural fiber containing products (composites) has widened the scope of their use as, for example, in the building industry that encourages the use of evironment-friendly alternative construction materials [17]. For instance, a thermal storage capacity similar with that of conventional building materials can be obtained by the incorporation of microencapsulated

phase change materials (PCMs) in natural composites in order to achieve an effect of thermoregulation [18]. This can contribute to reduce the thermal damping due to external temperature oscillations, making the in-house environment more comfortable.

In this paper, the moisture absorption/desorption capacity, the thermal and mechanical properties, and the thermoregulating ability of prepared ecosustainable composites will be discussed.

2. Experimental

2.1. Materials. Soy flour (defatted SF with 52% protein) was provided by Mangimifici Liverini-Telese (BN-Italy). Kenaf fibers were kindly supplied by Kenaf Eco Fibres Italia S.p.A (Guastalla-Italy) and Caroà fibers were kindly supplied by Federal University of Campina Grande, Brazil.

PHBV ENMAT Y 1000P was supplied by Tianan Biological Material Co., Ltd. Ningbo-China. Analytical grade glycerol (GLY), 99% solution in water and glutaraldehyde (GA), 25% solution in water were obtained from Sigma Aldrich. Microencapsulated PCMs characterized by the phase transition temperature at 28°C (MCPCM28) were supplied by Microtek Laboratories (USA). Microcapsule diameters range from 5 to 40 μm.

2.2. Preparation of Composites

2.2.1. Soy Flour-Based Composites. SF powder was mixed with distilled water in 1 : 9 ratio (by weight), and, if requested, 15 wt.% of GLY plasticizer was added. The SF suspension was homogenized using a magnetic stirrer for 15 minutes, the pH of the mixture was adjusted to 11 at 70°C, and after 30 minutes 40% by SF weight of GA as cross-linking agent was added, causing colour change of the mixture from olive green to brown, when most of water was evaporated out.

The precured resin was mixed with natural fibers (0.5 cm length) in a Brabender-like apparatus (Rheocord EC of HAAKE, NJ, USA) at room temperature in order to obtain a series of eco-composites. Formulations are listed in Table 1. The blends were dried for 5 days at room temperature and then pressed for 45 minutes at 120°C under 50 bar in a Collin hydraulic hot press for finalizing the curing process.

As for thermoactive soy panels, 10% by SF weight of microcapsules were added to the mixture.

2.2.2. PHBV-Based Composites. Polymer composites containing 40 and 60 wt.% of kenaf fibers were prepared using a lab-scale mixer (Thermo Haake Rheomix) at 190°C and 16 rpm mixing rate for 15 min. Polymer pellets were first fed into the mixer and then fibers (previously dried) were added as soon as the torque indicated melting of the polymer (about 2 minutes), the following 13 minutes being enough to reach torque stabilization that means homogeneous mixing of filler and matrix.

Samples from the mixer were compression moulded at 190°C and 100 bar for 10 min using a Collin polymer press to form squared plates (thickness 3.5 mm) for further characterizations.

As for thermoactive PHBV panels, 10% by PHBV weight of microcapsules were blended with the matrix.

Table 1: Ecocomposites formulations.

Samples		*Kenaf* (wt.%)		*Caroà* (wt.%)	
SOY based	15 wt.% GLY	40	60	40	60
	No GLY	40	60	40	60
PHBV based		40	60	—	

2.3. Moisture Absorption/Desorption. Moisture uptake of natural fibers and moisture uptake/release of soy-based composites was measured gravimetrically. The samples were conditioned in a vacuum oven at 70°C for 24 h, cooled in a desiccator and immediately weighted.

The weighted samples were then placed in a closed chamber at 90% relative humidity and room temperature for absorption test.

As for kenaf and caroà fibers, the same amount by weight of dried fibers was used for absorption measurements, performed for 60 hours. The water uptake has been calculated by the weight increase of the fibers normalized to their initial weight.

As for absorption test of soy-based composites, the preconditioned and weighted sample (60 mm length, 10 mm width, and 3.5 mm thick) containing 40 wt.% of kenaf was first placed in a closed chamber at 90% relative humidity and room temperature for 25 hours. When the sample reached a constant weight, the desorption measurement was immediately started on the same specimen, putting it in a desiccator filled with silica gel desiccant for 72 hours. The water uptake has been calculated by the weight increase of the specimen normalized to its initial weight.

2.4. Thermogravimetric Analysis. Thermal properties of ecocomposites were analysed by TGA. Samples were heated up to 50°C, and 30 min isothermal step was carried on in nitrogen atmosphere, then a ramp from 50°C up to 600°C at a scanning rate of 10°C/min in air was performed by using a TGA Q5000 from TA Instruments.

2.5. Flexural and Impact Tests. Three-point flexural test was performed using an Instron model 4504 machine at a deformation speed of 1 mm/min and with a span length of 48 mm to evaluate the flexural modulus under 1 kN load cell according to ASTM D790 test method.

Fracture tests were carried out with a Charpy Ceast Resil Impactor equipped with a DAS 4000 Acquisition System, using an impact energy of 3.6 J, an impact speed of 1 m/s and a span length of 48 mm. Samples (60 mm length, 10 mm width, and 3.5 mm thick) with a notch depth to width ratio of 0.3 were fractured at room temperature according to ASTM D256 test method. For each material, 5 specimens were fractured, and the average value of resilience was calculated.

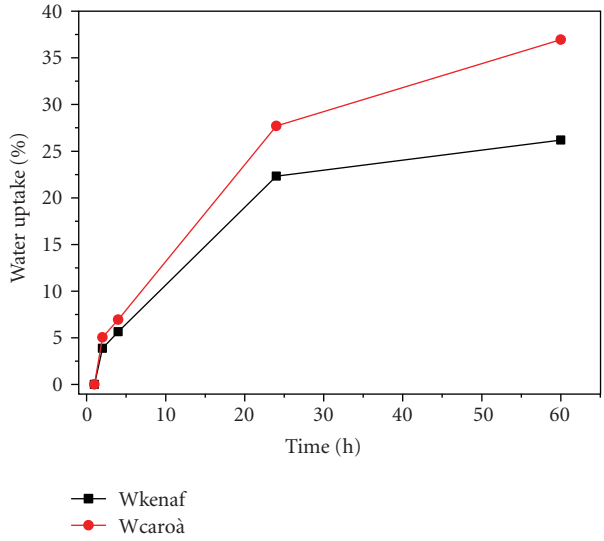

Figure 1: Moisture uptake % of caroà and kenaf fibers.

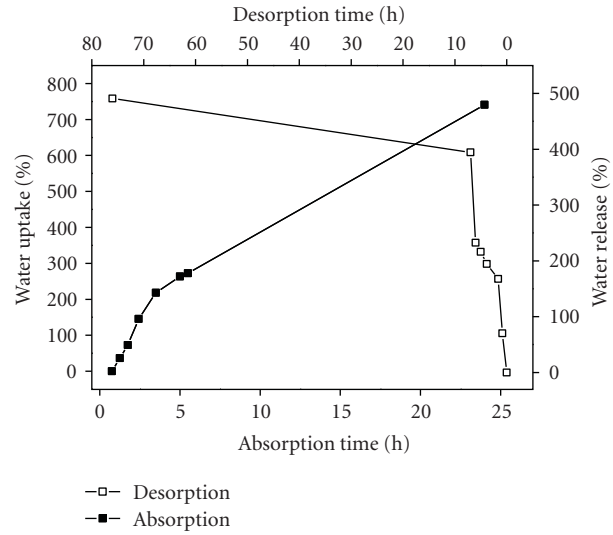

Figure 2: Absorption/desorption tests on 40 wt.% soy/kenaf composites.

2.6. Thermoregulating Test. Time-temperature images during heating and cooling of samples were recorded by means of an infrared thermocamera. The experimental equipment designed to test the thermoregulating effect was composed as follows [19]:

(1) Peltier-effect device, for heating and cooling the samples,

(2) plexigas chamber, in order to avoid thermal influences by external environment,

(3) electrical waves generator, consisting of a PID controller (that checks on the temperature and induces the rely to invert) and the inverter which is an electrical or electromechanical device that produces a sinusoidal waveform,

(4) infrared thermocamera to record images of thermal performance (FLIR SYSTEMS, Thermo Vision A40 M Researcher).

Specimens size (4 mm length, 2 mm width, 2 mm thick) has been selected in respect of this experimental setup.

3. Results and Discussion

3.1. Absorption/Desorption Test. In Figure 1 the percentage of water uptake of caroà and kenaf due to moisture penetration is reported.

As can be noted, caroà absorbs a slight higher quantity of water compared with kenaf. As reported from literature [16], several factors such as density, chemical composition, and structural parameters contribute to the differences in water absorbability of fibers.

The amount of water absorbed is an important factor in composites characterization, since it can have undesired effects on their mechanical properties and dimensional stability, and the hydrophilic character of natural fiber contributes to moisture absorption [20]. Since kenaf is reported to have the less moisture content [16] and is found to absorb less quantity of water, only kenaf-based composites were considered for further absorption and desorption tests.

Figure 2 shows the water uptake an release of soy-based composites containing 40 wt.% of kenaf. The weight of the sample increased as a consequence of water absorption up to about 700% of its initial weight in 24 h. The desorption test was started immediately after, placing the same sample in a desiccator filled with the desiccant agent at room temperature. The specimen released the water absorbed in 72 h, without application of any heating process. This "sponge" like behaviour can be considered suitable for indoor applications in wet environment.

It was observed that the moisture penetration does not depend only on the fiber but also on the type of resin in addition to other effect such as the quality of fiber matrix interface, the relaxation of the resin in presence of moisture, the void content in the resin, and the binding of water molecules on its molecular structure [20].

However, adsorption/desorption experiments (not reported) performed on PHBV-based systems revealed that a really small amount of moisture penetration is achieved in thermoplastic composites.

3.2. Thermogravimetric Analysis. The thermal resistance of the soy neat resin was compared with that exhibited by the resin reinforced with 40 wt.% of both caroà and kenaf fibers (Figure 3).

Starting from 50°C, when the samples are water-free, they are almost thermally stable in air flux up to 200°C despite of the presence of natural fibers. Probably, their degradation leads to the formation of some ash that can hinder further oxygen diffusion through the resin.

TGA traces of PHBV and its composites are shown in Figure 4. The curves revealed that PHBV composites undergo massive thermal degradation above 250°C. The

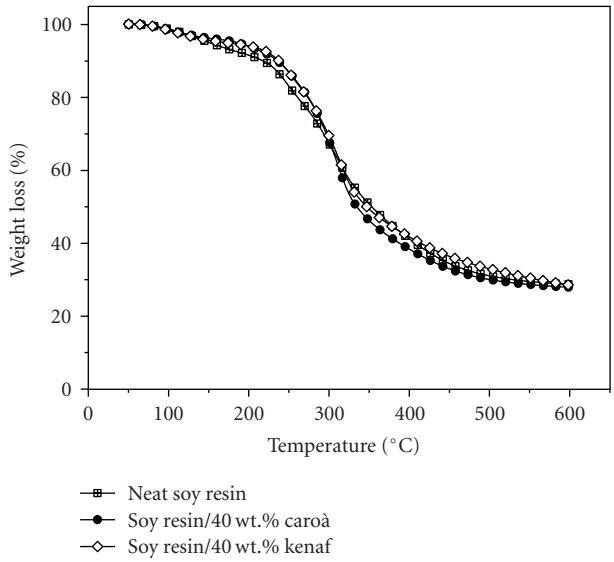

Figure 3: Thermogravimetric curves for soy-based systems.

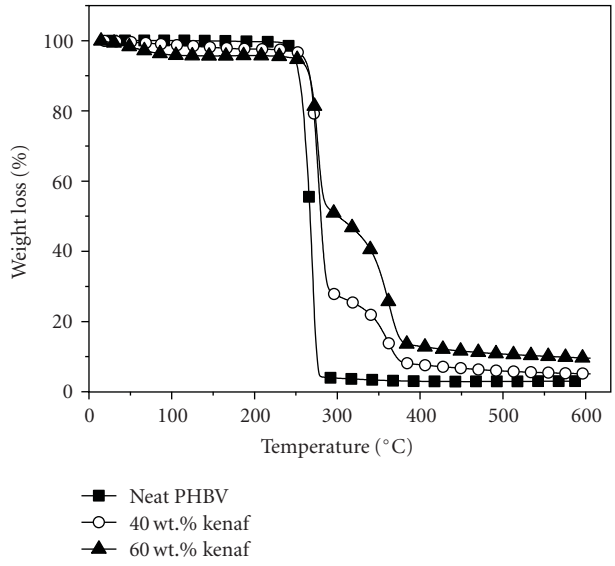

Figure 4: Thermogravimetric curves for PHBV-based systems.

onset of thermal degradation of composites was similar to that of neat PHBV. This can be attributed to the fact that PHBV is thermally unstable and starts degrading drastically above 250°C due to chain scission reactions leading to the reduction of molecular weight and resulting in the formation of the volatile acid products such as crotonic acid. Crotonic acid is also supposedly known to cause hydrolysis of the cellulose content of natural fiber and could result in defibrillation [21]. TGA curves of composite systems also suggested that there was no additional thermal degradation of PHBV with incorporation of kenaf fibers. There was formation of different amounts of residue, the amount was higher in composites having a higher content of fibers.

3.3. Mechanical and Impact Properties. Mechanical tests were performed in order to evaluate the flexural ultimate strength of soy based composites. The results are listed in Table 2. Both kenaf and caroà systems not containing glycerol displayed quite similar values of flexural strength. When glycerol is used in the formulation flexural values are lower, confirming its plasticization efficiency for the soy resin [22, 23]. Additionally, the higher is the fibers content, the higher is the flexural strength caused by the bridging formed in between them.

Table 2: Flexural ultimate strength of soy composites.

Kenaf (wt.%)	Flexural strength (MPa)	
	0 wt.% gly	15 wt.% gly
40	24.5 ± 5.8	7.0 ± 0.4
60	29.5 ± 1.2	13.7 ± 3.4
Caroà (wt.%)		
40	27.4 ± 6.1	9.6 ± 0.4
60	30.3 ± 7.1	21.4 ± 4.6

Table 3: Flexural and impact properties of PHBV composites.

Samples	Flexural modulus (MPa)	Flexural strength (MPa)	Impact strength (KJ/m^2)
Neat PHBV	1280 ± 120	28.2 ± 1.1	0.85 ± 0.15
40 wt.% kef	3605 ± 230	16.7 ± 4.0	2.25 ± 0.32
60 wt.% kef	4020 ± 370	14.1 ± 3.5	1.70 ± 0.10

Flexural and impact properties of kenaf reinforced thermoplastic composites are listed in Table 3. The flexural modulus is representative of intrinsic plastic deformation ability of virgin matrices, and PHBV exhibits a very limited deformation to fracture in comparison with other thermoplastic polymers. Nevertheless, PHBV composites show a significant increase of flexural modulus values with respect to the corresponding neat matrix due to the presence of fiber reinforcement [24]. This finding could suggest that there is a considerable interfacial interaction in between the fibers and PHBV matrix, and, at the same time, fibers entanglements act as resistant junction points against deflection forces.

It should be reminded that in a flexural test the combination of tensile and compressive strength occurs, and therefore, any measurement is affected by both flexural and shear stresses [25]. It is interesting to analyze the flexural strength values of thermoset and thermoplastic composites. In the case of the soy-based system not containing glycerol, the flexural strength remains constant independently of fibers content. On the other hand, by using the glycerol plasticizer, it is possible to reduce the soy system brittleness, and this effect is more pronounced when 60 wt.% of fibers is used.

As for PHBV, the response of the composite based on a brittle matrix will be affected by the properties of the constituents and by the interaction between them. It was observed that flexural strength decreased as a result of the incorporation of stiffness and flexible fibers.

The impact strength of a short fibre composite is determined by the energy required for the plastic deformation of matrix and fibers, for the fracture of matrix and fibers, for

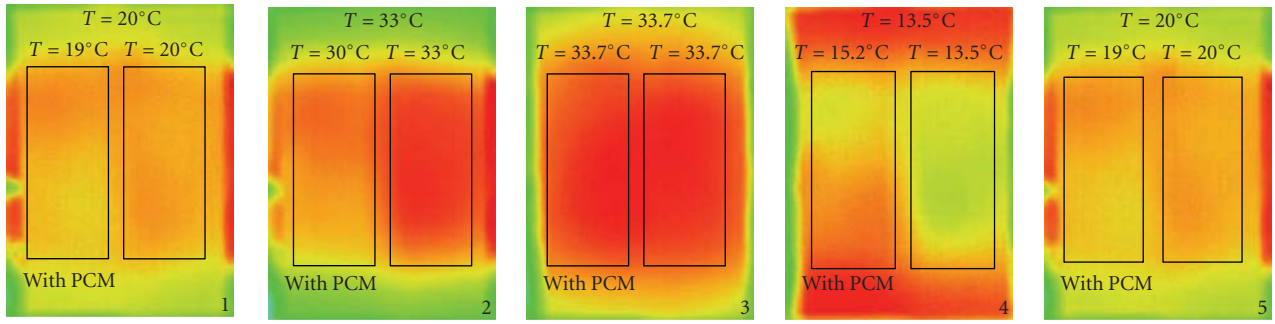

Figure 5: Colour images of soy resin measured by infrared thermocamera.

fiber-matrix debonding at the interface and for overcoming the friction following the debonding during pullout [26]. The nature of composite, fibers, and type of impact test are critical factors for the increase or decrease in the apparent impact strength. An Izod impact test is basically a flexural test with a transient load being applied. In the case of composites, their characteristics are related to the ability of both the matrix and the fiber-matrix interface to absorb the high speed impact.

Low fracture toughness was measured for neat PHBV, but the addition of fibers enhances its impact performances. The slight improvement from 0.85 up to 2.25 KJ/m^2 can be attributed to the energy dissipation mechanism occurring as a consequence of the good level of fiber-matrix adhesion and fiber aspect ratio (l/d).

3.4. Effects of Thermoregulation. Infrared (IR) thermographic systems provide images that represent surface temperatures by measuring the magnitude of infrared radiation emitted by the surface of an object. To perform the temperature distribution analysis, a thermal vision camera can be used to detect IR radiation and convert this information into an image, where each pixel corresponds to a temperature value. Modern IR imagers resolve surface temperature differences of 0.1°C or less. With this high sensitivity, they can provide a nondestructive evaluation of thermal phenomena, which are only revealed in the form of slight temperature gradients. Infrared thermography can be used as both a qualitative and a quantitative tool. The thermal qualitative effect due to the presence of micro-PCMs can be evaluated by recording colour images using the infrared thermocamera, as displayed in Figure 5.

The soy composite sample containing PCMs (reported on SX side of each frame) placed on the surface of the Peltier cell is able to delay and soften the thermal response in comparison with the sample without PCMs (reported on DX side of each frame), since microcapsules absorb heat during the melting process of paraffin waxes [19].

Temperature magnitude in a thermograph can be visualized by a colour scale in which each colour is related to a temperature range. From the hottest to the coldest temperature, the colours are so scaled: red, orange, yellow, green, and blue, the exact value depending on the experimental set fixed. In this experiment, the image was equivalent in the temperature range from 19°C to 40°C.

When the heating/cooling cycle starts, the samples are at the same temperature (step 1), both showing yellow colour (T = 19°C). During the heating cycle, the sample containing PCMs (SX side) turns orange, while reference composite (DX side) is red (step 2). Such colour differences indicate that the temperature of the sample containing PCMs is lower than that of composite not containing them. In this process, PCMs act as a thermal buffer material by absorbing heat delaying the heating of the panel.

When the heating cycle stops, the samples are at the same temperature as confirmed by the red colour for both (step 3, T = 33.7°C).

During the cooling cycle, the sample with PCMs is orange, while reference composite is green (step 4). This colour difference indicates that the temperature of the sample with PCMs is higher than that of reference composite, since part of the available heat is used for wax crystallization, postponing the panel cooling. When the cooling cycle stops, samples reach the same temperature and their colour is orange (step 5).

The same qualitative behaviour (not reported) was observed on PHBV thermoactive ecocomposites: the thermoregulation features are related to the presence of microencapsulated PCMs despite the substrate considered. Moreover, it is possible to tailor the thermoregulation efficiency of panels by using more or less amount of microcapsules in the formulation. In general, the higher is the PCMs content, the greater is the thermal buffer extent.

4. Conclusions

In this work some characteristics of SF- and PHBV-based composites reinforced by kenaf and caroà fibers have been studied in order to evaluate their potential in technological terms. These composites based on natural fibers and eco-sustainable matrices, both thermoset and thermoplastic, are expected to represent a new generation of materials engineered for secondary applications in the field of buildings construction or for the design of innovative bioarchitecture solutions.

As for the moisture uptake/release, soy/kenaf systems act in the same way as a sponge: they are able to take water and then lose it in a dry surrounding environment without forced heating procedures. On the contrary, PHBV/kenaf composites are not hygroscopic, thus representing a promising starting point for durability.

The mechanical characteristics of kenaf reinforced PHBV panels obtained by hot pressing suggested that fibers are able to improve the flexural modulus while promoting the dissipation of impact energy. The soy/kenaf composites mechanical properties are affected, on the other hand, by the use of glycerol as resin plasticizer.

The thermoregulation ability of all the systems can be tailored by using more or less amount of microcapsules in the formulation. In general, it was observed that the higher is the PCMs content, the greater is the thermal buffer extent. However, the thermal stability of thermoset and thermoplastic composites was found to be approximately the same up to 250°C.

Aknowledgments

The authors wish to express thanks to Professor Laura Hecker de Carvalho of Federal University of Campina Grande (Brazil) for the supply of Caroà fibers, Adolfo Izzo Renzi for IR thermography tests, and Mr. Vincenzo Di Lello for assistance during mechanical tests.

References

[1] A. K. Mohanty, M. Misra, and L. T. Drzal, "Sustainable bio-composites from renewable resources: opportunities and challenges in the green materials world," *Journal of Polymers and the Environment*, vol. 10, no. 1-2, pp. 19–26, 2002.

[2] V. K. Mathur, "Composite materials from local resources," *Construction and Building Materials*, vol. 20, no. 7, pp. 470–477, 2006.

[3] H. Y. Cheung, M. P. Ho, K. T. Lau, F. Cardona, and D. Hui, "Natural fibre-reinforced composites for bioengineering and environmental engineering applications," *Composites Part B*, vol. 40, no. 7, pp. 655–663, 2009.

[4] S. Chabba and A. N. Netravali, "'Green' composites part 1: characterization of flax fabric and glutaraldehyde modified soy protein concentrate composites," *Journal of Materials Science*, vol. 40, no. 23, pp. 6263–6273, 2005.

[5] S. Chabba and A. N. Netravali, "'Green' composites part 2: characterization of flax yarn and glutaraldehyde/poly(vinyl alcohol) modified soy protein concentrate composites," *Journal of Materials Science*, vol. 40, no. 23, pp. 6275–6282, 2005.

[6] S. Chabba, G. F. Matthews, and A. N. Netravali, "'Green' composites using cross-linked soy flour and flax yarns," *Green Chemistry*, vol. 7, no. 8, pp. 576–581, 2005.

[7] P. Lodha and A. N. Netravali, "Characterization of phytagel modified soy protein isolate resin and unidirectional flax yarn reinforced "Green" composites," *Polymer Composites*, vol. 26, no. 5, pp. 647–659, 2005.

[8] A. K. Mohanty, P. Tummala, W. Liu, M. Misra, P. V. Mulukutla, and L. T. Drzal, "Injection molded biocomposites from soy protein based bioplastic and short industrial hemp fiber," *Journal of Polymers and the Environment*, vol. 13, no. 3, pp. 279–285, 2005.

[9] S. Philip, T. Keshavarz, and I. Roy, "Polyhydroxyalkanoates: biodegradable polymers with a range of applications," *Journal of Chemical Technology and Biotechnology*, vol. 82, no. 3, pp. 233–247, 2007.

[10] L. Yu, K. Dean, and L. Li, "Polymer blends and composites from renewable resources," *Progress in Polymer Science (Oxford)*, vol. 31, no. 6, pp. 576–602, 2006.

[11] R. A. Shanks, A. Hodzic, and S. Wong, "Thermoplastic biopolyester natural fiber composites," *Journal of Applied Polymer Science*, vol. 91, no. 4, pp. 2114–2121, 2004.

[12] M. Shibata, S. Oyamada, S. I. Kobayashi, and D. Yaginuma, "Mechanical properties and biodegradability of green composites based on biodegradable polyesters and lyocell fabric," *Journal of Applied Polymer Science*, vol. 92, no. 6, pp. 3857–3863, 2004.

[13] D. G. Silveira, F. Vidigal Duarte Souza, C. R. Pelacani, A. Silva Souza, C. A. Silva Ledo, and J. R. Ferreira de Santana, "Micropropagation and in vitro conservation of Neoglaziovia variegata (Arr. Cam.) mez, a fiber producing bromeliad from Brazil," *Brazilian Archives of Biology and Technology*, vol. 52, no. 4, pp. 923–932, 2009.

[14] A. M. Mohd Edeerozey, H. M. Akil, A. B. Azhar, and M. I. Z. Ariffin, "Chemical modification of kenaf fibers," *Materials Letters*, vol. 61, no. 10, pp. 2023–2025, 2007.

[15] M. Z. Rong, M. Q. Zhang, Y. Liu, G. C. Yang, and H. M. Zeng, "The effect of fiber treatment on the mechanical properties of unidirectional sisal-reinforced epoxy composites," *Composites Science and Technology*, vol. 61, no. 10, pp. 1437–1447, 2001.

[16] G. Bogoeva-Gaceva, M. Avella, M. Malinconico et al., "Natural fiber eco-composites," *Polymer Composites*, vol. 28, no. 1, pp. 98–107, 2007.

[17] J. E. G. van Dam, "Environmental benefits of natural fibre production and use," in *Proceedings of the Symposium on Natural Fibres*, 2009.

[18] V. V. Tyagi and D. Buddhi, "PCM thermal storage in buildings: a state of art," *Renewable and Sustainable Energy Reviews*, vol. 11, no. 6, pp. 1146–1166, 2007.

[19] A. Izzo Renzi, C. Carfagna, and P. Persico, "Thermoregulated natural leather using phase change materials: an example of bioinspiration," *Applied Thermal Engineering*, vol. 30, no. 11-12, pp. 1369–1376, 2010.

[20] H. J. Kim and D. W. Seo, "Effect of water absorption fatigue on mechanical properties of sisal textile-reinforced composites," *International Journal of Fatigue*, vol. 28, no. 10, pp. 1307–1314, 2006.

[21] R. Bhardwaj, A. K. Mohanty, L. T. Drzal, F. Pourboghrat, and M. Misra, "Renewable resource-based green composites from recycled cellulose fiber and poly(3-hydroxybutyrate-co-3-hydroxyvalerate) bioplastic," *Biomacromolecules*, vol. 7, no. 6, pp. 2044–2051, 2006.

[22] P. Chen and L. Zhang, "New evidences of glass transitions and microstructures of soy protein plasticized with glycerol," *Macromolecular Bioscience*, vol. 5, no. 3, pp. 237–245, 2005.

[23] P. Tummala, W. Liu, L. T. Drzal, A. K. Mohanty, and M. Misra, "Influence of plasticizers on thermal and mechanical properties and morphology of soy-based bioplastics," *Industrial and Engineering Chemistry Research*, vol. 45, no. 22, pp. 7491–7496, 2006.

[24] S. Singh and A. K. Mohanty, "Wood fiber reinforced bacterial bioplastic composites: fabrication and performance evaluation," *Composites Science and Technology*, vol. 67, no. 9, pp. 1753–1763, 2007.

[25] G. Canché-Escamilla, J. Rodriguez-Laviada, J. I. Cauich-Cupul, E. Mendizábal, J. E. Puig, and P. J. Herrera-Franco, "Flexural, impact and compressive properties of a rigid-thermoplastic matrix/cellulose fiber reinforced composites," *Composites—Part A*, vol. 33, no. 4, pp. 539–549, 2002.

[26] A. Keller, "Compounding and mechanical properties of biodegradable hemp fibre composites," *Composites Science and Technology*, vol. 63, no. 9, pp. 1307–1316, 2003.

Hindawi Publishing Corporation
International Journal of Polymer Science
Volume 2011, Article ID 592906, 10 pages
doi:10.1155/2011/592906

Research Article

Effect of Different Parameters on Mechanical and Erosion Wear Behavior of Bamboo Fiber Reinforced Epoxy Composites

Anu Gupta,[1] Ajit Kumar,[1] Amar Patnaik,[2] and Sandhyarani Biswas[3]

[1] *School of Engineering and Technology, IGNOU, New Delhi 110068, India*
[2] *Department of Mechanical Engineering, N I T, Hamirpur 177005, India*
[3] *Department of Mechanical Engineering, N I T, Orissa, Rourkela 769008, India*

Correspondence should be addressed to Amar Patnaik, amar_mech@sify.com

Received 30 March 2011; Revised 15 May 2011; Accepted 14 June 2011

Academic Editor: Bibin Mathew Cherian

The application of natural fibers as reinforcement in polymer composites has been continuously growing during the last few decades. These composites find diverse applications in hostile environment where they are exposed to external attacks such as solid particle erosion. Also, in many respects, the mechanical properties of different polymer composites are their most important characteristics. Therefore, improvement of the erosion resistance and mechanical behavior of polymer composites are the prime requirements in their applications. Bamboo fiber which is rich in cellulose, relatively inexpensive, and abundantly available has the potential for reinforcement in polymers. To this end, an attempt has been made in this paper not only to study the utilization potential of bamboo fiber in polymer composites but also to study the effect of various parameters on mechanical and erosion wear performance of bamboo fiber reinforced epoxy composites.

1. Introduction

Fiber-reinforced polymers are increasingly becoming potential candidates for replacing conventional materials due to their many advantages. These composites are finding applications in diverse fields starting from appliances to spacecrafts. The application of natural fibers as reinforcement in polymer composites has been continuously growing during the last few years. The main advantages of such fibers are their low cost, renewability, biodegradability, low specific gravity, abundance, high specific strength, and stiffness. Among the various natural fibers, bamboo finds widespread use in housing construction around the world and is considered as a promising construction material for housing applications in both developed and underdeveloped countries. Being a conventional construction material since ancient times, bamboo fiber is a good candidate for use as natural fibers in composite materials. The reason that many studies focus on bamboo is because bamboo is an abundant natural resource in Asia, and its overall mechanical properties are comparable to those of other related wood composites. Furthermore, bamboo can be renewed much more rapidly compared with wood. Bamboo is an extremely light weight, functionally graded, and high strength natural composite. Polymer composites find various applications in hostile environment where they are subjected to external attacks such as solid particle erosion. In many respects, the mechanical properties of different polymer composites are their most important characteristics. Therefore, improvement of the erosion resistance and mechanical behavior of polymer composites are the prime requirements in their applications.

The properties of polymer composites are greatly influenced by many factors. The effect of fiber loading, fiber length, fiber and orientation has significant influence on mechanical behavior of polymer composites and is studied by many investigators [1–4]. Also, the influence of parameters such as concentration, impact velocity, impingement angle, fiber geometry, and shapes of the particles on erosion rate is very significant, and any changes in them can considerably affect the rate of material loss [5]. The erosive wear behavior of polymer composite systems as a function of fiber [6, 7], particle [8, 9] and fabric content [10, 11], fiber and filler type [6, 12], fiber orientation [7, 13, 14], fiber length [7, 15], impingement angle [6–8, 12–14, 16],

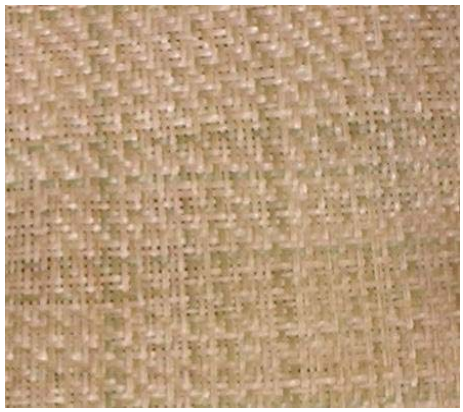

Figure 1: Bidirectional roving bamboo fiber.

impact velocity [8, 13], and erodent mass direction [16] has been studied previously. Although a great deal of work has been made on effect of various parameters on mechanical and wear behavior of different class of polymer composites, research on effect of parameters on natural-fiber-based polymer composites is rare. To this end, in the present research work, an attempt has been made to study the effect of various parameters on mechanical and erosion wear behavior of bamboo fiber reinforced epoxy composites.

2. Experimental Details

2.1. Composite Fabrication. Bidirectional bamboo fibers are collected from local sources. Epoxy LY 556 and the corresponding hardener (HY951) are supplied by Ciba Geigy India Ltd. In general, bamboo culm is a thin-walled hollow cylinder separated with nodes. In the present study, three straight internodes, 250–300 mm in length and 150 mm in diameter, obtained from the midheight of 3-year-old bamboo are used. These "tubes" are then divided into rods of average diameter 2.5 mm and length of 150 mm. These rods are then separated into several types of strips depend on individual requirements. The extracted fibers are dried in an oven at 45°C for 4 h to remove moisture. Each ply of roving bidirectional bamboo mat (Figure 1) is of dimension 150 × 150 mm^2. The average diameter of bamboo fibers is about 2.5 mm. Composites slabs are made by reinforcing bamboo mats in epoxy resin using simple hand lay-up technique followed by light compression molding, as hand lay-up technique is a simple method for composite production. A mold must be used for hand-lay-up parts unless the composite is to be joined directly to another structure. The mold can be as simple as a flat rectangular sheet. For some shapes, molds must be joined in sections, so they can be taken apart for part removal after curing. Before layup, the mold is prepared with a release agent to insure that the part will not adhere to the mold. Reinforcement fibers can be cut and laid in the mold. It is up to the designer to organize the type, amount, and direction of the fibers being used. Resin must then be catalyzed and added to the fibers. A brush, roller or squeegee can be used to impregnate the fibers with the resin. The lay-up technician is responsible for controlling the amount of resin and the quality of saturation. The castings are put under load for about 24 h for proper curing at room temperature. The composites of five different compositions (0 wt%, 10 wt%, 20 wt%, 30 wt%, and 40 wt% fiber loading) are made. After the curing process, test samples are cut to the required sizes as per individual test requirements.

Table 1: Test parameters.

Erodent	Silica sand
Erodent size (μm)	125–300
Erodent shape	Irregular, square pyramidal
Impingement angle (α, $\circ$)	15, 30, 60, 90
Impact velocity (m/s)	30 ± 4, 52 ± 4, 60 ± 4, 88 ± 4
Erodent feed rate (g/min)	4.7 ± 0.3
Test temperature	RT
Nozzle to sample distance (mm)	10
Nozzle diameter (mm)	4

2.2. Physical and Mechanical Properties. The theoretical density of composite materials is obtained as per the equation given by Agarwal and Broutman [17]. The actual experimental density of the composites is determined by simple water immersion technique, and finally the volume fractions of the composites are calculated. Tensile testing of the composites specimen is carried out using an Instron universal testing machine, Model 1195, at a crosshead speed of 10 mm min^{-1}. Rectangular specimens of size 150 × 10 × 3 mm^3 were used for testing. Flexural tests (three-point bend test) were conducted on all the composite samples in the universal testing machine Instron 1195. The dimension of each specimen is 60 mm ×10 mm × 4 mm. Span length of 40 mm and the cross-head speed of 10 mm/min are maintained. Charpy impact tests on specimens were performed using a pendulum impact testing machine. The standard specimen size as per ASTM D 256 is 64 mm × 12.7 mm × 3.2 mm and the depth under the notch is 10 mm. For evaluation of tensile, flexural, and impact properties, five specimens were tested and average values are reported.

2.3. Erosion Test. The set up for the solid particle erosion wear test (as per ASTM G76) used in this study is capable of creating reproducible erosive situations for assessing erosion wear resistance of the prepared composite samples. The erosion test rig is used for erosion testing of composite samples with the different test parameters given in Table 1. The solid particle erosion test rig consists of a compressor, drying unit, a conveyor belt-type particle feeder which helps to control the flow of sand particle, and an air-particle mixing and accelerating chamber. The compressed air is then mixed with the selected range of silica sand which is fed constantly by a conveyor belt feeder into the mixing chamber and then passing the mixture through a convergent brass nozzle of internal diameter of 3 mm.

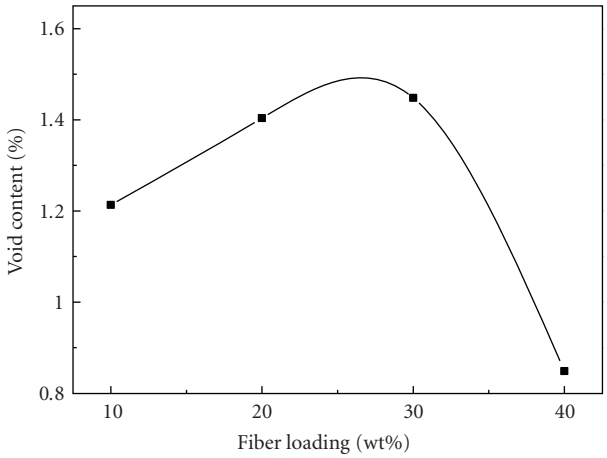

Figure 2: Effect of fiber loading on void content of composites.

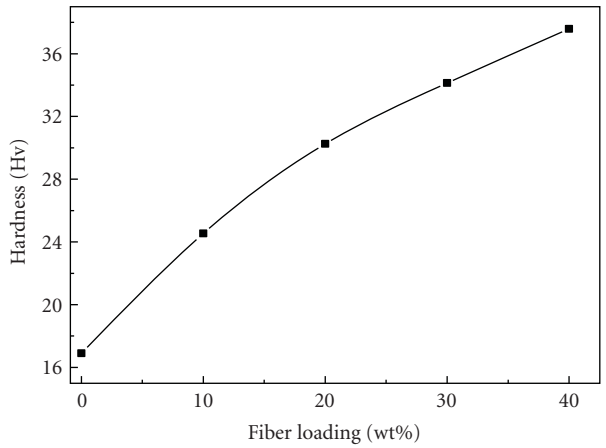

Figure 3: Effect of fiber loading on hardness of composites.

The erodent particles impact the specimen which can be held at different angles with respect to the direction of erodent flow using a swivel and an adjustable sample holder. The velocity of the eroding particles is determined using standard double disc method [18]. In the present study, pyramidal-shaped dry-silica sand of different particle sizes are used as erodent. After each experimental run, the eroded samples are cleaned in acetone and dried for 5 minutes and then weighed to an accuracy of ± 0.01 mg using an electronic balance. The weight loss is recorded for subsequent calculation of erosion rate. The process is repeated till the erosion rate attains a constant value called steady state erosion rate.

2.4. Scanning Electron Microscopy (SEM). The surfaces of the specimens are examined directly by scanning electron microscope (SEM) JEOL JSM-6480LV. The eroded samples are mounted on stubs with silver past. To enhance the conductivity of the eroded samples, a thin film of platinum is vacuum evaporated onto them before the photomicrographs are taken.

3. Results and Discussion

3.1. Effect of Fiber Loading on Physical and Mechanical Properties of Composites. The density is a material property which is of prime importance in several weight sensitive applications. There is always a difference between the theoretical and the measured density values of a composite due to the presence of voids and pores. It is well documented that presence of voids is one of the main factors influencing the mechanical performance of composites and the knowledge of void content is desirable for estimation of the quality of the composites. Porosity is identified as air-filled cavities formed inside the composites, and is often an unavoidable part in all composites. The void may be developed during the mixing and consolidation of two or more different material parts. Månson et al. [19] studied different processing and manufacturing techniques for synthetic fiber composites and considerable knowledge has been accumulated from the study to diminish the porosity part (i.e., to volume fractions below 0.01). In contrast, porosity in plant-fiber-reinforced composites makes usually a noteworthy contribution to the overall composite volume (i.e. weight fractions up to 40 wt%) (Figure 2). Larger porosity content in plant fiber-reinforced composites may be caused by a number of factors: (i) the existence of luminal cavities in plant fibers [20], (ii) the complex surface chemistry of plant fibers which complicates fiber/matrix compatibilization, (iii) the heterogeneous form and dimensions of plant fibers which restrict matrix impregnation [21, 22], and (iv) the low packing ability of plant fiber assemblies which limits the maximum obtainable fiber volume fraction [23]. Figure 2 shows the effect of fiber loading on void content of composites. From the figure, it is clearly observed that with the increase in fiber weight fraction the void content of the composites increases. However, on further increase in fiber loading (>30 wt%), the void content of the composite continuously decreases, and there may be perfect combination of fiber weight fraction and the matrix material. Hence, based up on the above analysis, it is clearly demonstrated that with increase in fiber loading the void content of the composites goes on decreasing.

Surface hardness of the composites is considered as one of the most important factors that govern the erosion resistance. The test results show that with the increase in fiber loading, the hardness (Hv) value of the bamboo-epoxy composites is improved (Figure 3). Oksman [24] reported clearly that inclusion of bamboo fiber in the epoxy matrix body results in improving the hardness of the composites although this improvement is marginal. This is because hardness is a function of the relative fiber volume and modulus [25].

With increasing wt% of bamboo fiber, the tensile strength of bamboo-epoxy composites decreases, as would be expected. Generally the tensile strength depends on the weakest part of the composites, and, may be, the interfacial interaction between epoxy and bamboo fiber is weak. Therefore, the tensile strength of the bamboo-epoxy composites decreases with increasing wt% of bamboo fibers. Mwaikambo and Bisanda reported that, for polyester/cotton fabric composites, the tensile strength of the composites

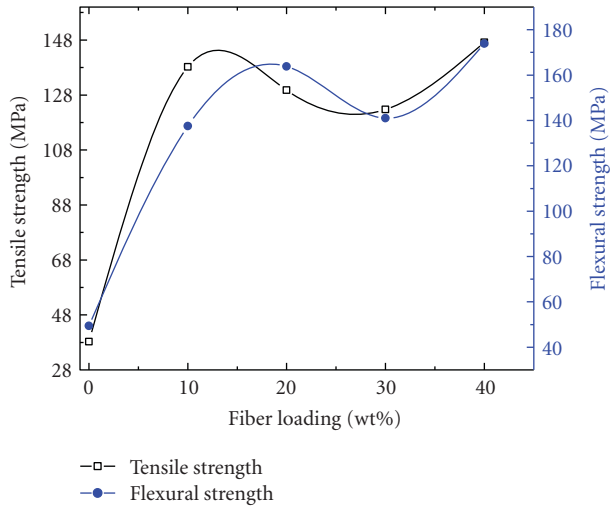

Figure 4: Effect of fiber loading on strength of composites.

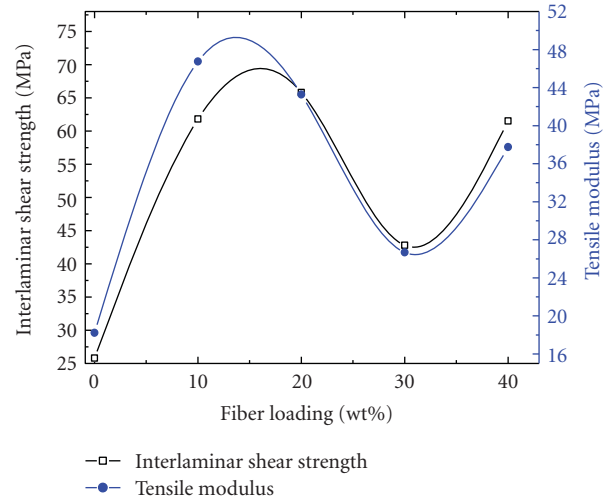

Figure 5: Effect of fiber loading on interlaminar shear strength and tensile modulus of composites.

decreased with increasing content of the cotton fabric, possibly because the void content increases with increasing fabric volume fraction [26]. However, in case of neat epoxy resin, the load increases linearly with displacement. Compared to other types of bamboo fiber composites, both peak load and displacement at failure of neat epoxy resin (0 wt% of fiber loading) are the lowest. Such behaviour generally characterizes the brittleness nature of neat epoxy resin. This is the common observation for thermosetting polyester resin [27, 28].

Similar observation is also observed in the present research work as shown in Figure 4. With the increasing in fiber loading, the void content increases as reported in Figure 2. However, at 40 wt% of bamboo fiber reinforced epoxy composites, the void content decreases. Similarly, the tensile strength decreases with increasing in fiber loading. However, at 40 wt%, fiber loading tensile strength of composite increases mostly due to less void content (Figure 2). The difference in the tensile strength depending on the kind of fiber can also be caused by other factors, such as the fiber length and hydrophilicity, as well as the difference in the chemical nature of the fiber.

The influence of fiber loading on flexural strength of bamboo-epoxy composite is also studied which also shows a similar observation, but a slight deviation is observed at 20 wt% fiber loading as shown in Figure 4. For the composites with 20 wt% of fiber loading, the flexural strength of the composites increases, and, with increasing fiber loading up to 30 wt%, it decreases drastically. However, on further increase of fiber loading up to 40 wt%, the composite shows maximum flexural strength. This behavior is similar to that of the tensile strength of composite except fiber loading of 10 wt%. Adversely, as shown in Figure 4, the flexural strength increased by the increase of fiber loading up to 20 wt% fiber loading. For instance, flexural strength of bamboo-epoxy composite is increased from 137.5 MPa to 163.8 MPa and then decreased from 163.8 MPa to 140.9 MPa, that is, up to 30 wt%, but on further increase in fiber loading the flexural strength increases from 140.9 MPa to 173.8 MPa.

According to Ismail et al. [29] and Yao and Li [30], this decrease is attributed to the inability of the fiber to support stresses transferred from the polymer matrix and poor interfacial bonding generates partially spaces between fiber and matrix material which generates a weak structure. For a composite to be used in structural application, it must possess higher flexural strength because it is one of the important mechanical properties of the composites.

Short-beam shear strength is applied to the laminated bamboo epoxy composites to determine the interlaminar shear strength (ILSS) of composites fabricated with different fiber loading. With the addition of fiber loading from 0 wt% to 10 wt%, the ILSS of laminates increases slightly, and, further increase in fiber loading up to 30 wt%, the ILSS starts decreasing drastically, but again with the increase in fiber loading up to 40 wt%, it shows quite different behaviour as shown in Figure 5.

The reduction may be related with the formation of voids in the matrix which is generally located at the interlaminar region of composites (Figure 2). The tendency of void formation is higher in 30 wt% fiber loading composite (void content: 1.448%) as compared to 10 wt% bamboo fiber composite (void content: 1.213%). This variation in property may be due to that the shear stress distribution is not parabolic and analysis is thus more complex than the conventional strength of materials analysis. The failure mode is strongly dependent on the ratio between length to support thickness, and the standard test methods suggest different ratios according to the type of material tested [31]. Similar observation is also reported in case of tensile strength as shown in Figure 5. The improvement in mechanical properties is due to the improvement in shear strength of the fiber/matrix interface bonding and also simultaneously may be an improvement in the macroscopic properties of the composite. However, the decrease in mechanical properties

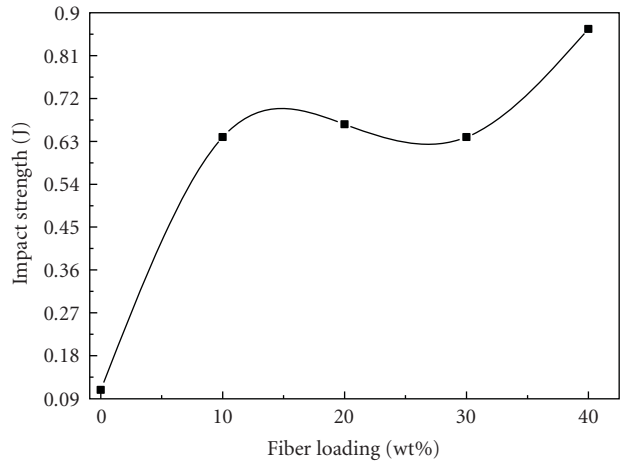

Figure 6: Effect of fiber loading on impact strength of composites.

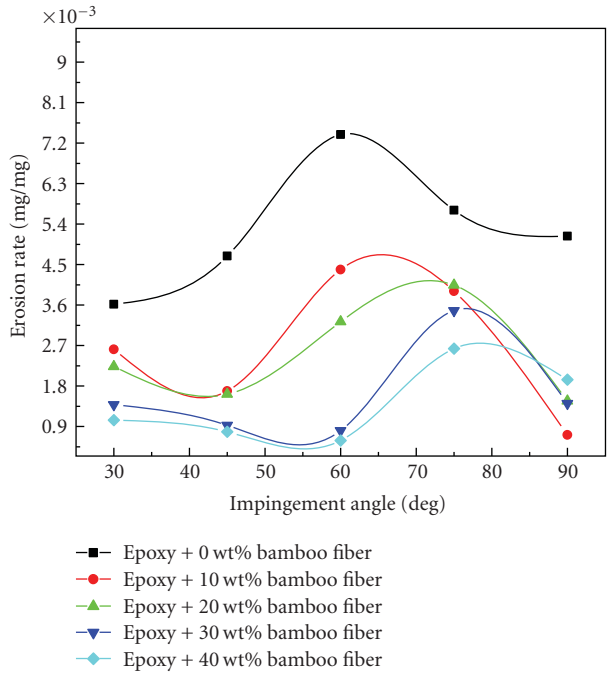

Figure 7: Effect of impingement angle on the erosion wear rate of the composites.

of any composites can be due to the poor interaction between matrix and fibers, which would make the fibers as the site of stress concentration. It induces microspaces between the fiber and matrix polymer, and as a result causes numerous microcracks when impact occurs, which induce crack propagation easily and decrease the impact strength of the composites [32, 33]. This result proves that kenaf has higher properties [34] and can be less weakening agent than rice husk [35].

The impact strength of these composite materials is measured, and the results are reported in Figure 6. In this case, the impact strength increases linearly with increasing fiber loading from 0 wt% to 20 wt% (i.e., from 0.639 J to 0.666 J) and then decreases nominal amount of energy (0.639 J), but, on further increase in fiber loading, the impact strength increases gradually with the increase in impact strength (0.866 J) as shown in Figure 6.

3.2. Effect of Impingement Angle on Erosion Rate. Erosion wear involves several wear mechanisms which are largely controlled by various parameters such as the angle of impingement, impact velocity, and particle size, particle material.

The angle of impingement is the angle between the eroded surface and the trajectory of the particle immediately before impact. In cases when erosion shows a maximum at low impingement angles, it is concluded that the "ductile mode of erosion wear" prevails [36, 37]. Conversely, if the maximum erosion rate is found at high impingement angles, then the "brittle mode" is assumed [36, 37]. The effect of impingement angle on erosion rate of bamboo-epoxy composite is studied, and results are shown in Figure 7. It is evident from the figure that impingement angle has significant influence on erosion rate and the maximum erosion is occurring at an impingement angle of 60°–75° for all composite samples irrespective of fiber loading. So the mode of wear is neither a ductile erosion mode nor brittle erosion wear mode, it is behaving like semiductile/semibrittle mode of erosion wear.

3.3. Surface Morphology. The SEM observations explain to the results presented in the Figure 7 for bamboo fiber reinforced epoxy composites under steady state erosion rate studied at constant impact velocity 45 m/sec, erodent size 250 μm, and stand-off distance of 65 mm at controlled conditions with variations of impingement angle (30 to 90°). Figure 8 shows the SEM of surfaces of the bamboo-epoxy composite eroded under various test conditions. Figures 8(a) and 8(b) show the bamboo-epoxy composites with 10 wt% fiber loading which appears that composites under consideration exhibit several stages of erosion and material removal process. Very small craters and short cracks are seen on the eroded surface of the composite (Figure 7) at 30° impingement angle. Increase in impingement angle to 45° under similar operating conditions shows slight increase in erosion rate as evident from Figure 7 to 20 wt% fiber loading. This indicated that the initiation of matrix material loss from the surface and the matrix is chipped off and the bamboo fibers are slightly visible beneath the matrix layer after the impact of dry silica sand particles as shown in Figures 8(c) and 8(d). But as the erosion tests are carried out with further higher impingement angle (60°) at constant impact velocity 45 m/sec, erodent size 250 μm, and stand-off distance 65 mm, the morphology of the eroded surface becomes different as in Figure 8(e) (Figure 7).

Such cracks are clearly noticed in Figure 8(e) and distinctly illustrate a crater formed due to material loss and the arrays of broken/semibroken bamboo fibers. Due to repeated impact of hard silica sand and higher impingement angle, the sand particles try to initiate cracks on the matrix body, and as erosion progresses gradually, these cracks

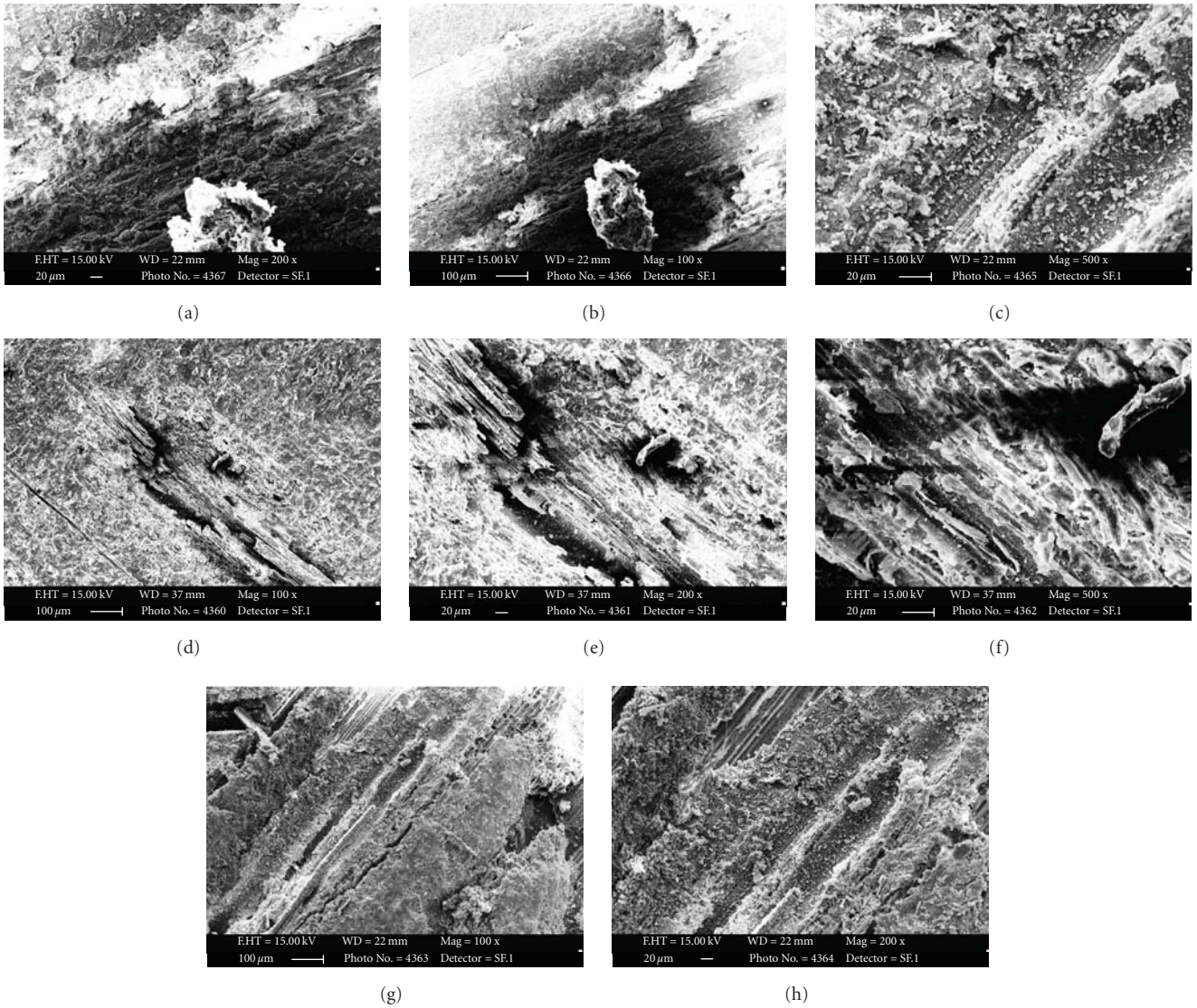

Figure 8: SEM observations of eroded samples with the variations of impingement angle.

subsequently propagate on the fiber bodies both in transverse as well as in longitudinal manner. But on further increase in impingement angle from 60° to 75°, almost all the composites showed maximum erosion rate (Figure 7) as shown in Figure 8(f) for 30 wt% fiber loading. However, the SEM micrograph in Figures 8(g) and 8(h) shows less cracks or craters on the composite surface after erosion at an impingement angle of 90°, and matrix removal is less as compared with other impingement angles (Figures 8(a)–8(f)). As bamboo fiber reinforced epoxy composites are not as ductile as metals, the surface shows mixed-damage processes. As discussed earlier for ductile materials, repeated impacts lead to plastic deformation processes and heavily strained regions on the composite surface. In the case of brittle materials on other hand, the propagation of cracks grows towards the surface and their intersection to form a wear particle separated from the surface leads to additional mass loss of the composite.

3.4. Effect of Impact Velocity on Erosion Rate. The speed of erosive particle has a very strong effect on the wear process. If the speed is very low, then the stresses at impact are insufficient for plastic deformation to occur and wear proceeds by surface fatigue. When the speed increases, it is possible for the eroded material to deform plastically on particle impact. In this contest, effect of impact velocity of particle on erosion rate is studied, and the results are represented in Figure 9. It is evident from the figure that at low impact velocity from 35 m/sec to 45 m/sec, there is not much variation in erosion rate (denoted as phase-1).

However, with the further increase in impact velocity, the erosion rate is significantly increasing, that is, up to 55 m/sec (denoted as phase 2). This may be due to the fact that at higher impact velocity, the erosion is occurring due to plastic deformation and more amount of material is removed. On further increase in impact velocity, all the composites show

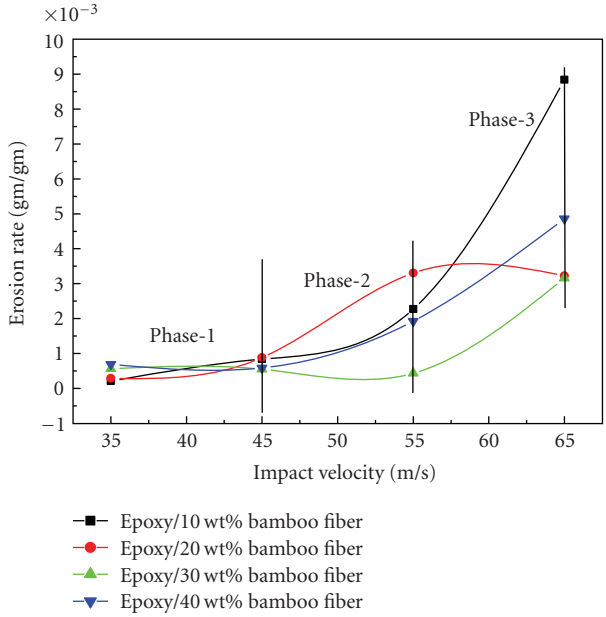

Figure 9: Effect of impact velocity on the erosion wear rate of the composites.

gradual increase in erosion rate except 20 wt% bamboo-fiber-reinforced epoxy composites which shows quite reverse in trend as shown in Figure 9.

3.5. Surface Morphology. Figure 10 shows the SEM observations of the eroded surfaces as a function of impact velocity under constant operating conditions such as impingement angle 60°, stand-off distance 65 mm, and erodent size 250 μm for bamboo-epoxy composites, respectively. Figures 10(a) and 10(b) show the micrograph of the same composite surface (10 wt%) eroded at an impingement angle of 60° and an impact velocity of 35 m/sec. The matrix covering the fiber seems to be chipped off, and the crater thus formed shows the fiber body which is almost intact. The signs of plastic deformation of the matrix material, and when, impacting at such a low impact velocity (35 m/sec), the hard erodent particles penetrate the surface and cause material removal mostly. Figures 10(c) and 10(d) show fragmentation of the fibers as a result of cracks, and multiple fractures are also distinctly shown in micrograph under similar impingement angle (60°). After the local removal of matrix, the arrays of fibers are normally exposed to erosive environment. At low impact velocity (45 m/sec) and impingement angle (60°), the damage to the surface is minimal as seen in Figures 10(e) and 10(f). Subsequently the material removal becomes faster. The wear trace is distinctly visible, and there is protrusion of fibers beneath the matrix layer as seen in Figure 10(g). The broken fiber, seen in Figure 10(h) are mixed with the matrix microflake debris, and the damage of the composite is characterized by separation and detachment of this debris at an impingement angle of 60°. Regions were formed due to simultaneous generation of cracks characteristic of brittle materials. The extent of plastic indentation, however, decreased as the angle of impingement decreased as seen in other micrographs (Figures 10(i) and 10(j)).

3.6. Effect of Erodent Size on Erosion Rate. The erosion rate of bamboo-fiber-reinforced epoxy composites have been studied by varying erodent size from 125 μm to 350 μm at constant impact velocity (45 m/sec), impingement angle (60°), and stand-off distance (65 mm) as shown in Figure 11. From Figure 11, it is observed, that with the increase in erodent size from 125 μm–175 μm, the erosion rate almost remained constant.

In contrast, the erosion rate increased appreciably on further increasing the erodent size from 175 μm to 275 μm, and on further increasing the erodent size from 275 μm to 350 μm, the erosion rate starts decreasing. As reported by Biswas and Satapathy [38, 39] and Patnaik et al. [40], for glass fiber-reinforced polymer composites, with the increase in erodent size, the erosion rate increases gradually irrespective of fiber loading. It is also observed that the composite with 40 wt% of bamboo fiber loading shows most erosion resistant closely followed by the composite with 20 wt%, 30 wt%, and 10 wt% of bamboo fiber loading.

4. Conclusions

This mechanical and the erosion behaviour of bamboo-fiber-reinforced epoxy composites leads to the following conclusions.

(1) The composites which are suitable for applications in highly erosive environments can be prepared by reinforcement of bamboo fibers in epoxy resin. The erosion wear performance of these composites improves quite significantly by addition of bamboo fibers.

(2) It is evident from this study that the void content increases with increase in fiber loading and is maximum for composites with 30 wt% fiber loading. However, on further increase in fiber loading, the void content starts decreasing. As far as hardness is concerned for bamboo-epoxy composites, with increase in fiber loading, the hardness increases gradually from 24.5 Hv to 37 Hv.

(3) The tensile strength shows maximum at 40 wt% fiber loading among other composites. The difference in the tensile strength depending on the kind of fiber can also be caused by other factors, such as the fiber length, and hydrophilicity as well as the difference in the chemical nature of the fiber.

(4) The flexural strength increased with the increase in fiber loading up to 20 wt%. For instance, flexural strength of bamboo-epoxy composite is increased from 137.5 MPa to 163.8 MPa, and then decreased from 163.8 MPa to 140.9 MPa, that is, up to 30 wt% but, on further increase in fiber loading, the flexural strength increases from 140.9 MPa to 173.8 MPa. However, as far as interlaminar shear strength and

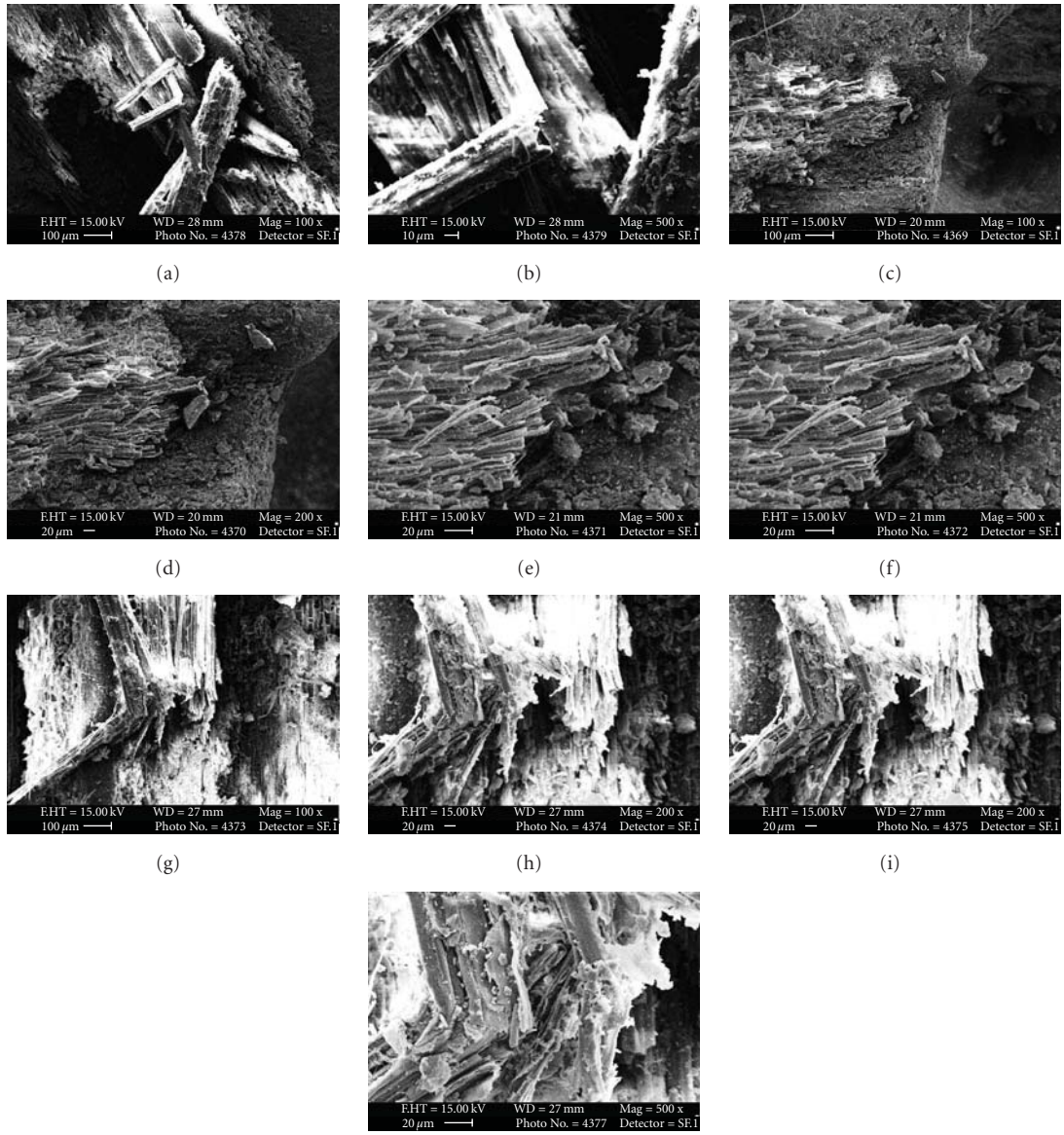

Figure 10: SEM observations of eroded samples with the variations of impact velocity.

tensile modulus are concerned, 20 wt% fiber loading show maximum strength and modulus.

(5) In this study, the impact strength increases linearly with increase in fiber loading from 0 to 20 wt%, that is, from ~0.639 to 0.666 J, and then decreases nominal amount of energy (0.639 J), but, on further increase in fiber loading, the impact strength increases gradually with the increase in impact strength (0.866 J).

(6) Study of influence of impingement angle on erosion rate of the composites filled with different weight percentage of fiber loading reveals their semibrittle nature with respect to erosion wear. The peak erosion rate is found to be occurring at 60° to 75° impingement angle for all the composite samples under various experimental conditions irrespective of fiber loading.

(7) For bamboo fiber composite, severe deterioration of both fiber and matrix, microploughing in the matrix, transverse shearing, stripping, and fibrillation of fiber are identified, and composite debonding, pulling, and fiber fracture are the characteristic features of damage in bamboo fiber.

(8) Possible use of these composites in components such as pipes carrying coal dust, helicopter fan blades, desert roof structures, industrial fans, and low cost housing is recommended. In future, this study can be extended to new hybrid composites using potential

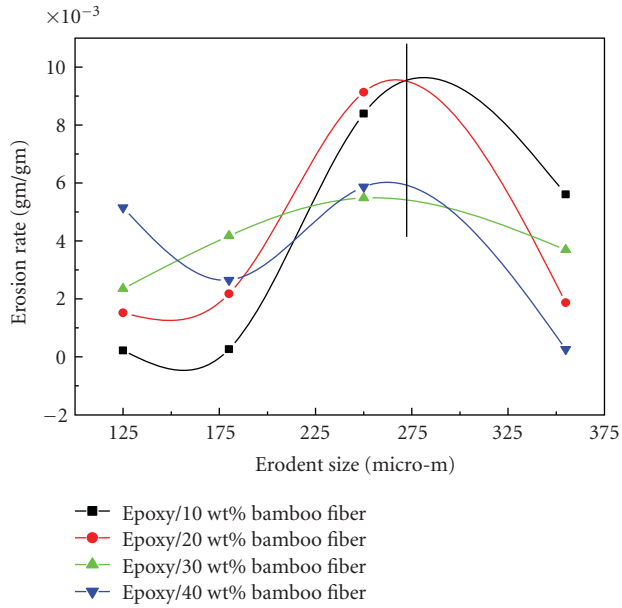

Figure 11: Effect of erodent size on the erosion wear rate of the composites.

fillers, and the resulting experimental findings can be similarly analyzed.

(9) The applications of natural fibers as reinforcement for polymer composites are reduced by the hydrophilic nature of natural fibers. The poor moisture resistance and poor wettability of natural fibers with hydrophobic polymers affect the interaction bonding between fiber and matrix interface. Therefore, chemical treatment of the fiber may improve the mechanical properties and wear resistance of the bamboo fiber-epoxy composites significantly as compared with the untreated bamboo-fiber-reinforced composites. However, fabrication techniques have also depended on the improvement of physical, mechanical, and wear resistance. It is recommended that the use of injection moulding technique to fabricate composite samples for testing is more precise and it reduced much of human factor's error, such as machining the composite to testing specimen which has critical dimensions.

References

[1] S. Öztürk, "Effect of fiber loading on the mechanical properties of kenaf and fiberfrax fiber-reinforced phenol-formaldehyde composites," *Journal of Composite Materials*, vol. 44, no. 19, pp. 2265–2288, 2010.

[2] S. Biswas, S. Kindo, and A. Patnaik, "Effect of fiber length on mechanical behavior of coir fiber reinforced epoxy composites," *Fibers and Polymers*, vol. 12, no. 1, pp. 73–78, 2011.

[3] J. W. Kim, J. J. Lee, and D. G. Lee, "Effect of fiber orientation on the tensile strength in fiber-reinforced polymeric composite materials," *Key Engineering Materials*, vol. 297–300, pp. 2897–2902, 2005.

[4] E. S. AL-Hassani and S. R. Areef, "The effect of fiber orientation on creep behavior and flextural strength in epoxy composites," *Engineering & Technology Journal*, vol. 28, no. 7, pp. 1281–1289, 2010.

[5] H. M. Clark, "Particle velocity and size effects in laboratory slurry erosion measurements OR... do you know what your particles are doing?" *Tribology International*, vol. 35, no. 10, pp. 617–624, 2002.

[6] A. P. Harsha and A. A. Thakre, "Investigation on solid particle erosion behaviour of polyetherimide and its composites," *Wear*, vol. 262, no. 7-8, pp. 807–818, 2007.

[7] N. M. Barkoula and J. Karger-Kocsis, "Effects of fibre content and relative fibre-orientation on the solid particle erosion of GF/PP composites," *Wear*, vol. 252, no. 1-2, pp. 80–87, 2002.

[8] V. K. Srivastava, "Effects of wheat starch on erosive wear of E-glass fibre reinforced epoxy resin composite materials," *Materials Science and Engineering A*, vol. 435-436, pp. 282–287, 2006.

[9] R. Zhou, D. H. Lu, Y. H. Jiang, and Q. N. Li, "Mechanical properties and erosion wear resistance of polyurethane matrix composites," *Wear*, vol. 259, no. 1–6, pp. 676–683, 2005.

[10] R. Rattan and J. Bijwe, "Influence of impingement angle on solid particle erosion of carbon fabric reinforced polyetherimide composite," *Wear*, vol. 262, no. 5-6, pp. 568–574, 2007.

[11] J. Bijwe and R. Rattan, "Influence of weave of carbon fabric in polyetherimide composites in various wear situations," *Wear*, vol. 263, no. 7-12, pp. 984–991, 2007.

[12] V. K. Srivastava and A. G. Pawar, "Solid particle erosion of glass fibre reinforced flyash filled epoxy resin composites," *Composites Science and Technology*, vol. 66, no. 15, pp. 3021–3028, 2006.

[13] U. S. Tewari, A. P. Harsha, A. M. Häger, and K. Friedrich, "Solid particle erosion of unidirectional carbon fibre reinforced polyetheretherketone composites," *Wear*, vol. 252, no. 11-12, pp. 992–1000, 2002.

[14] U. S. Tewari, A. P. Harsha, A. M. Häger, and K. Friedrich, "Solid particle erosion of carbon fibre- and glass fibre-epoxy composites," *Composites Science and Technology*, vol. 63, no. 3-4, pp. 549–557, 2003.

[15] H. Zhang, Z. Zhang, and K. Friedrich, "Effect of fiber length on the wear resistance of short carbon fiber reinforced epoxy composites," *Composites Science and Technology*, vol. 67, no. 2, pp. 222–230, 2007.

[16] A. Patnaik, A. Satapathy, M. Dwivedy, and S. Biswas, "Wear behavior of plant fiber (Pine-Bark) and cement kiln dust-reinforced polyester composites using Taguchi experimental model," *Journal of Composite Materials*, vol. 44, no. 5, pp. 559–574, 2010.

[17] B. D. Agarwal and L. J. Broutman, *Analysis and Performance of Fiber Composites*, John Wiley and Sons, New York, NY, USA, 2nd edition, 1990.

[18] A. W. Ruff and L. K. Ives, "Measurement of solid particle velocity in erosive wear," *Wear*, vol. 35, no. 1, pp. 195–199, 1975.

[19] J. A. E. Månson, M. D. Wakeman, and N. Bernet, "Composite processing and manufacturing—an overview," in *Comprehensive Composite Materials*, A. Kelly and C. Zweben, Eds., vol. 2, chapter 2, pp. 577–607, Elsevier, Amsterdam, The Netherlands, 2000.

[20] H. Lilholt and A. B. Bjerre, "Composites based on jute-fibres and polypropylene matrix, their fabrication and characterization," in *Proceedings of the 18th Risø International Symposium on Materials Science, Polymeric Composites – Expanding the*

Limits, pp. 411–423, Risø National Laboratory, Roskilde, Denmark, 1997.

[21] B. Madsen, *Properties of plant fibre yarn polymer composites–an experimental study*, Ph.D. thesis, Technical University of Denmark, Department of Civil Engineering, 2004.

[22] A. Thygesen, *Properties of hemp fibre polymer composites–an optimisation of fibre properties using novel defibration methods and detailed fibre characterization*, Ph.D. thesis, The Royal Veterinary and Agricultural University, Danish Centre for Forest, Landscape and Planning, 2005.

[23] B. Madsen and H. Lilholt, "Compaction of plant fibre assemblies," in *Proceedings of the 23rd Risø International Symposium on Materials Science, Sustainable Natural and Polymeric Composites–Science and Technology*, pp. 239–250, Risø National Laboratory, Roskilde, Denmark, 2002.

[24] K. Oksman, "Mechanical properties of natural fibre mat reinforced thermoplastic," *Applied Composite Materials*, vol. 7, no. 5-6, pp. 403–414, 2000.

[25] T. H. Ferrigno, *Handbook of Fillers and Reinforcements for Plastics*, Van Nostrand Reinhold, New York, NY, USA, 1978.

[26] L. Y. Mwaikambo and E. T. N. Bisanda, "Performance of cotton-kapok fabric-polyester composites," *Polymer Testing*, vol. 18, no. 3, pp. 181–198, 1999.

[27] L. W. H. Leonard, K. J. Wong, K. O. Low, and B. F. Yousif, "Fracture behaviour of glass fibre-reinforced polyester composite," *Proceedings of the Institution of Mechanical Engineers, Part L*, vol. 223, no. 2, pp. 83–89, 2009.

[28] K. J. Wong, B. F. Yousif, K. O. Low, Y. Ng, and S. L. Tan, "Effects of fillers on the fracture behaviour of particulate polyester composites," *Journal of Strain Analysis for Engineering Design*, vol. 45, no. 1, pp. 67–78, 2010.

[29] H. Ismail, M. R. Edyham, and B. Wirjosentono, "Bamboo fibre filled natural rubber composites: the effects of filler loading and bonding agent," *Polymer Testing*, vol. 21, no. 2, pp. 139–144, 2002.

[30] W. Yao and Z. Li, "Flexural behavior of bamboo-fiber-reinforced mortar laminates," *Cement and Concrete Research*, vol. 33, no. 1, pp. 15–19, 2003.

[31] M. Bagueri, "The Three-points Bending Test," in *Critical Review Proceedings of the 8th Japan-US Conference on Composite Materials*, pp. 683–692, Technomic Publ., Baltimore, Md, USA, 1998.

[32] Q. Zhao, J. Tao, R. C. M. Yam, A. C. K. Mok, R. K. Y. Li, and C. Song, "Biodegradation behavior of polycaprolactone/rice husk ecocomposites in simulated soil medium," *Polymer Degradation and Stability*, vol. 93, no. 8, pp. 1571–1576, 2008.

[33] H. S. Yang, H. J. Kim, J. Son, H. J. Park, B. J. Lee, and T. S. Hwang, "Rice-husk flour filled polypropylene composites; mechanical and morphological study," *Composite Structures*, vol. 63, no. 3-4, pp. 305–312, 2004.

[34] M. S. Huda, L. T. Drzal, A. K. Mohanty, and M. Misra, "Effect of fiber surface-treatments on the properties of laminated biocomposites from poly(lactic acid) (PLA) and kenaf fibers," *Composites Science and Technology*, vol. 68, no. 2, pp. 424–432, 2008.

[35] H. G. B. Premalal, H. Ismail, and A. Baharin, "Comparison of the mechanical properties of rice husk powder filled polypropylene composites with talc filled polypropylene composites," *Polymer Testing*, vol. 21, no. 7, pp. 833–839, 2002.

[36] J. C. Arnold and I. M. Hutchings, "Erosive wear of rubber by solid particles at normal incidence," *Wear*, vol. 161, no. 1-2, pp. 213–221, 1993.

[37] J. C. Arnold and I. M. Hutchings, "Model for the erosive wear of rubber at oblique impact angles," *Journal of Physics D*, vol. 25, no. 1A, pp. A222–A229, 1992.

[38] S. Biswas and A. Satapathy, "Erosion wear analysis of SiC filled glass-epoxy composites using Taguchi technique," *International Polymer Processing*, vol. 25, no. 1, pp. 23–33, 2009.

[39] S. Biswas and A. Satapathy, "An assessment of erosion wear response of SiC filled epoxy composites reinforced with glass and bamboo fibers," *International Polymer Processing*, vol. 25, no. 3, pp. 205–222, 2010.

[40] A. Patnaik, A. Satapathy, S. S. Mahapatra, and R. R. Dash, "Erosive wear assesment of glass reinforced polyester-flyash composites using taguchi method," *International Polymer Processing*, vol. 23, no. 2, pp. 192–199, 2008.

Hindawi Publishing Corporation
International Journal of Polymer Science
Volume 2011, Article ID 963549, 7 pages
doi:10.1155/2011/963549

Research Article

Manufacturing and Structural Feasibility of Natural Fiber Reinforced Polymeric Structural Insulated Panels for Panelized Construction

Nasim Uddin and Rahul R. Kalyankar

Department of Civil, Construction, and Environmental Engineering, University of Alabama at Birmingham, AL 35205, USA

Correspondence should be addressed to Nasim Uddin, nuddin@uab.edu

Received 14 April 2011; Accepted 28 April 2011

Academic Editor: Susheel Kalia

Natural fibers are emerging in the fields of automobile and aerospace industries to replace the parts such as body panels, seats, and other parts subjected to higher bending strength. In the construction industries, they have the potential to replace the wood and oriented strand boards (OSB) laminates in the structural insulated panels (SIPs). They possess numerous advantages over traditional OSB SIPs such as being environmental friendly, recyclable, energy efficient, inherently flood resistant, and having higher strength and wind resistance. This paper mainly focuses on the manufacturing feasibility and structural characterization of natural fiber reinforced structural insulated panels (NSIPs) using natural fiber reinforced polymeric (NFRP) laminates as skin. To account for the use of natural fibers, the pretreatments are required on natural fibers prior to use in NFRP laminates, and, to address this issue properly, the natural fibers were given bleaching pretreatments. To this end, flexure test and low-velocity impact (LVI) tests were carried out on NSIPs in order to evaluate the response of NSIPs under sudden impact loading and uniform bending conditions typical of residential construction. The paper also includes a comparison of mechanical properties of NSIPs with OSB SIPs and G/PP SIPs. The results showed significant increase in the mechanical properties of resulting NSIP panels mainly a 53% increase in load-carrying capacity compared to OSB SIPs. The bending modulus of NSIPs is 190% higher than OSB SIPs and 70% weight reduction compared to OSB SIPs.

1. Introduction

The structural insulated panels (SIPs) have come forward as an excellent alternative to conventional brick and concrete construction. They are an excellent material for wall, partitions, flooring, and slabs. They possess numerous advantages over traditional wooden and concrete construction [1]. The main component of SIPs consists of two laminates or skin plates and a core as shown in Figure 1.

The laminates are used to carry tensile and compressive loads in the SIPs and core is used to carry the shear load [2]. The laminates in SIPs can be typically made up of oriented strand boards (OSB) that are adhered to the expanded polystyrene (EPS) foam core material to form SIPs. OSB SIPs are commonly used for the structural application due to their ease of manufacturing and ease of availability. OSB SIPs are energy efficient, cost efficient, and require less construction and maintenance time. Significant weight reduction is possible with OSB SIP construction [2]. They provide several design choices, manufacturing alternatives, and also provide excellent aesthetic to the building structures [2]. They provide excellent bending properties and shear resistance along with excellent resistance to wind and seismic forces [3]. These mechanical properties play a key role for the structural applications such as wall panels, building panels, flooring, and slabs [4].

Although OSB SIPs have numerous advantages, they require wood for manufacturing the laminates in SIPs which results in large consumption of natural resources and reduces the greatly concerned resources. There are fire safety issues associated with the OSB SIPs [5]. OSB SIPs are of organic nature, so, to avoid the damages due to mold buildup and

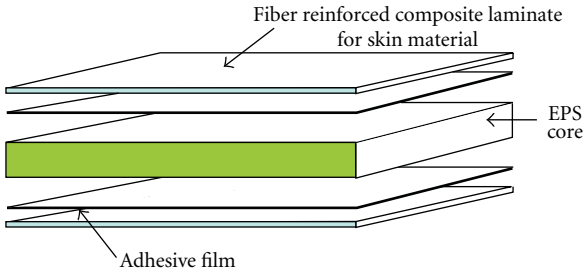

Figure 1: Typical layout of NSIPs.

termite attack, the special chemical treatment is needed to use OSB SIPs in the building construction [6]. The impact resistance of the OSB SIPs is always a major concern for their application in building industries. Windborne missiles can damage the OSB SIPs and may result in damage in the properties and even in the loss of life. One of the notable examples of this type of failure is hurricane Katrina in New Orleans which resulted in great loss of life and property damages [6]. OSB SIPs can have adverse effects of flood due to their poor water-resistant nature [7].

To overcome these issues, several advancements were carried to the OSB in the SIPs with more advanced composite laminates. Several fiber and matrix combinations can be used to manufacture the laminates such as glass-polypropylene, carbon-epoxy, and glass-epoxy. The research was carried out on application of glass/polypropylene (G/PP) which has emerged as an excellent material in the structural application to replace OSB laminates in SIPs [7].

G/PP shows excellent mechanical properties such as superior strength and stiffness which makes them an ideal material for manufacturing the SIPs [7]. Although they have superior mechanical properties, the main disadvantages with this material are their large energy consumption during manufacturing and their adverse effect on the manufacturing tools. They are manufactured in factory and so require significant manufacturing cost [8]. These issues direct the construction industry to a type of material which has higher strength than OSB and can be reproducible so as to reduce the environmental concerns and recyclability issues. These requirements can be well furnished by using natural fiber to replace the OSB and G/PP in the laminates.

Natural fiber reinforced polymeric (NFRP) composites are successfully being used worldwide in automobile parts such as doors, and body panels of cars [9] and in computer industry for manufacturing body panels [10]. Composites reinforced with these fibers are being studied worldwide for their low-cost application against other synthetic fibers such as glass and carbon fibers. There are wide ranges of natural fibers being used worldwide in composite applications such as bast, jute, sisal, cotton, coir, hemp, and kenaf. Natural fibers have numerous advantages which make them suitable to use as the structural material [11]. They require less energy for manufacturing and do not affect adversely the manufacturing tools. They are lightweight, cost efficient, recyclable, biodegradable, and possess a high specific modulus. In the current work the jute/polypropylene laminates along with EPS foam core were selected for the manufacturing of NSIPs due to their excellent mechanical properties [12].

Jute fibers have high specific strength and stiffness, making them suitable as reinforcement in polymeric matrices. The advantages of agro-based jute fibers were their cost effectiveness, ease of availability, and nonabrasive nature. They allow high filling level and reduce the cost of the composite material. The cellular structure of jute fiber provides very good heat and noise insulation [13]. On the other hand the polypropylene (PP) possesses excellent mechanical properties such as tensile strength, fire resistance, and low price. PP is recyclable and so reduces the problems of waste disposal [14].

The primary goal of this work is to study the structural behavior of natural fiber reinforced structural insulated panels (NSIPs) for the structural application and their advantages over traditional OSB SIPs and advanced glass/polypropylene (G/PP) SIPs. To this end, flexural test was carried out on NSIPs to know the mechanical properties such as bending modulus, bending strength, shear strength, shear modulus, and the failure criteria. The flexural test was carried on NSIPs and comparison was made with OSB SIPs and G/PP SIPs as discussed in Section 4. The vulnerability of composite material against out-of-plane impact forces is always a major design concern for the laminated structural composites. To overcome the issue of low-velocity impact and to check the failure criteria, the LVI test along with flexural test was carried out on as described in Section 5. The LVI test results on NSIPs were compared with traditional OSB SIPs and G/PP SIPs in order to validate the use of NSIPs in building construction.

2. Pretreatments Given to Jute Fibers

The mechanical properties of jute fibers, such as density, tensile strength, and modulus, depend on their internal structure and chemical composition [15]. Jute fibers possess a lower tensile strength than glass fibers, and on the other hand a higher specific Young's modulus. The main disadvantage of jute in composite manufacturing is its hydrophilic nature, which affects the bonding with the PP materials. Therefore the mechanical properties such as strength and stiffness are highly affected. This limits the use of the polymer matrix to the low melting temperature plastics due to their low processing temperature. For the improvement of composite properties, several pretreatments such as mercerization, bleaching, and UV radiation may be given to the fibers prior to use them with PP.

The jute fibers consist of 50–60% cellulose, 20–25% hemicelluloses, and 12–15% lignin in their chemical composition [16]. These fibers consist of a long chain of cellulosic molecules and lignin whereas the hemicellulose acts as cementing agent in giving strength and stability to the fibers. Lignin is the main ingredient of jute fibers which absorb moisture when exposed to the air. The fiber constitutes pendant hydroxyl and various polar groups which leads the fibers to the serious problem of moisture absorption. This moisture absorption ultimately leads toward poor interfacial bonding with resin. These fibers thus become unsuitable to use in

manufacturing NFRP laminates. To overcome this issues, in common practice, several treatments are given to the fibers prior to use them in NFRP composite manufacturing along with PP. These treatments includes bleaching, mercerization, and UV radiation treatment. But for the sake of brevity of this paper and based on ease of availability only bleaching treatment is given to the fibers for this study.

2.1. Bleaching. Bleaching is the most common method in which jute fibers are treated with oxidizing agents, such as sodium hypochlorite. A reaction takes place on the jute fibers in which the coloring agents get oxidized. Lignin is cementitious material which contributes mainly in the tensile strength of the fibers. The oxidizing agent mainly modifies the lignin from the fibers. Removal of lignin from the fibers provides jute fibers permanent white color, but simultaneously affects the tensile strength and young's modulus of fibers. To maintain the tensile strength of fiber the proportion of lignin should be retained as much as possible. The fibers are subjected to bleaching treatment using sodium hypochlorite (NaOCl). The raw jute fibers are soaked in 10% and 20% NaOCl for 4 hrs and washed with deionized water for 20 minutes to remove any chemicals present in it. The jute fibers are then allowed to air dry at room temperature [17]. NaOCl is the hypochlorous acid in which hypochlorite ions act as bleaching agent. Bleaching of jute fiber with NaOCl improves its brightness [17]. This deterioration of brightness of jute treated with alkali solution attributes to the removal of lignin from the structure of jute fibers. Bleaching of jute fibers, thus, results in reduction of tensile strength by 15%–20% due to the removal of lignin. The alkali treatment carried on jute fibers shows an increase in the elongation properties besides decreasing the tensile strength of the fibers [17]. In the bleaching treatment, the capillaries present in the fiber contract. The angle of contact increases due to the bleaching treatment. Young's modulus of jute fibers decreases after bleaching due to the removal of lignin [18]. The reduction of lignin from jute fibers improves their hydrophobicity, making them suitable for bonding with PP. Jute fibers treated with 10% NaOCl show greater moisture absorption than the jute fibers treated with a 20% NaOCl solution [9]. From the study, it is seen that the increase in NaOCl content also improves the resistance to humidity of the natural fibers [18]. The bleaching process affects stress strain curve and reduces the young's modulus of the fibers. It has been observed that there was a 220% increase in tensile strength of jute fibers treated with 10% NaOCl and 250% increase in tensile strength of jute fibers treated with 20% NaOCl to the raw jute fibers [18].

As the bleaching treatment demonstrated improved structural properties of the resulting laminate, the NFRP for the fabrication of NSIP panels for this study was manufactured using the bleached jute fibers.

3. Manufacturing of NFRP Laminates

Laminates can be manufactured using several methods such as extrusion blown molding, programmable powder perform process (P4), injection molding, film stacking, and hot melt impregnation method. In general, the laminate manufacturing process mainly governed by profit and loss ratio of particular production. All the processes vary according to the equipment cost and operating cost. The most suitable method for composite manufacturing is film stacking method [14]. This is a compression molding method in which fibers and matrices are subjected to predefined temperature and pressure. This method is cheaper than any other method used for manufacturing the laminates due to its low initial investment [14]. The fibers of desired size and desired directional orientation can be used for manufacturing the laminates. In this method the alternate layers of fibers and matrices are placed in position. This whole assembly is treated under predefined temperature and pressure up to the melting point of the matrix for certain time period and then allowed to cool at room temperature. Due to the melting of matrix it penetrates through the fibers. This penetration results in wetting of fibers and thus forming strong bond between fiber and matrix. After cooling the matrix the whole assembly turns into stiff and stable compound called as laminate.

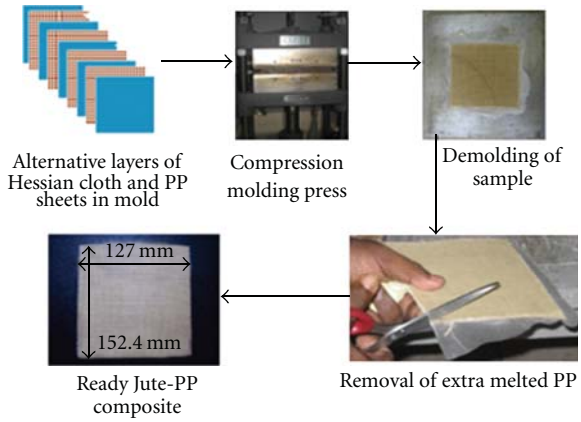

Figure 2: Detailed schematic of film stacking method for NFRP laminates.

In order to manufacture the NFRP laminates, bleached jute fibers were used along with polypropylene (PP). The alternate layers of fibers and PP films were used for manufacturing the laminates. Figure 2 shows the step by step illustration for manufacturing NFRP laminates.

NFRP laminates were manufactured at processing temperature 180°C and processing time 20 minutes at the applied pressure of 10 Tons [14].

4. Flexure Test of NSIP Samples

The main goal of flexure test was to check the suitability of NSIPs in flooring, and slab application to provide better alternative to the traditional OSB SIPs. Flexure test was carried on NSIPs to check the behavior of the specimen under different loading conditions and to check the deflection and failure types of the specimens. The prefabricated NFRP laminates with of 6.25 mm thickness were taken for manufacturing the NSIPs along with expanded polystyrene foam (EPS) with 25.4 mm thickness and 1.6×10^{-5} g/mm^3

(a) Crushing of NSIPs foam during flexure test

(b) Delamination of NSIPs facesheets during flexure test

(c) Delamination of NSIPs during flexure test

Figure 3: Failure modes of NSIPs during flexure test.

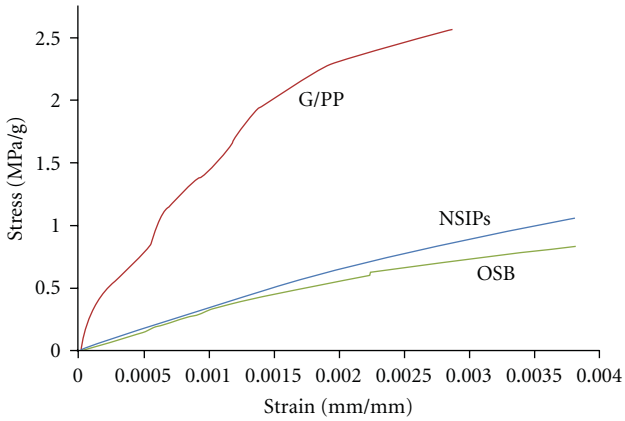

Figure 4: Comparison of normalized stress strain curves for different SIPs.

density for the core using hot melt spray adhesive to bond the NFRP with EPS [19].

Three-point bending setup was used for carrying out the flexure test on NSIPs and the stress-strain and load-deflection curves were obtained for these NSIPs. The load was applied at the center of specimen through rounded edge steel bars at constant rate of 2 mm/min as per ASTM C 393 [19]. The maximum load and deflection were recorded for all specimens. The load deflection curve was plotted to determine the sandwich stiffness. Four specimens of average dimensions 590 mm × 101 mm × 25.4 mm and average weight of 700 gm were used for the test and average stress strain curve was plotted for all specimens. For measuring the central deflection, dial gauge was placed at the bottom side of center of specimen. The strain gauge was placed at the center of specimen in order to record the strain induced. Figures 3(a)–3(c) shows different failure modes of NSIPs obtained during flexure test.

During the flexure test it was observed that the NSIPs failed due to shear failure of core and delamination of the facesheet and core as shown in Figure 3. From the flexure test on the NSIPs various parameters were obtained using numerical formulae given in ASTM C-393 [19]. Normalization of stress strain curves were carried out by dividing obtained stresses by the final weight of the specimen tested in order to validate the comparison of specimens with respect to weight. Figure 4 provides normalized average stress strain relationships for NSIPs, OSB SIPs, and G/PP SIPs obtained from three-point flexural test.

From Figure 4 it can be observed that the average stress-strain curve for NSIPs is higher than that of traditional OSB SIPs. The NSIPs shows more a consistent curve than OSBs. Failure observed was due to slippage of specimens from the supports due to excessive bending without any crack to the laminates. The shear cracks and delamination of laminates were observed during flexure test on NSIPs. Table 1 summarizes the results of flexure test for NSIPs, OSB SIPs, and G/PP SIPs.

From the Table 1 it has been observed that the bending modulus of NSIPs was more than traditional OSB SIPs by 190%. Also the bending stress at the extreme fibers of facesheet was 189% more than OSB SIPs and 80% of G/PP SIPs. The overall deflection obtained for NSIPs was 64% less than G/PP SIPs. On the other hand the average weight of NSIPs was 30% less than the traditional OSB which results in great reduction of weight of components.

5. Low-Velocity Impact (LVI) Test

The objective of low-velocity impact (LVI) test was to represent the resistance offered by the NSIPs under LVI conditions such as impact of hammer, tool drops, and nails as well as thrown object from outside that damage the skin material of wall. LVI test were carried on NSIPs to investigate the dynamic deformation, failure mode, and the response of sandwich composites against sudden weight drops. The LVI test provides knowledge regarding damage-resistant properties of NSIPs that are very useful for design and material selection [8]. The usual tendency of composite structures against small impact results in delamination of stronger and stiffer facesheet from the comparatively less strong core material. The common mode of failure in LVI

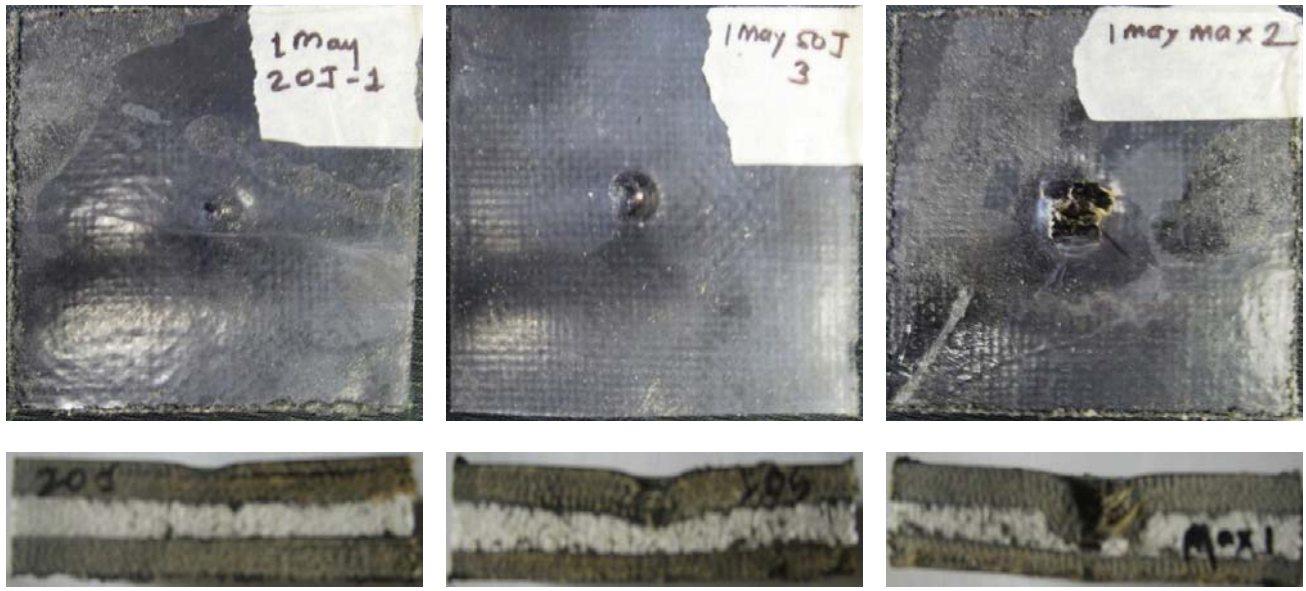

(a) LVI test NSIPs 20 J (b) LVI test NSIPs at 50 J (c) LVI test NSIPs 65 J

Figure 5: LVI failures of NSIPs at energy of 20 J, 50 J, and 65 J.

Table 1: Parameter obtained from flexural test on NSIPs, G/PP SIPs, and OSB SIPs.

Description	Load at failure (N)	Deflection obtained (mm)	Bending modulus (MPa)	Maximum bending stress (MPa)	Weight of material (gm)
NSIPs	511.52	27.83	1.71E3	5.41	518.4
OSB SIPs	978.56	18.84	0.90E3	2.86	732.8
G/PP SIPs	266.88	43	9.74E3	6.78	379.6

were surface cracking, laminate buckling, and debonding between laminate and core.

To know the LVI response, the impact tests were performed on NSIPs using a drop tower device with a free-falling mass. The damage was imparted through out of plane, concentrated impact perpendicular to the laminate using Instron 8250 drop-weight impact machine with instrumented striker assembly. Impacts of mass were carried out at the center of NSIPs, sufficiently away from the edges to avoid interaction of stresses at the edges and stresses at the impact location during damage formation. Damage resistance of composite depends on several factors such as thickness of plate, stiffness of material, mass, and boundary conditions.

NSIPs with variable laminate thickness were cut into piece of 101.6 mm × 101.6 mm size for the test. These specimens were placed in the fixture with two-plate assembly used to hold the specimens in perpendicular direction to the freely falling mass. The fixture was then tied with screws in order to prevent the specimen movement and provide fixed end conditions. The drop weight impactor was then raised to the desired height and allowed to fall freely on the specimen in order to create required impact force on the specimen. All data such as force at the time of impact and break and velocity of hammer was recorded with data acquisition software. The specimens were subjected to impact energy of 20 J, 50 J, and 65 J. From the LVI test various parameters such as impact energy absorbed by specimens, peak load at the time of failure, total energy, and impact velocity were calculated. Figure 5(a)–5(c) shows failures observed on NSIPs during LVI test.

From Figure 4, various failure modes were observed for the NSIPs. At energy of 20 J, the NSIPs showed indentation to the top laminate without any damage. On the other hand, at 50 J and 65 J, the top laminates were damaged due to impact. A crushed core and slight indentation to the bottom laminates have been observed at 65 J. The LVI test were also carried out on OSB SIPs and G/PP SIPs in order to compare the results obtained in all cases so as to replace the NSIPs with OSB SIPs and G/PP SIPs. Figure 6(a)–6(c) shows load versus time and energy versus time curve at 20 J, 50 J, and 65 J.

From Figure 6(a) it can be observed that G/PP SIPs and OSB SIPs followed the same energy and load paths. The maximum load attained by them was 2.04 KN and 2.09 KN respectively, whereas, in case of NSIPs the maximum load

Table 2: Comparison of Impact response of NSIPs with OSB and G/PP SIPs.

Impact energy (J)		20			50			65	
Velocity (m/s)		2.6			4.0			4.7	
Impact height (m)		0.33			0.82			107	
Specimen	NSIP	G/PP	OSB	NSIP	G/PP	OSB	NSIP	G/PP	OSB
Total energy (J)	16.6	13.8	14.9	44.3	30.4	6.97	68.6	42.7	20.3
Energy at yield (J)	18.5	2.13	0.89	—	0	0	—	0	−13.6
Energy at failure (J)	17.4	14.8	15.5	46.2	34.8	6.90	69.1	48.8	20.0
Maximum load (KN)	3.2	2.04	2.09	4.9	6.57	0.74	5.0	8.23	2.03
Load at yield (KN)	3.1	0.73	1.44	0.02	0	−0.02	0	0	−0.85
Load at failure (KN)	0.6	0.40	0.40	0.9	1.30	0.13	0.9	1.62	0.39
Defl. at max. load mm)	14.0	17.5	10.9	19.7	20.8	12.5	22.7	23.5	61.0
Defl. at yield (mm)	13.4	3.98	1.20	—	0	0	—	0	45.8
Defl. at failure (mm)	11.4	11.0	8.67	19.1	15.0	21.0	28.8	18.4	74.1
Total deflection (mm)	7.5	5.64	5.71	11.8	6.04	22.3	27.5	7.86	75.6

attained by specimen prior to failure was 3.2 KN which is 57% higher than G/PP and 53% higher than OSB SIPs. The energy absorbed by NSIPs was 16.6 J which is 20% higher than G/PP and 11% higher than OSB SIPs. It can be observed from Figure 6(b) that the total energy attained by NSIPs was 44.3 J which is 45% higher than G/PP SIPs. Also at 65 J as shown in Figure 6(c), maximum load attained by the NSIPs was 5 KN which is 246% higher than OSB SIPs. The maximum energy absorbed by NSIPs is 68.6 J which is 60% higher than G/PP SIPs. From the LVI results and the curve plotted the information was obtained, as summarized in Table 2.

From the LVI tests on NSIPs, it can be concluded that the NSIPs showed comparable results in terms of energy absorption with G/PP and OSB SIPs. The LVI test was carried out on NSIPs manufactured using bleached jute fiber, considering their superiority over other type of treated fibers. The LVI test was also carried out on G/PP and OSB SIPs in order to compare the NSIPs with traditional OSB and G/PP SIPs. The following are the conclusions obtained from NSIPs, OSB SIPs, and G/PP SIPs LVI tests.

(1) The total energy absorbed by NSIPs at 20 J was 12% higher than G/PP SIPs and 11% higher than OSB SIPs.

(2) The energy absorbed by NSIPs at 50 J was 45% higher than G/PP and 64% higher than OSB SIPs.

(3) The energy absorbed by NSIPs at 65 J was 60% higher than G/PP.

(4) The maximum load taken by NSIPs was higher in all cases in which it showed an increase of 53% increase in maximum load at 20 J and 146% at 65 J compared to OSB SIPs.

The overall performance of NSIPs in all cases resulted in a significant improvement in the energy absorption as well as mechanical properties of NSIPs compared to traditional OSB SIPs and G/PP SIPs.

6. Summary

Flexural strength tests and low-velocity impact tests were carried out on the reduced scale NSIP panels to determine the behavior of NSIPs in bending and impact conditions. The EPS foam with 25.4 mm thickness was used for the core along with NFRP laminates in the resulting manufacture of the NSIPs. Structural characterization of innovative, reduced scale NSIPs was presented in this paper, and the following conclusions were drawn from this study.

(i) Bending modulus of NSIPs is 190% higher than OSB SIPs. Also the bending stress at the extreme fibers of facesheet is 189% more than OSBs and is 80% of G/PP SIPs.

(ii) There is great savings in the material as the weight of NSIPs is 30% less than the weight of OSB SIPs.

(iii) G/PP SIPs and OSB SIPs followed the same energy and load path in which the maximum load attained by them was 2.04 KN and 2.09 KN.

(iv) The maximum load attained by NSIPs prior to failure was 3.2 KN which is 57% higher than G/PP and 53% higher than OSB SIPs.

(v) In case of 20 J impact energy, The energy absorbed by NSIPs was 16.6 J which is 20% higher than G/PP and 11% higher than OSB SIPs. In case of 50 J impact energy, total energy attained by NSIPs was 44.3 J which is 45% higher than G/PP SIPs. Also in case of 65 J impact energy, the maximum load attained by the NSIPs was 5 KN which is 246% higher than OSB SIPs. The maximum energy absorbed by NSIPs is 68.6 J which is 60% higher than G/PP SIPs.

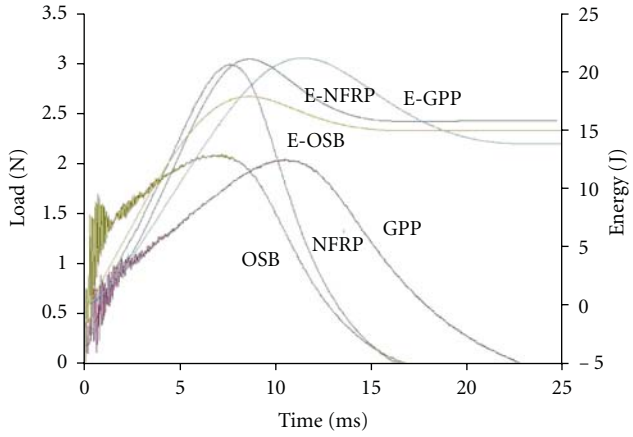

(a) Load versus time and energy versus time curve at 20 J

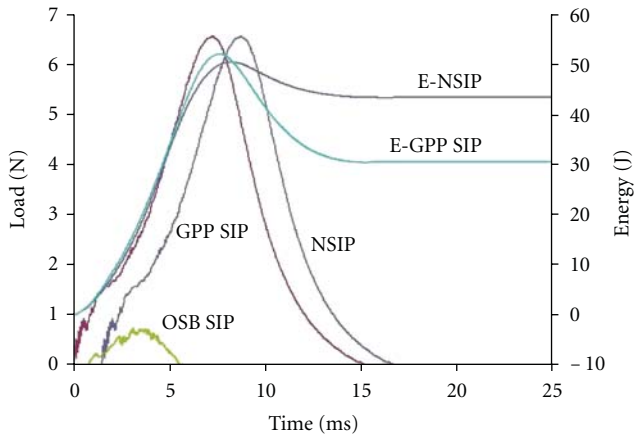

(b) Load versus time and energy versus time curve at 50 J

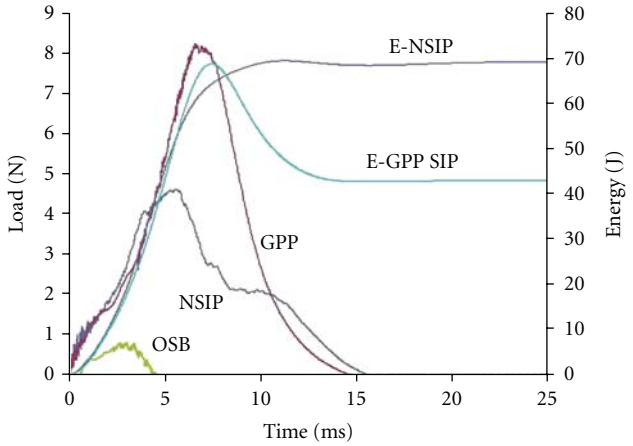

(c) Load versus time and energy versus time curve at 65 J

Figure 6: Load versus time versus energy curve for NSIPs, G/PP, and OSB SIPs at 20 J, 50 J, and 65 J.

Hence it can be concluded that the NSIPs can be used as a better alternative to OSB SIPs and G/PP SIPs in structural applications such as flooring and walls.

Acknowledgment

The authors gratefully acknowledge funding and support provided by National Science Foundation (NSF) for this research project (CMMI-825938).

References

[1] 2011, http://www.ibpanels.com.
[2] 2011, http://www.toolbase.org.
[3] 2011, http://www.sips.org.
[4] The Engineered Wood Association (APA) The engineered wood association product guide.
[5] 2009, http://www.sipsupply.com.
[6] "Performance of physical structures in hurricane Katrina and hurricane Rita (2006): a reconnaissance report," Tech. Rep., National Institute of Standards and Technology, Gaithersburg, Md, USA.
[7] A.S Vaidya, N. Uddin, and U. Vaidya, "Structural characterization of thermoplastic composite structural insulated panels (CSIPs)," *Journal of Materials in Civil Engineering*, 2008.
[8] B. C. Ray, *Thermal Shock on Interfacial Adhesion of Thermally Conditioned Glass Fiber/Epoxy Composites*, Department of Metallurgical and Materials Engineering, NIT Rourkela, India, 2004.
[9] Der Fakultät Maschinenwesen, *Investigation on jute fibers and their composites based on polypropylene and epoxy matrices*, Ph.D. Dissertation, University of Dresden Vietnam, 2006.
[10] B. C. Suddel and W. J. Evans, "The increasing use and application of natural fiber composite materials within the automotive industry," in *Proceedings of the 7th International Conference on Wood Fiber-Plastic Composites*, pp. 7–14, Madison, Wis, USA, 2003.
[11] A. R. Sanadi, D. F. Caulfield, R. E. Jacobson, and R. M. Rowell, "Renewable agricultural fibers as reinforcing fillers in plastics: mechanical properties of kenaf fiber-polypropylene composites," *Industrial and Engineering Chemistry Research*, vol. 34, no. 5, pp. 1889–1896, 1995.
[12] 2009, http://www.epspackaging.org/.
[13] Daimler-Benz, "The corporate units in the Daimler Benz group," Tech. Rep. 2, 1995, http://www.daimler-benz.com/mb/mb_e.html.
[14] P. K. Pal, "Jute reinforced plastics: a low cost composite material," *Plastics and Rubber Processing and Applications*, vol. 4, no. 3, pp. 215–219, 1984.
[15] 2011, http://www.ibpanels.com.
[16] 2011, http://www.mcmaster.com.
[17] A. K. Bledzki and S. Reihmane, "Thermoplastics reinforced with wood fillers: a literature review," *Journal of Polymer Plastic Technology and Engineering*, vol. 37, no. 4, pp. 451–468, 1998.
[18] M. A. Mannan Khan, *Characterization of Raw, Delignified and Bleached Jute Fibres by Study of Absorption of Moisture and Some Mechanical Properties*, Physics Department, Curzon Hall, Dhaka University, Dhaka, Bangladesh, 1996.
[19] ASTM D 790 M-93; Standard Test Method for flexural properties of Unreinforced and Reinforced Plastics and Electrical Insulating Materials.

Hindawi Publishing Corporation
International Journal of Polymer Science
Volume 2011, Article ID 569871, 14 pages
doi:10.1155/2011/569871

Research Article

Natural Fibre-Reinforced Biofoams

Anne Bergeret and Jean Charles Benezet

Centre des Matériaux de Grande Diffusion, Ecole des Mines d'Alès, 6 avenue de Clavières, 30319 Alès, France

Correspondence should be addressed to Anne Bergeret, anne.bergeret@mines-ales.fr

Received 8 April 2011; Accepted 24 June 2011

Academic Editor: James Njuguna

Starches and polylactic acids (PLAs) represent the main biobased and biodegradable polymers with potential industrial availability in the next decades for "bio" foams applications. This paper investigates the improvement of their morphology and properties through processing and materials parameters. Starch foams were obtained by melt extrusion in which water is used as blowing agent. The incorporation of natural fibres (hemp, cellulose, cotton linter, sugarcane, coconut) in the starch foam induced a density reduction up to 33%, a decrease in water absorption, and an increase in mechanical properties according to the fibre content and nature. PLA foams were obtained through single-screw extrusion using of a chemical blowing agent that decomposed at the PLA melting temperature. A void content of 48% for PLA and 25% for cellulose fibre-reinforced PLA foams and an improvement in mechanical properties were achieved. The influence of a fibre surface treatment was investigated for both foams.

1. Introduction

Global warming, growing awareness in environmental and waste management issues, dwindling fossil resources, and rising oil prices are some of the reasons why lightweight "bio" products such as "bio" foams are increasingly promoted regarding sustainable development in material applications.

In this context, "bio" foams based on starches and biopolyesters such as polylactic acids (PLAs) have a great industrial potential, since starch foams can be considered as good candidates to substitute expanded polystyrene used for food trays in packaging industries. Moreover, PLA foams are promising alternatives to polyolefin-based foams for many automotive parts. They could be also used as efficient carriers for active pharmaceutical ingredients allowing drug release to be controlled and bioavailability to be enhanced.

Starches and PLA can be associated to biodegradable fillers leading to commonly named "bio" composites.

The poor mechanical properties of starchy materials compared to conventional oil-based polymers can be improved by adding natural fibres. Starches have been yet associated to numerous fibres among which jute fibres [1], ramie fibres [2], flax fibres [1, 2], tunicin, whiskers [3], bleached leafwood fibres [4], wood pulp [5] or microfibrils from potato pulp [6]. Most of these studies showed a high compatibility between starch and natural fibres leading to higher stiffness. A reduction in water absorption was also obtained thanks to the higher hydrophobicity of natural fibres which was linked to the high crystallinity of cellulose. The improvement of the properties of natural fibre reinforced starch biocomposites foams was ascribed to the formation of a tight three-dimensional network between carbohydrates through hydrogen bonds.

PLA was also associated to kenaf fibres [7], jute fibres [8], flax fibres [9], rice, and wheat husks [10]. Much literature was focused on fibre surface treatments able to improve fibre/PLA interactions, among them physical (corona [11], cold plasma [12], mercerization [13]...) and chemical treatments (silane agents [14], isocyanates [15]...).

This paper exposes investigations carried out on natural fibre reinforced starch and PLA foams. The relationships existing between the material formulations, the processing conditions, the cellular morphology, and the final biocomposites foams properties, especially the mechanical properties, were highlighted in this paper.

2. General Aspects on Polymer Foams

Polymer foams are made of a solid and a gas phase mixed together upon processing. Foams with air bubbles or cells

being either closed-cells or open-cells are obtained, open-cell foams being usually more flexible than closed-cell foams. The gas used as blowing agent is either a chemical or a physical blowing component. Chemical blowing agents react in the extruder to give off the foaming gas, mainly through thermally induced decomposition reactions. Physical blowing agents are gases that do not chemically react during the foaming process and are therefore inert towards the polymer matrix.

In this study, starch foams are obtained by melt extrusion in which water is used as blowing agent as it turns into steam under temperature and pressure conditions of the extrusion. To enhance the number of cells and to homogenise the cellular microstructure, additives such as nucleating agents, that is, talc, are used. PLA foams are obtained by melt extrusion using a chemical blowing agent (called CBA) which decomposes at the PLA melting temperature.

The foaming capacity of the polymer materials was assessed by the measurement of the void content of the final product after extrusion. The experimental results allow defining an optimum set of extrusion conditions (screw profile and speed, cooling temperature, extrusion temperatures along the screw…) and material formulations (CBA content, fibre content and nature…) to improve void content and foams properties. The cell morphology (number, dimensions, shape…) and the mechanical properties (tensile, bending…) are analyzed.

3. Natural Fibre-Reinforced Starch Foams

3.1. Materials and Processing Equipments. Potato starch from Roquette Co. (France) (10–25 wt% amylose, 75–80 wt% amylopectin, 0.05 wt% proteins based on dry weight) was used for this study. Starch was mixed with different natural fibres, such as cotton linter fibres, hemp fibres, cellulose fibres, sugarcane fibres, and coconut fibres. Table 1 summarizes natural fibres main characteristics. Sugarcane and coconut fibres were submitted to specific a surface treatment described in Section 3.4.

A single-screw extruder (FairEx, 720 mm length, 30 mm diameter, 1.5 × 40 mm flat die, 2.31 compression rate) with 6 heating zones and a corotating twin-screw extruder (Clextral BC21, 900 mm length, 25 mm diameter, 1.5 × 40 mm^2 flat die) with 12 heating zones extruder were used for foams extrusion. Water was added with a peristaltic pump and sheet-shaped samples were obtained by calendaring of the extruded foams. Three fibre contents were compared: 7, 10, and 15 wt%. Regular expansion was achieved by adding 2 wt% of talc (Rio Tinto Minerals, France) and 2 wt% of CBA (Hydrocerol ESC5313 supplied by Clariant Masterbatches Co, France).

3.2. Determination of an Optimum Set of Extrusion Conditions. Most of the formulations were produced through twin-screw extrusion, except one which was produced through single-screw extrusion which is the industrial processing commonly used for food packaging.

3.2.1. Twin Screw Extrusion. The following processing parameters were optimized for twin-screw extrusion: screw profile, screw speed, temperature profile, mass flow rate, and water content. Restrictive elements (such as reverse pitch screws) in corotating twin-screw extrusion increase the local pressure along the barrel which favour the polymer transport as well as the expansion at the extruder die. Using screw profile 1 (see Table 2) at 200 rpm with a temperature profile from 30 to 120°C from input to die, pressure was increasing too quickly and the torque exceeded its maximum working point (110 Nm) so that the material could not be convoyed through the extruder. As a consequence, the best set of extrusion conditions was obtained without restrictive elements and a full conveying system (profile 2) (Table 3). Screw rotation speed must be high enough to reduce the residence time in the extruder but at the same time, this one must not increase shear rate within the extruder. The influence of screw speed was studied in the range of 190–430 rpm, and the optimum was found at 300 rpm. In this case, several die temperatures (from 100 to 180°C) were compared for a given screw speed of 200 rpm. It was observed that no expansion occurred for a die temperature below 100°C and a maximum expansion for 160°C. Table 4 describes the optimum temperature profile along the 12 heating zones of the extruder.

A low polymer flow (2 kg/h) should be used to avoid starch degradation. Water acts as a foaming agent as well as a plasticizer. The water content must be carefully adjusted. This optimization is difficult because starch inherently contains some water that can vary according to the storage conditions (residence time, relative humidity). It is commonly known [16] that water content ranged between 15 and 30%. Based on the twin-screw and temperature profiles defined on Tables 3 and 4, respectively, an optimized value of 17% of water gave the best expansion. In these conditions, all formulations were processed with specific mechanical energy (SME) values between 60 and 90 W·h/kg.

3.2.2. Single Screw Extrusion. For single-screw extrusion, only two processing parameters need to be studied: screw rotation speed and barrel temperature profile. Screw rotation speeds ranging from 10 to 120 rpm were compared, with the best expansion being obtained at 50 rpm corresponding to a torque between 30 and 40 Nm.

The barrel temperature profile was similar to the previous one used for the twin-screw extrusion (heating zone 1: 30°C; die: 160°C). A heterogeneous material was obtained with nonmelted granules within low expanded foam. Increasing the temperature of the feeding zone (Table 5) leads to a foam similar to the one produced by twin-screw extrusion.

3.3. Influence of the Fibre Nature and Content on the Starch Foam Characteristics

3.3.1. Density, Expansion Index, and Cell Morphology. It has to be noticed that the addition of fibres contributes to decrease the biocomposite density except for hemp fibres (Table 6). The lowest foam density was obtained with the

Table 1: Main characteristics of the different natural fibres used in this study.

Fibre type	Length (mm)	Cellulose content (%)	Supplier
Cotton linter	2.1	80–85	Maeda Co (Brazil)
Hemp	3.2	70–72	Chanvrière de l'Aube (France)
Cellulose	0.13	98-99	Rettenma & Söhne (Germany)
Sugarcane	12.5	80–85	Edro Ecosystems Co (Brazil)
Coconut	23.5	33	Mercedes Benz (Brazil)

Table 2: Twin screw profiles with two restrictive elements (noted "Rev") (profile 1).

Screw elements	Dir	Dir	Dir	Rev	Dir	Dir	Rev
Screw thread (mm)	33	25	16.6	−33	33	16.6	−33
Screw length (mm)	325	150	50	25	100	200	50

Table 3: Best set of twin screw extrusion conditions with a full conveying system (profile 2).

Screw elements	Dir	Dir	Dir	Dir	Dir
Screw thread (mm)	33	25	33	25	16.6
Screw length (mm)	250	175	50	175	250

Table 4: Temperature profile of the twin screw extruder.

	barrel										die	
Heating zone	1	2	3	4	5	6	7	8	9	10	11	12
Temperature (°C)	30	30	50	60	70	80	90	90	100	120	120	160

Table 5: Temperature profile of the single screw extruder.

	barrel					die
Heating zone	1	2	3	4	5	6
Temperature (°C)	70	90	100	120	120	160

biocomposite foam reinforced by cellulose fibres. Moreover, it has been observed that the presence of fibres reduces the expansion ratio of starch foam at the exit of the die except for the biocomposite foam reinforced by cotton fibres. These contradictory effects should result from two competitive mechanisms: on one side, fibres tend to increase the viscosity of the moulded starch and, on the other side, fibres act as nucleating agents providing surfaces for cell growth. As a consequence, reinforced starch foams exhibit smaller size cells with thinner walls as shown on Table 7 and Figure 1. Results showed an open-cell structure for all formulations (about 80–82%) with low variations between them. This parameter was mainly influenced by processing conditions and especially cooling speed at the extruder die.

3.3.2. Water Absorption. Water absorption contents of the different fibres (Table 8) and of the starch-based biocomposites foams (Table 9) were measured after samples storage at various relative humidity ratios (33, 56, and 75 RH%) for 200 h. Differences of water absorption are observed between the fibres. Cotton linter fibres are less hydrophilic than hemp and cellulose fibres. These variations do not influence significantly the hydrophilicity of biocomposites foams. Indeed the presence of fibres leads to a slight decrease in starch hydrophilicity, about 1%, which does not depend on the fibre nature [17]. This decrease could be related to the interactions between the fibres and the matrix (formation of hydrogen bonds). It can be noticed that values for starch are closed to those obtained by Soykeabkaew et al. [1].

3.3.3. Mechanical Properties. In Figure 2, bending properties (flexural modulus, maximum stress, maximum strain, modulus/density ratio, so-called specific modulus) are shown as a function of fibre nature and relative humidity (after 7 days conditioning at 33, 56, and 75 RH%) for starch foam and 10 wt% reinforced biocomposites foams.

A reinforcing effect of the fibres was observed according to the fibre nature. The best reinforcing effect was obtained with hemp fibres, followed by cellulose fibres and finally cotton linter fibres. This can be explained by the differences in fibre stiffness and length. Similar results were discussed in the literature. Several authors studied the mechanical properties of starch foams reinforced by flax, jute [1], and aspen [18, 19]. They assumed that the reinforcement effect of fibres is related to a good adhesion between fibres and matrix. In fact, starch and fibres have similar chemical structures which should favour the formation of hydrogen bonds between them. In view of the large standard deviations, it can be assumed that there are no variations of elongations at break according to the fibre nature. The values of the specific

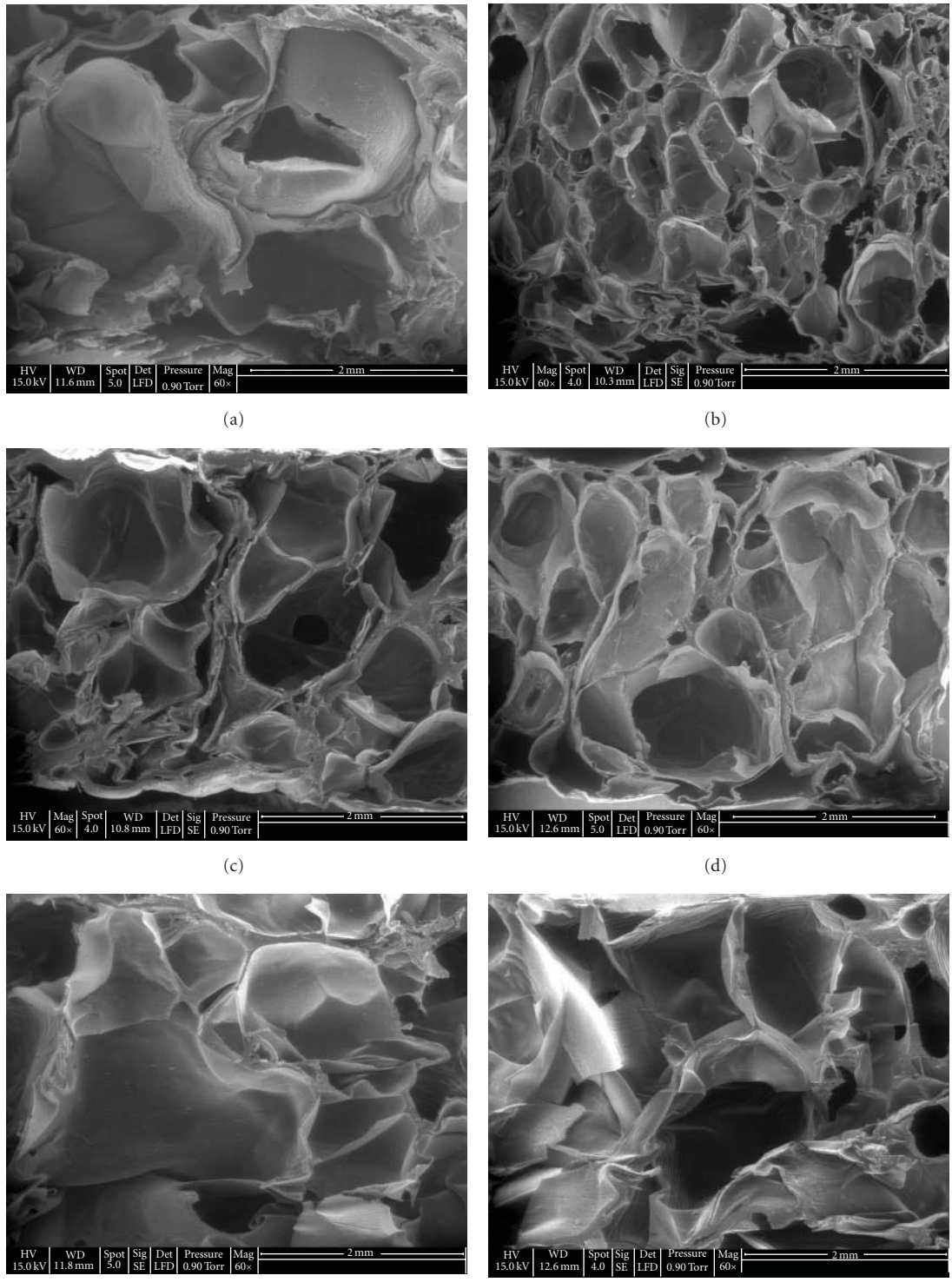

Figure 1: Cell morphology (a) starch foam; biocomposites foams reinforced by 10 wt% of (b) cotton linter (c) hemp and (d) cellulose fibres and 7 wt% of (e) sugarcane (f) coconut fibres.

modulus are the highest in the case of formulations with lower densities (cotton linter and cellulose fibres). According to the literature [20], this can be explained by the fact that there is no fibre orientation and that fibres are located on the surface or in the cell-wall of the starch foam Moreover, the reinforcing effect is decreased when relative humidity increased (from 33 to 75% RH). Lawton et al. [18] observed the same phenomenon in the case of starch foams reinforced

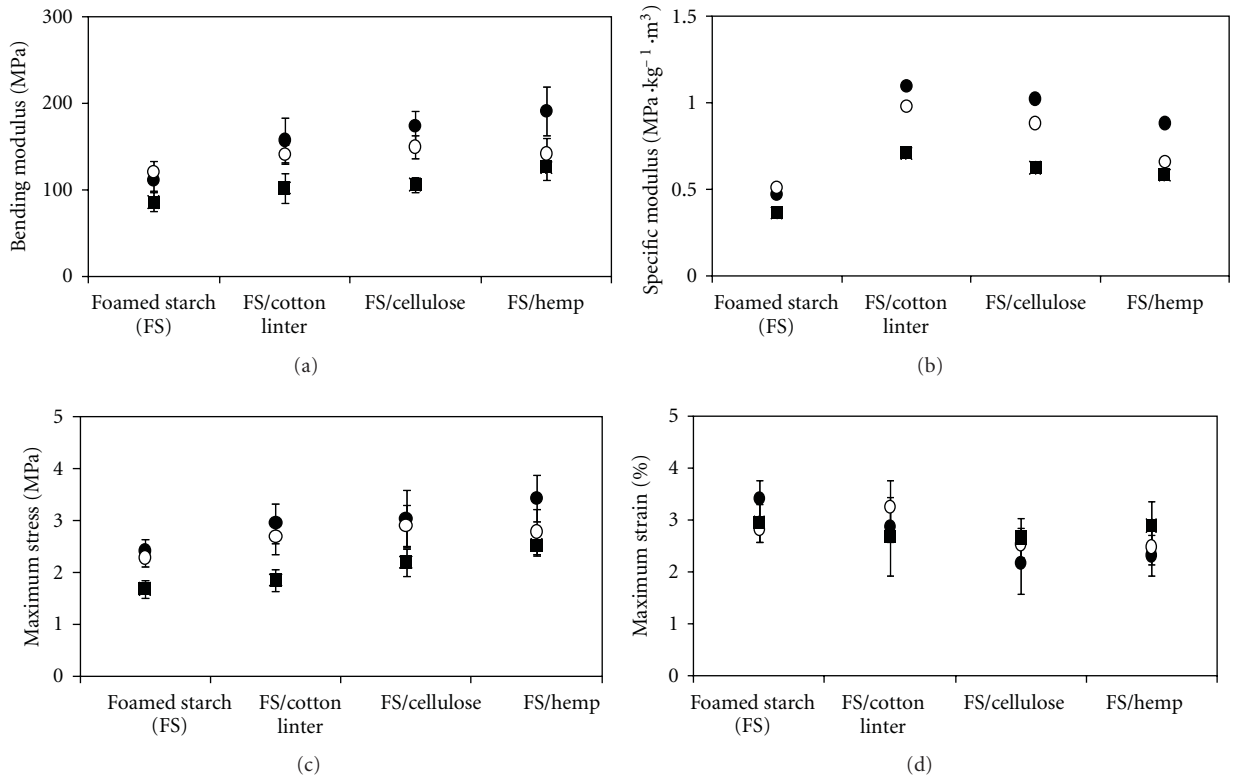

Figure 2: Mechanical properties of starch foam and 10 wt% reinforced biocomposites foams as a function of the fibre nature and the relative humidity: ● 33 RH%, ○ 56 RH%, ■ 75 RH%, (a) bending modulus, (b) bending modulus/density ratio, (c) maximum stress, (d) maximum strain.

Table 6: Densities and expansion ratios of starch-based biocomposites foams compared to starch foam.

Material	Content (wt%)	Density (g/cm^3)	Expansion ratio
Starch foam (SF)	—	0.236 ± 0.016	2.919 ± 0.213
SF/cotton linter	10	0.175 ± 0.008	3.360 ± 0.169
SF/hemp	10	0.242 ± 0.010	2.844 ± 0.171
	7	0.161 ± 0.004	2.847 ± 0.075
SF/cellulose	10	0.170 ± 0.007	2.787 ± 0.123
	15	0.158 ± 0.004	2.366 ± 0.109

with aspen fibres. It was explained by a higher plasticization of starch when relative humidity is high. The material becomes softer, and the mechanical properties decrease. Nevertheless, Soykeabkaew et al. [1] did not observe the same trends for composites reinforced by 10 wt% of jute and flax fibres. They measured an improvement of mechanical properties with increasing RH during storage from 11 to 43% and then degradation with increasing RH from 43 to 75%.

In Figure 3, bending properties are shown as a function of the cellulose fibre content and of the relative humidity (after 7 days conditioning at 33, 56, and 75 RH%). Maximum stress increases for starch foams reinforced by 7 and 10 wt% of cellulose fibres, then remained constant over 10 wt%. Results in the literature showed the same trend depending on the fibre content. Lawton et al. [18] observed an improvement in mechanical properties with fibre contents ranging from 2.5 to 15 wt%. Similarly, they noticed a decrease in mechanical properties with increasing moisture content during storage. Regarding the evolution of the specific modulus values, an increase was observed for increasing fibre content.

3.4. Influence of the Fibre Surface Treatment. To reduce the water hydrophilicity of fibres and increase the interfacial affinity between fibres and starch foam, or change the hydrophilic/hydrophobic behavior of surfaces, some physical and/or chemical treatments are largely used. Low temperature plasma techniques were studied for polymeric surface modifications especially in presence of oxygen. Several reactors geometries have been studied to achieve the more efficient surface modification on materials.

In this part of the study, a low temperature plasma treatment was applied on sugarcane and coconut fibres

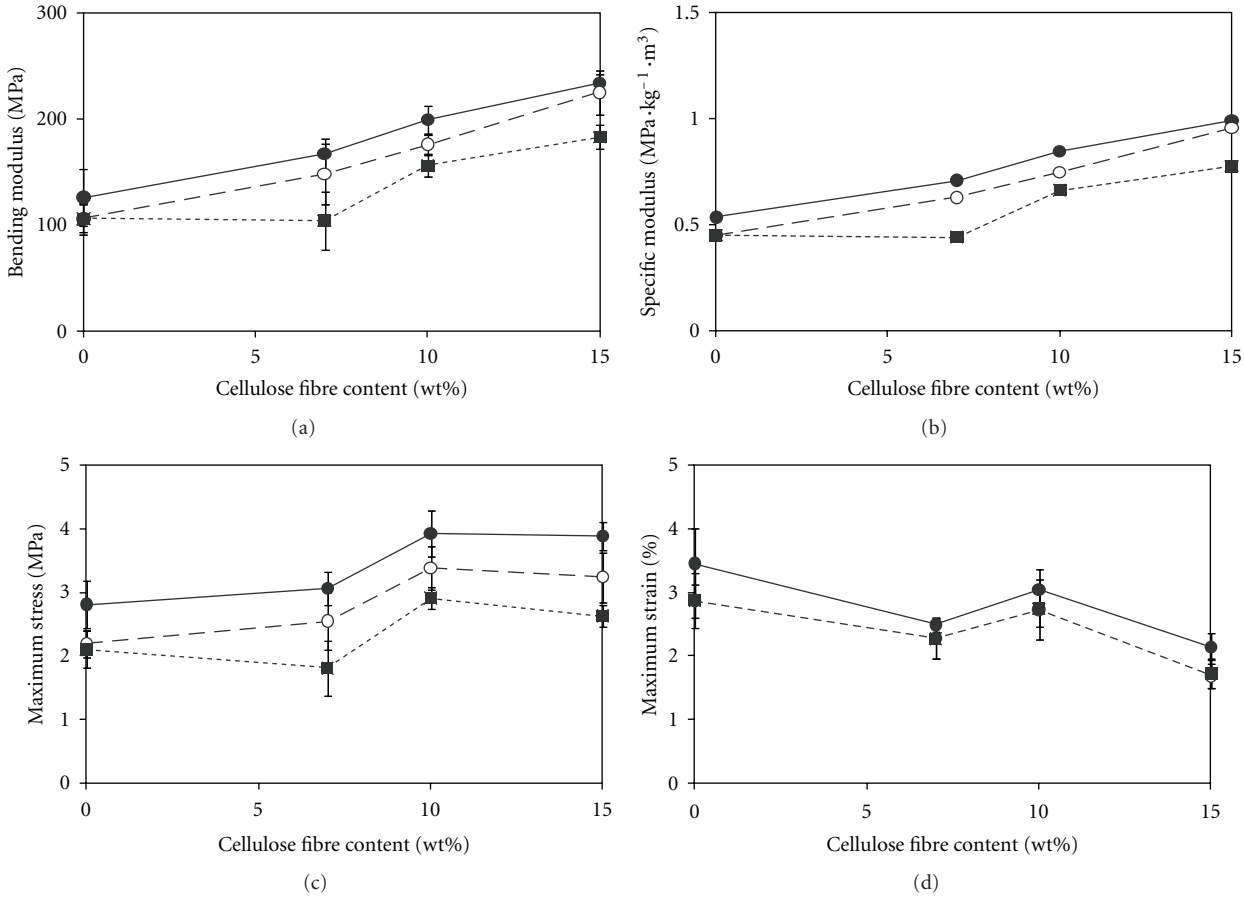

Figure 3: Mechanical properties of starch and biocomposites foams as a function of the cellulose fibre weight content and the relative humidity: ● 33 RH%, ○ 56 RH%, ■ 75 RH%, (a) bending modulus, (b) bending modulus/density ratio, (c) maximum stress; (d) maximum strain.

Table 7: Size (mean diameter in number d_n, mean diameter in weight d_w, wall thickness of cells e, polydispersity index PDI, and sphericity I_s) and open cell ratio C_o of biocomposites foams reinforced by 10 wt% of fibres compared to starch foam.

Material	d_n (μm)	d_w (μm)	PDI	e (μm)	I_s	C_o (%)
Starch foam (SF)	875.0	1046.6	0.84	21.52	0.72	80.5 ± 0.71
SF/cotton linter	648.9	734.1	0.88	15.12	0.70	81.0 ± 0.00
SF/hemp	784.1	966.9	0.81	17.39	0.70	82.5 ± 0.71
SF/cellulose	577.6	730.7	0.79	12.54	0.70	82.0 ± 0.00

(Table 1). A tubular plasma reactor was used (gas: oxygen, power: 57 W, mass treated: 15–20 g/30 min, pressure: 0.17–0.25 Pa, frequency: 13.56 MHz).

The single-screw extruder previously described was used for sample preparation. Water was added with a peristaltic pump and sheet-shaped samples were made by calendaring of the extruded foams. A fibre content of 7 wt% was tested. Regular expansion was achieved by adding 2 wt% of talc, 2 wt% of CBA, and 17 wt% of water.

Mechanical properties of biocomposites foams reinforced either by coconut or sugarcane fibres are presented on Table 10 after 6 days conditioning at 54 RH%. Foams reinforced by coconut fibres present higher mechanical properties than foams reinforced by sugarcane fibres. This result could be explained by the difference in the initial length of these two fibres (23.5 mm against 12.5 mm). A decrease in flexural modulus is observed with plasma surface treatment whatever the fibre type but it must be noticed that standard deviations are significant. The other mechanical properties were not impacted by the treatment.

3.5. Conclusion. The physicochemical and mechanical properties were studied depending on the composition of the biocomposites foams. A decrease of the density was observed with the addition of fibres, while the expansion ratio varied depending to the fibre nature. The water absorption of the matrix was reduced by the incorporation of fibres, possibly due to the lowest hydrophilicity of fibres as compared

Table 8: Water absorption contents of natural fibres at various relative humidity ratios.

Material	RH (%)	Water absorption (%)
Cotton linter	33	3.78
	56	6.12
	75	9.02
Hemp	33	4.98
	56	7.84
	75	11.81
Cellulose	33	5.31
	56	7.72
	75	11.50

Table 9: Water absorption contents of starch-based biocomposites foams compared to starch foam.

Material	Content (wt%)	RH (%)	Water absorption (%)
Starch foam (SF)	—	33	9.10
		56	12.52
		75	16.78
SF/cotton linter	10	33	8.84
		56	11.93
		75	16.34
SF/hemp	10	33	8.75
		56	11.97
		75	16.43
SF/cellulose	7	33	9.16
		56	12.49
		75	16.72
	10	33	8.78
		56	11.51
		75	15.68
	15	33	9.11
		56	12.17
		75	15.92

to starch. The study of mechanical properties showed an improvement in the flexural behavior of biocomposites foams compared to starch foam. The highest mechanical properties were obtained with coconut fibres, and plasma treatment with oxygen did not improve their mechanical properties.

4. Natural Fibre-Reinforced Biopolyester Foams

4.1. Industrial Context. PLA is currently one of the most promising biopolymers. During the last decade, PLA has been the subject of an abundant literature with several reviews and book chapters [21–25]. Processable by many techniques (blowing films, injection moulded pieces, calendared and thermoformed films…), a wide range of PLA grades is now commercially available with companies such as Cargill (USA), Mitsui Chemical (Japan), Galactic (Belgium), Shimadzu Co (Japan), Purac (The Netherlands), and many others [26].

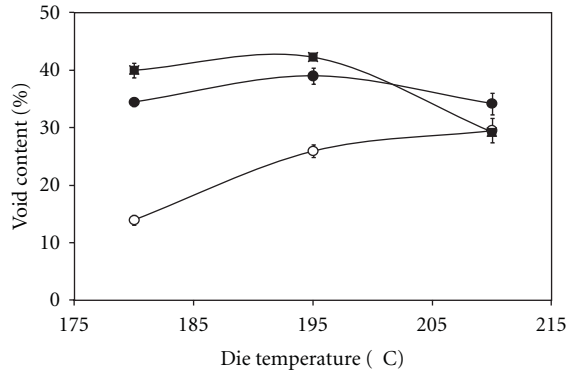

Figure 4: Evolution of the void content as a function of the die temperature and screw speed (●: 10 rpm, ○: 20 rpm, ■: 30 rpm) (PLA 7000D; 2 wt% CBA1; temperature profile A; free cooling).

With the aim of reducing the environmental impact of plastics, PLA-based foams products are of major industrial interest, replacing heavy items by lighter biobased products with identical performance levels. In this paper, chemically foamed structure is studied.

The objective of the studies concerned is to optimize either the processing conditions (extrusion flow rate, temperature, cooling system) or the material formulation (nature and content of chemical blowing agent, PLA characteristics) to improve foam expansion and mechanical performances. The influence of the incorporation of cellulose fibres is also studied. Different fibre aspect ratios were used, and a silane coupling agent was applied to optimize the fibre/PLA adhesion.

4.2. Determination of an Optimum Set of Extrusion Conditions. PLA 7000D (Mn = 199 600 Da, polydispersity index = 1.78 (SEC, THF, 25°C), Tg = 61°C, Tm = 153°C) provided by Nature Works LCC (USA) and Hydrocerol OMAN698483 called CBA1 (gas yield = 55 mL/g, initial and final decomposition temperatures = 160 and 220°C) provided by Clariant Masterbatches (France) were used as polymer matrix and chemical blowing agent, respectively. 2 wt% of CBA1 was incorporated in PLA.

Single-screw extrusion (FairEx, screw length = 720 mm, screw diameter = 30 mm, flat die = 40 × 1.5 mm^2, compression rate = 2.31) was used for foaming. Two cooling conditions, that is, a free cooling system and a confined cooling system in a three-calendaring rolls system at controlled temperature were used. Two temperature profiles (noted profile A and profile B) (Table 11) and three screw speeds ranging from 10 to 30 rpm were considered. For temperature profile A, three die temperatures were compared.

4.2.1. Influence of the Die Temperature and the Screw Rotation Speed. For a given temperature profile (profile A), results showed that the void fraction of the extruded foams reached a maximum value for an intermediate die temperature of 195°C and a screw speed of 30 rpm (Figure 4). This evolution was already reported by other authors [27, 28], and it

Table 10: Impact, flexural, and tensile properties for biocomposites foams (54 RH%).

Material	Impact resistance (kJ/m^2)	Flexural modulus (MPa)	Tensile strength (MPa)	Tensile elongation (%)
FS/Sugarcane	0.35 ± 0.08	98 ± 22	1.8 ± 0.4	2.9 ± 0.4
FS/treated sugarcane	0.34 ± 0.09	82 ± 22	1.9 ± 0.3	3.3 ± 1.0
FS/Coconut	0.69 ± 0.22	138 ± 70	2.8 ± 1.8	3.4 ± 1.3
FS/treated coconut	0.61 ± 0.25	110 ± 42	2.5 ± 1.1	3.3 ± 1.3

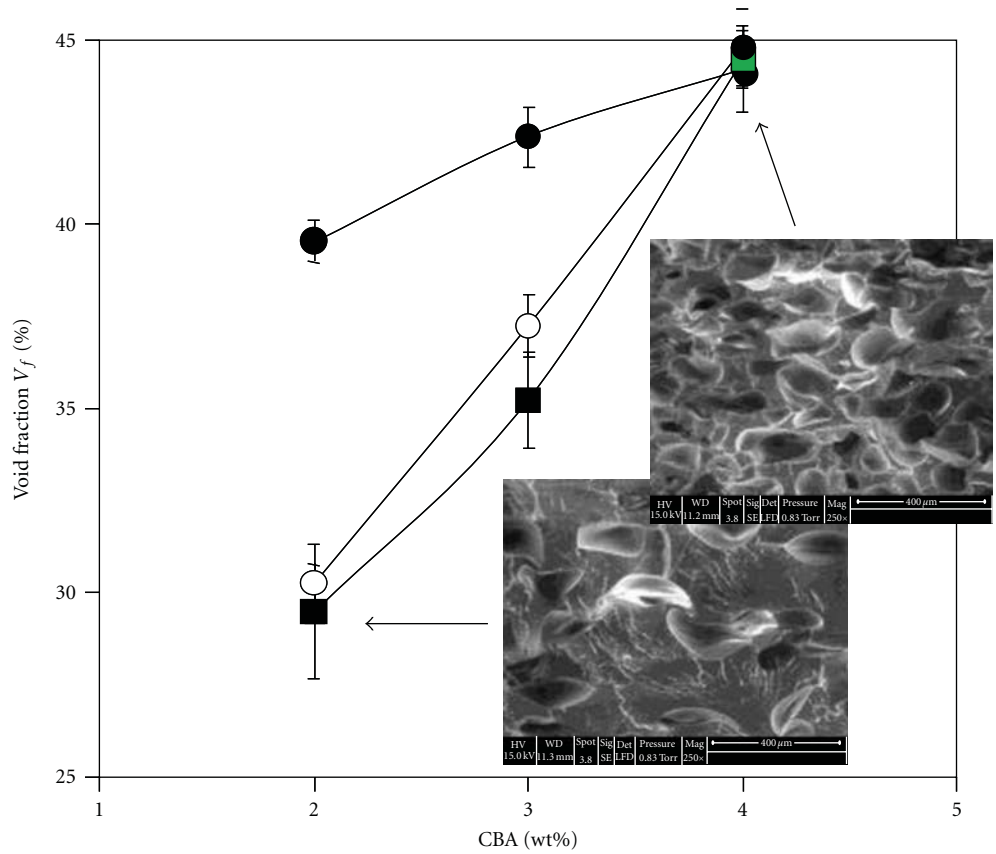

Figure 5: Void fraction of PLA foams as a function of the chemical blowing agent content (CBA1), the processing conditions (temperature profile: ● A; ■, ○ B) and the PLA nature (○ PLA4032D; ●, ■ PLA7000D) and corresponding microstructures (ESEM observations; magnitude 250x).

could result from a competition between two antagonist mechanisms. On one hand, an increase in temperature could favour the chemical blowing agent decomposition and thus allow the gas formation. But on the other hand, an increase in temperature could reduce the polymer viscosity and favour gas loss by diffusion through the polymer. It seems that the chemical blowing agent decomposition is predominant at low temperatures while the diffusion process is preponderant at high temperatures. Nevertheless, results obtained at the intermediate screw speed (20 rpm) are different. The void content increases with the die temperature. The simulation of the polymer flow (in particular the evaluation of temperature and viscosity distribution in the barrel and the die) are required to be able to evaluate the relative level of these two competitive mechanisms.

4.2.2. Influence of the Temperature Profile. The density and the void content of the foam extruded with the temperature profile A were equal to 767 kg/m^3 and 42%, respectively, as values of 893 kg/m^3 and 33% were obtained for the foam extruded with the temperature profile B for a given die temperature (195°C) and screw rotation speed (30 rpm). It can be noticed that the temperature profile B presents higher temperatures for the first barrel zones than those of temperature profile A. Therefore, with temperature profile B, an earlier gas formation should occur (i.e., before the complete melting and the pressurization of the polymer within the barrel) leading to a significant gas loss through the hopper. The quantity of CO_2 available for the expansion process in the die should then be reduced leading to a lower void content [29].

4.2.3. Influence of the Cooling Rate. Table 12 shows that the cooling rates induced by the two cooling systems used in this study are not different enough to induce important modification of the void content and the cellular structure.

Table 11: Temperature profiles for PLA chemical foaming through single-screw extrusion.

Temperature profile	Temperature (°C)					
	Barrel (from hopper to die)					Die
	1	2	3	4	5	6
A	130	150	165	165	170	180-195-210
B	150	170	170	170	180	195

Table 12: Effect of the cooling system on the void content and the cellular structure (PLA 7000D, 2 wt% CBA1, temperature profile A, screw speed 30 rpm, die temperature 195°C)—Void content V_f, cell dimensions (d_n, d_w), cell size polydispersity (PDI), cell density (N_c), cell-wall thickness (δ)—( ) = standard deviation.

Cooling system	V_f (%)	$\overline{d}_n$ (μm)	$\overline{d}_w$ (μm)	PDI	N_c (cells/cm^3) $\times 10^4$	δ (μm)
free	47 (1)	107	122	0.88	7.38	49.26
confined	45 (1)	92	105	0.88	10.86	45.59

These results are similar to those reported by other authors [30].

4.3. Influence of the Material Formulation. PLA7000D was compared to PLA4032D (Mn = 183 800 Da, polydispersity index = 1.95 (SEC, THF, 25°C), Tg = 69°C, Tm = 173°C) also provided by Nature Works LCC (USA). A significant difference in melting temperatures was observed between these two PLAs and was attributed to different optical purities (6.4% and 2.4% of D-lactic units for PLA 7000D and PLA 4032D, resp.).

CBA1 was compared to Hydrocerol CT3108 (gas yield = 50 mL/g, initial and final decomposition temperatures = 150 and 210°C, resp.) called CBA2 and also provided by Clariant Masterbatches (France). Each CBA was incorporated in PLA at contents varying from 2 to 4 wt%.

Single-screw processing was performed based on the optimal set of conditions previously described, that is, a screw speed of 30 rpm, a die temperature of 195°C, specific temperature profiles (A and B), and a confined cooling system.

4.3.1. Influence of the PLA Nature. The nature of PLA has no major effect on the void content of the foams extruded with a same temperature profile (B). Indeed the density varies between 894 and 879 kg/m^3 corresponding to a density reduction of 33% and 34% for PLA7000D and PLA4032D, respectively, for a given content of CBA1 (2 wt%). It can be notified that the foaming of PLA4032D is not possible using the temperature profile A. The barrel temperature in the feeding and melting zones is lower than the polymer melting temperature and then not adapted for extrusion process. Nevertheless, because of the high temperatures used in the first barrel zones for temperature profile B, one can anticipate significant gas losses during extrusion. This result confirms that a compromise should be found between all processing parameters [27, 29, 31].

4.3.2. Influence of the Chemical Blowing Agent Content. Figure 5 shows that the void content increases linearly (the foam density decreases) with the CBA1 content, regardless of the PLA type or the temperature profile. This evolution is related to the amount of gas formed and available during the expansion process [27]. Similar results were reported for extruded foams based on polyolefins [29, 32].

As shown on Table 13, the two studied PLAs provide foams with a homogeneous cellular structure (polydispersity PDI close to 1) with a relatively low open-cells ratio (between 11 and 27%). This is in agreement with results reported for polyolefin foams [27, 33, 34]. An increase in the open-cell ratio with the CBA1 content is observed which is related to the amount of gas release. This trend was already reported by other authors [27, 29]. A higher open-cell ratio range was obtained for PLA4032D (ratio between 19 and 27% for CBA1 content between 2 and 4 wt%) compared to PLA7000D (ratio between 12 and 19% for CBA1 content between 2 and 4 wt%). This is related to the higher temperatures involved in the temperature profile B used for PLA4032D compared to profile A inducing then a higher gas yielding as well as a lower PLA viscosity. According to Klempner and Sendijarevic [27], during initial cell growing, cells are closed. As the polymer viscosity decreases, the cell-wall thickness decreases so that they should break because of an increased pressure within the cell. Regarding PLA7000D (temperature profile A), an increase in CBA1 induces an increase in the average cell diameter (about 16% for d_n). Nevertheless, the cell-wall thickness remains constant (between 46 and 49 μm). These results are related to an increase in gas volume available for cell growing and may explain the increase in void content (Figure 4). Results performed on PLA4032D are different. The variation of the average cell diameter is not linear with the CBA1 content, and larger cells are obtained for extreme CBA1 contents (2 and 4 wt%). It can be assumed that several competitive mechanisms should occur (i) the increase in gas yielding and decrease in viscosity due to the higher barrel temperatures of profile B, (ii) the plasticization induced by the gas products during decomposition, and (iii) the presence of a higher content of nucleating agents present in the CBA1 master batch. Complementary works are in progress to evaluate their relative contributions. The average cell diameter and the cell-wall thickness measured in the present study are similar to those reported for polyolefins foamed with CBA1 [27, 29], but significantly higher than those reported by other authors for microcellular PLA foams [33]. Nevertheless, the cases reported in the literature concern mainly physical foaming processes, and

Table 13: Cell dimensions (d_n, d_w), cell size polydispersity (PDI), cell density (N_c), cell-wall thickness (δ) as a function if the chemical blowing agent content (CBA1) (PLA 7000D temperature profile A and PLA 4032D temperature profile B; screw speed 30 rpm; die temperature 195°C; free cooling)—( ): standard deviation.

PLA	CBA1 (%wt)	d_n (μm)	d_w (μm)	PDI	N_c (cells·cm^{-3}) $\times 10^5$	δ (μm)	C_o (%)
7000D	2	90	105	0.86	11.25	48.14	10.91 (0.24)
	3	95	104	0.91	10.13	46.46	14.72 (1.08)
	4	107	122	0.88	7.38	49.26	19.22 (0.69)
4032D	2	134	144	0.93	2.72	95.39	19.12 (1.47)
	3	125	174	0.72	4.02	70.80	24.49 (1.3)
	4	130	152	0.86	4.19	57.89	26.76 (1.11)

Table 14: PLA-foams tensile properties as a function if the chemical blowing agent content (CBA1) (PLA 7000D temperature profile A and PLA 4032D temperature profile B; screw speed 30 rpm; die temperature 195°C; free cooling)—σ_{max}: yield stress, ε_{max}: elongation at yield stress, σ_r: ultimate stress, ε_r: ultimate elongation—( ): standard deviation.

PLA	CBA1 (wt%)	Void fraction (%)	σ_{max} (MPa)	ε_{max} (%)	σ_r (MPa)	ε_r (%)
7000D	0	—	60.51 (1.58)	10.33 (0.94)	57.34 (1.36)	11.12 (0.86)
	2	42 (1)	36.00 (2.84)	8.41 (0.32)	33.38 (2.18)	9.95 (0.71)
	3	45 (1)	25.65 (1.33)	8.84 (0.39)	21.51 (1.72)	11.59 (0.92)
	4	47 (1)	23.71 (0.90)	8.37 (0.55)	20.49 (1.08)	10.28 (1.16)
4032D	0	—	59.51 (2.26)	9.40 (0.42)	54.61 (4.99)	10.19 (0.61)
	2	34 (1)	40.54 (3.27)	10.24 (0.89)	37.91 (3.90)	11.51 (1.23)
	3	41 (1)	30.68 (2.40)	8.61 (0.70)	27.14 (3.44)	10.43 (1.11)
	4	48 (1)	26.77 (1.24)	9.44 (1.36)	22.87 (1.12)	11.50 (1.60)

PLA modified by nanofillers (which act as cell nucleating agents) and/or chain extenders.

Finally, for both types of PLA, the increase in CBA1 content leads to a reduction in tensile yield and ultimate stresses (Table 14), due to the increase in void content (reduction of the effective sample cross-section) and in number of cells (which act as damage initiators). On the contrary, yield and ultimate elongations are both about 10% and independent on CBA1 content. Similar results were reported in the literature for PVC and PUR-based foams [35, 36]. It is all the more interesting to evaluate the ratio tensile stress/density (so-called specific stress) to determine the efficiency of the PLA foaming. These ratios are about 46 MPa·cm^{-3}·g^{-1} for yield stress and 43 MPa·cm^{-3}2·g^{-1} for ultimate stress for unfoamed PLA and for PLA foamed with 2 wt% of CBA1. Above 2 wt% of CBA1, a significant decrease in the specific stress is observed (about 34 MPa·cm^{-3}·g^{-1} for yield stress and 29 MPa·cm^{-3}·g^{-1} for ultimate stress). This behavior is independent on PLA nature.

4.3.3. Influence of the Chemical Blowing Agent Nature. PLA7000D was foamed through identical processing conditions (temperature profile A, die temperature 195°C, screw speed 30 rpm, confined cooling) with 4 wt% of CBA1 and CBA2. Similar void contents were obtained (45% for CBA1 and 43% for CBA2). The slight difference should result from small differences in gas yielding between both CBA. Nevertheless, the cellular morphology could be different but was not evaluated here.

4.4. Influence of the Incorporation of Raw and Surface Treated Cellulose Fibres in PLA Foams

4.4.1. Fibres Characteristics and Processing. PLA7000D was reinforced by pure cellulose fibres (cellulose content = 99.5%) provided by Rettenmaier and Söhne (Germany). Four fibres (two Short Cellulose Fibres (SCF) and Cellulose MicroFibres (CMF)) were compared according to their shape factor as described in Table 15.

A silane surface treatment was applied on one of these fibres, that is, CMF1, according to an experimental procedure described by Huda et al. [37]. 5 wt% of aminopropyltriethoxysilane (APS) compared to the fibre was dissolved for hydrolysis in a mixture of water ethanol (40 : 60 w/w). The pH of the solution was adjusted to 4 with acetic acid and stirred continuously during 1 h. Next, the fibres were soaked in the solution for 3 h. Fibres were then washed and kept in air for 3 days. Lastly, the fibres were oven dried at 80°C for 12 h.

Biocomposites (20 and 30 wt% of fibres) were compounded with a twin-screw extruder (Clextral BC21, length 900 mm, diameter 25 mm, 12 heating zones). Then, foaming

Table 15: Characteristics of the short cellulose fibres (SCF) and the cellulose microfibres (CMF) used for the study.

	Length (μm)	Diameter (μm)	Shape factor	Density (g/l)	S_{BET} (m^2/g)
SCF1	130	20	6,5	155–185	0.642
SCF2	60	20	3	180–220	0.813
CMF1	40	20	2	190–250	0.780
CMF2	18	15	1,2	230–300	1.192

Table 16: Cell dimensions (d_n, d_w), cell density (N_c), cell size polydispersity (PDI), cell-wall thickness (δ), and open-cell ratio (C_o) as a function of the fibre nature and fibre content (PLA7000D, 3 wt% CBA2 for biocomposites foams, 4 wt% CBA2 for PLA foam, temperature profile A, screw speed 30 rpm, die temperature 195°C, free cooling)-( ): standard deviation.

	Fibre (%wt)	d_n (μm)	d_w (μm)	PDI	N_c (cells·cm^{-3}) × 10^5	δ (μm)	C_o (%)
7000D	0	106	131	0.81	6.98	54.74	21.68 (2.31)
SFC1	20	81	104	0.78	3.67	172.11	29.69 (0.90)
	30	59	72	0.81	—	—	30.89 (1.55)
SFC2	20	62	87	0.71	9.47	118.98	26.00 (1.39)
	30	55	70	0.79	—	—	33.25 (1.42)
CMF1	30	67	92	0.72	15.80	67.66	36.42 (2.10)
CMF2	30	79	107	0.73	6.87	109.33	38.42 (1.26)

processing was achieved with a single-screw extruder (3 wt% CFA2, temperature profile A, screw speed 30 rpm, die temperature 195°C). All results are compared to unreinforced PLA (4 wt% of CBA2).

4.4.2. Void Content and Cell Morphology. It was observed (Figure 5) that the presence of cellulose fibres induced a sharp decrease in the void content compared to unreinforced PLA7000D. It can be noticed that it was not possible to process PLA foams reinforced by 20 wt% of microfibres because of a too low viscosity. Indeed, other investigations have shown that a drastic decrease in molecular weight occurs for these compounding samples. For 20 wt% reinforced foams, the void content is about 11% for short fibres (SFC1 and SFC2) while it is very low, for the 30 wt% reinforced foams. This could suggest that void content decreases with fibre content for PLA foaming, which is in accordance with the literature [38]. For 30 wt% microfibers, void contents of 25 and 17% were obtained for CMF1 and CMF2, respectively. Similar results were obtained for PVC/wood flour and PP/wood flour composites [39–42].

As shown on Table 16, cell diameters decrease with the increase in fibre content whatever the shape factor of the fibres. This result could be related to an increase in the number of nucleating sites induced by the fibre surface. Cell diameters and cell densities seem to be independent of the fibre length for a given fibre weight content of 30 wt%. The cell-wall thickness is much higher for cellulose fibre reinforced PLA foams compared to unreinforced PLA foam. Moreover, the polydispersity index variations are heterogeneous in presence of fibres. These behaviors should be related to fibre distribution within PLA matrix and to the fibre/matrix interactions. Indeed, these two parameters have a direct impact on the rheological behavior and therefore on the foam morphology. Local debondings at the fibre/matrix interface induce gas losses that will decrease the cell growing ability, and on the other hand, a heterogeneous distribution of the cell size (i.e., a low polydispersity index) is obtained when a disorganized repartition of fibres in the PLA matrix occurs. Results show also an increase in the open-cell ratio in presence of fibre compared to unreinforced PLA foam. This could be related to a low interfacial adhesion inducing microholes between fibres and polymer as suggested by other authors [39]. A linear correlation between the open-cell ratio and the developed surface of the fibres (considered as the ratio between the specific surface of the fibres determined through BET measurements and the weight content of fibres) was established.

4.4.3. Mechanical Properties. Tensile tests performed on composite foams (Table 17) do not show any significant variations according to the fibre content and length. Yield stress and strain are about 20 MPa and 7%, respectively, for all materials. Moreover, it can be observed similar specific yield and ultimate stresses (stress/density ratio) for all composites with lower values (ranging from 20 to 29 MPa·cm^{-3}·g^{-1}) than those of unreinforced PLA foam (42 MPa·cm^{-3}·g^{-1}). Similar data were obtained by other authors [43, 44] for PLA reinforced by hemp, microcrystalline cellulose, and wood flour. This decrease was attributed to a lack of adhesion between reinforcement systems and PLA. Nevertheless, Huda et al. [45] show inverse results for PLA reinforced by recycled cellulose fibres. These specific properties are different according to the fibre length. A slight decrease with the fibre content was observed for SFC1 as no variation can be observed for SFC2.

4.4.4. Improvement of the Interfacial Adhesion Fibre/Matrix. As shown on Figure 6, a sharp unexpected decrease in void content is obtained for $CMF1_{APS}$ compared to CMF1. It can

Table 17: PLA-foams tensile properties as a function of the fibre nature, the fibre content, and the fibres surface treatment ($CMF1_{APS}$) (PLA7000D, 3 wt% CBA2 for biocomposites foams, 4 wt% CBA2 for PLA foam, temperature profile A, screw speed 30 rpm, die temperature 195°C, free cooling)—σ_{max}: yield stress; ε_{max}: elongation at yield stress; σ_r: ultimate stress; ε_r: ultimate elongation—( ): standard deviation.

	Fibre (%wt)	Void fraction (%)	σ_{max} (MPa)	ε_{max} (%)	σ_r (MPa)	ε_r (%)
7000D	0	43 (1)	17.81 (1.41)	7.57 (0.98)	16.27 (1.33)	8.34 (1.14)
SFC1	20	10 (1)	20.12 (2.20)	7.07 (0.72)	19.89 (2.18)	7.15 (0.73)
	30	—	21.50 (1.11)	7.47 (0.33)	21.32 (1.22)	7.52 (0.33)
SFC2	20	12 (1)	23.7 (1.76)	7.30 (0.71)	23.59 (1.75)	7.34 (0.70)
	30	—	18.94 (2.59)	6.61 (0.61)	18.92 (2.58)	6.63 (0.61)
CMF1	30	25 (0)	19.69 (1.22)	6.94 (0.69)	19.55 (1.24)	6.98 (0.70)
$CMF1_{APS}$	30	7 (3)	22.95 (3.33)	8.77 (0.72)	22.92 (3.32)	8.79 (0.73)
CMF2	30	17 (1)	17.91 (1.69)	7.16 (0.50)	17.84 (1.68)	7.18 (0.51)

be noticed that discrepancies exist in the literature. As an example, some authors [39] observed an increase in the void content (6 to 12% regardless to the composite) in the case of HDPE/wood flour composites. But the chemical blowing agent nature should also be considered. Besides, it could be interesting to evaluate the grafting level of silane molecules onto the cellulose fibre surface. Regarding tensile properties (Table 17), no significant improvement was observed in presence of APS surface treatment, nevertheless mean values are higher. Further investigations should be achieved to optimize the silane grafting on cellulose fibres.

4.5. Conclusion. Experimental results show that, depending on processing conditions and material formulation, a single-screw extrusion process based on chemical foaming can lead to a significant reduction in weight of unreinforced PLA foam (up to 48%) and cellulose fibre reinforced PLA foams (up to 25%) as well as an improvement in mechanical properties (tensile strength up to 30%). Nevertheless, it requires an optimized control of all process and material parameters.

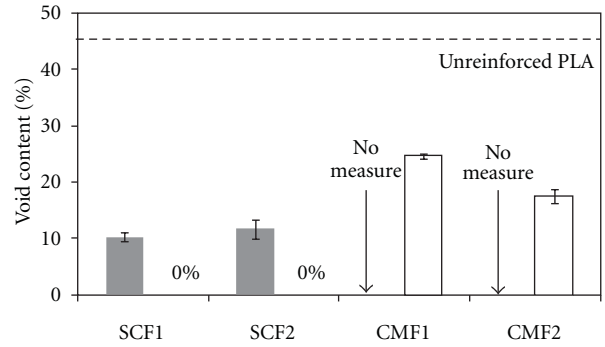

Figure 6: Void fraction of cellulose reinforced PLA foams as a function the fibre content: ■ 20 wt%; □ 30 wt% (PLA7000D, 3 wt% CBA2 for biocomposites foams, 4 wt% CBA2 for PLA foam, temperature profile A, screw speed 30 rpm, die temperature 195°C, free cooling).

5. Further Investigations

The influence of natural fibres on foaming ability needs to be clarified, as well as the influence of the fibre/matrix adhesion on the cell growing rate. For PLA-based biocomposites foams, a posterior plasma treatment could be performed to stabilize the initial plasma treatment and avoid loss of surface features. An optimization of the silane grafting conditions (preparation of polysiloxane solution, grafting duration, drying conditions…) could also be achieved. Other studies are conducted to understand the mechanisms that govern the formation of open-cells or closed-cells.

Regarding the foam properties, only mechanical properties (bending and tensile modes) were analyzed in this paper. Experiments have been achieved to study the influence of different parameters (processing and material parameters) on the biodegradation rate (mainly Biological Demand in Oxygen, BDO).

Many further investigations will be performed to understand competitive mechanisms that govern the cell formation during extrusion, especially for PLA foams, among them (i) the decrease in viscosity due to extrusion conditions that favour gas losses by diffusion through the polymer, (ii) the increase in gas yielding with increasing temperature that can induce a plasticization by the gas products, and (iii) the nucleating effects of nucleating agents and/or of natural fibres present within the polymer.

Acknowledgments

The authors are very indebted to Ph. D. students that were strongly involved in the presented studies, that is, Dr. A. Stanojlovic-Davidovic (for starch foams) and Dr. J. M. Julien (for PLA foams). Specific thanks are also devoted to Pr H. M. Viana (Centro Universitário Fundação Santo André, Santo André, SP, Brazil) for its active contribution to the study on sugarcane and coconut fibres, as well as to Pr. S. Borros (Universitat Ramon Ull, Barcelona, Spain) for the realization of the plasma treatments. Authors are also grateful to financial organization ADEME, to Vitembal Company (Remoulins. France), and to French academic institutions (Université de Toulon et du Var; Ecole des Mines de Douai).

References

[1] N. Soykeabkaew, P. Supaphol, and R. Rujiravanit, "Preparation and characterization of jute-and flax-reinforced starch-based composite foams," *Carbohydrate Polymers*, vol. 58, no. 1, pp. 53–63, 2004.

[2] M. Wollerdorfer and H. Bader, "Influence of natural fibres on the mechanical properties of biodegradable polymers," *Industrial Crops and Products*, vol. 8, no. 2, pp. 105–112, 1998.

[3] M. N. Angles and A. Dufresne, "Plasticized/ tunicin whiskers nanocomposite materials. 2. Mechanical properties," *Macromolecules*, vol. 34, no. 9, pp. 2921–2931, 2001.

[4] L. Averous, C. Fringant, and L. Moro, "Plasticized starch-cellulose interactions in polysaccharide composites," *Polymer*, vol. 42, no. 15, pp. 6571–6578, 2001.

[5] A. J. F. de Carvalho, A. A. S. Curvelo, and J. A. M. Agnelli, "Wood pulp reinforced thermoplastic starch composites," *International Journal of Polymeric Materials*, vol. 51, no. 7, pp. 647–660, 2002.

[6] A. Dufresne, D. Dupeyre, and M. R. Vignon, "Cellulose microfibrils from potato tuber cells: processing and characterization of starch-cellulose microfibril composites," *Journal of Applied Polymer Science*, vol. 76, no. 14, pp. 2080–2092, 2000.

[7] T. Nishino, K. Hirao, M. Kotera, K. Nakamae, and H. Inagaki, "Kenaf reinforced biodegradable composite," *Composites Science and Technology*, vol. 63, no. 9, pp. 1281–1286, 2003.

[8] D. Plackett, A. T. Logstrup, P. W. Batsberg, and L. Nielsen, "Biodegradable composites based on L-polylactide and jute fibres," *Composites Science and Technology*, vol. 63, no. 9, pp. 1287–1296, 2003.

[9] K. Oksman, M. Skrifvars, and J. F. Selin, "Natural fibres as reinforcement in polylactic acid (PLA) composites," *Composites Science and Technology*, vol. 63, no. 9, pp. 1317–1324, 2003.

[10] H. S. Yang, H. J. Kim, H. J. Park, B. J. Lee, and T. S. Hwang, "Effect of compatibilizing agents on rice-husk flour reinforced polypropylene composites," *Composite Structures*, vol. 77, no. 1, pp. 45–55, 2007.

[11] M. N. Belgacem, P. Bataille, and S. Sapieha, "Effect of corona modification on the mechanical properties of polypropylene/cellulose composites," *Journal of Applied Polymer Science*, vol. 53, no. 4, pp. 379–385, 1994.

[12] J. C. Benezet, R. B. Christensen, H. Viana, A. Bergeret, L. Ferry, and S. Borros, "Biodegradable composites from starch foam and surface plasma treated natural fiber," in *Recent Advances in Research on Biodegradable Polymers and Sustainable Composites*, vol. 1, Nova Science Publishers, New York, NY, USA, 2008.

[13] N. E. Zafeiropoulos, C. A. Baillie, and J. M. Hodgkinson, "Engineering and characterisation of the interface in flax fibre/polypropylene composite materials. Part II. The effect of surface treatments on the interface," *Composites Part A*, vol. 33, no. 9, pp. 1185–1190, 2002.

[14] A. K. Bledzki and J. Gassan, "Composites reinforced with cellulose based fibres," *Progress in Polymer Science*, vol. 24, no. 2, pp. 221–274, 1999.

[15] G. Siqueira, J. Bras, and A. Dufresne, "New process of chemical grafting of cellulose nanoparticles with a long chain isocyanate," *Langmuir*, vol. 26, no. 1, pp. 402–411, 2010.

[16] G. D. Valle, Y. Boché, P. Colonna, and B. Vergnes, "The extrusion behaviour of potato starch," *Carbohydrate Polymers*, vol. 28, no. 3, pp. 255–264, 1995.

[17] A. Stanojlovic-Davidovic, *Matériaux biodegradables à base d'amidon expanse renforcé de fibres naturelles. Application à l'emballage alimentaire*, Ph.D. thesis, Université du Sud Toulon-Var, 2006.

[18] J. W. Lawton, R. L. Shogren, and K. F. Tiefenbacher, "Aspen fiber addition improves the mechanical properties of baked cornstarch foams," *Industrial Crops and Products*, vol. 19, no. 1, pp. 41–48, 2004.

[19] R. L. Shogren, J. W. Lawton, and K. F. Tiefenbacher, "Baked starch foams: Starch modifications and additives improve process parameters, structure and properties," *Industrial Crops and Products*, vol. 16, no. 1, pp. 69–79, 2002.

[20] Z. Liu, C. S. L. Chuah, and M. G. Scanlon, "Compressive elastic modulus and its relationship to the structure of a hydrated starch foam," *Acta Materialia*, vol. 51, no. 2, pp. 365–371, 2003.

[21] L. Averous, "Biodegradable multiphase systems based on plasticized starch: A review," *Journal of Macromolecular Science. Polymer Reviews*, vol. C44, no. 3, pp. 231–274, 2004.

[22] D. Garlotta, "A literature review of poly(lactic acid)," *Journal of Polymers and the Environment*, vol. 9, no. 2, pp. 63–84, 2002.

[23] R. Auras, B. Harte, and S. Selke, "An overview of polylactides as packaging materials," *Macromolecular Bioscience*, vol. 4, no. 9, pp. 835–864, 2004.

[24] R. Mehta, V. Kumar, H. Bhunia, and S. N. Upadhyay, "Synthesis of poly(lactic acid): a review," *Journal of Macromolecular Science. Polymer Reviews*, vol. C45, no. 4, pp. 325–349, 2005.

[25] A. Sodergard and M. Stolt, "Properties of lactic acid based polymers and their correlation with composition," *Progress in Polymer Science*, vol. 27, no. 6, pp. 1123–1163, 2002.

[26] L. Shen, J. Haufe, and M. K. Patel, "Product overview and market projection of emerging bio-based plastics," Utrecht University 2009, www.epnoe.eu.

[27] D. Klempner and V. Sendijarevic, *Polymeric Foams and Foam Technology*, Hanser Garner, Munich, Germany, 1991.

[28] M. Parikh, R. A. Gross, and S. P. McCarthy, "The influence of injection molding conditions on biodegradable polymers," *Journal of Injection Molding Technology*, vol. 2, no. 1, pp. 30–36, 1998.

[29] C. H. Lee, K. J. Lee, H. G. Jeong, and S. W. Kim, "Growth of gas bubbles in the foam extrusion process," *Advances in Polymer Technology*, vol. 19, no. 2, pp. 97–112, 2000.

[30] M. Sauceau, C. Nikitine, E. Rodier, and J. Fages, "Effect of supercritical carbon dioxide on polystyrene extrusion," *Journal of Supercritical Fluids*, vol. 43, no. 2, pp. 367–373, 2007.

[31] A. Greco, A. Maffezzoli, and O. Manni, "Development of polymeric foams from recycled polyethylene and recycled gypsum," *Polymer Degradation and Stability*, vol. 90, no. 2, pp. 256–263, 2005.

[32] S. T. Lee, L. Kareko, and J. Jun, "Study of thermoplastic PLA foam extrusion," *Journal of Cellular Plastics*, vol. 44, no. 4, pp. 293–305, 2008.

[33] S. S. Ray and M. Okamoto, "Biodegradable polylactide and its nanocomposites: opening a new dimension for plastics and composites," *Macromolecular Rapid Communications*, vol. 24, no. 14, pp. 815–840, 2003.

[34] Y. Ema, M. Ikeya, and M. Okamoto, "Foam processing and cellular structure of polylactide-based nanocomposites," *Polymer*, vol. 47, no. 15, pp. 5350–5359, 2006.

[35] E. Kabir, M. C. Saha, and S. Jeelani, "Tensile and fracture behavior of polymer foams," *Materials Science and Engineering A*, vol. 429, no. 1-2, pp. 225–235, 2006.

[36] H. R. Lin, "The structure and property relationships of commercial foamed plastics," *Polymer Testing*, vol. 16, no. 5, pp. 429–443, 1997.

[37] M. S. Huda, L. T. Drzal, A. K. Mohanty, and M. Misra, "Effect of fiber surface-treatments on the properties of laminated biocomposites from poly(lactic acid) (PLA) and kenaf fibers," *Composites Science and Technology*, vol. 68, no. 2, pp. 424–432, 2008.

[38] L. M. Matuana and O. Faruk, "Solid state microcellular foamed PLA and PLA/wood flour composites: morphology and property characterization," in *Proceedings of the 4th International Symposium on wood polymer composites*, Bordeaux, France, 2009.

[39] Q. Li and L. M. Matuana, "Foam extrusion of high density polyethylene/wood-flour composites using chemical foaming agents," *Journal of Applied Polymer Science*, vol. 88, no. 14, pp. 3139–3150, 2003.

[40] F. Mengeloglu and M. M. Laurent, "Foaming of rigid PVC/wood-flour composites through a continuous extrusion process," *Journal of Vinyl and Additive Technology*, vol. 7, no. 3, pp. 142–148, 2001.

[41] L. M. Matuana and M. Fatih, "Manufacture of rigid PVC/wood-flour composite foams using moisture contained in wood as foaming agent," *Journal of Vinyl and Additive Technology*, vol. 8, no. 4, pp. 264–270, 2002.

[42] S. Pilla, S. G. Kim, G. K. Auer, S. Gong, and C. B. Park, "Microcellular extrusion-foaming of polylactide with chain-extender," *Polymer Engineering and Science*, vol. 49, no. 8, pp. 1653–1660, 2009.

[43] A. P. Mathew, K. Oksman, and M. Sain, "Mechanical properties of biodegradable composites from poly lactic acid (PLA) and microcrystalline cellulose (MCC)," *Journal of Applied Polymer Science*, vol. 97, no. 5, pp. 2014–2025, 2005.

[44] R. Masirek, Z. Kulinski, D. Chionna, E. Piorkowska, and M. Pracella, "Composites of poly(L-lactide) with hemp fibers: morphology and thermal and mechanical properties," *Journal of Applied Polymer Science*, vol. 105, no. 1, pp. 255–268, 2007.

[45] M. S. Huda, L. T. Drzal, A. K. Mohanty, and M. Misra, "Chopped glass and recycled newspaper as reinforcement fibers in injection molded poly(lactic acid) (PLA) composites: a comparative study," *Composites Science and Technology*, vol. 66, no. 11-12, pp. 1813–1824, 2006.

Hindawi Publishing Corporation
International Journal of Polymer Science
Volume 2011, Article ID 736474, 7 pages
doi:10.1155/2011/736474

Research Article

Kenaf Bast Fibers—Part II: Inorganic Nanoparticle Impregnation for Polymer Composites

Jinshu Shi,[1] Sheldon Q. Shi,[1] H. Michael Barnes,[1] Mark F. Horstemeyer,[2] and Ge Wang[3]

[1] *Forest Products Department (FPD), Mississippi State University (MSU), Box 9820, Starkville, MS 39762-9601, USA*
[2] *Center for Advanced Vehicular Systems (CAVS), Mississippi State University, Box 5405, Starkville, MS 39762-5405, USA*
[3] *International Center for Bamboo and Rattan, No. 8 Futong Dongdajie, Wangjing Area, Chaoyang District, Beijing 100102, China*

Correspondence should be addressed to Sheldon Q. Shi, sshi@cfr.msstate.edu

Received 1 April 2011; Revised 18 June 2011; Accepted 5 July 2011

Academic Editor: Bibin Mathew Cherian

The objective of this study was to investigate an inorganic nanoparticle impregnation (INI) technique to improve the compatibility between kenaf bast fibers and polyolefin matrices. The Scanning Electron Microscopy (SEM) was used to examine the surface morphology of the INI-treated fibers showing that the $CaCO_3$ nanoparticle crystals grew onto the fiber surface. Energy-dispersive X-ray spectroscopy (EDS) was used to verify the $CaCO_3$ nanoparticle deposits on the fiber surface. The tension tests of the individual fiber were conducted, and the results showed that the tensile strength of the fibers increased significantly (more than 20%) after the INI treatments. Polymer composites were fabricated using the INI-treated fiber as reinforcement and polypropylene (PP) as the matrix. The results showed that the INI treatments improved the compatibility between kenaf fibers and PP matrix. The tensile modulus and tensile strength of the composites reinforced with INI-treated fibers increased by 25.9% and 10.4%, respectively, compared to those reinforced with untreated kenaf fibers.

1. Introduction

Lignocellulosic fiber is a renewable and biodegradable natural polymer which has been used in a variety of applications, such as textile, pulp and paper, and so forth. In recent years, there has been an increasing interest in utilizing natural fibers to replace synthetic glass or carbon fibers to fabricate sheet molding compound (SMC) composites for automobile structural component design. Natural fibers are light weight, economical and environmentally friendly. However, in the processing of lignocellulosic fiber-reinforced polymer composites, the following issues should be addressed. The cell wall structure of natural fibers contains many micropores. If a chemical pulping process is used, additional micropores would be created since some of the lignin and hemicellulose of natural fibers are removed [1]. The presence of these micropores in the cell wall structure could cause manufacturing defects in composites, such as interfacial failure and air pockets. Compatibility between the fiber surface and polymer matrix has been a major issue for lignocellulosic fiber-reinforced polymer composites processing [2–5]. As it was reported in the first paper of this series [6] that the kenaf fibers retted using an alkaline solution by a hermetical process had poor compatibility with the polypropylene (PP) matrix resulting in delaminations of the composites. A common way to improve the compatibility between the cellulosic natural fibers and the polymer matrix is to use coupling agents [7]. However, the organic coupling agents are usually costly and also cause environmental concern. Previous study indicated that the deposited nanoparticles on the fiber surface served as nucleation sites to initiate the crystalline orientation of the molten polymer matrix [8]. Therefore, a proper process to introduce nanoparticles onto the fiber surface serving as attraction force manipulators to polyolefin matrixes has a potential to improve the crystalline formation in the polymer matrix. Since the mechanical behavior of a composite material strongly depends on the adhesion between the reinforced fibers and the matrix, the properties of the composites should be enhanced [9].

Directly impregnating the commercial nanoparticles into the micropore cell wall structure of the cellulosic nature fibers can be difficult and costly. For the inorganic nanoparticle impregnation (INI) process in this study, the primary salt, Na_2CO_3, and secondary ionic salt, $CaCl_2$, were impregnated

into micropores of the fiber cell wall consecutively. The two chemicals react at certain temperature and pressure conditions, and the inorganic nanoparticles of $CaCO_3$ are formed. The chemical reaction is described as follows:

$$CaCl_2 \cdot H_2O + Na_2CO_3 \xrightarrow{H_2O} CaCO_3 + 2NaCl + 2H_2O. \quad (1)$$

The INI technology has been used in pulp, paper, and surface coating industries [10]. The main purpose of INI in pulp and paper was to improve the printability of the papers. The inorganic nanoparticles loaded into cell wall and on the surface may provide strong static electric attractive forces to nonpolar polymer surface [11], and hence the compatibility between the fibers and the polymer matrix may be improved. These nanoparticle-impregnated fibers can be incorporated readily into the existing manufacturing process to make fiber sheets for composite products. The impregnation of the inorganic nanoparticles into the micropore structure of the fiber cell walls can reduce the microvoid volumes in the fiber, as well as reduce air bubble formation during the composite fabrication process. This process is low cost (using inexpensive ionic salts), has little environmental concern (weak chemical solutions are used and can be reused), and simple (the inorganic nanoparticles form directly). The products can be potentially used as vehicle components because of their light-weight, good mechanical properties and environmental friendliness.

In this study, the kenaf bast fibers retted from the hermetical alkaline process were further treated with INI processes. The objectives of this study were to optimize the INI process for the kenaf bast fibers and to evaluate the potentials on the property improvement for the kenaf fiber-PP composites.

2. Materials and Methods

2.1. Materials. The Kenaf stalks were obtained from MSU North Farm. After the separation of the kenaf core and bast, the bast was cut into 50.8 mm lengths and dried to a moisture content of 7.4% at 103°C. Sodium hydroxide (NaOH) solution (5%, w/v) prepared with NaOH beads (Lab grade, Thermo Fisher Scientific Inc.) and distilled water was used as digestion agent. Glacial acetic acid (17.4 N, Regent grade, Thermo Fisher Scientific Inc.) was used as a pH neutralizer. Sodium carbonate (Na_2CO_3) aqueous solutions (0.1 mol/L) and calcium chloride ($CaCl_2$) aqueous solutions (0.1 mol/L and 0.2 mol/L) were prepared, respectively, using distilled water. The sodium carbonate and calcium chloride were supplied by Fisher Scientific Inc. Polypropylene (PP) films (CO-EX Oriented Polypropylene), provided by Plastic Suppliers, Inc. Dallas, Tex, USA, and were used to fabricate kenaf fiber/PP composites.

2.2. INI Treatments. The flowchart on the treatment details is described in Figure 1 [5, 12, 13]. Kenaf bast was retted with a 5% NaOH solution (fiber: NaOH solution = 1 : 30, g/mL) in a hermetical reactor (Parr Instrument Co. 251 M) at 160°C. The retting process took one hour and was aided with a mechanical stirring. The autogenous vapor pressure was 0.60 MPa. After the retting process, the pH of the retting liquid and retted fibers was adjusted to 7.0 using acetic acid. The neutralized fibers were washed with water to remove chemicals from the fibers. These fibers were used as the control fibers. The control fibers and 0.1 mol/L Na_2CO_3 water solution (fiber: solution = 5 : 400, g/mL) were mixed in the hermetic reactor with mechanical stirring at 70°C with autogenous vapor pressure of 0.1 MPa for 30 minutes. The excessive primary ionic solution was removed from kenaf fibers by gravity. The secondary ionic solution was used to impregnate the fibers at three different temperatures and autogenous vapor pressures (100°C, 0.15 MPa; 130°C, 0.30 MPa, and 160°C, 0.70 MPa) for 15 minutes. The controlled molar ratios of Na_2CO_3 to $CaCl_2$ were 1 : 1 and 1 : 2 by the concentration of $CaCl_2$ solution, 0.1 mol/L or 0.2 mol/L. Three temperatures and the corresponding pressures provided a total of six INI treatment conditions. After the impregnation of the two ionic solutions, the primary ionic salt (Na_2CO_3) reacted with the secondary ionic salt ($CaCl_2$) in kenaf bast fibers to generate $CaCO_3$ nanoparticles in the micropore structure of the fiber cell wall, from which the nanoparticle crystals may grow onto the fiber surface. The impregnated fibers were washed to remove excess $CaCO_3$ particles and other ions on fiber surface.

2.3. Determination of $CaCO_3$ Loading. The percentage $CaCO_3$ loading in the fibers was calculated based on the difference in ash contents between the untreated fibers and INI-treated fibers. The ash content was determined by burning the material in a muffle furnace first at 400°C for 30 minutes, then at 850°C for 45 minutes.

2.4. Characterization of INI-Treated Fibers. Surface morphology, tensile properties of individual fibers, surface hardness, and elastic modulus of the fibers were examined in the same procedures described in the first paper of this series [6]. Elements determination was conducted using a Bruker Quantax 200 X Flash Energy-Dispersive X-ray Spectrometer (EDS) System (LN2-free high speed 30 mm^2 SDD Detector).

2.5. Composites Fabrication. The composites were fabricated with a sheet molding compound process. The control fibers and INI-treated kenaf fibers were dispersed in water by vigorous mechanical stirring. The fiber suspension was poured into a 355 mm × 355 mm deckle box and then passed through a screen (mesh 35), on which the fiber sheets were formed as the water flowed down gravitationally. The fiber sheets were dried in an oven set at 80°C. The fiber sheets and PP films were cut into a dimension of 15.2 cm × 15.2 cm and laminated alternatively. The fiber to PP weight ratio in the composite panel was 50 : 50. The laminated mats were pressed at 200°C and 0.7 MPa for 2.5 minutes. The pressure was not released until the platen was cooled to room temperature. The kenaf fiber/PP panels were removed from the press and stored in a desiccator with the silica gel for two days before preparing the mechanical testing specimens. Three panels were fabricated for each formula. The density of all of the kenaf fiber/PP composites (including the control

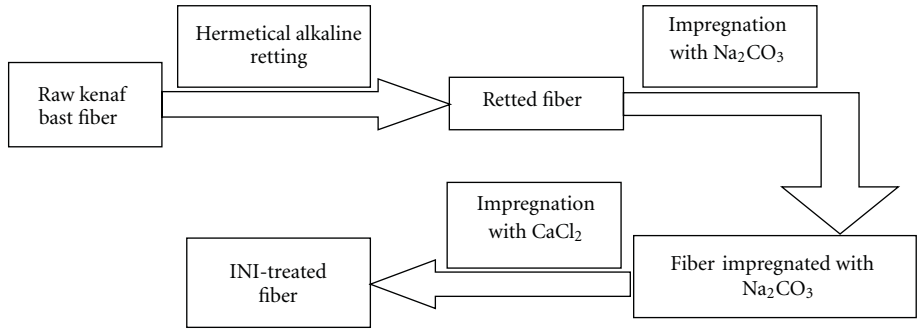

Figure 1: Flowchart of INI treatment.

fibers reinforced and INI-treated fibers-reinforced composites) was $0.88 \pm 0.03\ g/cm^3$.

2.6. Composites Tensile Properties Testing. Tensile properties of the INI-treated fiber/PP composites and control fiber (untreated fiber)/PP composites were tested with Instron 5869 (load cell 50 kN). The crosshead extensions were used as the specimen deformations. Composites samples were kept in desiccators for one week before tensile testing. The procedures referred to ASTM 1037. The crosshead speed during the tension testing was 2.5 mm/min. Nine replicates of each composite formulation were tested. Multiple comparison of the results was conducted with Fisher's Least Square method at $\alpha = 0.05$ using SAS 9.2 software (SAS Institute Inc. NC, USA). The fracture surfaces of the samples were observed using scanning electron microscopy (SEM, Zeiss Supra TM 40).

3. Results and Discussion

3.1. CaCO3 Loading. Table 1 shows the loading percentage of $CaCO_3$ in the fibers. Each specimen was examined twice, and the errors were less than 0.1%. The fibers treated at 130°C (Na_2CO_3 to $CaCl_2 = 1:1$, mol : mol) had the highest $CaCO_3$ loading. Although the differences in the loading percentages of $CaCO_3$ among the impregnation variables were no more than 1%, a small increase in $CaCO_3$ nanoparticle loading could result in a significant change in surface characteristics of the fibers since the particles impregnated in were in nano scales and with a high specific surface area. A small amount of $CaCO_3$ nanoparticles may give a large surface area, which may have a significant impact on the interfacial compatibility between the fiber and the polymer matrix.

3.2. Surface Morphology and Element Determination. Figure 2 shows the SEM images of the fiber surfaces treated with INI. As the temperature increased, the inorganic nanoparticle size increased, indicating that temperature played an important role in the formation of $CaCO_3$ crystals. The sizes of the $CaCO_3$ nanoparticles in the fibers treated at 100°C and 130°C were smaller than 90 nm. However, some $CaCO_3$ particles generated at 160°C ($Na_2CO_3 : CaCl_2 = 1:1$, mol : mol) grew to a diameter over nanoscale.

Table 1: $CaCO_3$ loading percentages of the INI-treated fibers.

INI treatment conditions		
Temperature (°C)	$Na_2CO_3 : CaCl_2$ (mol : mol)	$CaCO_3$ loading (%)
100	1 : 1	1.91
100	1 : 2	2.30
130	1 : 1	2.86
130	1 : 2	2.57
160	1 : 1	2.43
160	1 : 2	2.21

The EDS spectrum and elements maps are shown in Figures 3 and 4. In the spectrum, calcium (Ca), carbon (C), and oxygen (O) were detected indicating that the $CaCO_3$ nanoparticles exist in the fibers. Calcium may exist as calcium ion (Ca^{2+}) with Cl^- ion or in $CaCO_3$ molecule. Since, neither sodium (Na) nor chlorine (Cl) was detected from the EDX. Therefore, Calcium can only exist in $CaCO_3$. This evidence testified that the reaction between Na_2CO_3 and $CaCl_2$ occurred during the INI process and the $CaCO_3$ was synthesized. The byproduct, NaCl, would have been washed off after the INI treatment. The peaks for gold (Au) and palladium (Pd) came from the specimens coating treatment for the SEM and EDS.

3.3. Surface Hardness and Elastic Modulus. Table 2 shows the surface hardness and elastic modulus of the INI-treated fibers.

The fibers treated at 130°C (0.30 MPa) yielded a 52.6–76.9% increase in modulus and a 47.0–59.1% increase in hardness. The improvement of the hardness and modulus properties was found for the other INI treated fibers also compared with the untreated fiber. The micropores in the cell wall of the lignocellulosic fibers were filled up by the $CaCO_3$ particles, which enhanced the stress transfer between cellulose fibrils resulting a higher hardness and modulus. A higher variation in the hardness and modulus properties was found in Table 2. This may be because that some indentation tests are on the $CaCO_3$, while others on the fibers. In addition, the component variation at different locations of

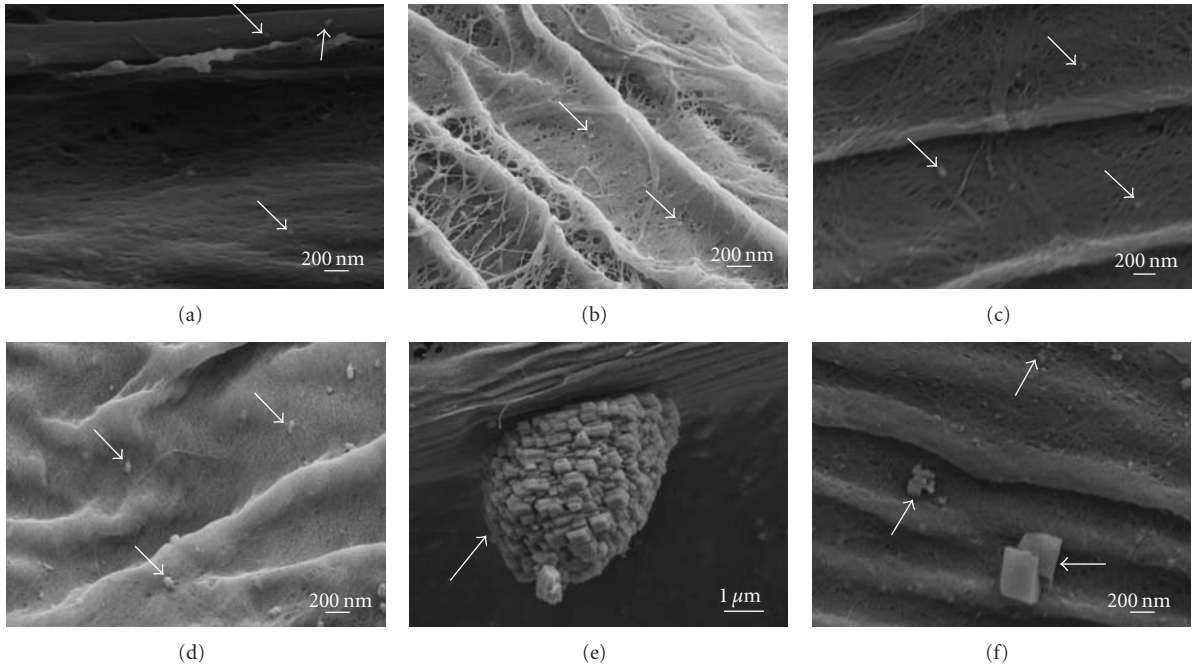

Figure 2: SEM images of INI-treated fibers. (a) 100°C (Na_2CO_3 : $CaCl_2$ = 1 : 1, mol : mol), (b) 100°C (Na_2CO_3 : $CaCl_2$ = 1 : 2, mol : mol), (c) 130°C (Na_2CO_3 : $CaCl_2$ = 1 : 1, mol : mol), (d) 130°C (Na_2CO_3 : $CaCl_2$ = 1 : 2, mol : mol) at 1 : 2, (e) 160°C (Na_2CO_3 : $CaCl_2$ = 1 : 1, mol : mol), and (f) 160°C (Na_2CO_3 : $CaCl_2$ = 1 : 2, mol : mol). The white arrows designated the $CaCO_3$ particles.

Table 2: Surface hardness and elastic modulus of the INI treated fibers.

INI treatment conditions		Surface hardness (MPa)			Elastic modulus (GPa)		
Temperature (°C)	Na_2CO_3 : $CaCl_2$, mol : mol	Mean	Stdev.	LSD	Mean	Stdev.	LSD
	Untreated fiber	287.91	113.75	A	4.64	1.73	A
100	1 : 1	264.83	26.36	A	4.88	0.43	A
100	1 : 2	272.31	51.35	A	5.40	0.68	A
130	1 : 1	423.25	47.89	B	7.08	0.78	B
130	1 : 2	458.19	112.81	B	8.21	1.03	B
160	1 : 1	213.26	87.56	A	4.30	1.00	A
160	1 : 2	295.57	42.39	A	5.28	0.50	A

Stdev.: means standard deviation. Average of four samples. Means with the different letter are significantly different at $\alpha = 0.05$.

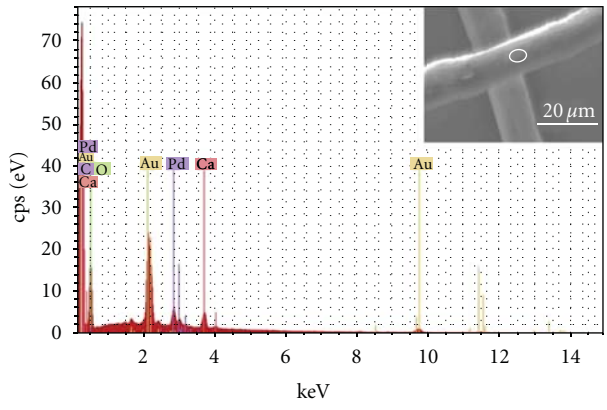

Figure 3: EDS spectrum of kenaf fiber treated with INI process at 100°C, Na_2CO_3 : $CaCl_2$ = 1 : 2, mol : mol. The white circle designated the point that was analyzed.

the fiber itself would also cause the variation in hardness and modulus properties.

3.4. Tensile Properties of Individual Fibers. The tensile properties of the individual fibers are shown in Table 3.

Table 3 shows the tensile property comparison for the INI-treated and -untreated fibers. The results showed that the INI treatments improved the tensile properties. While the improvement in tensile modulus did not show statistically different (α = 0.05), the tensile strength of the fibers increased significantly after the INI treatments. A 27% increase in tensile strength (from 810 MPa to 1,032 MPa) was obtained for the fiber treated at 160°C (Na_2CO_3 : $CaCl_2$ = 1 : 2, mol : mol). The improvement in the tensile strength should be attributed to the impregnation of $CaCO_3$ particles in fiber cell wall, which increases the density of the fibers and

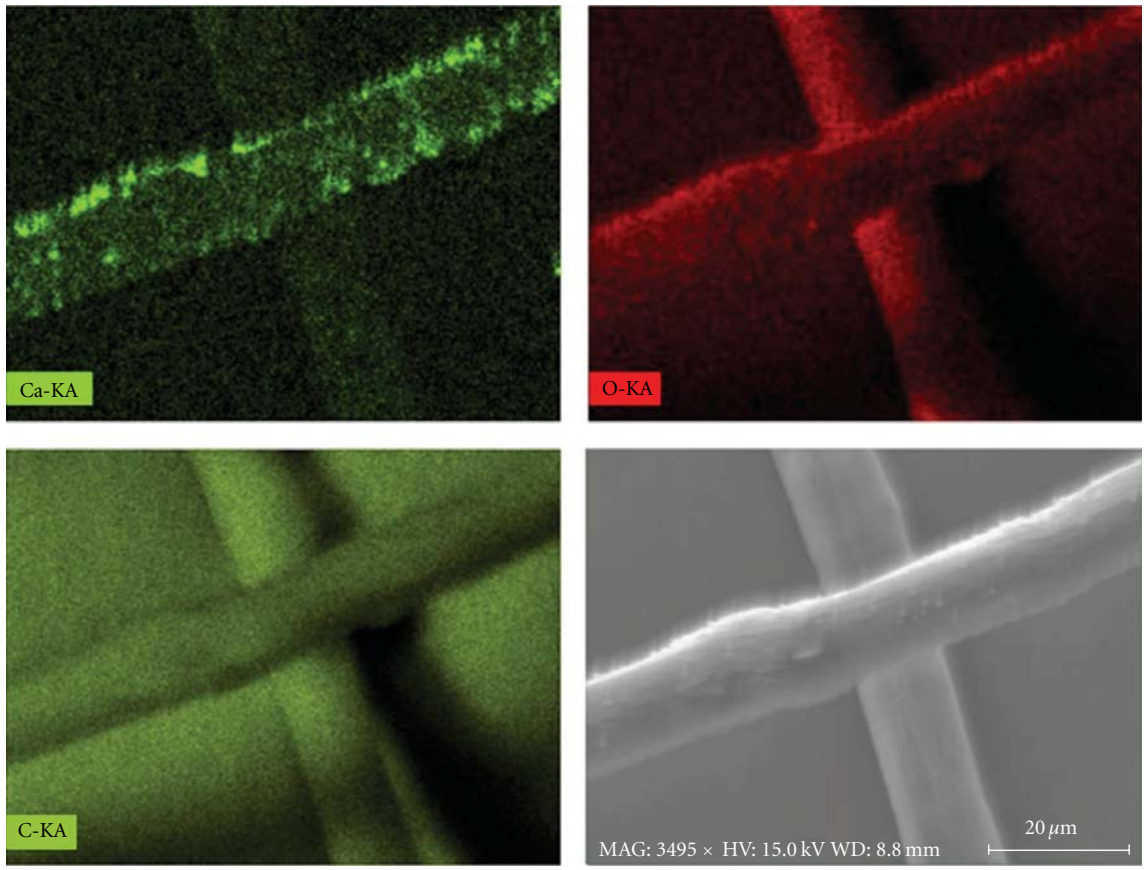

Figure 4: EDS elements mapping of kenaf fiber treated with INI process at 100°C ($Na_2CO_3 : CaCl_2 = 1 : 2$, mol : mol). Left top: calcium (Ca). Right top: oxygen (O). Left bottom: carbon (C). Right bottom: SEM image.

reduces the defect for the fiber by filling up the micropores. The $CaCO_3$ particles in the fiber also helped for the stress transfer between the cellulose fibrils, yielding the overall tensile strength improvement.

3.5. Tensile Properties of INI Treated Fiber/PP Composites. The tensile strength and tensile modulus of INI treated fiber/PP composites are shown in Table 4.

For most of the treatment conditions, the PP composites reinforced with the INI-treated fibers showed improvement in both tensile strength and tensile modulus. Except for the fibers treated at 100°C ($Na_2CO_3 : CaCl_2 = 1 : 1$, mol : mol), significant improvement in tensile strength was found for all other combinations. The INI treatment condition at (100°C, $Na_2CO_3 : CaCl_2 = 1 : 2$, mol : mol) showed the best reinforcing effects compared to other conditions, with about 10.4% increase in tensile strength. No significant difference in tensile strength was found among the six INI treatment conditions.

The improvement in tensile modulus of the composites does correlate with the INI treatment conditions. INI treatment significantly increased tensile modulus for all combinations. The composites reinforced with the fibers treated at 160°C ($Na_2CO_3 : CaCl_2 = 1 : 1$, mol : mol) gave the highest tensile modulus, which was 25.9% higher than those reinforced with untreated fibers.

Table 3: Tensile properties of individual fibers.

INI treatment conditions	Modulus (GPa)	LSD Test	Strength (MPa)	LSD test
Untreated fiber	13.5	A	810	A
100°C, 1 : 2	14.7	A	1001	B
160°C, 1 : 2	14.6	A	1032	B

1 : 2 means the molar ratio of Na_2CO_3 to $CaCl_2$. Average of 30 samples. Means with the different letter are significantly different at $\alpha = 0.05$.

The typical stress-strain curves of the INI-treated fiber/PP composites are shown in Figure 5. Since the load taken up by the fibers decreases as the strain increases [14], the tensile behaviors of the composites drive to plastic deformation, and the slopes of the stress-strain curves become smaller as the strain increases. The dislocation of INI-treated kenaf fibers in the composites may occur under a higher load than untreated fibers do because $CaCO_3$ particles modified the compatibility between kenaf fiber and PP matrix. Therefore, the initial slopes of the stress-strain curves are higher for the INI-treated fiber/PP composites than that for the untreated fiber/PP composites, and the elongations of the

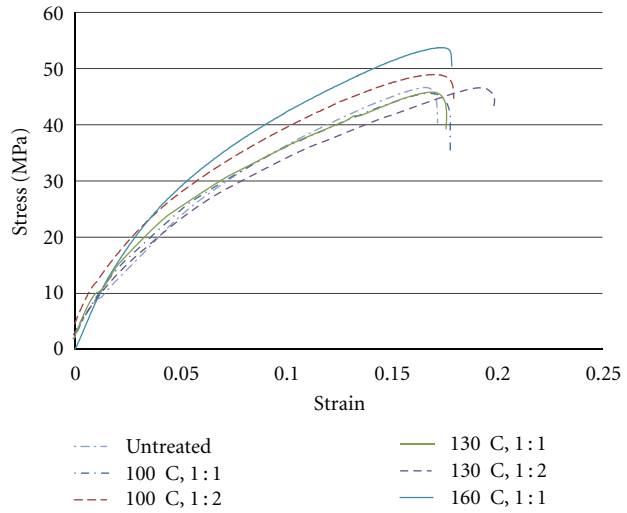

Figure 5: Stress-strain curves of the INI-treated fiber/PP composites. The labels mean the INI treatments conditions for the kenaf fibers. Untreated fiber is the control fiber that has been retted at 160°C but not treated with INI processes.

Table 4: Tensile strength and tensile modulus of INI treated fiber/PP composites.

	Tensile Strength (MPa)			Tensile Modulus (GPa)		
INI treatments	Mean	Stdev.	LSD Test	Mean	Stdev.	LSD Test
Untreated	46.77	3.43	A	1.70	0.20	A
100°C, 1 : 1	49.23	3.77	AB	1.88	0.11	B
100°C, 1 : 2	51.65	2.57	B	1.96	0.15	BC
130°C, 1 : 1	50.20	3.30	B	1.93	0.22	BCD
130°C, 1 : 2	51.61	2.51	B	2.05	0.11	DE
160°C, 1 : 1	51.41	4.33	B	2.14	0.22	E
160°C, 1 : 2	50.94	4.31	B	1.99	0.16	BE

1 : 1 and 1 : 2 means the molar ratio of Na_2CO_3 to $CaCl_2$. Average of 27 samples. Means with the same letter are not significantly different at $\alpha = 0.05$. Stdev: standard deviation of the mean.

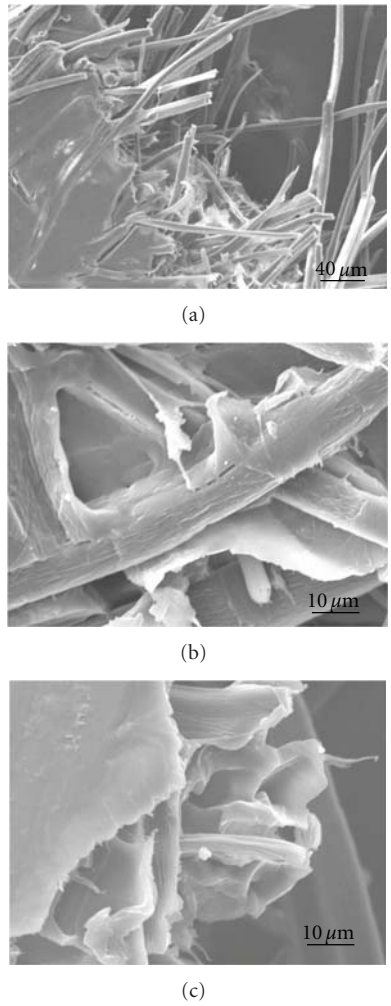

Figure 6: SEM images of the fracture surfaces of kenaf fiber/PP composites. (a) PP composites reinforced with untreated fibers; (b) PP composites reinforced with INI-treated fibers (INI treatment conditions were 100°C, $Na_2CO_3 : CaCl_2 = 1 : 2$, mol : mol), and (c) PP composites reinforced with INI-treated fibers (INI treatment conditions were 160°C, $Na_2CO_3 : CaCl_2 = 1 : 1$, mol : mol).

INI-treated fiber/PP composites were higher than that of the untreated fiber/PP composites.

The mechanical property improvement for the kenaf fiber/PP composites should be attributed to the improvement in interfacial bonding between the fiber and PP matrix. Figure 6 shows the SEM images for the fracture surfaces of fiber/PP composites with both the INI-treated fibers (two treatment conditions) and -untreated fibers. Fiber pullout is clearly shown at the fracture surface for the composites with untreated fibers (Figure 6(a)) indicating poor interfacial compatibility between untreated fibers and PP. However, for the composites with INI-treated fibers, more simultaneous failure was observed. The interfacial compatibility between the INI-treated fiber and PP matrix was much improved compared to the control samples, indicating stronger adhesion between the fiber and the PP matrix. It may be reasoned that the inorganic nanoparticles deposited on the fiber surface served as the nucleation sites to initiate the crystalline formation of the semicrystalline polymer matrix around the fibers.

4. Conclusions

Inorganic nanoparticles ($CaCO_3$) were successfully impregnated into kenaf bast fibers. From the SEM images, the nanoparticle deposition is clearly observed on the fiber surfaces. INI treatment (at 130°C) increased the surface hardness of the fiber by 52.6–76.9% and the elastic modulus by 47.0–59.1%. The fibers treated at 160°C with INI processes yielded a 27% improvement in tensile strength. The impregnated inorganic nanoparticles improved the compatibility between the fibers and the PP matrix, resulting in an increase in tensile modulus and tensile strength of the kenaf fiber/PP composites. Based on the current lab condition, the INI treatment conditions including

(1) 130°C, 1 : 1 (Na_2CO_3 : $CaCl_2$, mol : mol), (2) 160°C, 1 : 1 (Na_2CO_3 : $CaCl_2$, mol : mol), and (3) 160°C, 1 : 2 (Na_2CO_3 : $CaCl_2$, mol : mol) produced the optimal kenaf fibers that had the best reinforcement effects for PP. The PP composites reinforced with the INI-treated (160°C, 1 : 1) fibers showed a 10.4% improvement in tensile strength and 25.9% in tensile modulus compared to those reinforced with untreated fibers.

Acknowledgments

The research work was supported by Department of Energy (DOE), funding no. 362000-060803 through Center for Advanced Vehicular System (CAVs) at Mississippi State University and National Science Foundation (NSF), fund no. CMMI0928641 09080796. Acknowledgments are given to Dr. Jinwu Wang for the help with the data analysis, Dr. Sangyeob Lee for the involvement of the project when he worked as a post-doc at Mississippi State University, and USDA-Forest Service Southern Research Station, Pineville, La, USA and the International Center for Bamboo and Rattan, Beijing, China for the instrumental support. The manuscript is approved for publication by Forest and Wildlife Research Center (FWRC), Mississippi State University. The FWRC Publication No. FP609.

References

[1] G. G. Allan, J. P. Carroll, A. R. Negri, M. Raghuraman, P. Ritzenthaler, and A. Yahiaoui, "The microporosity of pulp: the precipitation of inorganic fillers within the micropores of the cell wall," *TAPPI Journal*, vol. 75, no. 1, pp. 175–178, 1992.

[2] S. Q. Shi, D. J. Gardner, and J. Z. Wang, "Surface properties of polymer automobile fluff particles characterized by inverse gas chromatography and contact angle analysis," in *Proceedings of the 4th International Conference on Wood Fiber-Plastics Composites*, pp. 245–256, Forest Products Society, Madison, Wis, USA, May 1997.

[3] S. Y. Lee, *Transcrystallization behavior and interfacial strength of a semicrystalline polymer combined with thermomechanical pulp (TMP) fiber*, M.S. thesis, Moscow, Idaho, USA, University of Idaho, 2002.

[4] C. G. Ma, M. Z. Rong, M. Q. Zhang, and K. Friedrich, "Irradiation-induced surface graft polymerization onto calcium carbonate nanoparticles and its toughening effects on polypropylene composites," *Polymer Engineering and Science*, vol. 45, no. 4, pp. 529–538, 2005.

[5] S. Lee, S. Q. Shi, and M. H. Barnes, "Multifunctional nanoparticles at the hydrophilic and hydrophobic interface," in *Proceedings of the Advanced Biomass Science and Technology for Bio-Based Products*, pp. 173–181, Chinese Academy of Forestry, Beijing, China, May 2007.

[6] J. Shi, S. Q. Shi, H. M. Barnes, M. Horstemeyer, J. Wang, and E. B .M. Hassan, "Kenaf bast fibers—part I: hermetical alkali digestion," *International Journal of Polymer Science*, vol. 2011, Article ID 212047, 8 pages, 2011.

[7] C. Clemons and A. R. Sanadi, "Instrumented impact testing of kenaf fiber reinforced polypropylene composites: effects of temperature and composition," *Journal of Reinforced Plastics and Composites*, vol. 26, no. 15, pp. 1587–1602, 2007.

[8] S. Y. Lee, T. F. Shupe, L. H. Groom, and C. Y. Hse, "Heterogeneous nucleation of a semicrystalline polymer on fiber surfaces," in *Recent Developments in the Particleboard, Fiberboard, and Molded Wood Products Industry*, T. E. Shupe, Ed., pp. 99–105, Forest Products Society, 2006.

[9] J. M. Park, T. Q. Son, J. G. Jung, and B. S. Hwang, "Interfacial evaluation of single Ramie and Kenaf fiber/epoxy resin composites using micromechanical test and nondestructive acoustic emission," *Composite Interfaces*, vol. 13, no. 2-3, pp. 105–129, 2006.

[10] J. Kuusipalo, M. Kaunisto, A. Laine, and M. Kellomäki, "Chitosan as a coating additive in paper and paperboard," *Tappi Journal*, vol. 4, no. 8, pp. 17–21, 2005.

[11] S. Y. Lee, *Some factors affecting the interfacial interaction at thermomechanical fiber and polypropylene interphase*, Ph.D. Dissertation, Louisiana State University, Baton Rouge, La, USA, 2006.

[12] S. Q. Shi, S. Lee, and J. Shi, "Lamination process for chemical retted kenaf fiber/thermoplastic polymer composites," in *Proceedings of the 23rd Annual American Society for Composites Technical Conference*, Memphis. Tenn, USA, September 2008.

[13] S. Q. Shi, S. Lee, and M. Horstemeyer, "Natural fiber retting and inorganic nanoparticle impregnation treatment for natural fiber/polymer composites," in *Proceedings of the American Society for Composites*, University of Washington, Seattle, Wash, USA, September 2007.

[14] R. M. Rowell, R. Jacobson, and D. Caulfield, "Properties of kenaf/polypropylene composites," in *Kenaf Properties, Processing and Products*, chapter 32, pp. 381–392, Mississippi State University, Ag & Bio Engineering, Starkville, Miss, USA, 1999.

Hindawi Publishing Corporation
International Journal of Polymer Science
Volume 2011, Article ID 964193, 10 pages
doi:10.1155/2011/964193

Research Article

A Study of Nanoclay Reinforcement of Biocomposites Made by Liquid Composite Molding

Farida Bensadoun,[1] Nadir Kchit,[1] Catherine Billotte,[1] Simon Bickerton,[2] François Trochu,[1] and Edu Ruiz[1]

[1] *Department of Mechanical Engineering, Chair on Composites of High Performance (CCHP), Research Centre on Plastics and Composites (CREPEC), Ecole Polytechnique de Montréal, P.O. Box 6079, Station Centre-Ville, Montreal, QC, Canada H3C 3A7*
[2] *Centre for Advanced Composite Materials, Department of Engineering, University of Auckland, Private Bag 92019, Auckland 1142, New Zealand*

Correspondence should be addressed to Edu Ruiz, edu.ruiz@polymtl.ca

Received 1 March 2011; Accepted 3 May 2011

Academic Editor: Susheel Kalia

Liquid composite molding (LCM) processes are widely used to manufacture composite parts for the automotive industry. An appropriate selection of the materials and proper optimization of the manufacturing parameters are keys to produce parts with improved mechanical properties. This paper reports on a study of biobased composites reinforced with nanoclay particles. A soy-based unsaturated polyester resin was used as synthetic matrix, and glass and flax fiber fabrics were used as reinforcement. This paper aims to improve mechanical and flammability properties of reinforced composites by introducing nanoclay particles in the unsaturated polyester resin. Four different mixing techniques were investigated to improve the dispersion of nanoclay particles in the bioresin in order to obtain intercalated or exfoliated structures. An experimental study was carried out to define the adequate parameter combinations between vacuum pressure, filling time, and resin viscosity. Two manufacturing methods were investigated and compared: RTM and SCRIMP. Mechanical properties, such as flexural modulus and ultimate strength, were evaluated and compared for conventional glass fiber composites (GFC) and flax fiber biocomposites (GFBiores-C). Finally, smoke density analysis was performed to demonstrate the effects and advantages of using an environment-friendly resin combined with nanoclay particles.

1. Introduction

Recent advances in the composites field are related to the addition of nanoparticles such as carbon nanotubes, nanoclays, or silicates nanoparticles to improve the thermal, mechanical, and electrical properties. Nanoparticle additives, like nanoclay, are widely used in various industries such as cable coatings, adhesives, inks, pharmaceutical and automotive [1, 2]. One of the most common nanoclay forms is montmorillonite (MMT) with a particle thickness of 1 nm and 70 to 100 nm crosswise silica platelets [3, 4]. The choice and extensive use of montmorillonite nanoparticles in previous research is mainly due to the fact that they are commonly available and inexpensive [5]. Minimal content (1–5% wt) of such additives can improve the reinforcement of the polymer matrix by increasing flexural modulus by up to 31% and lowering the coefficient of linear thermal expansion [6–8]. However, the incorporation of nanoparticles into the liquid matrix is still a challenge, because it requires proper dispersion and exfoliation of the nanoclay. Since they are hydrophilic in their natural state and unevenly distributed, they must be organically modified to avoid agglomeration between the platelets in the dispersion media [9, 10]. This modification will increase the degree of exfoliation and thus, increase the level of surface interaction. This can be done through common dispersion techniques such as exfoliation-absorption, in situ polymerization, melt-intercalation, or sonication [9, 11–13]. Usually, in order to easily incorporate nanoparticles within the matrix, polymer dispersion media are used. The idea is that particle motion would be easier in a less viscous media than the polymer itself. Burgentzle et al.

[14] studied the behaviour of nanoclays in various solvents to evaluate the interaction between the particles and the dispersion media at different scales. They demonstrated that the surface energy of the dispersion media is superior to clay, which leads to an enhancement of the d-spacing, and therefore a balance between hydrophilic and hydrophobic natures which is the key to good dispersion. The choice of solvent will mainly depend on the matrix. If a media is used to disperse nanoparticles, and is then added to the resin, the quantity control will be crucial, otherwise an overall decrease of mechanical performances may result [12, 15]. This issue can be overcome for unsaturated polyester (UP) resins since they are composed of 35 to 38% wt of styrene monomer, which can be easily used as dispersion media without resorting to the use of another solvent.

Liquid composite molding (LCM) is widely used for manufacturing composite parts particularly because it is less expensive compared to autoclave process. LCM processes, such as resin transfer molding (RTM) and vacuum-assisted resin transfer molding (VARTM), are commonly used to manufacture glass fiber composites as well as nanoreinforced composites. Hussain et al. [16], using a resin infusion process, showed a significant improvement in mechanical properties of laminates made of glass fibers using 1% wt nanoclay. However, the infusion processes listed above are limited by the low viscosity required to impregnate the fibrous reinforcement [7, 12, 17] and knowing that the viscosity could significantly increase with the addition of nanoclays. Due to their exfoliation, the nanoclay content is often limited to a maximum of 5% wt. Thus, good knowledge of the matrix rheological behavior is mandatory and the viscosity should be controlled in order to properly impregnate the fibers and produce parts with variability in mechanical performances.

Green technologies are increasingly important on the world stage, and have been implemented in several industries. Bio-based materials appear to have a promising future, and could play an important role in solving current environmental issues. Using these materials could reduce the impact of petroleum based products, and generate lightweight and inexpensive composites. Most often, a bio component is introduced into the conventional resin, offering the significant advantage of reducing fossil fuel dependence for composite manufacturing and contributing to the reduction of greenhouse gas emissions. However, the addition of bio-based content slightly decreases the storage modulus and glass transition temperature (Tg), but increases the toughness [18, 19]. Given that stiffness and toughness are opposed performance parameters, a proper balance is then required to obtain an efficient composite by optimizing the percentages of bioproducts and nanoadditives. This can be done by the addition of layered silicates as shown in previous studies [20–22]. The simple replacement of a portion of the resin by a biocomponent reduces the overall mechanical properties, but if used in conjunction with the nanoclay, it counterbalances the properties, because the nanoparticles have greater affinity with bio-based resins [11, 16, 17].

Nowadays, natural fibers are well known, some proving to be as strong as standard glass fiber. Their use does not require any change in the current methods for composites manufacture [23]. Moreover, natural fibers can also be recycled, which is an added value [24–29]. In terms of mechanical performance, the use of flax fibers shows higher elongation at break than glass fibers, and thermal barrier properties are also improved. Table 1 illustrates the comparative properties of flax and glass fibers [30].

Safety regulations are becoming more restrictive as regards the response of polymers and polymer composites when exposed to fire. The main challenge remains that composite matrices have poor resistance to fire and generate large quantities of smoke, and industry needs to develop cost-effective and environmentally friendly flame-retardant systems [9]. Conventional flame retardants, such as ammonium polyphosphate (APP), are well known to be effective in thermoset resins by reducing the peak heat release (PHRR) and the total heat release (THR). However, to improve fire resistance to an acceptable level, very high amounts of APP, close to 30% wt, are required [31, 32]. In addition, conventional flame retardants are suspected to be harmful to the environment. This justifies their replacement by nanoclays particles, which have the advantage of acting as an effective flame retardant when mixed at low concentrations in a polymeric matrix [3, 9, 33]. Nazare et al. [9] as well as Gilman et al. [34–36] have shown that incorporating a small amount of nanoparticles (1–5% wt) can reduce the PHRR, THR, and fire growth index by 25%. Wilkie [37] also observed that flammability diminution is directly related to the surface treatment used to functionalize the nanoclay and its proportion in the matrix. Thus, it is necessary to optimize the combination between the resin and the type of nanoclay particles. Besides acting like a flame retardant, nanoclays also influence the UP resin cure by reducing cross-linking, which also lowers char formation, thus reducing flammability.

This study will focus on the manufacture of composites by LCM processes using nanocharged resins. Key parameters such as dispersion of nanoparticles will be analyzed thoroughly, as well as the mechanical properties and flammability performance. Two different resins and reinforcements will be considered, where one will lead to the manufacturing of a greener material. Three types of nanoclay particles will be investigated at weight fraction varying from 1 to 5%. The structure of the nanoreinforced thermoset matrices will be studied using rheology, in order to select the best dispersion while keeping in mind the processability of the resin for manufacturing. Glass and flax fiber reinforced composites will be fabricated and mechanically tested to obtain the elastic modulus (E) and the ultimate stress (σ). These composites will also be evaluated in terms of their flammability. Mechanical and flammability properties will be explored in this research project to determine and confirm the positive impact of the addition of nanofillers to the manufactured composites.

2. Experimental

2.1. Material. In this work, two resins were used to disperse the nanoclays particle and manufacture the composite

Table 1: Comparative mechanical properties of glass and flax fibers [23].

Fiber type	Density (g/cm^3)	Young's modulus (GPa)	Specific modulus (10^6 m^2/s^2)	Elongation at break (%)	Moisture absorption (%)
Glass	2.55	73	29	3	—
Flax	1.4	60–80	26–46	1.2–1.6	7

Table 2: Properties of nanoclay particles.

	Cloisite 11B	Cloisite 15A	Cloisite 30B
D-spacing	18.4 Å	31.5 Å	18.5 Å
Density	1.9–2.1 g/cc	1.66 g/cc	1.98 g/cc
Surface treatment	Benzy (hydrogenated tallow alkyl) dimethyl, salts with bentonite	Bis (hydrogenated tallow alkyl) dimethyl, salt with bentonite	Alkyl quaternary ammonium bentonite

laminates. Petroleum-based unsaturated polyester (R937-DPE24) from AOC was initially used to prepare nanoreinforced composites. Then, petroleum-based unsaturated polyester diluted with 8% of soy oil, Envirez Q11500 INF from Ashland, was used. Both resins were pre-promoted with cobalt ethylhexanoate (0.05%) and initiated using methyl ethyl ketone peroxide (MEKP925) from Norox at 1.5 parts per 100 parts of resin. Three different kinds of nanoclay particles were investigated in this work. Table 2 summarizes their properties. They are all montmorillonite-type nanoclays, which is an organically modified layered magnesium aluminum silicate, and are all provided by Southern Clay Products. Two types of fibrous reinforcement were also used in this study, a bidirectional 0°/90° glass fabric from JB Martin and 0°/90° flax fibers fabric.

2.2. Nanoclay Dispersion. Dispersion of nanoclay particles into the matrix is key to obtain the desired properties of the composite. In this work, three techniques were used to disperse the nanoparticles in the unsaturated polyester resin: hand mixing, three-roll-mill, and sonication. This paper reports the results obtained with the sonication technique, which proved to lead to the best mixing quality. In this study, a high-frequency ultrasonication bath from *Elmasonic* was used for nanoparticles dispersion at 35 kHz and 100 W during an hour. Four different procedures were studied to optimize the ultrasonication parameters and the mixing strategy. Figure 1 shows a flow diagram of the A0 to A4 techniques studied in this work. The dispersion media was either styrene, resin, or a mixture of both. Pure samples were sonicated using technique A0 in order to study the impact of ultrasonication on resin properties and to establish a comparative basis. After sonication, styrene is either removed or added to ensure the same percentage in all samples. Styrene quantity was measured by mass control and incorporated using a high-speed mechanical stirrer.

2.3. Fiber Reinforced Nanocomposite Manufacturing. Two liquid composite molding (LCM) processes were investigated in this research: the Seeman composite resin infusion molding process (SCRIMP), and resin transfer molding process (RTM). The SCRIMP process (see Figure 2) was modified using an aluminum plate on top of the laminate in order to better control the overall thickness of the manufactured composite, and create good surface finish on both sides. Usually, SCRIMP method requires the use of a distribution media, sitting on top of a layer of peel ply, on top of the laminate. In this work, these layers were removed, because of major nanoclays filtration problems. Laminates are composed of either six layers of 0°/90° woven glass fibers or eight layers of 0°/90° woven flax and glass fiber fabrics. The infusion pressure was chosen by taking into account the initial viscosity of the nanoreinforced resin and the minimum allowable pressure to prevent boiling and evaporation of styrene. The viscosity of the mixture is critical, because it will influence the filling time of the part and the impregnation of the fiber tows. Manufacture was followed by a 2-hour postcure at a 100°C. This step was preceded by a 3-hour post-cure at room temperature for SCRIMP composite plates only.

During the SCRIMP infusion process, the thickness of the part varies from the resin inlet to the vent location. This is due to the pressure gradient during resin flow and the decompaction of the fibers. After filling, the pressure in the cavity becomes uniform and the thickness equilibrates. However, this step, called postfilling, is very slow and often the resin cures before reaching the thickness equilibrium. To avoid this phenomenon, the filling time has to be relatively short compared to the post-filling stage [38]. Furthermore, if the resin flow is too fast, voids can be entrapped within the laminate reducing its mechanical performance. It has been demonstrated in previous work [39] that macro and micro voids are formed at, respectively, low and high capillary number. Since in this study resin viscosity will be affected by the presence of nanoparticles, then the pressure gradient in the mold has to be adjusted to ensure the same flow velocity (i.e., capillary number) for manufacture of all composite samples. To improve the robustness of the process, several composites plates were manufactured by SCRIMP using a polyester resin with different viscosities. The viscosity of the resin was modified by styrene dilution. At the same time, the vacuum pressure was varied for each laminate according to the viscosity of the applied resin. Figure 3(a) shows the resulting infusion times as a function of vacuum pressure. This evolution is found to be linear and can be illustrated by the model of the following (1) in terms of vacuum pressure, resin viscosity and infusion time:

$$\frac{t}{\mu} = -\frac{a}{P} + b \quad \text{or} \quad P = \frac{a}{b - t}\mu, \tag{1}$$

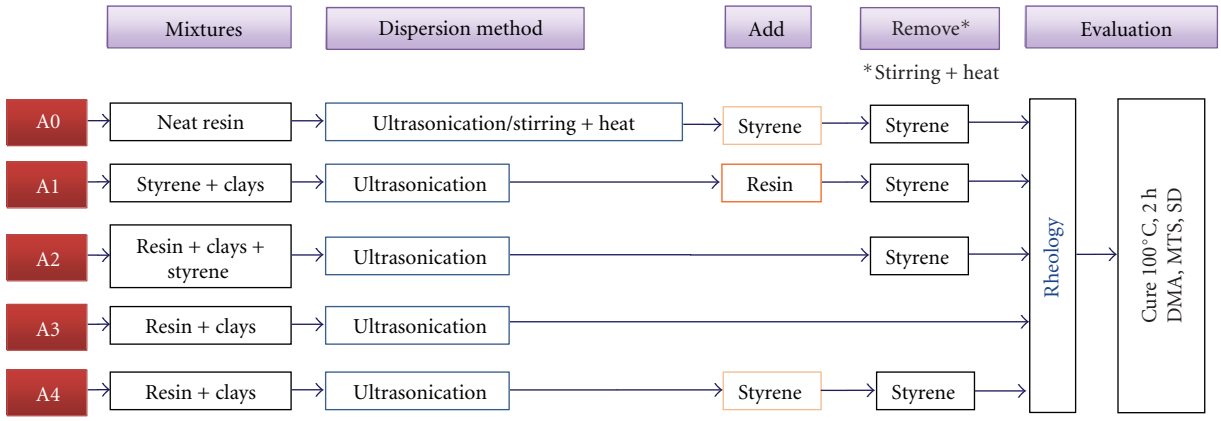

Figure 1: Nanoclay dispersion methods.

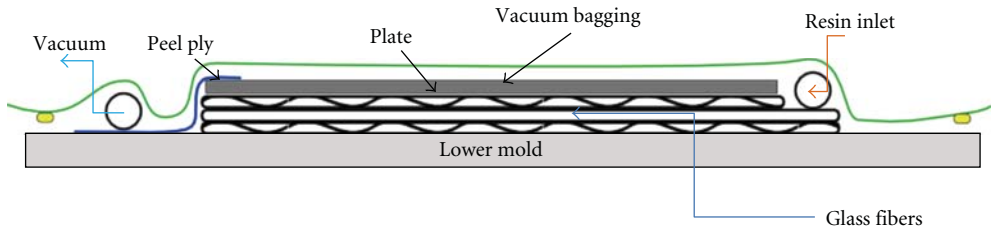

Figure 2: SCRIMP composite manufacturing setup. The liquid resin infusion was performed throug a classical VARTM process. The aluminum plate on top reduce thickness variation of the part. The reinforcement is a combination of oriented fibers and mat.

where t is the infusion time in minutes, P the vacuum pressure in kPa, μ the viscosity of the resin in Pa·s, and a and b are experimental parameters (resp., 928.7 and 3.18). In this work, the viscosity of the nanocharged resin will vary according to the nanoclay content. It is desirable to keep a constant capillary number for all samples. To do so, the infusion time has to be similar for all manufactured plates. Since the composite plates have a fixed length of 65 cm and the same reinforcement, by fixing a desired filling time, the vacuum pressure can be adjusted according to the viscosity of the resin. Figure 3(b) shows the experimental results for an infusion time of 6 min 20 sec with different resin viscosities. For this mold configuration and a fixed filling time, the previous model is used to adjust the vacuum pressure P as a function of nanocharged resin viscosity.

In addition to the SCRIMP process, an RTM manufacturing process was also implemented in this research. As shown in Figure 4, the fibers were placed between the two rigid aluminum mold parts and were clamped with a hydraulic press. The advantage of this process is that the thickness of the laminates is controlled by the mold cavity. A plate, used as a spacer, was added to adjust the depth of this cavity in order to obtain the same dimensions for both processes. Afterwards, the RTM setup was heated up to reduce the viscosity of the resin and improve impregnation of the fibers. Table 3 summarizes the manufacturing parameters used during SCRIMP and RTM experiments.

2.4. Material Characterization. Simple shear rheology tests were performed on the nanodispersed resins using a controlled stress rheometer MRC501 from Anton Paar with concentric cylinders and parallel plate geometries. Tensile and flexural mechanical tests were performed using a mechanical testing and simulation (MTS) machine from Lab Integration. A crosshead speed of 1.15 mm/min and a span length of 60 mm were used according to ASTM D790 standard. For all tests, a minimum of four samples were tested to ensure reproducibility. The flammability of the samples was studied by testing smoke density according to ASTM D2843. For this test, the flame strikes the sample at an angle of 45 degrees for a period of 4 minutes. Above the sample holder, a lamp and a light detector are located on each side of the chamber to measure the light transmission. The light intensity decreases with the smoke density generated by the burning sample. In other to obtain reproducible results, six samples of the same size were tested.

3. Nanoclay Dispersion and Processability Analyses

3.1. Nanoclay Dispersion Analysis. In this work, rheology was used to study the dispersion of the nanoclays in the liquid resin. The objective was to link the shear viscosity behavior to the level of dispersion and exfoliation of the nanoclay platelets in the mixture. Higher shear viscosity is associated with a better exfoliation of the structure [40, 41]. The shear viscosity can also be related to the ability of the polymer to bond to the nanoclays and will depend on the type of clay and its surface treatment.

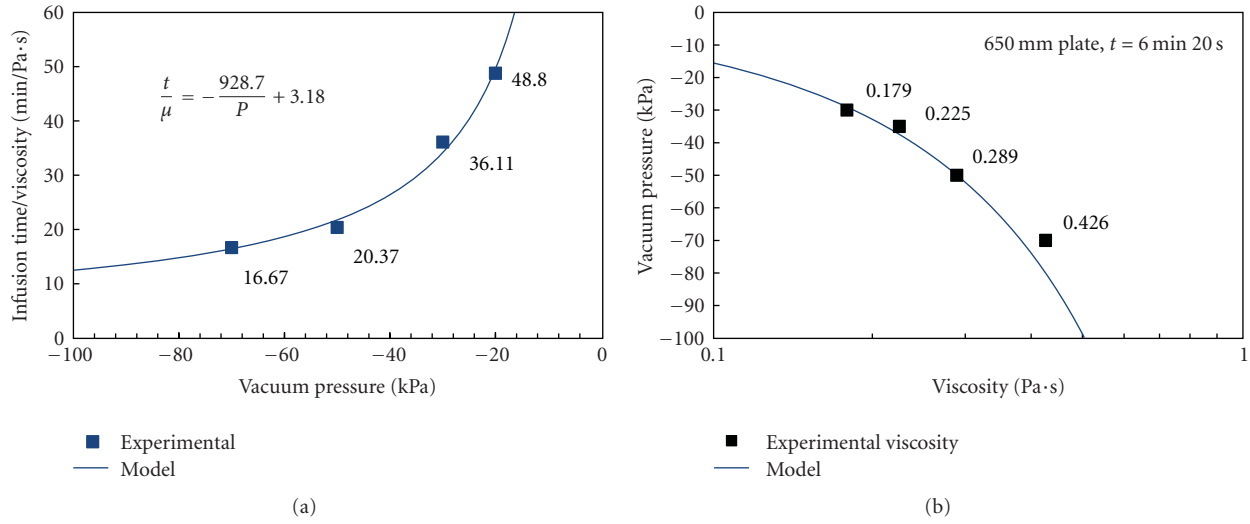

Figure 3: Optimization of SCRIMP process parameters (a) infusion time and (b) vacuum pressure required to obtain the same filling time.

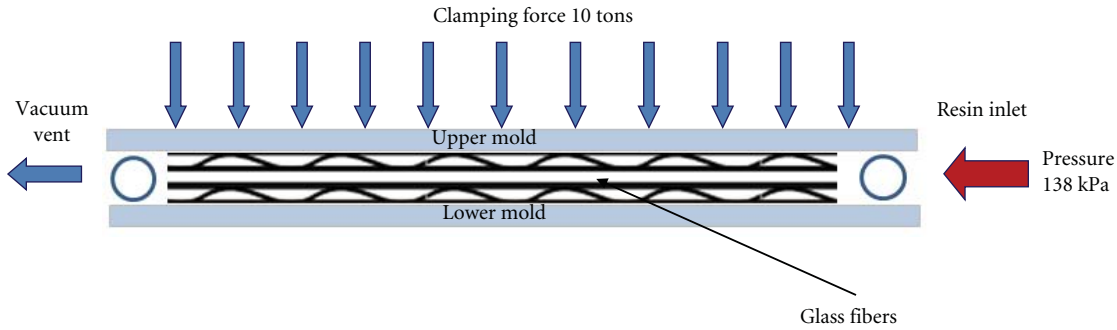

Figure 4: RTM composite manufacturing setup.

Shear experiments were carried out on resin-nanoclay mixtures dispersed by methods A1 to A4 in order to verify the impact of clay addition on viscosity. As illustrated in Figure 5, the viscosity increases by up to four-times if compared to the neat resin A0, with 3% wt of nanoclay content. However, the A1 blend shows a non-Newtonian shear-thinning behaviour while blends A2 to A4 exhibit a nearly Newtonian behaviour similar to the neat resin A0. The non-Newtonian behaviour of mix A1 may be a direct consequence of the creation of links between the nanoparticles and the resin. It can be concluded from these results that only the dispersion technique A1 would be able to produce a well-dispersed and probably intercalated/exfoliated structure. An exfoliated structure would result in higher surface interaction due to the physical properties of the montmorillonite clay itself and intercalation due to the polymer diffusion into the galleries of the nanoclays [42–44]. Durán et al. [45] observed a similar behavior for montmorillonite suspensions under shear experiments, and Sinha [3] showed that the linear viscoelastic performance of the polymer chains are indeed altered by the addition of the nanoparticles in the composition. The dispersion method chosen requires the use of styrene as the dispersion media. Due to its low viscosity (0.762 m Pa·s) the styrene allows better movement of the particles. Adding the resin afterwards seals the internal structure and maintains the intercalated-exfoliated structure.

Figure 6 shows the results of shear viscosity tests carried out on the Envirez Q11500 UP bioresin charged with 3% wt of Cloisite 30B nanoclays dispersed with the A1 technique. In this analysis, successive shear tests were conducted to study the reorientation of the nanoclays platelets along the rotation axis. During the first rotation, the viscosity of the blends at a shear rate of 0.1 sec^{-1} is 0.8 Pa·s, reducing to 0.3 Pa·s for a shear rate of 100 sec^{-1}. This shear thinning behaviour is related to the reorientation of the nanoclays platelets around the rotational axis. When the test is held for one minute before starting the second rotation, the nanoclays tend to reorganize in their original random position. As a consequence, the viscosity at low shear rates during the second sweep is lower than for the first. This phenomena is also reproduced for the third shear rate sweep. However, for all three cases, the viscosity of the blends is the same for high shear rate of 100 sec^{-1}, showing that the same reorientation of nanoparticles appears after all three sweeps.

Figure 7 shows the initial viscosity at a constant shear rate of 0.1 s^{-1}, for various types and percentage of Cloisite nanoclay dispersed in the bioresin Q11500. Generally, the viscosity increases with the nanoparticles content. It is notable

Table 3: SCRIMP and RTM process parameters.

	Part size (mm)	Fiber volume content V_f (%)	Resin injection pressure (kPa)	Mold and preform temperature (°C)	Vacuum pressure (kPa)	Closing mold pressure (tons)
RTM	300 × 100 × 2.19	40	138	80	70	10
SCRIMP	650 × 300 × 2.12	41	—	Room Temperature	30–70	—

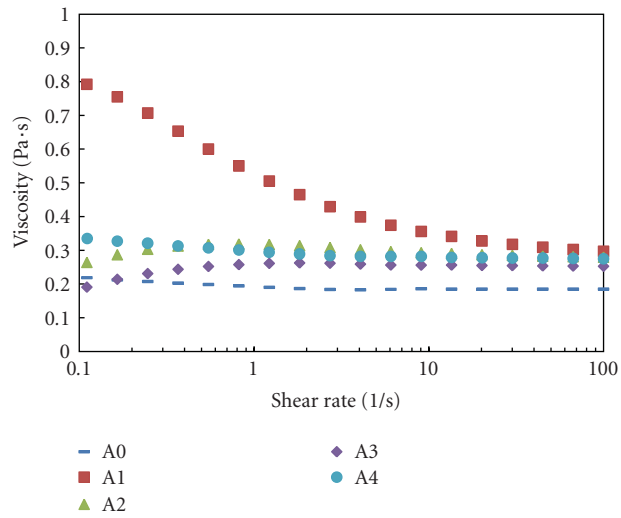

Figure 5: Shear viscosity sweep at 23°C for 3% wt C30B nanoclay dispersed in petroleum-based resin R937 by different methods.

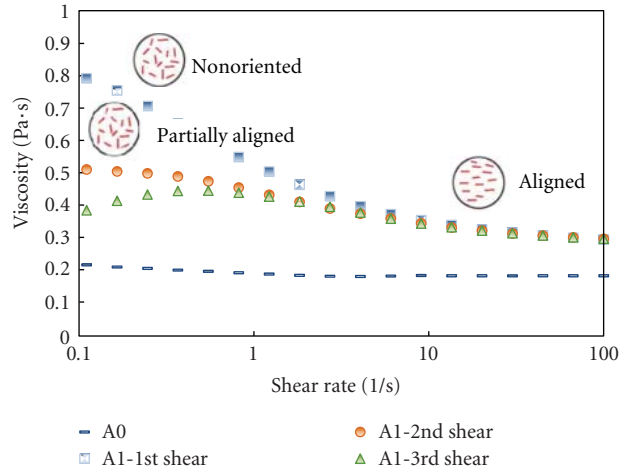

Figure 6: Successive shear viscosity sweeps at 23°C for 3% wt C30B nanoclay dispersed in petroleum-based resin R937 using the A1 mixing method.

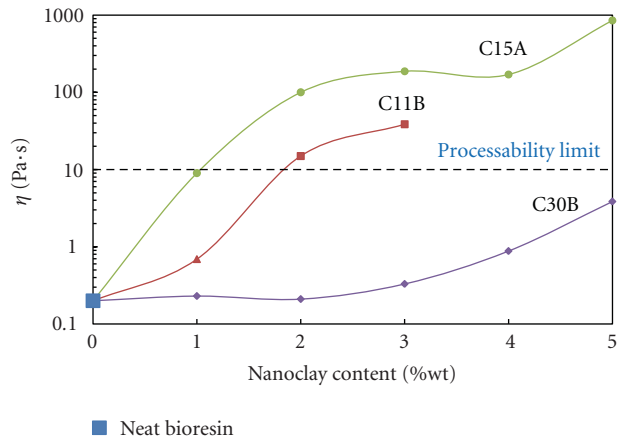

Figure 7: Viscosity at 23°C for various types of nanoclays and percentage. The dotted line indicates the maximum viscosity allowed for liquid composite molding.

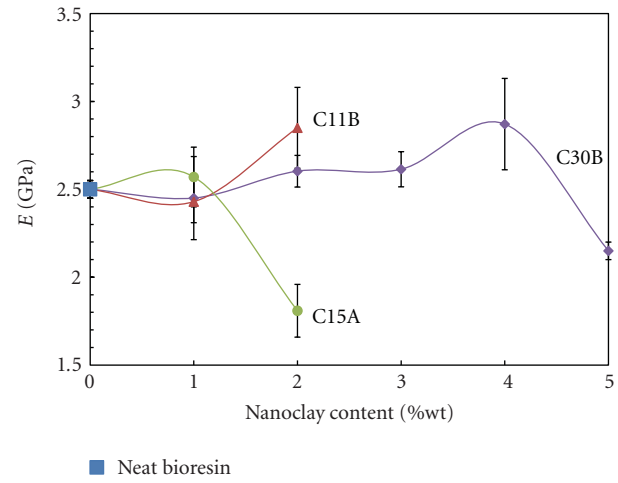

Figure 8: Flexural modulus of nanoclays reinforced polyester bioresin (matrix only).

that for the same amount of nanoclay, the viscosity is higher for C15A than for C11B and C30B. This phenomenon can be related to the higher surface interaction between the nanoclays and the UP resin which leads to a possible better dispersion for C15A. This difference can be explained by the chemical treatment and d-spacing between nanoclay platelets. The latter can also have an impact on the capacity of the particle to exfoliate with sonication energy. As described in Table 1, even if particles C15A and C11B have almost the same chemical treatment, C15A has a higher d-spacing. This higher d-spacing will facilitate the diffusion of the polymer macromolecules between the platelets resulting in higher surface interaction and higher viscosity. For C30B and C11B, the d-spacing is similar, but their chemical treatment was different. This will affect the initial viscosity value, respectively, 0.28 Pa·s and 0.8 Pa·s.

3.2. Processability Analysis. In LCM processes, the impregnation of the fibrous preform and time required to fill up the mold are intimately related to the viscosity of the resin.

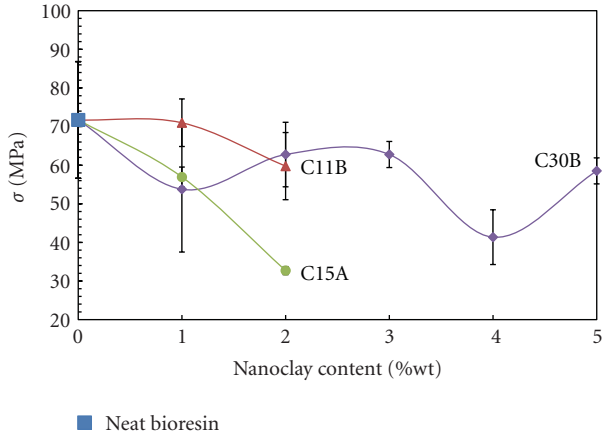

Figure 9: Ultimate strength of nanoclays reinforced polyester bioresin (matrix only).

These manufacturing processes are limited to low viscosities due to the very dense nature of typical porous media to be infiltrated (i.e., compacted fibers) and relatively low infusion pressures compared to injection molding of pure plastics. In practice, resin viscosity is limited to 1 Pa·s for SCRIMP process and 10 Pa·s for RTM. This processability limit of the nanocharged resin is illustrated in Figure 7 by the dotted line at 10 Pa·s. These manufacturing requirements limit the application of nanoclays to 1% for C15A, 2% for C11B, and 5% for C30B. These nanoclay concentrations are applied in this study for the manufacture of composite laminates with the nanocharged bioresin.

3.3. Mechanical Properties of Nanoclay Composites. In this work, different types and percentages of nanoclays were used to study their impact on mechanical properties of the composite laminate. The resulting flexural properties for C11B, C15A, and C30B nanocharges are shown in Figures 8 and 9. As illustrated in Figure 8, the addition of 1% wt of nanoclays does not have an impact on flexural modulus. This is most probably due to the low interaction between nanoparticles dispersed in the matrix. However, significant increases are observed for contents above 2% wt.

The flexural modulus of the nanofilled resin samples decreases to 1.6 GPa with the addition of 2% wt of Cloisite 15 A. This decrease in elastic properties is related to the very high viscosity of the mix (see Figure 7) and the limitations of the processability by the SCRIMP technique. For samples manufactured with Cloisite 11B and 30B, an increase in elastic modulus is observed for 2 to 4% wt of nanoclays content. Dispersion of nanoparticles in the resin is limited to 2% for C11B and 5% for C30B. In these cases, significant agglomerates were observed after dispersion, which have decreased the elastic response of the composite laminates. It can be concluded from Figure 8 that the elastic modulus of the nanocharged bioresin can be improved with the addition of 2% of Cloisite 11B and 3 to 4% of C30B.

Figure 9 shows the resulting ultimate strengths of the nanocharged bioresin manufactured at different proportions of nanoclays. It was observed that for all samples, the ultimate

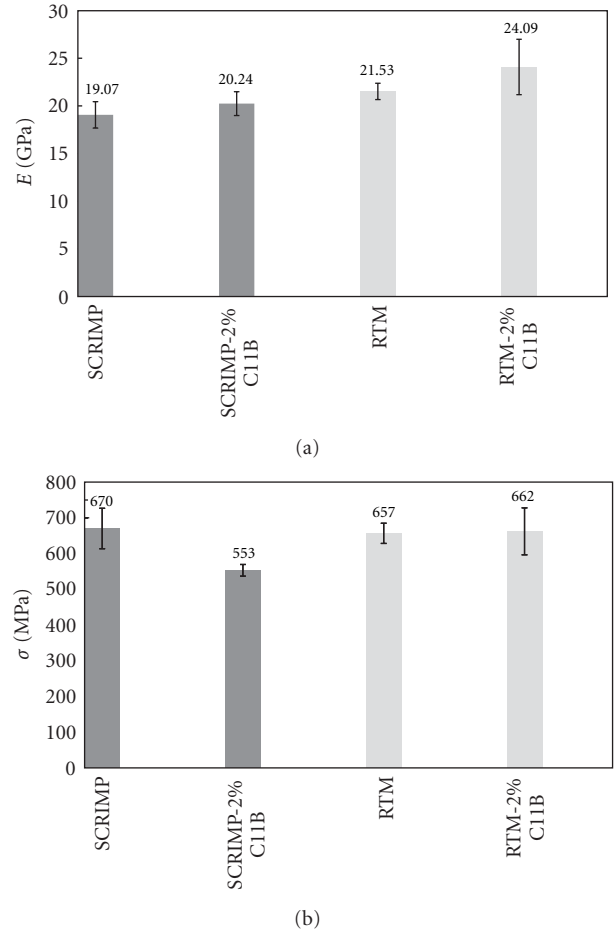

Figure 10: Mechanical properties of composite laminates made by RTM and SCRIMP processes: (a) flexural modulus, (b) utimate strength.

strength is lower than the neat resin, and the worst case is for 2% wt of C15A. This decrease in the ultimate strength is probably due to the fact that the nanoclays platelets are probably well dispersed but not exfoliated. Due to the relatively large amount of resin required to manufacture the composite plates, the ultrasonication technique used in this work may not guarantee full dispersion and exfoliation of the nanoclays. If agglomerates are present in the nanocharged resins, polymer chains will not diffuse between the clay platelets creating voids inside the agglomerate. This material discontinuity will initiate microcracking that decreases the ultimate strength of the composite laminate, which may explain the variability in the data for Cloisite 30B. It can also be concluded from Figures 8 and 9, that Cloisite 15 A is not appropriate to be used as reinforcement for the Q11500 bioresin. Moreover, both C11B and C30B, at 2 and 3% wt, respectively, are suitable as nanoreinforcements for composite laminates manufactured by SCRIMP and RTM processes. For the remainder of this study, which will focus on the manufacturing, the Cloisite 11B was chosen at a concentration of 2% wt.

In order to study the feasibility of nanoreinforced composites, rectangular plates were injected using the processes

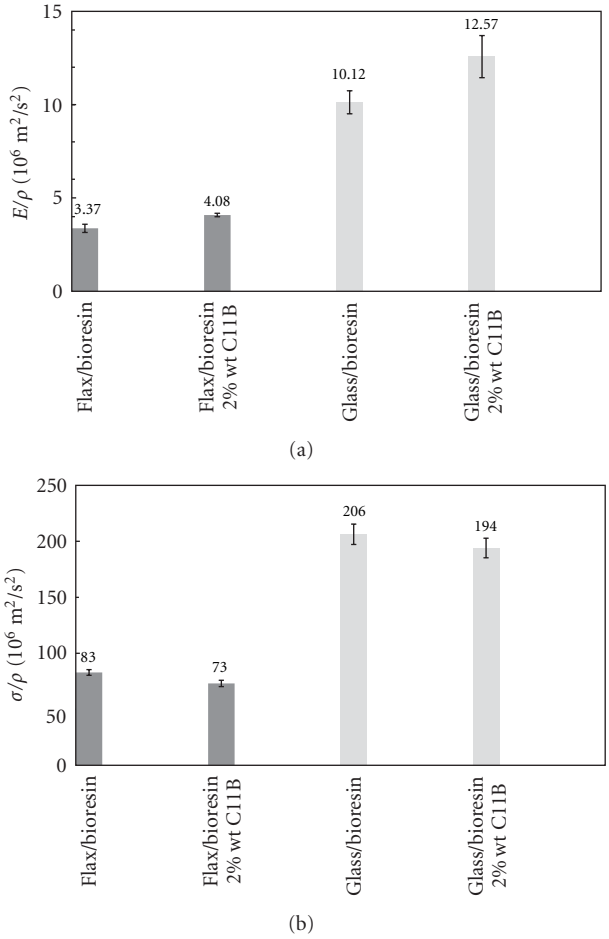

Figure 11: Mechanical properties of glass and flax reinforced nanoclays composite made by SCRIMP process: (a) specific flexural modulus (b) specific ultimate strength.

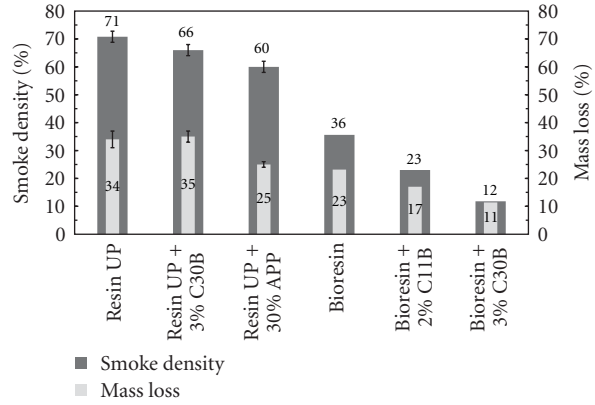

Figure 12: Results of the flammability tests carried out on various composite laminates made by SCRIMP process.

described above. These composite plates were manufactured using bidirectional glass fibers as described in Table 1. The Q11500 UP bioresin containing 8% of soy oil was mixed with 2% of C11B nanoclays. Prior to RTM injection, the mold was heated to 80°C to reduce cycle time and improve impregnation of the fibers. Table 2 summarizes the parameters used for RTM processing. Figure 10 illustrates the resulting mechanical properties of the composite plates with pure resin, and with resin nanoreinforced with 2% wt of C11B. These experimental data show that the RTM process results in improved mechanical properties as compared to the SCRIMP process. This was due to the higher molding temperature which improves fibers impregnation, higher injection pressure, and rigid mold that ensure a constant thickness and thus, a constant fiber volume fraction.

The addition of 2% of nanoclay C11B provided an improvement of both the flexural modulus and ultimate strength for both processes. An improvement of 11% in flexural modulus results of RTM laminates whereas it was 6% for the SCRIMP laminates. No significant changes were observed in ultimate strength for both processes, taking into consideration the standard deviation. Even if this improvement of mechanical properties appears promising, it may be considered to be irrelevant due to the complexity of mixing the nanoparticles with the resin.

One of the purposes of this research was the manufacturing of green composite nanoreinforced with mineral particles. To do so, glass fibers were replaced by natural fibers and a green composite was made with soy-based resin injected with the SCRIMP process. The manufacturing conditions were the same as of the previous case, except that there were eight layers of 0°/90° flax or glass fibers instead of six. Figure 11 shows the results of the mechanical tests carried out on the green composites. Using the law of mixtures, it was found that the specific properties E/ρ and σ/ρ of natural composites are much lower than those of the glass fiber composites at an equivalent fiber volume fraction of 50%. This was identified as a limitation for the practical use of these green composites. The addition of 2% wt of nanoclays C11B improved the flexural modulus of flax laminates by 18%, which is in the same order of magnitude as for the glass laminates of Figure 10. However, the ultimate stress carried by the natural fiber composites was slightly reduced by the addition of nanoclays. These latter results would require further study to develop a better understanding of the underlying reasons.

4. Flammability Results

Flammability of composite parts is a major concern since the considerable amount of smoke and toxic fumes released during burning restrict their use in the transport and building applications. Additives such as ammonium polyphosphate (APP) are often used as flame retardants in replacement of more toxic additives used in the past. However, the addition of a significant amount of these particles decreases the mechanical properties of the resin. Thus, one of the aims of the present research was to study the use of nanoclays as a potential flame retardant.

To analyze the flame retardancy of nanoclay reinforced composites, glass fiber plates were produced by the SCRIMP process using the bioresin with different amounts of nanoclay. Figure 12 shows the resulting smoke density and mass

loss of the six tested laminates. These measurements were carried out with a smoke density test facility modified to fit the ASTM D2843 standard. Six samples were tested in order to get a good reproductability within the results. The first part of the study was conducted using a petroleum-based UP resin, resulting in a smoke density of 71% and a loss of one-third of the mass after burning. Then the glass fibers/petroleum-based UP resin laminates were manufactured adding 30% of APP flame retardant or 3% wt C30B nanoclay particle. The smoke density of these samples was reduced to 60 and 66%, respectively. The addition of 30% of APP resulted then in a diminution of 15% in the smoke density and 26% in the mass loss. The addition of 3% of nanoclays equals the improvement of the flame retardancy for these laminates.

In the second part of this study, the petroleum-based UP resin was replaced by the soy oil diluted resin Q11500. For the neat bioresin/glass fibers laminate, the smoke density was reduced to 36% and the mass loss to 23%. This is an improvement of more than 50% of the results obtained with the petroleum-based resin. The addition of 2% of C11B nanoclays to this soy-based resin reduced the smoke density to 23% and the mass loss to 17% while the addition of 3% wt C30B resulted in only 12% of smoke density and 11% of mass loss. These results clearly indicate the potential use of nanoclays as an effective, more environment friendly flame retardant for bio-composites. This difference between C11B and C30B can be explained by their chemical affinity to the soybean oil contained in the Q11500 resin.

5. Concluding Remarks

In this paper, rheology analyses were completed on different nanoclay mixtures dispersed in a styrene media. Experimental rheological and mechanical analyses have shown that the properties of the charged resin are directly dependent on the nanoclay content as well as on the chemical treatment used to functionalize the nanoclays. Two bidirectional reinforcements: glass and flax fibers, were used to manufacture parts using RTM and SCRIMP processes. Two types of resin: petroleum-based unsaturated polyester and soy oil-based resin were also investigated, with three types of nanoclays: Cloisite 11B, 30B, and 15A. The choice of nanoparticles for manufacturing was restricted to the processability limit of the nanocharged resin of 10 Pa·s. First, mechanical property evaluation showed that the elastic modulus of the nanofilled resin with only 2% of Cloisite 11B increased by 14%: however, the ultimate stress decreases by 16%. This type of nanoreinforcement was chosen for further manufacturing of laminates.

Composite plates manufactured with glass and flax fibers were mechanically tested showing an improvement of 6% with the SCRIMP process and 11% for RTM when adding 2 wt% of nanoclays. The laminates made with natural fibers showed an increase of 18% of the elastic modulus. Finally, fire resistance of nanocomposites was evaluated with the smoke density tests. The addition of 3 wt% of nanoclays improved the flammability by up to 30% compared to the conventional composite, and the combination of nanoclay and bioresins doubled this value. Moreover, replacing current flame retardant, such as APP, by nanoclay particles is ecological and also reduces the impact of petroleum and chemical-based products. This study illustrates that the use of well-dispersed nanoclays in polyester resin brings a global improvement and is suitable for resin infusion process.

Abbreviations

GFC:	Glass fibers composite
GF-NC:	Glass fibers nanocomposite
GFBiores-C:	Glass fibers bioresin composite
GFBiores-NC:	Glass fibers bioresin nanocomposite
FFBiores-C:	Flax fibers bioresin composite
FFBiores-NC:	Flax fibers bioresin nanocomposite
UP resin:	Unsaturated polyester resin
Phr:	Parts per hundred
Wt:	Weight percentage.

Acknowledgments

The authors acknowledge the support provided by the Chair of High Performance Composite (CCHP) and the Center for Applied Research on Polymers and Composites (CREPEC). The financial contribution of the Natural Sciences and Engineering Research Council of Canada (NSERC) is also greatly appreciated.

References

[1] S. Abend and G. Lagaly, "Sol-gel transitions of sodium montmorillonite dispersions," *Applied Clay Science*, vol. 16, no. 3-4, pp. 201–227, 2000.

[2] W.-F. Lee and Y.-T. Fu, "Effect of montmorillonite on the swelling behavior and drug-release behavior of nanocomposite hydrogels," *Journal of Applied Polymer Science*, vol. 89, no. 13, pp. 3652–3660, 2003.

[3] S. Sinha Ray and M. Okamoto, "Polymer/layered silicate nanocomposites: a review from preparation to processing," *Progress in Polymer Science*, vol. 28, no. 11, pp. 1539–1641, 2003.

[4] F. Gao, "Clay/polymer composites: the story," *Materials Today*, vol. 7, no. 11, pp. 50–55, 2004.

[5] L. A. Utracki, M. Sepehr, and E. Boccaleri, "Synthetic, layered nanoparticles for polymeric nanocomposites (PNCs)," *Polymers for Advanced Technologies*, vol. 18, no. 1, pp. 1–37, 2007.

[6] F. Laoutid, L. Bonnaud, M. Alexandre, J. M. Lopez-Cuesta, and P. Dubois, "New prospects in flame retardant polymer materials: from fundamentals to nanocomposites," *Materials Science and Engineering R*, vol. 63, no. 3, pp. 100–125, 2009.

[7] D. Dean, A. M. Obore, S. Richmond, and E. Nyairo, "Multiscale fiber-reinforced nanocomposites: synthesis, processing and properties," *Composites Science and Technology*, vol. 66, no. 13, pp. 2135–2142, 2006.

[8] J. Denault and B. Labrecque, "Groupe technologique sur les nanocomposites polymères—PNC-Tech," 2002, http://ww2.imi.nrc.ca/francais/PDF/factsheets/pnc-tech.pdf.

[9] S. Nazare, B. K. Kandola, and A. R. Horrocks, "Flame-retardant unsaturated polyester resin incorporating nanoclays," *Polymers for Advanced Technologies*, vol. 17, no. 4, pp. 294–303, 2006.

[10] M. Bartholmai and B. Schartel, "Layered silicate polymer nanocomposites: new approach or illusion for fire retardancy? Investigations of the potentials and the tasks using a model system," *Polymers for Advanced Technologies*, vol. 15, pp. 355–364, 2004.

[11] M. Alexandre and P. Dubois, "Polymer-layered silicate nanocomposites: preparation, properties and uses of a new class of materials," *Materials Science and Engineering R*, vol. 28, no. 1, pp. 1–63, 2000.

[12] M. Haq, R. Burgueno, A. K. Mohanty, and M. Misra, "Processing techniques for bio-based unsaturated-polyester/clay nanocomposites: tensile properties, efficiency, and limits," *Composites Part A: Applied Science and Manufacturing*, vol. 40, no. 4, pp. 394–403, 2009.

[13] T. J. Pinnavaia and G. W. Beall, *Polymer—8 Clay Nanocomposites*, vol. 51, John Wiley & Sons, Chichester, UK, 2000.

[14] D. Burgentzle, J. Duchet, J. F. Gerard, A. Jupin, and B. Fillon, "Solvent-based nanocomposite coatings: I. Dispersion of organophilic montmorillonite in organic solvents," *Journal of Colloid and Interface Science*, vol. 278, no. 1, pp. 26–39, 2004.

[15] I. Ortega, "Fabrication et caracterisation de nanocomposites a matrice epoxy," M.S. dissertation, Mechnanical Engineering, Ecole Polytechnique, Montreal, Canda, 2008.

[16] F. Hussain, D. Dean, A. Haque, and A. M. Shamsuzzoha, "S2 glass/vinylester polymer nanocomposites: manufacturing, structures, thermal and mechanical properties," *Journal of Advanced Materials*, vol. 37, no. 1, pp. 16–27, 2005.

[17] L. Y. Lin, J. H. Lee, C. E. Hong, G. H. Yoo, and S. G. Advani, "Preparation and characterization of layered silicate/glass fiber/epoxy hybrid nanocomposites via vacuum-assisted resin transfer molding (VARTM)," *Composites Science and Technology*, vol. 66, no. 13, pp. 2116–2125, 2006.

[18] H. Miyagawa, A. K. Mohanty, R. Burgueno, L. T. Drzal, and M. Misra, "Novel biobased resins from blends of functionalized soybean oil and unsaturated polyester resin," *Journal of Polymer Science Part B*, vol. 45, no. 6, pp. 698–704, 2007.

[19] M. Haq, R. Burgueno, A. K. Mohanty, and M. Misra, "Bio-based unsaturated polyester/layered silicate nanocomposites: Characterization and thermo-physical properties," *Composites Part A: Applied Science and Manufacturing*, vol. 40, no. 4, pp. 540–547, 2009.

[20] C. Weinong, S. Bo, L. Zengshe, and S. Erhan, "Compressive properties of epoxidized soybean oil/clay nanocomposites," *International Journal of Plasticity*, vol. 22, no. 8, pp. 1549–1568, 2006.

[21] Z. Liu, S. Z. Erhan, and J. Xu, "Preparation, characterization and mechanical properties of epoxidized soybean oil/clay nanocomposites," *Polymer*, vol. 46, no. 23, pp. 10119–10127, 2005.

[22] H. Uyama, M. Kuwabara, T. Tsujimoto, M. Nakano, A. Usuki, and S. Kobayashi, "Green nanocomposites from renewable resources: plant oil-clay hybrid materials," *Chemistry of Materials*, vol. 15, no. 13, pp. 2492–2494, 2003.

[23] R. Kozowski and M. Wadyka-Przybylak, "Flammability and fire resistance of composites reinforced by natural fibers," *Polymers for Advanced Technologies*, vol. 19, no. 6, pp. 446–453, 2008.

[24] N. R. C. o. Canada, "From fiber glass to biofibres," 2010, http://www.nrc-cnrc.gc.ca/eng/dimensions/issue3/flax.html.

[25] P. J. Roe and M. P. Ansell, "Jute-reinforced polyester composites," *Journal of Materials Science*, vol. 20, no. 11, pp. 4015–4020, 1985.

[26] M. K. Sridhar, G. Basavarappa, S. G. Kasturi, and N. Balasubramanian, "Mechanical properties of jute-polyester composites," *Indian Journal of Technology*, vol. 22, no. 6, pp. 213–215, 1984.

[27] A. N. Shah and S. C. Lakkad, "Mechanical properties of jute-reinforced plastics," *Fibre Science and Technology*, vol. 15, no. 1, pp. 41–46, 1981.

[28] E. T. N. Bisanda and M. P. Ansell, "The effect of silane treatment on the mechanical and physical properties of sisal-epoxy composites," *Composites Science and Technology*, vol. 41, no. 2, pp. 165–178, 1991.

[29] S. V. Prasad, C. Pavithran, and P. K. Rohatgi, "Alkali treatment of coir fibres for coir-polyester composites," *Journal of Materials Science*, vol. 18, no. 5, pp. 1443–1454, 1983.

[30] W. D. Brouwer, "Natural fibre composites in structural components: alternative applications for Sisal?" 2010, http://www.fao.org/docrep/004/y1873e/y1873e0a.htm.

[31] S. Horold, "Phosphorus flame retardants in thermoset resins," *Polymer Degradation and Stability*, vol. 64, no. 3, pp. 427–431, 1999.

[32] S. V. Levchik, "Halogen-free approach in fire retardancy of thermoplastic polyesters," *Recent Advances in Flame Retardancy of Polymers*, vol. 13, pp. 296–314, 2002.

[33] A. H. B. Kandola and D. Price, "Nanocomposites," in *Fire Retardant Materials*, chapter 6, Woodhead Publishing, Cambridge, UK, 2001.

[34] J. W. Gilman, C. L. Jackson, A. B. Morgan et al., "Flammability properties of polymer - Layered-silicate nanocomposites. Polypropylene and polystyrene nanocomposites," *Chemistry of Materials*, vol. 12, no. 7, pp. 1866–1873, 2000.

[35] J. W. Gilman, "Flammability and thermal stability studies of polymer layered-silicate (clay) nanocomposites," *Applied Clay Science*, vol. 15, no. 1-2, pp. 31–49, 1999.

[36] J. Gilman, T. Kashiwagi, A. Morgan et al., Flammability of polymer clay nanocomposites consortium: year one annual report, 2000.

[37] C. Wilkie, "Recent advanced in fire retardancy of polymerclay nanocomposite," in *Recent Advances in Flame Retardancy of Polymers* , vol. 13, pp. 206–217, Business Communications Company, Norwalk, Calif, USA, 2002.

[38] Q. Govignon, S. Bickerton, J. Morris, and P. A. Kelly, "Full field monitoring of the resin flow and laminate properties during the resin infusion process," *Composites Part A: Applied Science and Manufacturing*, vol. 39, no. 9, pp. 1412–1426, 2008.

[39] J. S. Leclerc and E. Ruiz, "Porosity reduction using optimized flow velocity in Resin Transfer Molding," *Composites Part A: Applied Science and Manufacturing*, vol. 39, no. 12, pp. 1859–1868, 2008.

[40] R. Wagener and T. J. G. Reisinger, "A rheological method to compare the degree of exfoliation of nanocomposites," *Polymer*, vol. 44, no. 24, pp. 7513–7518, 2003.

[41] R. Krishnamoorti, J. Ren, and A. S. Silva, "Shear response of layered silicate nanocomposites," *Journal of Chemical Physics*, vol. 114, no. 11, pp. 4968–4973, 2001.

[42] J. C. Pierre, C. R. D. K. Daniel, and P. C. Raj, *Rheology of Polymeric Systems: Principles and Applications*, Hanser Publishers, New York, NY, USA, 1st edition, 1997.

[43] T. Phillips, "The physics of whipped cream," 2008, http://science.nasa.gov/science-news/science-at-nasa/2008/25apr_cvx2.

[44] F. A. Morrison, *Understanding Rheology*, Oxford University Press, Nwe York, NY, USA, 2001.

[45] J. D. G. Durán, M. M. Ramos-Tejada, F. J. Arroyo, and F. González-Caballero, "Rheological and electrokinetic properties of sodium montmorillonite suspensions: I. Rheological properties and interparticle energy of interaction," *Journal of Colloid and Interface Science*, vol. 229, pp. 107–117, 2000.